NASA Contractor Report 174860

Aerodynamic Performance Investigation of Advanced Mechanical Suppressor and Ejector Nozzle Concepts for Jet Noise Reduction

C.D. Wagenknecht
E.D. Bediako

CONTRACT NAS3-23038
FEBRUARY 1985

NASA

NASA Contractor Report 174860

Aerodynamic Performance Investigation of Advanced Mechanical Suppressor and Ejector Nozzle Concepts for Jet Noise Reduction

C.D. Wagenknecht
E.D. Bediako
General Electric Company
Cincinnati, Ohio

Prepared for
Lewis Research Center
under Contract NAS3-23038

National Aeronautics
and Space Administration

Scientific and Technical
Information Branch

1985

TABLE OF CONTENTS

TABLE OF CONTENTS (Concluded)

LIST OF ILLUSTRATIONS

LIST OF ILLUSTRATIONS (Continued)

LIST OF ILLUSTRATIONS (Continued)

LIST OF ILLUSTRATIONS (Concluded)

LIST OF TABLES

1.0 SUMMARY

In pursuit of an acoustically acceptable, high performance exhaust system capable of meeting Federal Aviation Regulation Stage 3 (FAR 36 Stage 3) noise goals for an Advanced Supersonic Transport (AST) application, a design study was conducted to incorporate an acoustically treated ejector shroud into a 20-chute suppressor exhaust system. The resulting ejector shroud exhaust system, after a full scale mechanical design development, was tested along with the 20-chute and the coannular exhaust systems. The results of the test were evaluated in a mission analysis study to determine engine size and aircraft Takeoff Gross Weight (TOGW) necessary to complete a typical AST mission based on system installed performance and estimated acoustic suppression effectiveness.

The mission analysis results showed the ejector shroud nozzle to be the best among the three nozzle systems studied for the AST mission within the constraints of FAR 36 (1969) Stage 3 noise goals. Comparatively, the ejector shroud nozzle system has a 79,000 pounds advantage in TOGW over a commensurate aircraft fitted with the 20-chute nozzle. The coannular nozzle, on the other hand, appears not to be an attractive concept for AST application where noise suppression is a measure of acceptability.

Though the ejector shroud nozzle performs excellently at supersonic cruise and reasonably well at takeoff, it did not quite meet subsonic performance levels projected during the conceptual design phase. This resulted from the conflicting requirements where takeoff and supersonic cruise configurations are dominated by acoustics and aerodynamics, respectively, thereby compromising the intermediate subsonic cruise point. Solutions have been advanced, however, that will seek to restore or alleviate subsonic cruise performance deficits and push it towards the conceptual design goal.

The ejector nozzle takeoff configuration flow visualization test showed complex air induction characteristics by virtue of the action of the discrete 20-Chute conic nozzles. The ejector air induction pattern appeared characteristically different from conventional annular ejector systems, and it did change current thinking on ejector inlet sizing for Ejector Shroud systems.

It is believed that implementation of the recommendations will further improve the ejector shroud nozzle system and make it even more suitable for the AST mission.

2.0 INTRODUCTION

Background

Jet noise reduction and control has been one of the dominant forces in supersonic cruise aircraft research, and hence, the exhaust system, the primary component through which the noise abatement schemes are carried out, has received considerable attention. General Electric product design engines for the NASA Supersonic Cruise Research Program have proposed annular and, in particular, coannular nozzle concepts due to their potential for noise abatement. These exhaust nozzle system concepts have included both single stream and dual stream designs for conventional engines, as well as inverted flow coannular designs for single and double bypass Variable Cycle Engines (VCE). Figure 1 shows the single stream multi-chute mechanical suppressor nozzle with retractable chutes. The chutes are stored in the plug when not used for noise suppression during cruise modes. While the exhaust nozzle performance penalties are minimized by retracting the suppressor chutes during cruise, the single stream nozzle design resulted in a relatively heavy exhaust system, primarily due to the deep and long suppressor chute lobes. This weight penalty forced alternative approaches to be investigated, the first being the coannular suppressor exhaust system. The suppression potential of the coannular system is derived from inversion of core and fan flows through flow inverting struts where the lower velocity and temperature fan flow promotes rapid decay of the higher velocity outer annulus core jet. This suppression system demonstrated 4-6 Effective Perceived Noise (EPNdB) suppression on the YJ101 Acoustic test vehicle (Reference 1). Figure 2 shows the coannular Acoustic Nozzle Exhaust System.

Extensive scale model testing under various Government contracts (Reference 1) showed that the multi-chute mechanical suppressor could be installed in the outer (core) stream of the

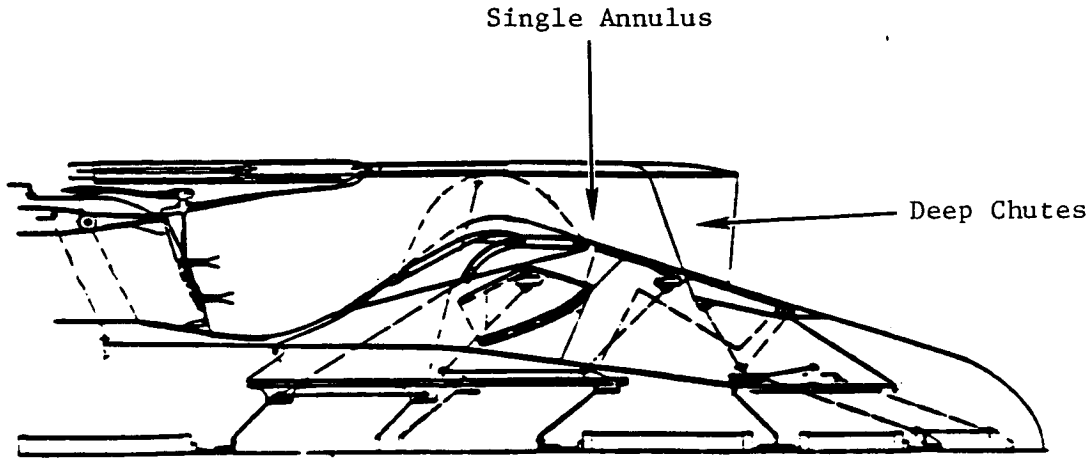

Figure 1. Fully Suppressed Single Stream Exhaust System

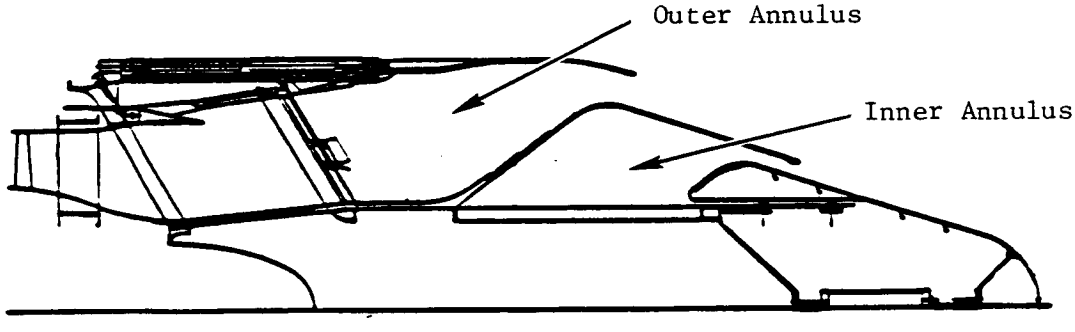

Figure 2. Coannular Acoustic Nozzle Exhaust System

coannular exhaust primary nozzle to provide additional noise reduction of 3-4 EPNdB over that of coannular exhaust system alone. Additionally, the small shallow chutes resulted in a lighter and a more reliable mechanical design compared to the single stream full suppressor nozzle concept. The most recent refinement of this type of jet noise suppression system was designed for the Variable Cycle Test Bed Engine Program, (Reference 2). This mechanical suppressor is a 20-chute, 1.75 nozzle-to-base area ratio, with moderate chute depth. Figure 3 shows the coannular nozzle with outer stream suppressor. The feasibility of implementation of these complex geometrical features in a full scale product design without excessive compromises in weight and aero/acoustic/mechanical design prompted a scale model program (Contract NAS3-21608) to measure jet noise characteristics of the 20-chute suppressor in the General Electric Anechoic Free Jet Facility. The test indicated a combined noise suppression potential of the two suppression schemes to be approximately 7-10 EPNdB.

The noise suppression effectiveness of all exhaust systems mentioned above are measured against the Federal Aviation Regulation, Part 36, 1969 (FAR 36, 1969) noise goals. These are noise goals to be complied with by all transport category large aircraft and turbojet powered aircraft by specific dates in the future. The noise milestones are categorized by stages, from FAR 36-Stage 1 through FAR 36-Stage 3. For the Supersonic Cruise Aircraft to be a viable proposition, it has to meet the FAR 36, Stage 3 noise regulation and also have acceptable performance and realistic takeoff gross weight (TOGW).

Each of the exhaust system concepts illustrated in Figures 1 through 3 successfully utilized the noise suppression schemes discussed above either singly or in combination to achieve the FAR 36-Stage 1 and Stage 2 noise goals with a reasonable engine size in the NASA AST-2 Aircraft (References 3 and 4), but they

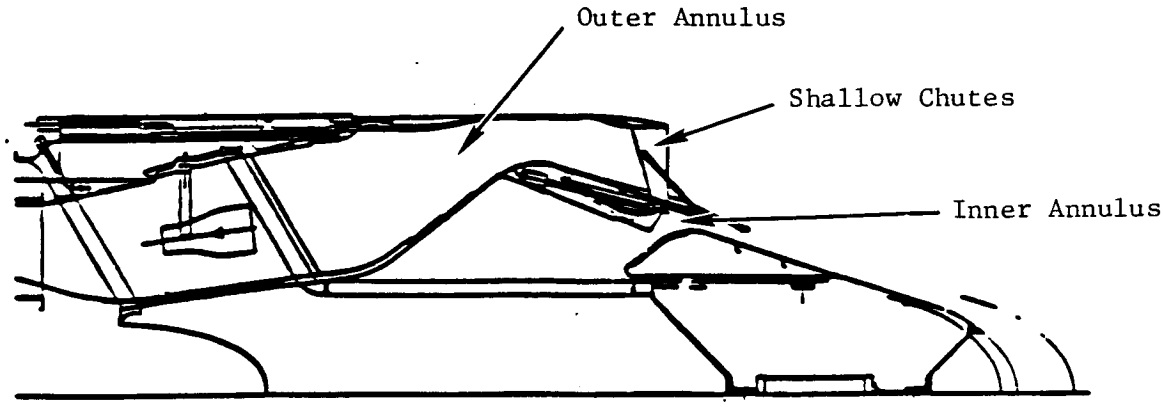

Figure 3. Coannular Nozzle with Outer Stream Suppressor

could not satisfy the Stage 3 goal. It was hypothesized that an acoustically treated ejector, when combined with a 20-chute mechanical suppressor and a coannular suppression scheme, could promote enough suppression to achieve the FAR 36-Stage 3 noise goal. The purpose of this program, therefore, was to conduct design studies to identify important exhaust systems features, followed by scale model testing to investigate aerodynamic performance of the fully integrated ejector shroud system at the important flight points.

3.0 SYMBOLS AND ABBREVIATIONS

A	Cross section area, in^2
A*	Sonic throat area, in^2
ΔA	Effective seal area change, in^2
A_I	Inner nozzle exit area, in^2
A_O	Outer nozzle exit area, in^2
AST	Advanced Supersonic Transport
C_D	Discharge coefficient, dimensionless
C_F	Friction drag coefficient, dimensionless
C_{FG}	Thrust coefficient, dimensionless
C_P	Pressure drag coefficient, dimensionless
C_T	Thrust coefficient, dimensionless
C_2	Axial balance readout, millivolts
dB	decibel
DOT	Department of Transportation
EPNdB	Effective Perceived Noise in decibel
EPNL	Effective Perceived Noise Level, decibels
f	Exit stream thrust parameter, $(H+P_aA_9)/{}^PT_8A_8$, dimensionless
F	Stream thrust, mV+PA, lbf
FAA	Federal Aviation Administration
FAR	Federal Aviation Regulation
FAR 36 Stage 1	Federal Aviation Regulation, Part 36 Stage 1 noise goal
FI	Ideal thrust, lbf
ft	feet

G	Real-gas stream thrust correction factor, dimensionless
g	Acceleration of gravity, 32.174 ft/sec^2
GE	General Electric Company
H	Net thrust (static) or thrust-minus-drag (wind-on), lbf
H_o	Axial balance force, lbf
in	inches
K	Real-gas mass flow function, $°R^{1/2}/sec$
K_2	Balance force calibration factor, lbf/millivolt
km	kilometers
kps	kilo pounds (1,000 lbs)
Ls	Ejector shroud length, inches
m	meters; mass flow rate, slugs/sec
M	Mach number, dimensionless
NASA	National Aeronautics and Space Administration
N.M.	Nautical Miles
NPR	Nozzle Pressure Ratio
P	Pressure, static unless otherwise specified by subscript, psia
ΔP	Static pressure differential across seal, psi
R	Gas constant, 1716.32 $ft^2/sec^2-°R$
RN	Reynolds number, dimensionless
RSPD	Rapid Solidification Process Deposition
S	Ejector setback from suppressor shroud boattail, in
SCA	Supersonic Cruise Aircraft
SCAR	Supersonic Cruise Aircraft Research
SCR	Supersonic Cruise Research

STC	Stream Tube Curvature fluid dynamics analysis program
T	Temperature, °R
TOGW	Takeoff Gross Weight, lbs
V	Velocity, ft/sec
V_j	Nozzle core jet velocity, ft/sec
V_{mix}	Mass averaged mixed stream velocity, ft/sec
V_R	Velocity ratio, V_{89}/V_9, dimensionless
W	Mass flow rate, lbm/sec
W_x	Dead-weight calibration load, lbf
X	Ejector setback, full scale, in. (See def. for 5 on page 10).
Δ	Incremental quantity
λ	Total to ambient pressure ratio, P_t/P_a, dimensionless
θ	Meridian angle measured clockwise from vertical
θ_i	Angle of observer relative to inlet axis, degrees
γ	Specific heat ratio, dimensionless
Σ	Summation

Subscripts

a	Ambient
b	Base
e	Exit station
i	Ideal
j	Counter for summations
o	Freestream conditions
t	Total conditions

Subscripts (Continued)

x	x component
1	Inner passage flow ASME metering nozzle station
2	Inner passage flexible seal station
4	Balance cavity
5	Outer passage flow ASME metering nozzle stations
6	Outer passage flexible seal station
7	Outer nozzle charging station
8	Outer passage throat area station
9	Outer nozzle discharge
87	Inner nozzle charging station
88	Inner nozzle throat station
89	Inner nozzle discharge

Superscripts

*	Sonic flow
'	Referenced to base pressure

4.0 PROGRAM APPROACH

The overall program consisted of three major tasks. These are:

- Task 1 - Coannular and 20-Chute Suppressor Nozzle Aerodynamic Performance Test Program
- Task 2 - Acoustically Treated Ejector Shroud Study
- Task 3 - Ejector Shroud Nozzle Aerodynamic Performance Test Program.

Although Task 1 was independent of Tasks 2 and 3, Task 2 was initiated first as illustrated in the work flowchart, shown in Figure 4. This provided an ejector shroud design early enough in the program to enable Tasks 1 and 3 to be conducted in parallel. By combining the Tasks 1 and 3 experimental programs, the associated model hardware were designed simultaneously to take advantage of parts commonality for cost effectiveness. In addition, the overall time required to complete the program was reduced relative to a sequential order of accomplishing the three tasks. The following summarizes the work accomplished from each of the tasks.

Task 1 - Model Coannular and 20-Chute Suppressor Nozzle Aerodynamic Performance Test Program

The objective of this task was to measure and evaluate the aerodynamic performance of a model coannular plug nozzle with a 20-chute mechanical noise suppressor in the outer stream. The evaluation was conducted at simulated takeoff, subsonic cruise, and supersonic cruise flight conditions representative of an advanced supersonic transport. The basis for the model design

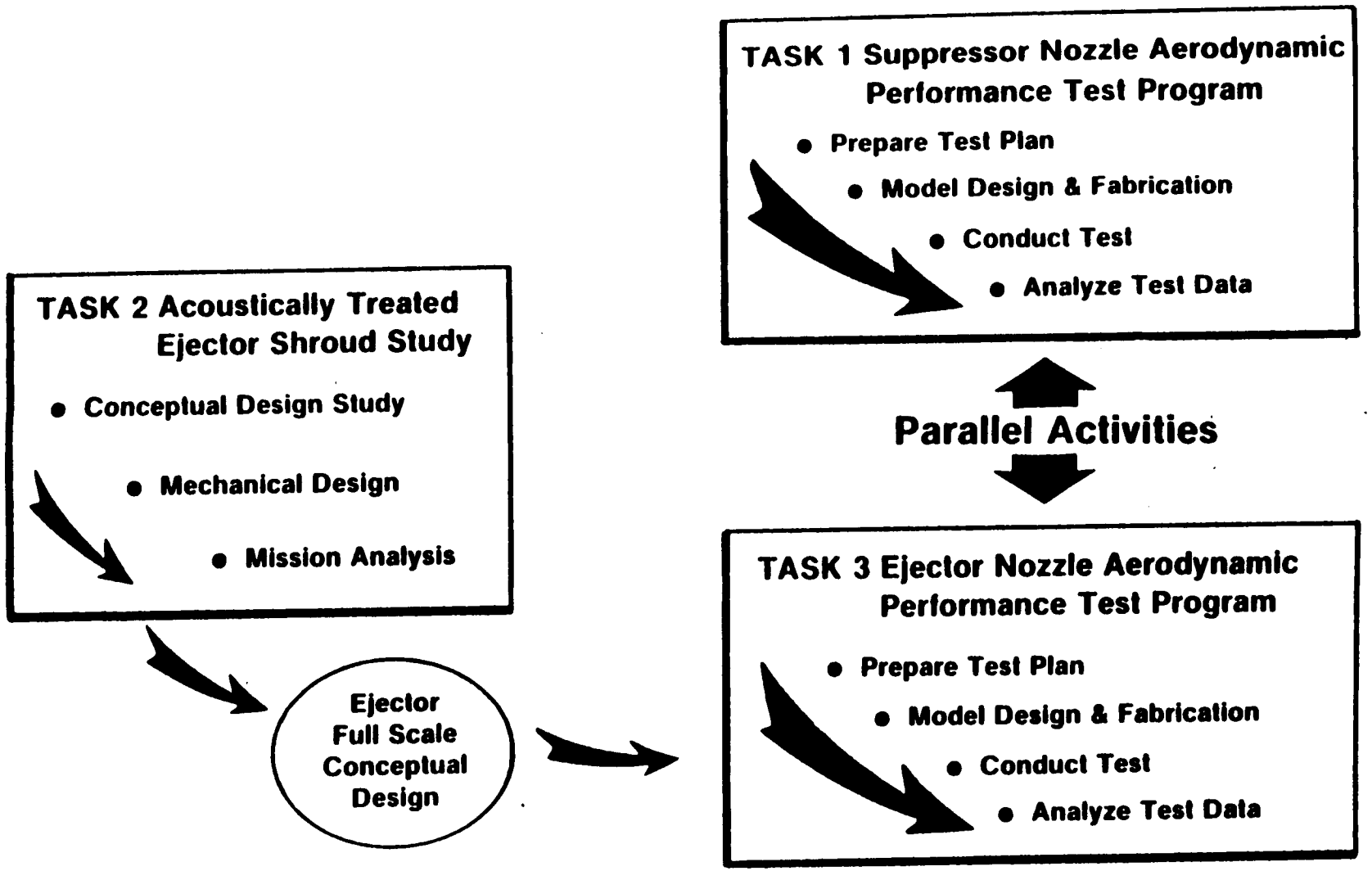

Figure 4. Program Work Flow

was a full scale product type nozzle design shown in Figure 5 and reported in Reference 2. This particular concept utilized an 18° half-angle plug which was revised in Task 1 to incorporate a 15° half-angle plug. This revision was accomplished first in Task 1 to provide the basis for the model design in subsequent tasks.

The aerodynamic performance of a "baseline" unsuppressed nozzle was also investigated in Task 1. An existing product type unsuppressed coannular nozzle, shown in Figure 6, was also revised from 18° plug half-angle to 15° plug half-angle design for aerodynamic enhancement. This revision was also accomplished early in Task 1 to provide a basis for the unsuppressed coannular model design. The remainder of the task activities involved (1) formulation of test plan, (2) design and fabrication of scale model hardware, (3) wind tunnel and static testing, and (4) data analysis.

Task 2 - Acoustically Treated Ejector Shroud Study

The objective of this task was to conduct a design study to identify a candidate full scale ejector shroud coannular plug nozzle exhaust system for an advanced supersonic transport incorporating an outer stream 20-chute mechanical suppressor with an acoustically treated ejector shroud for additional jet noise reduction. The full scale design was used as the basis for defining scale models for Task 3. The work elements for this task included (1) conceptual design study, (2) mechanical design study, and (3) mission analysis.

Conceptual Design Study

A preliminary design study was conducted to incorporate an acoustically treated ejector shroud into the 20-chute mechanical suppressor and coannular acoustic exhaust system (20-chute nozzle). The design began with a baseline GE21/V50C double bypass

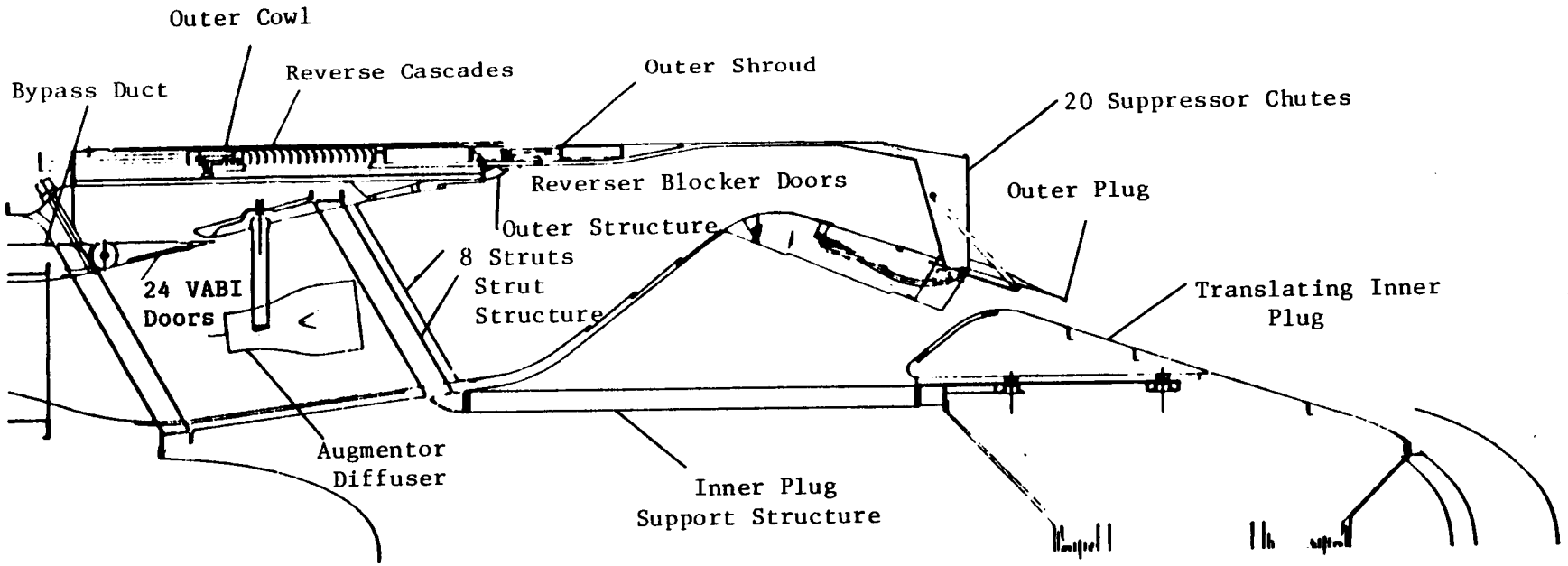

Figure 5. 20-Chute Coannular Nozzle (18 degree plug).

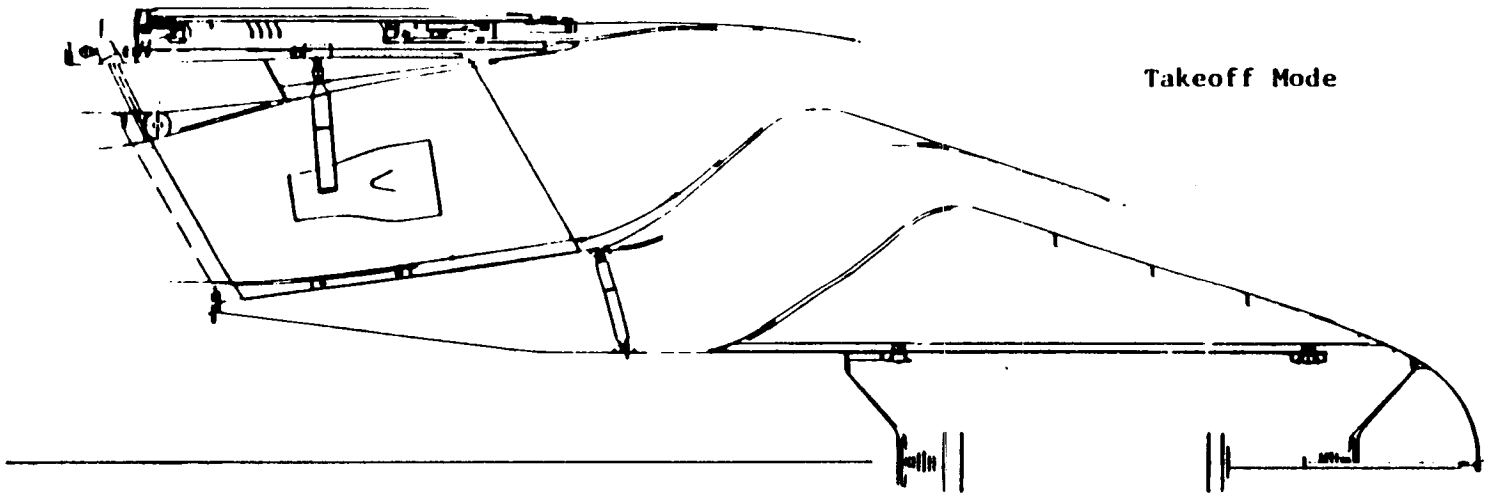

Figure 6. Coannular Nozzle (18 degree plug), Takeoff Mode.

variable cycle engine (Reference 4). Design factors considered during this conceptual design phase included ejector flap length and thickness, as well as plug truncation, all of which affected aerodynamic performance, weight and acoustic suppression characteristics. Several ejector shroud nozzle configurations were defined and developed to provide the pertinent information required to make the selection.

Performance estimates were based on prediction methodologies presented in the Noise Abatement Nozzle Design Guide for High Velocity Jet Noise Source Location and Reduction Program, Reference 5, and current GE Fluid Dynamics Analysis Programs. The analysis results were used to update the engine cycle to reflect prevailing engine takeoff performance data needed to estimate takeoff noise levels. It was the goal of the entire design process to satisfy the FAR 36-Stage 3 noise goals without undue aerodynamic and mechanical design compromises, and the work proceeded accordingly. Noise from all engine related sources was examined; fan and core turbomachinery additions to exhaust jet noise were evaluated to check compliance with the noise goals. Based on the analysis data, a trade study was conducted to select the most promising ejector shroud configuration for full scale mechanical design development.

Mechanical Design Study

The aero-acoustic exhaust nozzle configurations defined in the conceptual design study provided the basic internal contours for the mechanical design study. Important aspects of the exhaust system mechanical design were covered. The study analyzed pressures, temperatures and stresses for proper selection of materials; details of deployment and retraction of the mechanical suppressor and ejector shroud; cooling requirements of nozzle components; actuation system types and quantities, thrust

reverser installation and actuation, weights and dimensions. A design cross section was generated to show the layout and operational feasibility.

Mission Analysis

The aerodynamic performance data from the Conceptual Design and the Exhaust System Weight studies were evaluated using the mission analysis program. This program used the AST-2 Airplane (References 3 and 4) and flew the AST Mission "B" with an initial 600 N.M. subsonic cruise segment followed by a Mach 2.32 (hot day) supersonic cruise. The output yielded takeoff gross weight to perform the 4,000 N.M. mission. Also available from the Mission Analysis were Mission parameter sensitivities (derivatives) which would enable calculation of change in takeoff gross weight as a figure of merit in response to changes in installed performance, exhaust system weight, or noise level.

Task 3 - Model Ejector Nozzle Aerodynamic Performance Test Program

The objective of this task was to measure and evaluate the aerodynamic performance of the 20-chute nozzle from Task 1 with an integrated ejector at simulated takeoff, subsonic cruise, transonic acceleration, and supersonic cruise flight conditions representative of an advanced supersonic transport.

As was previously discussed and illustrated in the work flowchart of Figure 4, Task 3 was conducted in parallel with Task 1 in order to improve efficiency. The models tested in Task 3 were based on the 20-chute nozzle with an integrated ejector concept as defined in the Task 2 study. Work elements in Task 3 were the same as for Task 1, namely: (1) formulation of test plan, (2) design and fabrication of scale model hardware, (3) wind tunnel and static testing, and (4) data analysis.

5.0 CONCEPTUAL DESIGN

Design Philosophy

Deployment of aircraft noise abatement schemes present a special challenge to gas turbine engine exhaust system design technology because design features that promote noise abatement generally detract from system performance potential. In addition to the performance potential decrement, they promote mechanical design complexity, increase exhaust system weight and complicate the inter-relationships between mission performance parameters like propulsion efficiency, fuel requirements and Takeoff Gross Weight (TOGW) assessment. Introduction of acoustics into the exhaust system selection criteria means that the selection of a particular exhaust system over others will be on the basis of its capability to minimize the TOGW for a specific mission profile at a specific noise level (EPNdB) as outlined in FAR 36 (1969).

Since TOGW is the sum of payload, aircraft system weight and fuel, it becomes apparent that any weight minimization process hinges heavily on aircraft system efficiency improvements. Reduction of aircraft system weight and improvement of propulsion system efficiency are directly translated into TOGW reduction. Propulsion efficiency and aircraft system technology enhancements are derived from aerodynamics, mechanical design, and materials technology, among others. Improved aerodynamics means less drag, more efficient fuel usage and lower TOGW. Advanced mechanical design reduces aircraft weight, saves fuel, and reduces TOGW. Use of advanced light weight, higher temperature resistant materials improves specific thrust, and reduces aircraft system weight as well as fuel requirements and TOGW.

As indicated earlier, jet noise abatement dominates supersonic cruise aircraft exhaust system design, and the evaluation of the net cumulative effects of the three identified suppression

schemes is the primary task of this program. Reduction of jet noise is accomplished through coannular inverted flow suppression, direct suppression through use of multi-chute mechanical suppressors and the deployment of acoustically treated ejector shroud. Any or all of these contribute heavily towards exhaust system weight increase and the higher the suppression desired, the greater the weight contribution. This means that the acceptability of an exhaust system must be based on the best compromise between acoustics, aerodynamic performance, and weight.

The strategy of Task 2 was to develop the ejector shroud nozzle and evaluate it against the other two baseline nozzles (i.e., the baseline coannular nozzle and the 20-chute suppressor nozzle) for required engine size (lb/sec of air intake) and TOGW, with the aircraft flying a specific mission profile, at an allowable noise level using a specific supersonic cruise aircraft. The following portions of the report present problem synthesis and analysis methods.

Noise Goals

Several factors influence aircraft performance. Among these are operational, technological and regulatory factors. Operational factors are characterized by payload, mission profile, fuel, aircraft system, propulsion efficiency, etc. The technology factors are dominated by acoustics, aerodynamics, mechanical design, materials, aircraft system, propulsion efficiency and others. The most obscured, yet the most dominant of the aircraft performance influencing factors are the regulatory factors, either for safety or for noise abatement. With the acoustics being such a dominant force in supersonic aircraft systems design, it is worth a few moments to examine how the FAR 36-Stages 1 through 3 are formulated.

The FAR 36-Stages 1 through 3 are noise goals to be complied with by all transport category large aircraft and turbojet powered aircraft by specific dates in the future. These noise goals are categorized by stages from Stage 1 through Stage 3, in order of increasing stringency.

Noise Measuring Points

Compliance with the noise goals is determined by measuring Effective Perceived Noise Level (EPNL) of the concerned aircraft at three reference points along or parallel to the runway or runway extended. These noise measuring (reference) points are (1) Takeoff (Community), (2) Approach, and (3) Sideline. Takeoff noise is measured at a point 21,325 feet (6,500 meters) from the start of the takeoff roll on the extended centerline of the runway, and Approach noise is measured at a point 6,562 feet (2,000 meters) from the threshold on the extended centerline of the runway. Likewise, the Sideline noise is measured at a point on a line parallel to and 1,476 feet (450 meters) from the extended centerline of the runway where the noise level after liftoff is greatest, except for airplanes powered by more than three turbojet engines, where this distance is 0.35 nautical miles for the purpose of showing compliance with Stage 1 or stage 2 noise limits as applicable. Figure 7 shows the FAR 36 (1969) Noise Measuring Points

Noise Levels

Compliance with noise levels is determined by flight test at the prescribed measuring points shown in Figure 7 and at the appropriate FAR 36 stage.

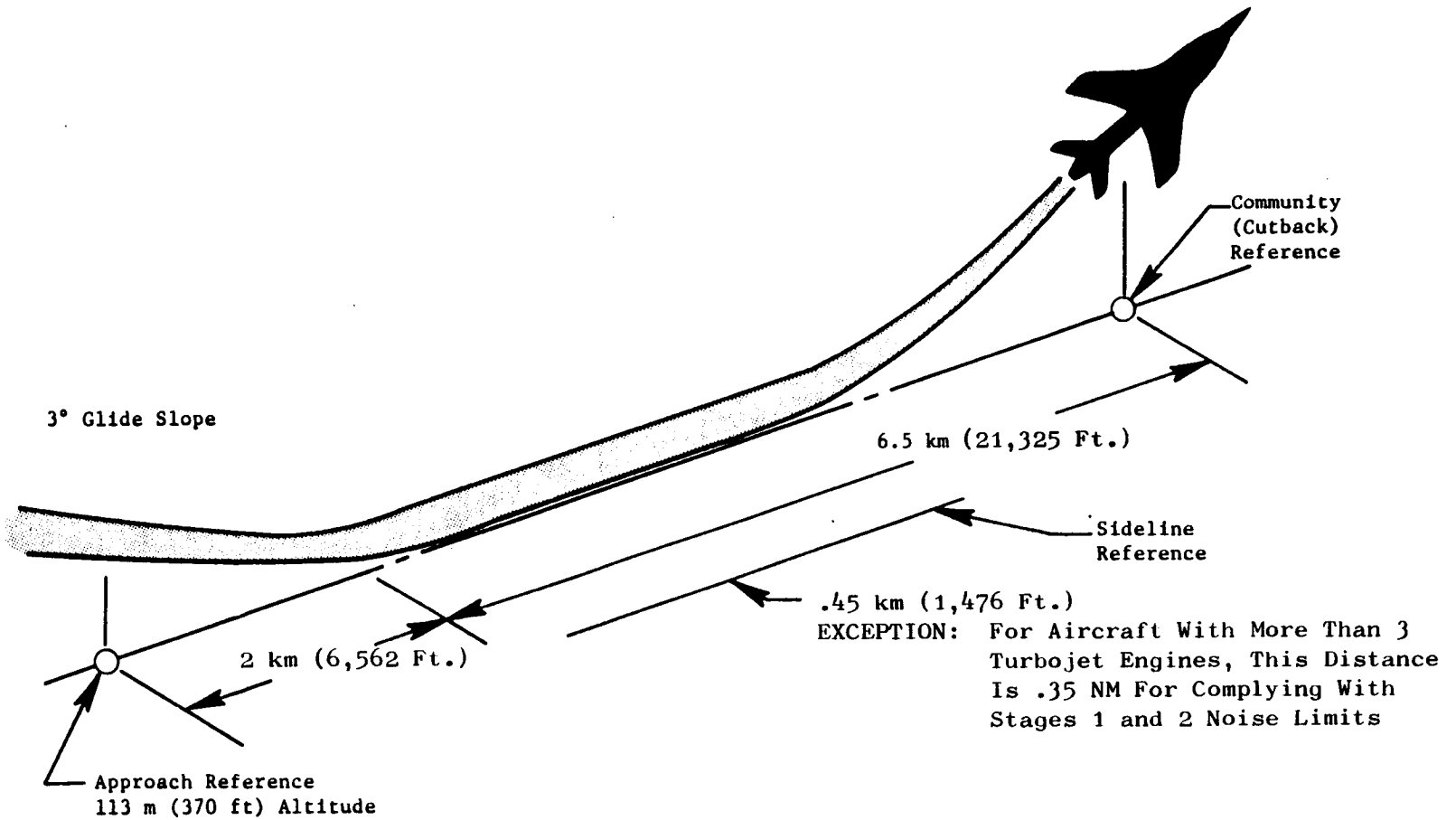

Figure 7. FAR 36 (1969) Noise Measuring Points

Stage 1 Noise Limits

The Stage 1 maximum noise limit is 108 EPNdB regardless of the number of engines and must not exceed the noise level indicated by an appropriate interpolation between weights as shown in Figure 8a. Only the Takeoff (Community) noise is to be satisfied in Stage 1.

Stage 2 Noise Limits

Stage 2 noise limits for airplanes regardless of the number of engines are as follows:

1. For Takeoff - 108 EPNdB for maximum weight of 600,000 pounds or more, reduced by 1 EPNdB per 60,000 pounds from the maximum weight down to 93 EPNdB for a maximum weight of 75,000 pounds and less.

2. For Sideline and Approach - 108 EPNdB for a maximum weight of 600,000 pounds or more reduced by 1 EPNdB per 150,000 pounds from the maximum weight down to 102 EPNdB weight for a maximum weight of 75,000 pounds and less. Stage 2 noise limits are illustrated in Figure 8b.

Stage 3 Noise Limits

Stage 3 noise limits are as follows:

1. Takeoff (Community)

   a. For airplanes with more than 3 engines, 106 EPNdB for maximum weight of 850,000 pounds or more, reduced by 1 dB per 106,250 pounds from the maximum weight down to 89 EPNdB for maximum weight of 44,673 pounds and less.

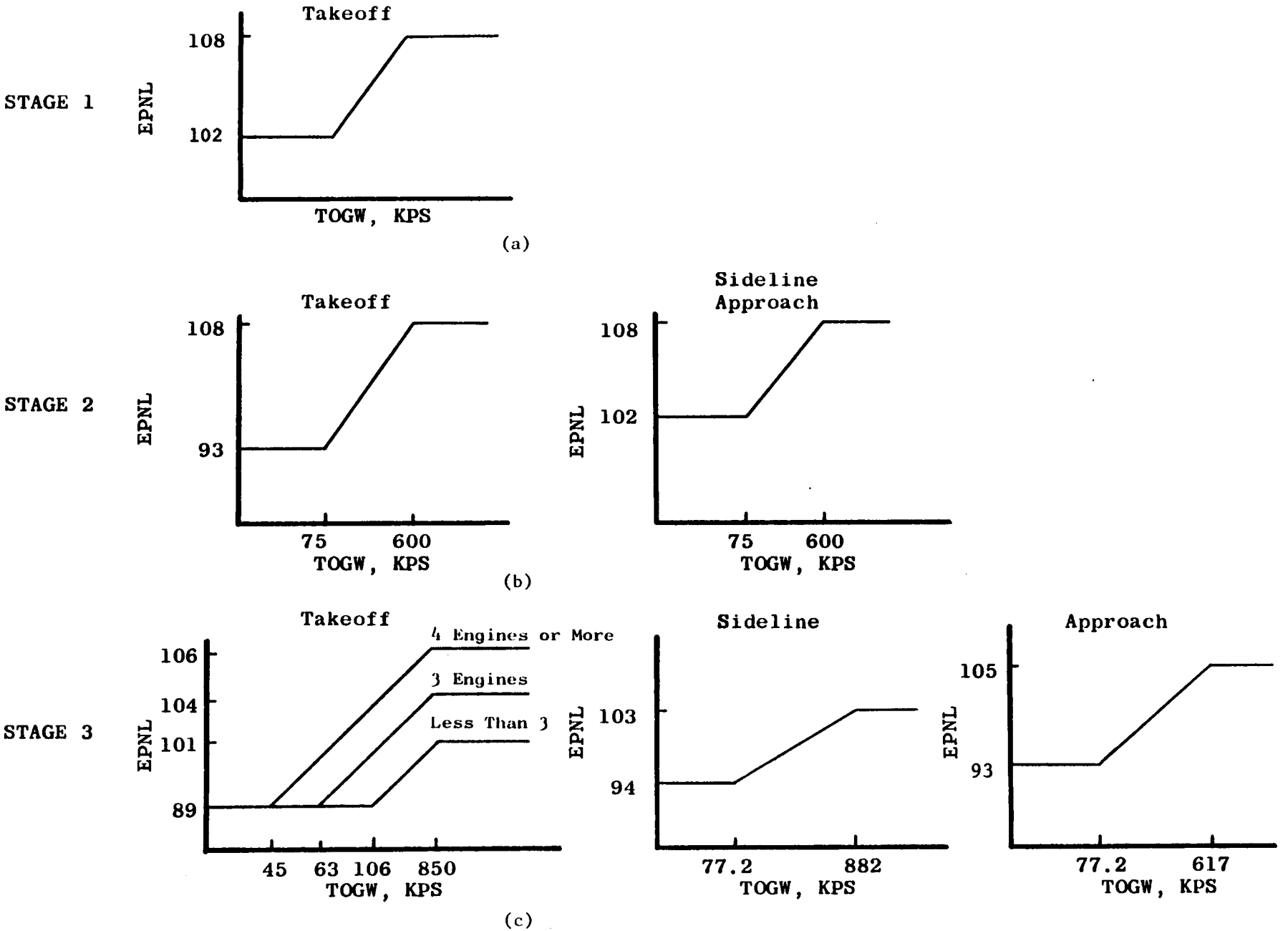

Figure 8. Federal Aviation Regulation Noise Goals
FAR 36, 1969, Stages 1, 2 & 3

b. For airplanes with 3 engines - 104 EPNdB for a maximum weight of 850,000 pounds or more, reduced by 1dB per 106,250 pounds from the maximum weight down to 89 EPNdB for a maximum weight of 63,177 pounds and less.

c. For airplanes with fewer than 3 engines - 101 EPNdB for a maximum weight of 850,000 pounds or more, reduced by 1 dB per 106,250 pounds from the maximum weight of 106,250 pounds and less.

2. For Sideline, regardless of the number of engines - 103 EPNdB for a maximum weight of 882,000 pounds or more, reduced by 1 dB per 172,270 pounds from the maximum weight down to 94 EPNdB for a maximum weight of 77,200 pounds and less.

3. For Approach, regardless of the number of engines - 105 EPNdB for maximum weights of 617,300 pounds or more, reduced by 1 dB per 132,468 pounds from the maximum weight down to 93 EPNdB for a maximum weight of 77,200 pounds or less. Stage 3 noise limits are illustrated in Figure 8c.

Throughout the study, the FAR 36 (1969) Stage 3 was used. After noise levels at the study conditions were determined, the values were "traded" in order to obtain an overall noise level.

"Trading" rules used are described in Appendix C of FAR 36 as follows:

"Tradeoff" - The noise levels may be exceeded at one or two of the measuring points if,

1. The sum of the exceedances is not greater than 3 EPNdB,
2. No exceedance is greater than 2 EPNdB, and
3. The exceedances are completely offset by reductions at other required measuring points.

Ejector Shroud Conceptual Design

The approach used in Task 2 to accomplish the conceptual design and ultimate selection of the final ejector nozzle configuration is illustrated schematically in Figure 9. The prototype mechanical design and engine cycle were redefined to suit program goals, refined through mechanical design, aerodynamics and acoustics trade studies, and followed by mission analysis to identify engine size and TOGW commensurate with the desired noise goals.

The conceptual design was started by selecting a prototype cycle and an ejector shroud design for development. These were reviewed and compared with previous NASA programs for development ideas. Several documents published under SST Technology, Follow-On Program - Phase II, Noise Suppressor/Nozzle Development, were studied to identify the variables that dominate ejector performance.

The following geometric features were identified to influence ejector performance:

- Setback - the axial distance from the suppressor exit plane to the flight lip hilite of the ejector.
- Minimum annular area between the ejector lip and suppressor chutes.
- Number of suppressor elements and geometry.
- Suppressor nozzle area ratio.
- Ejector shroud area ratio - inlet-to-exit ratio.
- Ejector length to diameter ratio.
- Suppressor radius ratio - suppressor exit inner radius divided by outer radius.

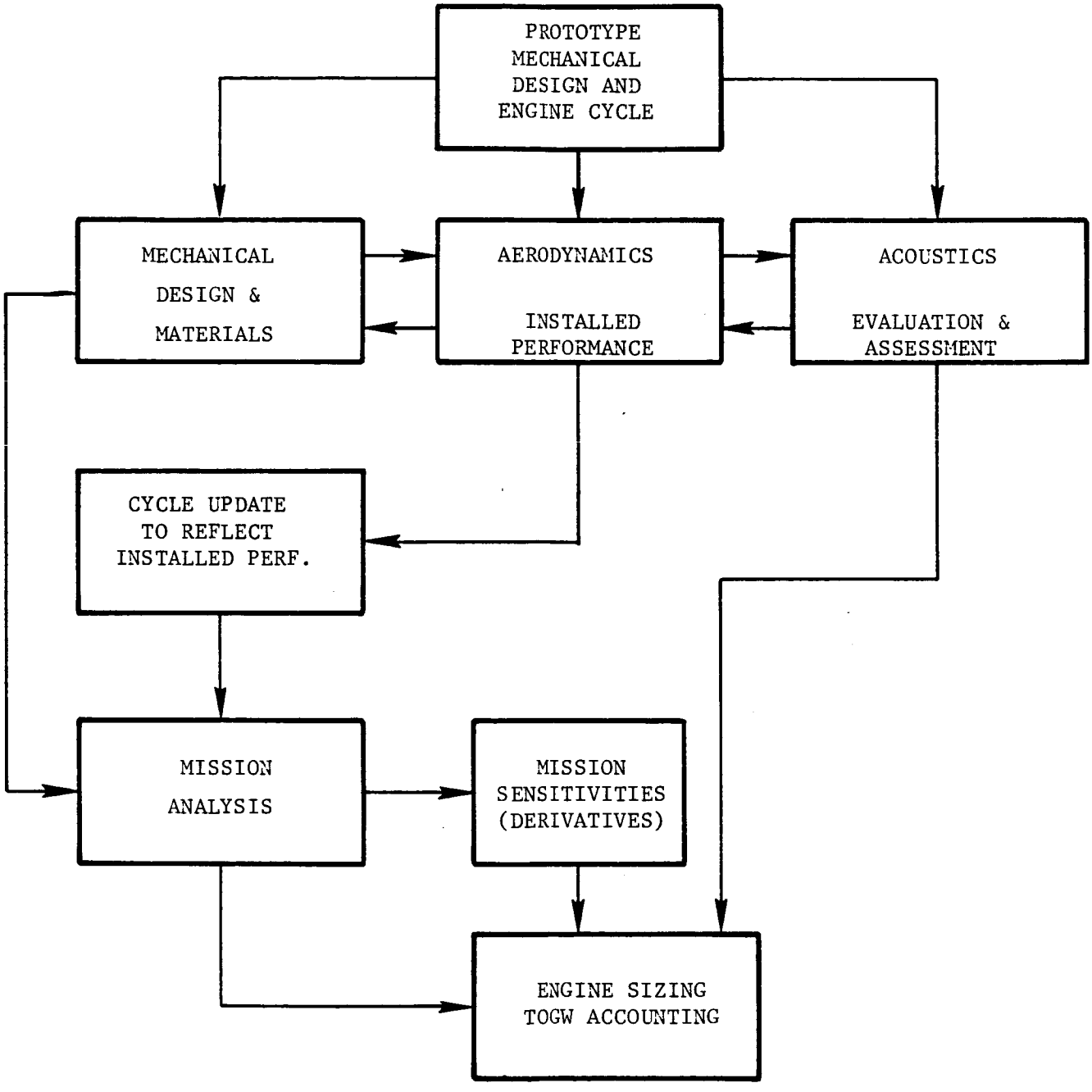

Figure 9. Task 2, Acoustically Treated Ejector Shroud Study and Evaluation Process

Some of these geometric parameters were set by virtue of the 20-chute suppressor to be used in the study. These include the suppressor area ratio, suppressor geometry and the number of elements. An early suppressor configuration spouting an 18°, truncated plug is shown in Figure 10.

The prototype 20-chute suppressor nozzle was revised to reflect the specific cycle being used in the study, i.e., the GE21-V50C engine cycle. The plug half-angle was changed from 18° to a 15° half-angle, to improve aero performance. The revised 20-chute suppressor nozzle was then used as the base for the integrated ejector design. Figure 11 shows the preliminary redesigned ejector-suppressor concept in the suppressed (Takeoff) mode, and Figure 12 shows the schematic of the ejector in the supersonic cruise mode. The suppressor has an area ratio of 1.75, a radius ratio of .717, and a depth-to-width ratio of the individual suppressor elements of 1.0.

After takeoff and during subsonic, transonic acceleration, and supersonic modes, the suppressor is retracted and stowed within the plug and the shroud is also translated forward to close the ejector inlet. The shroud consists of flaps and seals which allow the exit area to be varied to control exhaust gas expansion. The inner-to-outer nozzle area ratio which is about 0.2 at rotation, based on cycle data, is decreased to zero by translating the inner plug aft while opening the Variable Bypass Injector (VABI) to allow various degrees of mixing of the fan and core flows from partial to full at subsonic cruise, transonic acceleration and supersonic cruise modes, respectively.

The initial ejector shroud design was analyzed for potential aero/acoustic performance problems and later evaluated for weight, aerodynamic performance and acoustic characteristics. Flowpaths representing takeoff, subsonic cruise, transonic acceleration and supersonic cruise were defined and used to estimate

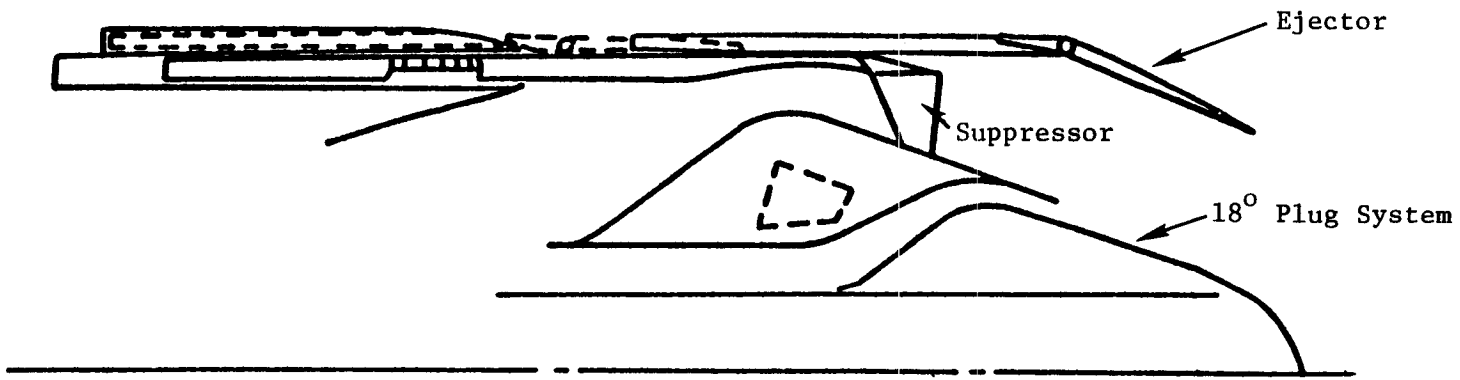

Figure 10. Early Chute Suppressor/Ejector Nozzle Configuration

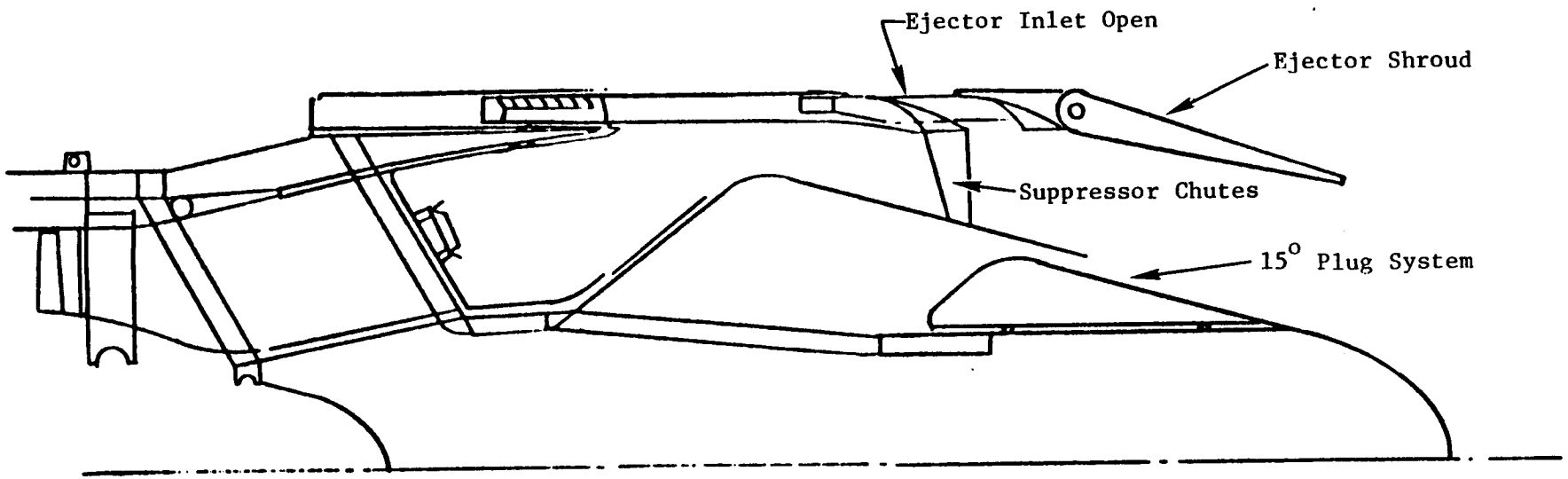

Figure 11. Conceptual Ejector Shroud Development; Take-off Mode

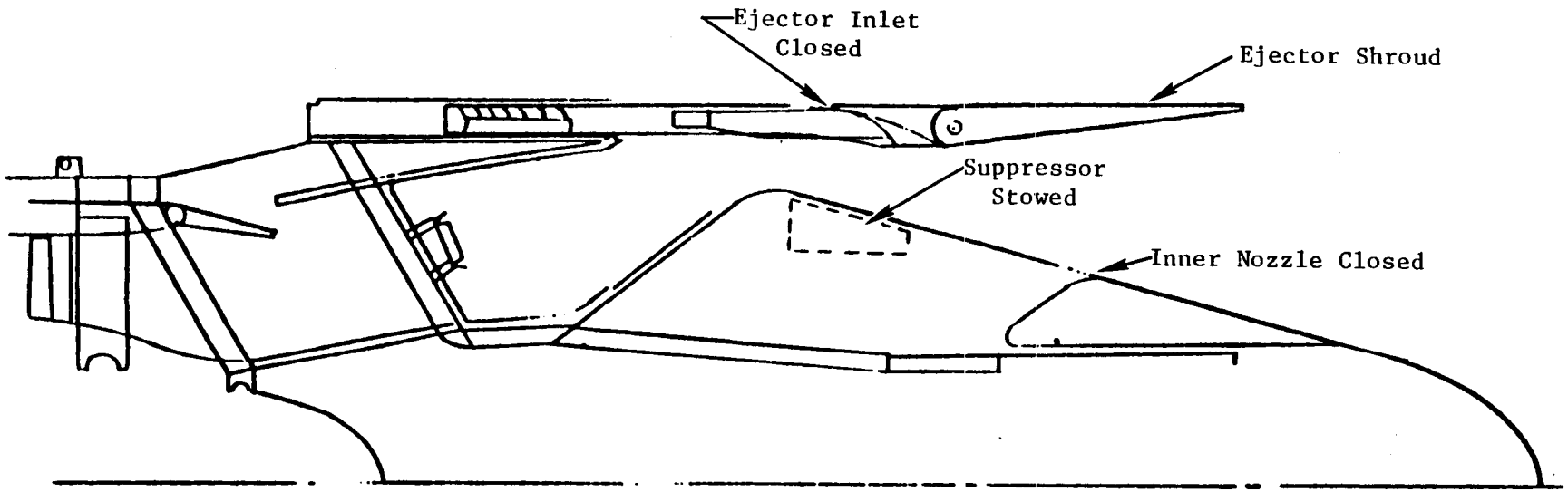

Figure 12. Conceptual Ejector Shroud Development; Supersonic Cruise Mode

performance, primarily at the design supersonic cruise point and other off-design points. The shroud length and other exhaust system parameters were varied to create several possible configurations to determine the effect of the variation on performance, acoustics, and exhaust system weight. Studies were conducted to estimate the weights of the various configurations as well as Stream Tube Curvature (STC) computer code fluid dynamics analysis for their supersonic cruise performance.

The analytical model of the ejector shroud nozzle in the supersonic cruise mode is shown in Figure 13. The main variable for the study was the shroud length, Ls. The nominal length of the shroud for the preliminary ejector design was 42.5 inches. To study the effect of shroud length on weight and aero/acoustic performance, a shroud 60 inches long was also analyzed. This represents a 41% increase in shroud length that could be acoustically treated. The preliminary weight study indicated that the baseline ejector nozzle weighed 5,375 lbs., or about 25% more than the unshrouded nozzle with 20-chute mechanical suppressor. Adding more shroud length while maintaining the same nacelle radius, R_{NAC}, increased the nozzle weight by an additional 1,750 lbs. for a 66% increase over the suppressor alone configuration. In order to reduce this substantial weight penalty, the nacelle radius was increased from 42.9 inches to 45 inches to allow a more efficient structure to be constructed and at the same time reduce the change in weight from 1,750 lbs. to 840 lbs., or 44% over the 20-chute suppressor configuration. The summary of the ejector shroud configurations weight study is shown in Table 1.

The weight reduction of the system was evaluated against performance loss associated with higher boattail drag (supersonic configuration) because of the increased nacelle diameter.

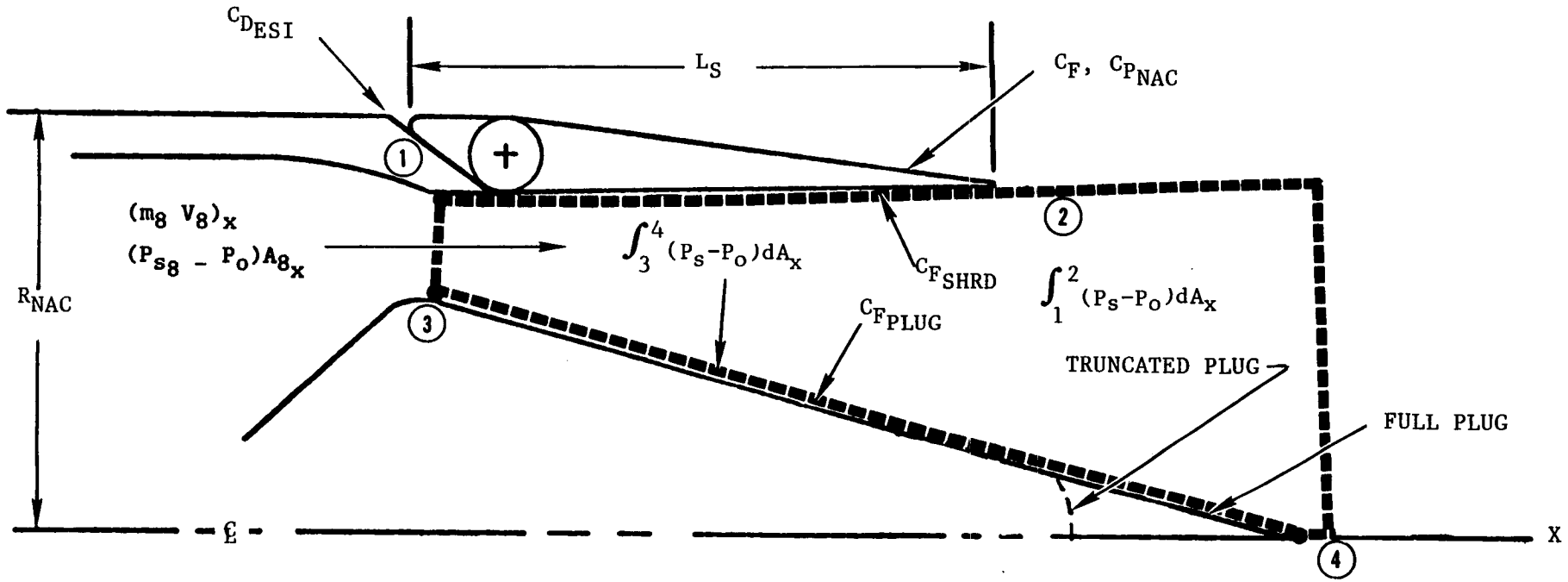

$$H = (m_8V_8)_x + \int_1^2 (P-Po)dAx + \int_3^4 (P-Po)dAx$$

$$C_T = H/Hi \text{ (Inviscid)}$$

$$Hi = mVi = m_8 \sqrt{2_g JC_p T_t \left[1-(P/Pt)^{\frac{\gamma-1}{\gamma}}\right]}$$

$$C_{T_{internal}} = C_{T_{inviscid}} - C_{F_{SHRD}} - C_{F_{PLUG}}$$

$$C_{T_{installed}} = C_{T_{internal}} - C_{F_{NAC}} - C_{P_{NAC}}$$

Figure 13. Ejector Shroud Supersonic Cruise Analytical Model and Nomenclature.

TABLE 1

EJECTOR SHROUD WEIGHT STUDY SUMMARY

CONFIGURATION	SHORT FLAP R_{NAC} = 42.9	LONG FLAP R_{NAC} = 42.9	LONG FLAP R_{NAC} = 45
ΔWEIGHT FOR EJECTOR SHROUD DESIGN RELATIVE TO BASELINE (LBS)	BASE	+ 1750	+ 840
TOTAL WEIGHT (LBS)	5375 LBS	7125	6215
FLAP WEIGHT (L_S)(IN)	42.5	60.0	60.0

The STC computer program was used to evaluate the effects of ejector shroud length and diameter on nozzle performance. Referring to Figure 13, the following represent increments in gross thrust coefficient:

$C_{P_{NAC}}$	--	Nacelle pressure drag
$C_{F_{NAC}}$	--	Nacelle friction drag
$C_{F_{PLUG}}$	--	Plug friction drag
$C_{F_{SHRD}}$	--	Shroud internal friction drag
$C_{F_{EI}}$	--	Ejector Interface drag

Initial STC runs on the ejector shroud configuration indicated a substantial loss in performance due to sub-ambient pressures on the plug in the curved region of the truncation. However, STC runs with a full plug (conical) alleviated that performance deficit. Plug pressure distribution plots indicating full plug performance characterized by no sub-ambient pressures and higher pressure recovery is shown in Figure 14. Typical flowfields differentiating between the truncated and the full plugs are shown in Figures 15 and 16, respectively. The results of the STC study showing effect of plug and shroud length is detailed in Figure 17. Though the short shroud (LS = 42.5) had the highest aerodynamic performance, it was not sufficient information to base the selection (short versus long shroud) on. The selection criterion would be based on the cumulative effect of aerodynamic performance, weight, and acoustics on aircraft mission.

Work was initiated to accumulate precise acoustic information to assess the merits of the long and short ejector shroud nozzles. Work elements included acoustic evaluation of the acoustically treated ejector shroud using the Motsinger & Sieckman (M & S) methodology (Reference 6) and identification of spectral distribution of the jet mixing and the shock cell noise for the different ejector lengths at typical takeoff conditions.

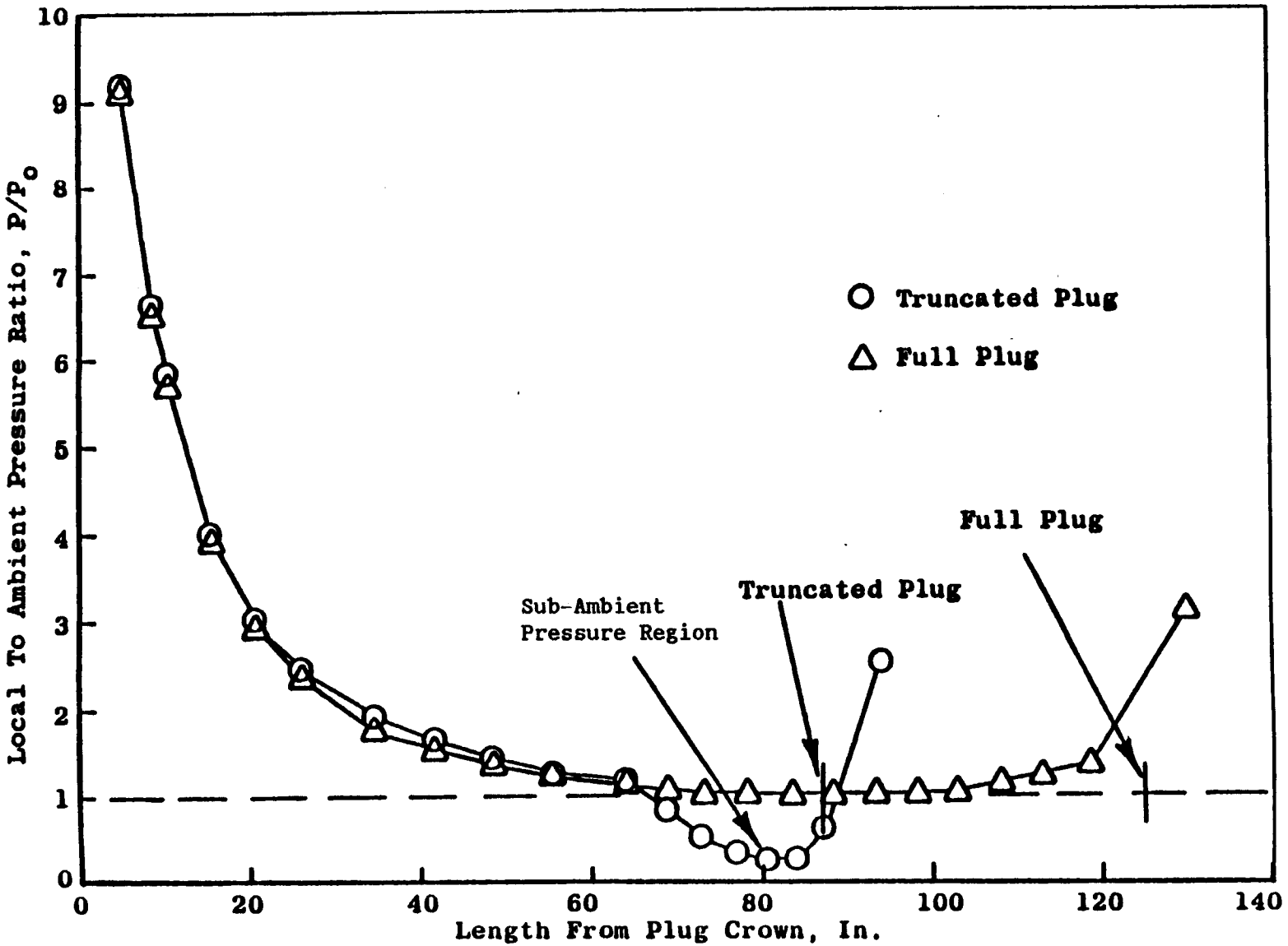

Figure 14. Plug Pressure Distributions Showing Superior Performance of the Full Plug Over the Truncated Plug.

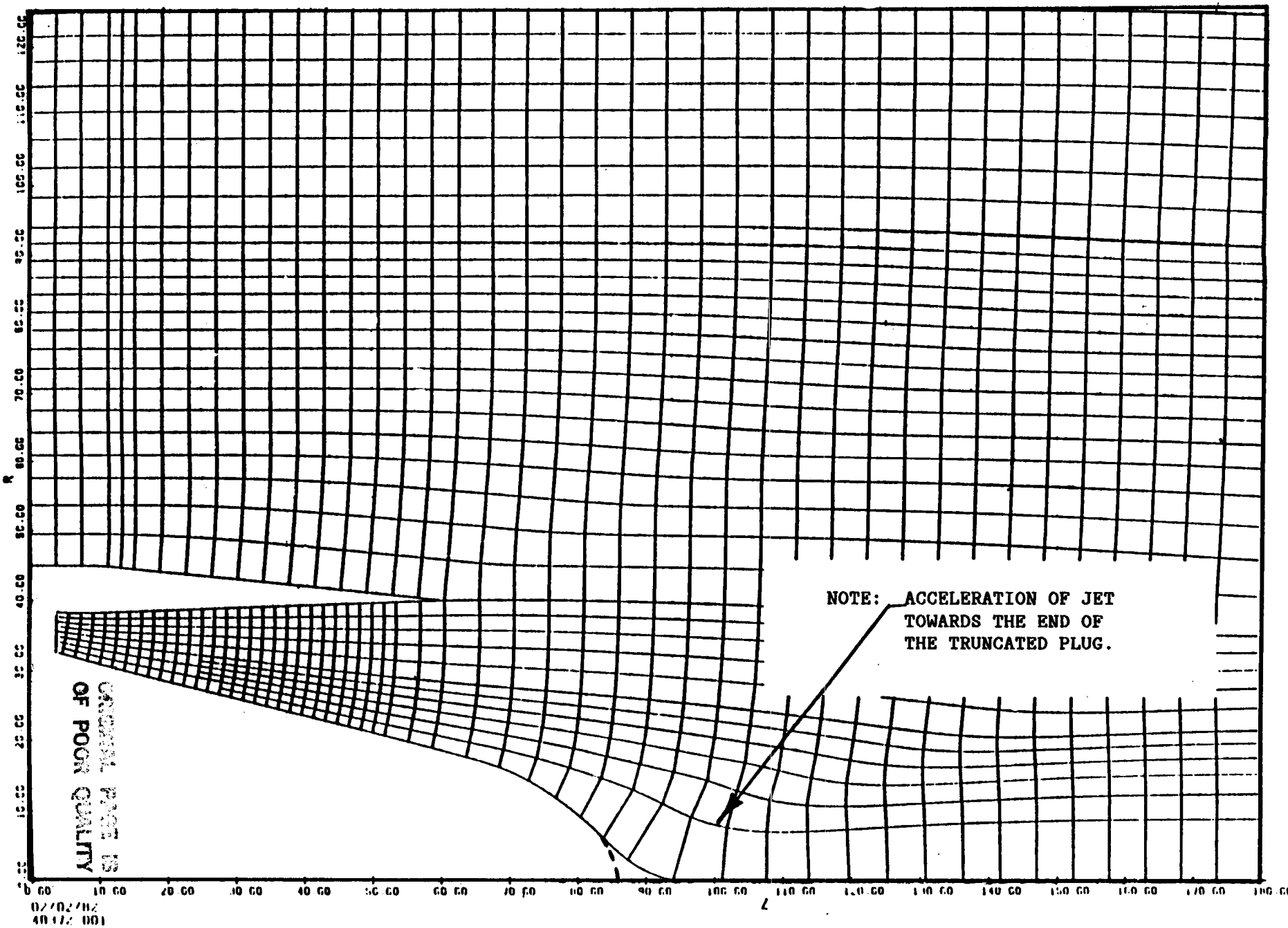

Figure 15. Streamline Development; Supersonic Cruise, Long Flap, Truncated Plug With External Flow.

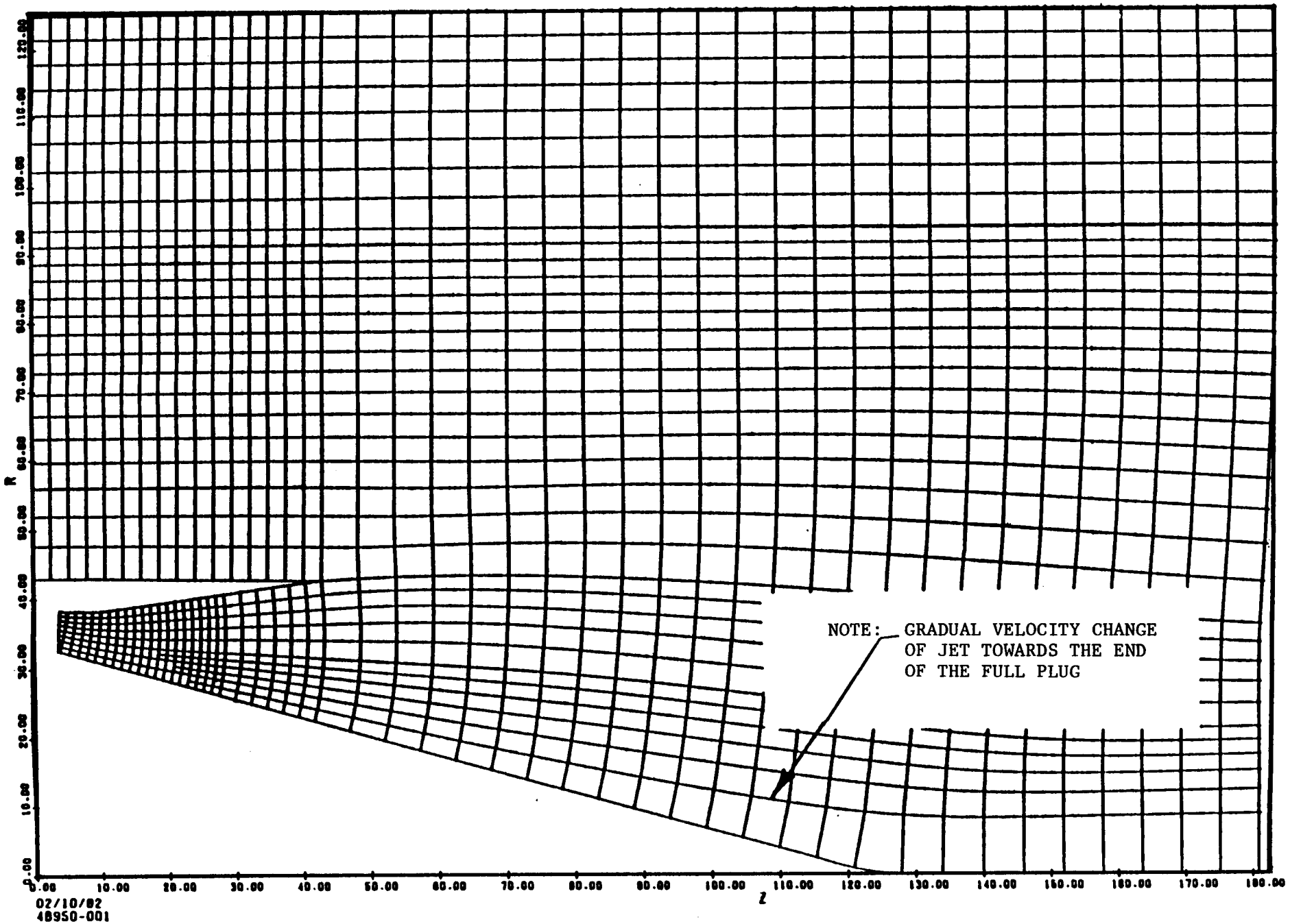

Figure 16. Streamline Development; Supersonic Cruise, Short Flap, Full Plug With External Flow

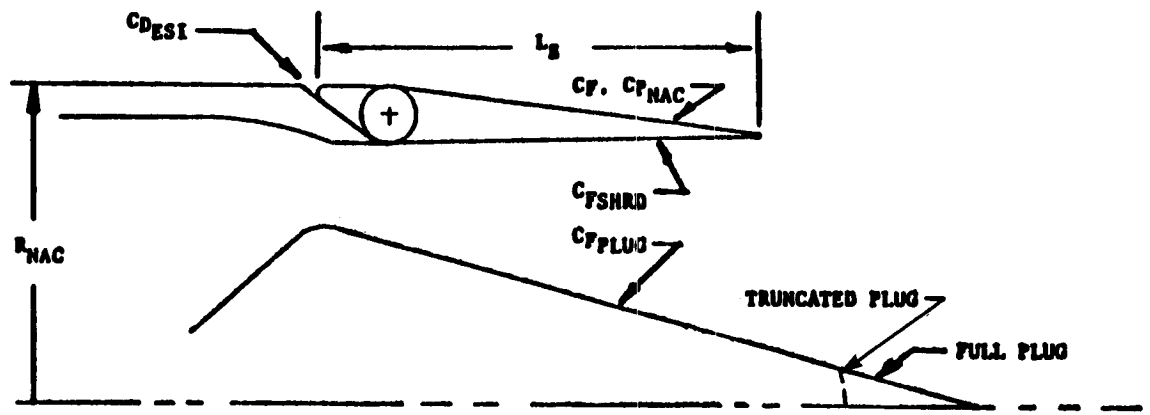

LS IN	42.5	42.5	60	60	60	60
R_{NAC} IN	42.9	42.9	42.9	42.9	45	45
PLUG	TRUNCATED	FULL	TRUNCATED	FULL	TRUNCATED	FULL
$CFG_{INTERNAL}$	.9749	.9855	.9799	.9869	.9799	.9869
$CFG_{INSTALLED}$	.9711	.9817	.9729	.9799	.9673	.9743

Δ = .0074

Figure 17. Ejector Shroud Nozzle Aerodynamic Performance Comparisons Based on Combinations of Long and Short Shrouds and Truncated and Full Plugs.

The completed acoustic study estimated total engine and component (jet, fan inlet, exhaust, turbomachinery) noise levels at FAR 36 (1969) Stage 3 measurement locations using the GE21-V50C engine cycle and ejector shroud nozzle at typical take-off cycle. The M & S engineering spectral correlation program was used to calculate the jet and shock cell noise associated with supersonic jet flows, and the AST prediction program, likewise, was used to predict the fan inlet, fan exhaust, and core turbomachinery noise estimates.

The synthesis of the above noise estimates plus the jet noise and other component noise estimates yielded the total noise estimate at FAR 36 (1969) Stage 2 measurement locations.

In order to study the impact of shock cell noise on the total engine noise, predictions were made with and without shock cell noise. Figures 18 and 19 summarize Perceived Noise Level (PNL) directivities of the total and component engine noise levels with and without shock cell noise control respectively. Definition of PNL directivities is shown in Figure 20. The predictions show that the long (LS = 60 in) treated ejector shroud has a takeoff sideline noise level of 103.0 EPNdB and could be reduced to 101.9 EPNdB if shock noise is effectively controlled. The reshaping of the 20-chute suppressor profile and the provision for a full length conical plug system were the principal means of controlling shock noise.

It is to be noted that at the cycle condition under consideration jet noise is the dominant component, and sideline noise is the most difficult noise goal to satisfy. Since the noise levels shown in Figures 18 and 19 were evaluated at FAR 36 Stage 2 measurement location, equivalent sideline noise increase when measured at Stage 3 noise measurement location was computed. The computation showed an increase of 2.84 dB. The computational algorithm and geometry of the Stages 2 and 3 measurement locations are shown in Figure 21. On the basis of above

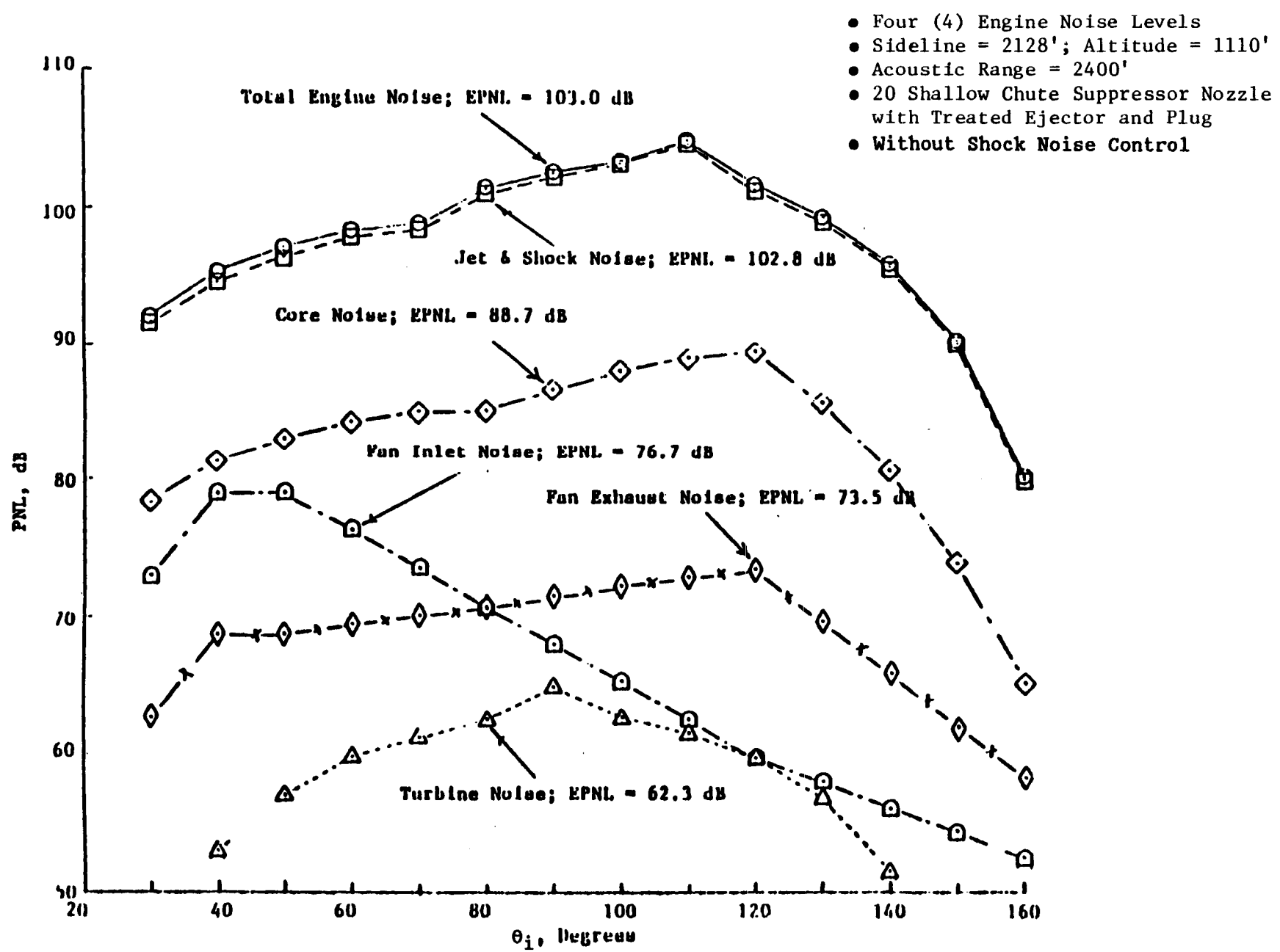

Figure 18. Total Engine and Component Noise Levels of the Ejector Shroud Nozzle with the G21-V50C Engine.

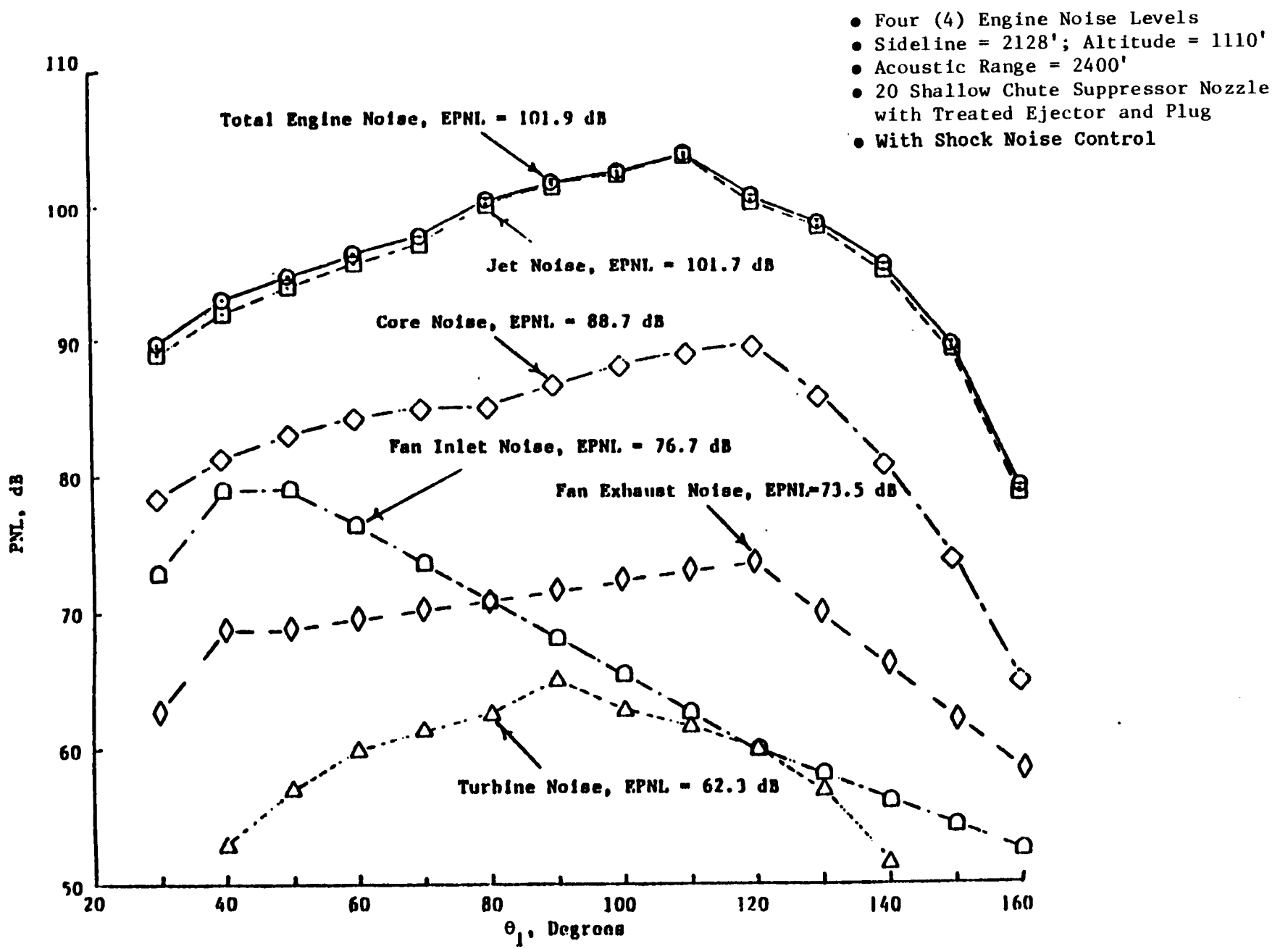

Figure 19. Total Engine and Component Noise Levels of the Ejector Shroud Nozzle with the G21-V50C Engine with Shock Noise Control.

- θ_i measured from nozzle inlet axis

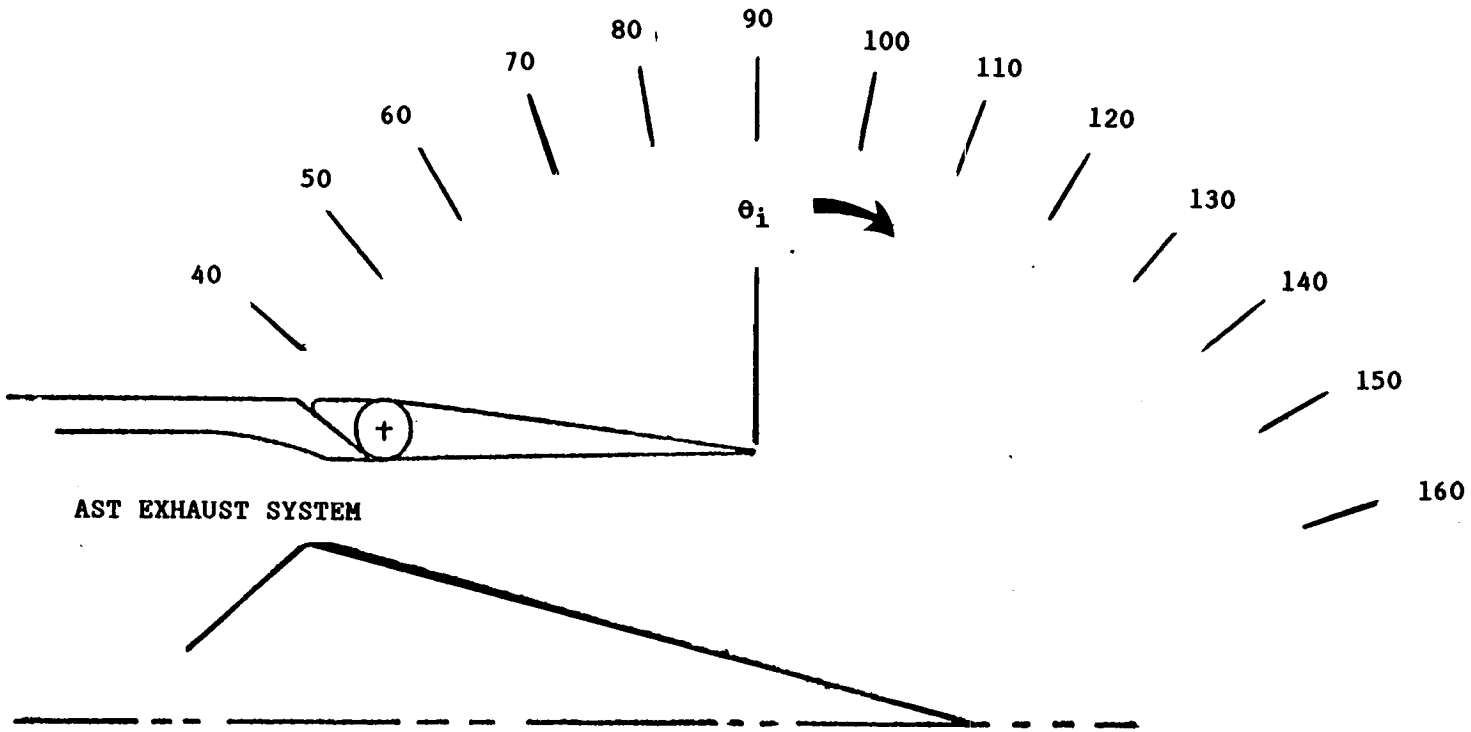

Figure 20. Definition of θ(degrees) for Perceived Noise Level Directivities.

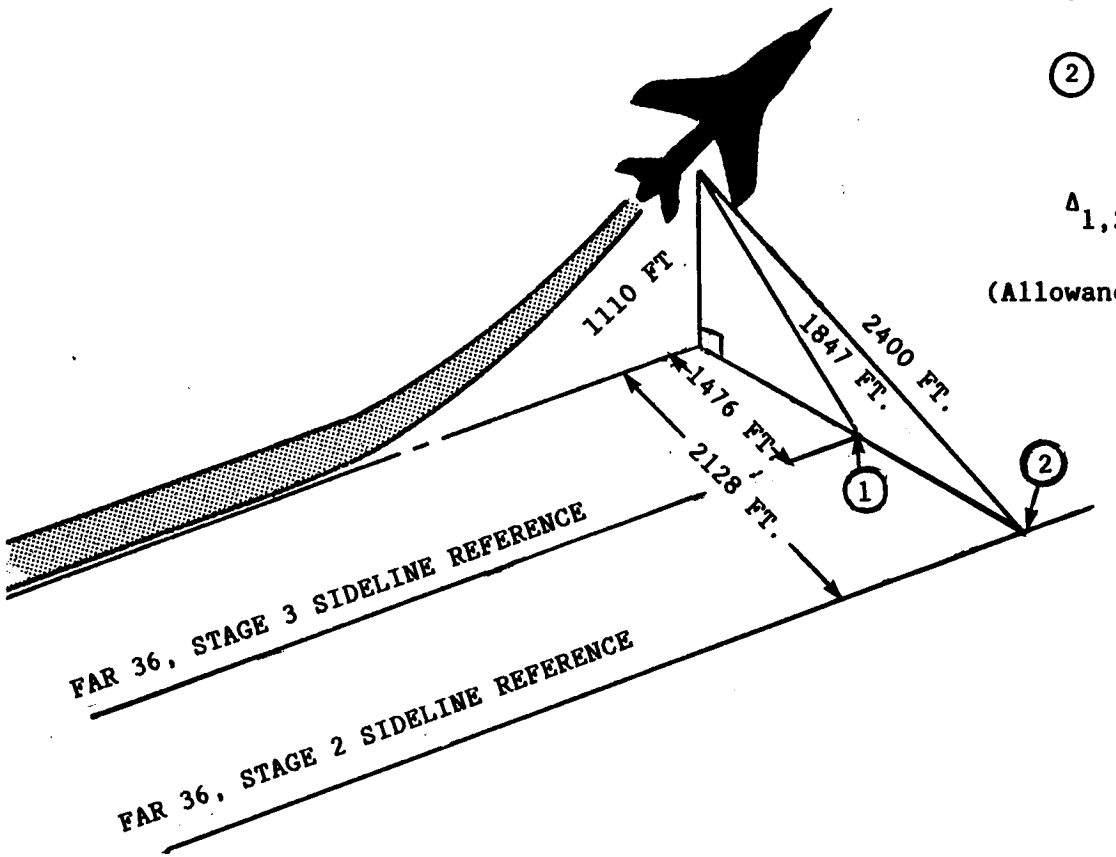

(1) - FAR 36, STAGE 3 SIDELINE NOISE MEASUREMENT LOCATION

(2) - FAR 36, STAGE 2 SIDELINE NOISE MEASUREMENT LOCATION

$$\Delta_{1,2}\ \text{PNdB} \approx 25 \log \left(\frac{2400}{1847}\right) \approx 2.84$$

(Allowance given for medium attenuation effects)

Figure 21. Approximate Perceived Noise Level Difference (ΔPNdB) Between FAR 36 Stages 2 and 3 Sideline Measurement Locations.

noise computation, the nominal sideline noise including shock noise control and under Stage 3 rules would be 104.74 PNdB for the long ejector shroud (Ls=60 in) and 105.49 PNdB for the short ejector shroud (Ls=42.5 in). The computational algorithm for calculating the difference in noise between the long and short ejector is shown in Table 2.

Conceptual Design Results

One of the penalties of noise reduction is system weight increase due to engine oversizing; and so when a specific noise level has to be achieved, component weight by itself becomes an item of secondary importance. Weight becomes a discriminating factor only when two competing acoustic systems satisfy the same noise goal. For this reason the 20-chute nozzle, which can only satisfy Stage 2 noise, gets automatically eliminated, though it is lighter in weight compared to the ejector shroud. With the foregoing, the choice between the short and the long ejector designs becomes easier when consideration is given to the fact that the short ejector shroud cannot meet the Stage 3 rules, even under the "Noise Tradeoff" rules without upward resizing of the engine whereas the long ejector shroud could under the "Noise Tradeoff" rules. This, then, makes the long ejector shroud the better choice for the application intended and the 840 pounds increase becomes the cost of achieving .75 PNdB extra noise suppression.

The following table shows the attributes of both ejector nozzles at an engine size of 858 lb/sec airflow, and using the short ejector shroud as reference:

TABLE 2

TOGW TRADE EQUIVALENTS FOR PERFORMANCE, ENGINE WEIGHT AND NOISE

- - 1% Δ CFG (SUPERSONIC) ≃ + 10,000 LBS TOGW
  + 1% Δ ENGINE WEIGHT ≃ + 1,700 LBS TOGW
  - 1 Δ DB NOISE ≃ + 5,000 LBS TOGW (20-CHUTE NOZZLE)

- NOISE SUPPRESSION POTENTIAL FOR LONG FLAP EJECTOR: LONGER SHROUD HAS MORE AREA AND THICKNESS FOR ACOUSTIC TREATMENT AND PACKING.

  ADDITIONAL SUPPRESSION IS EVALUATED THUS

  Δ PNDB = 5 LOG (L2/L1) WHERE
  WHERE = L2 = 60 AND L1 = 42.5

  L = THE LENGTH OF EJECTOR FLAP

  Δ PNDB = .75 DB

- BASELINE ENGINE WEIGHT = 13,150 LBS (GAS GENERATOR)

- BASELINE TOGW = 735,000 LBS

Item	Short Ejector Shroud	Long Ejector Shroud	Increment of Long Shroud Over Short
C_{FG}	.9817	.9743	-.0074 (-.75%)
Stage 3 Sideline Noise, PNdB	105.49	104.74	-.75
Engine Weight, Gas Generator + Exhaust System, lbs	18,525	19,365	+840 (+4%)

Comparing the two ejector shroud noise levels to that shown for FAR 36, Stage 3, sideline, in Figure 8, one concludes that none of the ejector shrouds absolutely satisfies the Stage 3 rules. However, interpreting the rules within the broader context of "Noise Tradeoff" enables the long ejector shroud to satisfy the Stage 3 rules with the knowledge that the sideline noise is exceeded by less than 2 PNdB and that there is adequate margin for noise reduction at community and approach to offset the increase at the sideline. See page 28 for the noise trading rules. The foregoing concludes that the short ejector shroud cannot meet the Stage 3 rules under any conditions without upward resizing of engine and airplane in spite of performance and weight superiority; and the long ejector shroud, therefore, becomes the choice for full scale prototype development.

The question may, however, be asked if the short ejector flap could be brought into noise compliance by resizing the engine, but the fact remains that the ideal critical noise parameters (V_{mix} and V_R) have been "tailored" during the matching to achieve maximum coannular and 20-chute noise suppression, so without a massive engine and cycle redesign, the long flap ejector appears to be the most reasonable way to go. From Table 3, it can be concluded that the cost of the .75 PNdB noise reduction, due to the long flap ejector (relative to the short flap), is approximately 15,150 lbs.

TABLE 3

COMPARISON BETWEEN THE SHORT AND LONG EJECTOR SHROUDS SHOWING TOGW EQUIVALENT FOR .75 EPNDB REDUCTION IN LONG SHROUD

- REFERENCE SHORT EJECTOR SHROUD.

- LONG EJECTOR SHROUD TRADES:

  - .0075 Δ CFG ≃ + 7,500 LBS IN TOGW
  + 4.5% Δ ENGINE WEIGHT = + 7,650 LBS IN TOGW
  - .75 EPNDB = ?

  COST OF .75 ΔEPNDB ≃ 15,150 LBS IN TOGW.

6.0 MECHANICAL DESIGN

Design Approach

Three nozzle layouts were completed to develop operating modes, materials, actuation mechanisms, structures and weights of the exhaust systems. These were the baseline coannular, the 20-chute suppressor, and the ejector shroud nozzles shown in Figures 22 through 24 respectively. Figure 25 shows the ejector shroud in the supersonic cruise configuration. The 20-chute suppressor and the ejector shroud nozzles required successive increases in diameter to satisfy the aero/acoustic requirements. The addition of the 20-chute suppressor to the baseline coannular nozzle increased the outer diameter by 5% in order to match the suppressor radius ratio requirements. Likewise, the addition of the ejector shroud to the 20-chute suppressor necessitated increase in the outer diameter by 11% to allow structural strength without the weight and also provide thickness and volume for acoustic material packing.

As a result of these changes, plug truncation, shroud translations and engine mount locations were adjusted accordingly to match the area ratio requirements for an overall improvement in performance.

Exhaust System Design Results

The AST exhaust system is a high radius ratio plug nozzle with a Fixed Primary Nozzle Cowl and a translating center plug nozzle. A translating outer shroud adjusts the exit area ratio for high performance throughout the pressure ratio range. The outer shroud inner surface is contoured to match closely the primary throat area requirements at the more important operating points. The translating center plug nozzle exhausts the excess bypass airflow that cannot flow through the primary nozzle throat.

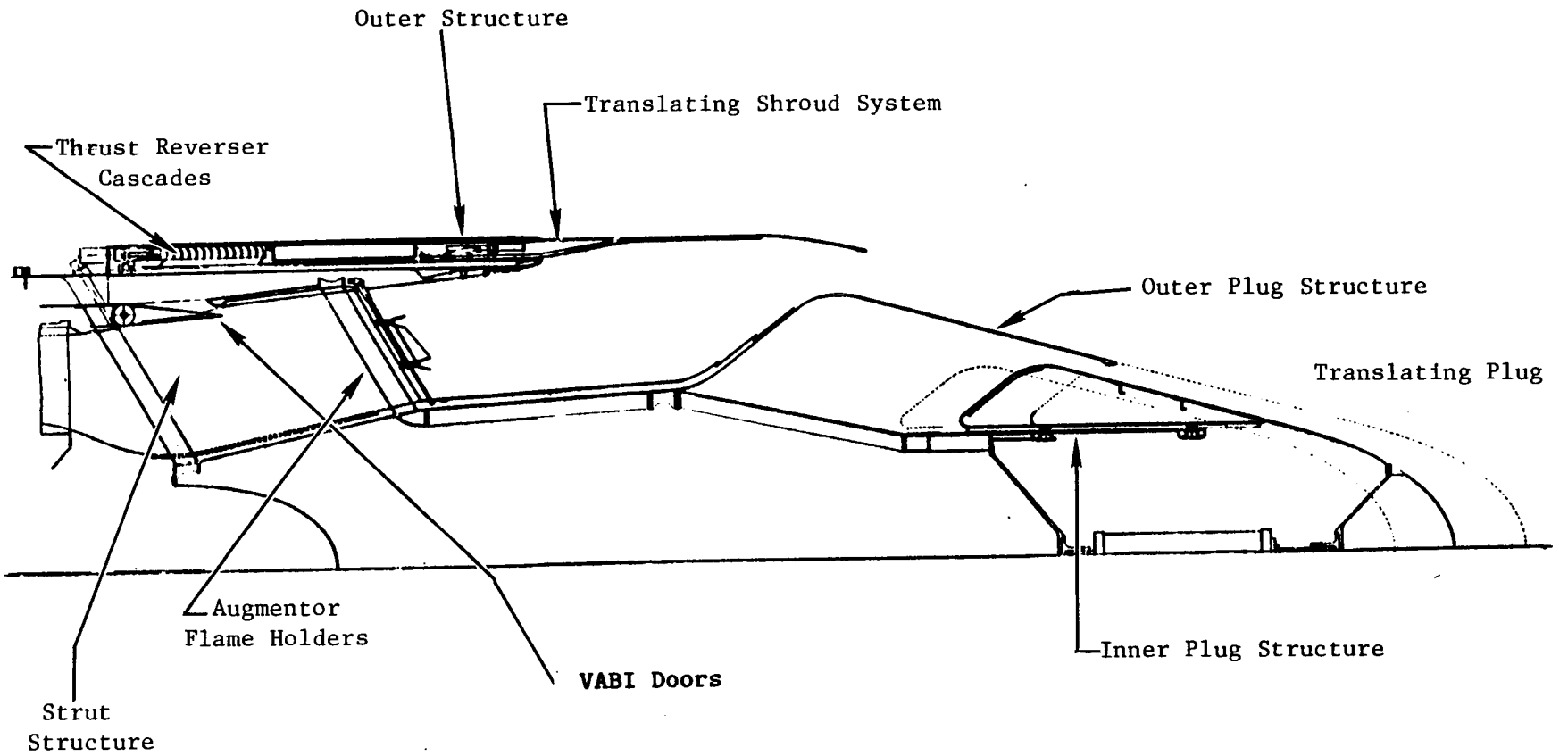

Figure 22. Coannular Nozzle.

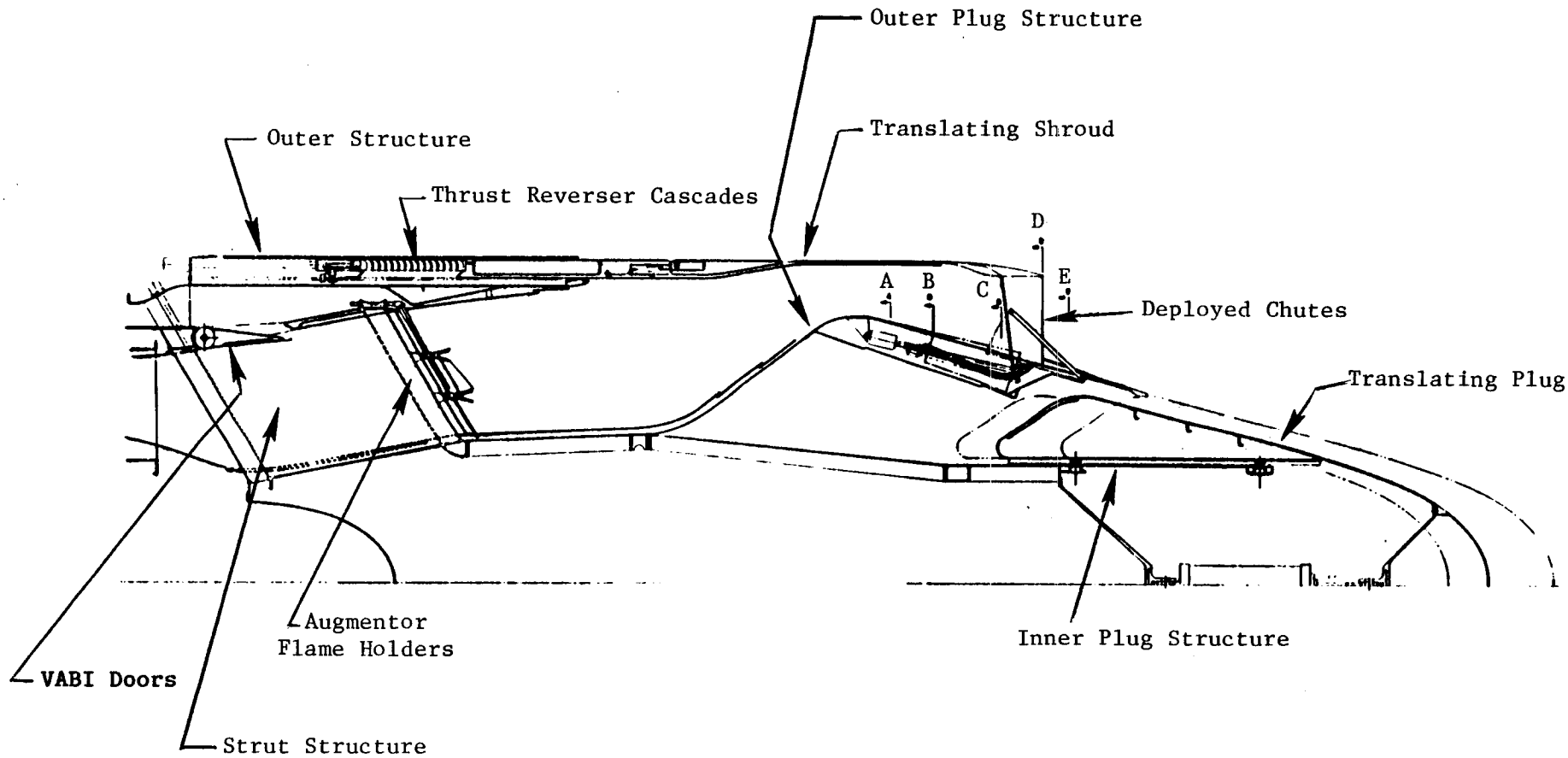

Figure 23. Baseline Coannular 20-Chute Suppressor Nozzle

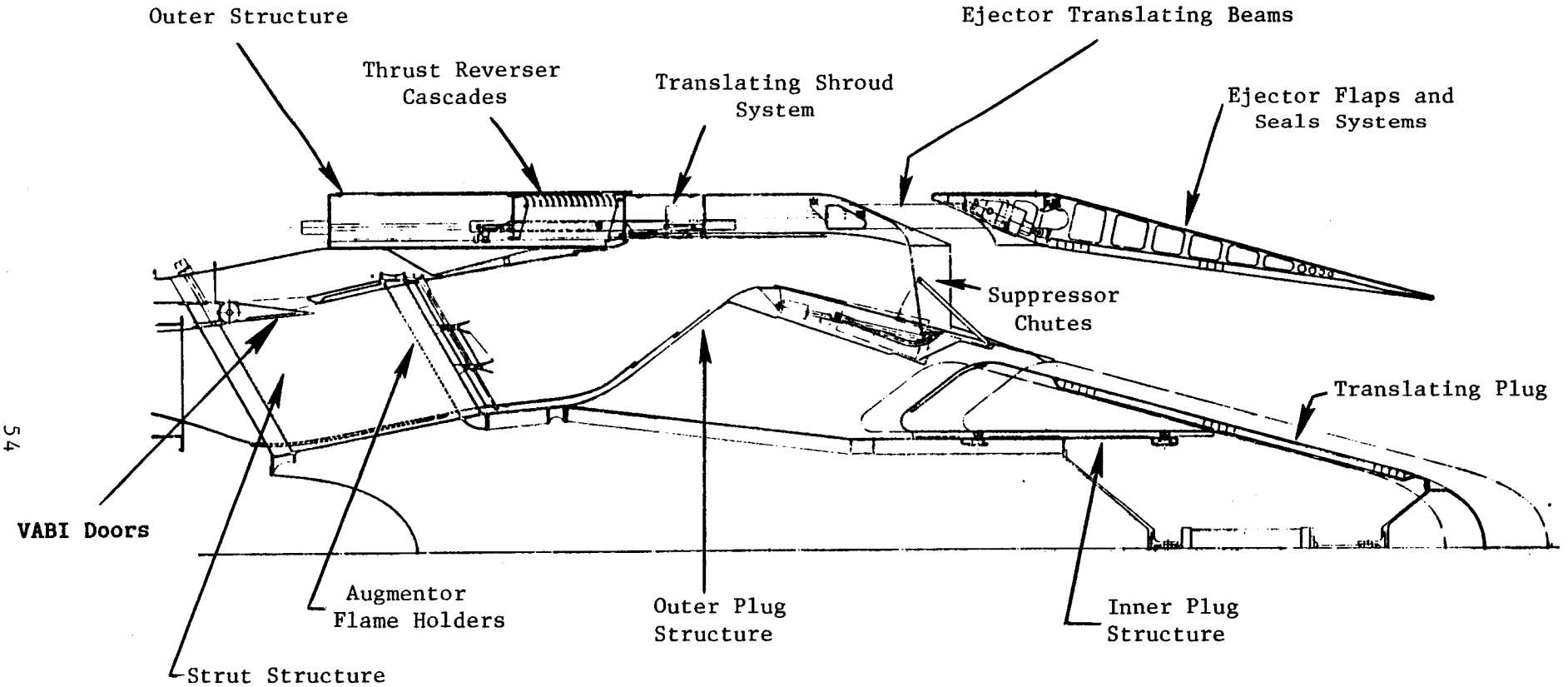

Figure 24. 20-Chute Suppressor Ejector Shroud Nozzle (Takeoff Mode)

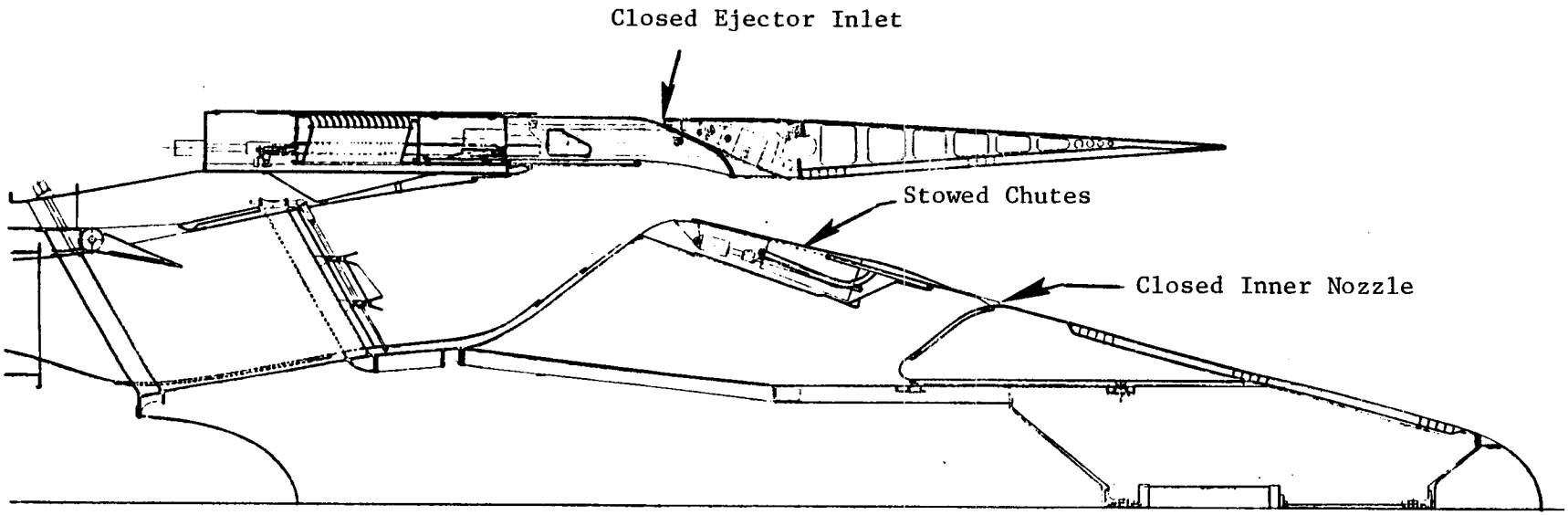

Figure 25. 20-Chute Suppressor Ejector Shroud Nozzle (Supersonic Cruise Mode)

During noise suppression takeoff, bypass flow is ducted from the outer fan passage through eight strut-ducts into the plug beam and then to the center plug nozzle. This arrangement along with the high radius ratio primary nozzle provides the characteristic inverted jet velocity profile co-annular suppression. Additional suppression is obtained by deploying 20 chutes in the outer stream during suppressed operation. Still higher suppression is obtained by shrouding the nozzle discharge with ejected ambient air and a mechanical shroud lined with sound absorbing material. The ejector shroud is attached to the aft end of the translating shroud. For unsuppressed operation, most of the bypass air is mixed with the core stream, the suppressor chutes are stowed in the nozzle plug outer surface, and the ejector inlet is closed for high internal performance. The ejector shroud is made of variable area flaps and seals so that the required expansion ratio for good performance can be met throughout the wide pressure ratio operating range.

The exhaust system includes a cascade type thrust reverser. The thrust reverser cascades are attached to the forward end of the translating outer shroud. When the shroud is fully extended, the cascades are exposed on the outside and inside and a shroud mounted door assembly is expanded to contact the fixed plug crown to block the flow through the primary nozzle. The cascades occupy three quarters of the circumference but may be positioned in the total circumference if the reverser discharge efflux can be controlled to prevent airframe impingement and engine reingestion. A low temperature rise augmentor is used in the exhaust system to provide augmented thrust during acceleration.

Translating Outer Shroud

The outer shroud is a cylindrically shaped fabrication made up of machined rings, sheet metal rolled rings and

honeycomb. The aft end is shaped to provide a path for ambient airflow ventilation of the backside of the suppressor chutes. Twelve reverser blocker doors are contained in a cavity near the middle of the cylinder. The thrust reverser cascade boxes are located near the forward end of the shroud. They occupy 270° of the circumference and can be arranged in any desired circumferential location to prevent exhaust gas impingement on the aircraft and/or engine hot gas reingestion. The forward end of the shroud supports the linkage which drives the reverser blocker doors. The inner liner of the shroud provides convective cooling for the shroud inner surface to the end of the liner and film cooling beyond the end of the liner. The aft cavity of the shroud contains the support and positioning system for the ejector shroud.

Ejector Shroud

The ejector shroud is composed of a flap support ring forming the aft surface of the ejector inlet and containing the flap actuators, 20 variable area flaps, 10 support beams and an actuating ring housed in the aft cavity of the translating outer shroud. The forward outer end of the flap support ring contains the seal for the ejector inlet in the inlet closed position. The inner surface of the support ring contains 20-chute inlet cavity fillers to provide a continuous inner flowpath when the inlet is closed. The flaps are conventional sheet metal fabrication and incorporate sound absorption panels on the inner surface of the flaps. The sound absorption panels are constructed similar to honeycomb with the chambers vented to the inner flowpath.

Outer Cowl

The outer cowl provides the outer flow surface between the aft end for the aircraft nacelle and the translating shroud. It also retains the cowl to shroud seal at the aft end and thus functions as the outer container wall for the bypass cooling air for the shroud liner.

Outer Structure

The outer structure is a cylindrical structure with a bulkhead at the forward end and a stiffening ring at the aft end. The outer forward end of the bulkhead has a step to provide for the nacelle-exhaust nozzle interface. The aft ring contains the inner shroud seal to separate the shroud cooling air from the main stream. Two sets of longitudinal tracks are contained in the cylindrical portion of the outer structure. One set of four tracks support the outer shroud. The other set of twelve tracks provide for positioning of the reverser block doors.

Strut Structure

The strut structure is composed of eight pairs of radial beams (slanted 60° to the engine centerline) joined by outer and inner circumferential rings. The forward outer ring is joined through vanes in the bypass stream to the bypass duct outer spacer ring. The supporting loads for the inner nozzle are thus transferred to the engine outer bypass duct through radial beams and strut sidewalls for the bypass air duct. Upper and lower cylindrical surfaces between struts form the boundary for the core engine airflow passage, and the upper surface support the VABI doors. This strut structure is encased with cooling air liners that blend with the turbine frame liner to form continuous struts from the turbine frame entrance to the bypass strut exit. A portion of the liner is sound absorbing material.

VABI Doors

Twenty-four Variable Area Bypass Injector doors in sets of three between each of the eight struts are hinged to the forward outer part of the strut structure. One power hinge per set of three doors maintains the VABI door position. The doors are conventional sheet metal structure with sound absorbing panels on the core flowpath side.

Outer Plug Structure

The outer plug structure is composed of welded sheet metal and machined rings to form the core flow inner flowpath. It is supported at the forward end by the strut structure aft inner ring. The aft end ring forms the outer flowpath of the inner nozzle. This structure also contains the suppressor chutes and their actuation mechanism.

Inner Plug Structure

The inner plug structure consists of a truss support attached at the forward end of the strut structure aft inner ring, a mid ring that supports an aft stiffened cylinder which in turn supports the four sets of guide rollers, and the actuator for the translating plug.

Translating Plug

The translating inner plug is composed of welded sheet metal and machined rings stiffened at the forward end with honeycomb and containing a honeycomb type sound absorption covering cone. Thus, the inner bypass flowpath contributes to the jet noise suppression. The inner plug is supported by four sets of guide tracks that engage the guide rollers on the plug structure.

Suppressor Chutes

Twenty suppressor chutes are mounted in the outer plug structure. Each chute is supported by a link and a set of two rollers engaging tracks attached to the plug. The chute construction can be sheet metal or cast. The 1.75 nozzle to base area ratio suppressor allows a lightweight simple stowed position arrangement that does not require a cover door and a cover door actuation system. The chutes are retracted into cavities on the

outer plug surface such that they blend with the plug outer contour to form the inner flowpath of the outer stream. Section drawings of the chutes stowed in the plug are shown in Figure 26 in Sections B-B and C-C. Section A-A shows a cut through the chute actuator, and Section E-E shows the plug blending aft of the stowed position chute. Section D-D shows the chutes in the deployed position.

Actuation

Six actuation systems are required for positioning the exhaust system components. Four synchronized rotary hydraulic motor driven ball-screw actuators are used to position the outer translating shroud for the suppressed and unsuppressed forward thrust modes and the reverse operating mode. Four similar actuators position the ejector shroud relative to the translating shroud. Twenty hydraulic piston actuators position the ejector flaps. Eight rotary hydraulic motors driving power hinges position the VABI doors. The inner plug is positioned by a single hydraulic piston actuator. Twenty rotary hydraulic motor driven ball-screw actuators are used to position the suppressor chutes. Alternate actuation methods such as air or hydraulic powered cable driven gear boxes for positioning the shroud, VABI doors and suppressor chutes are possible options. Future detailed trade studies outside this contract will provide the optimum choice.

Augmentor

The augmentor for the AST exhaust nozzle is a low ΔT burner, producing 600 to 1000°F temperature rise primarily for transonic acceleration. It consists of two flameholders, fuel spraybars and an ignitor. The flameholder is a molded ceramic "V" gutter. The spraybars are radial tubes supplied by a single fuel manifold.

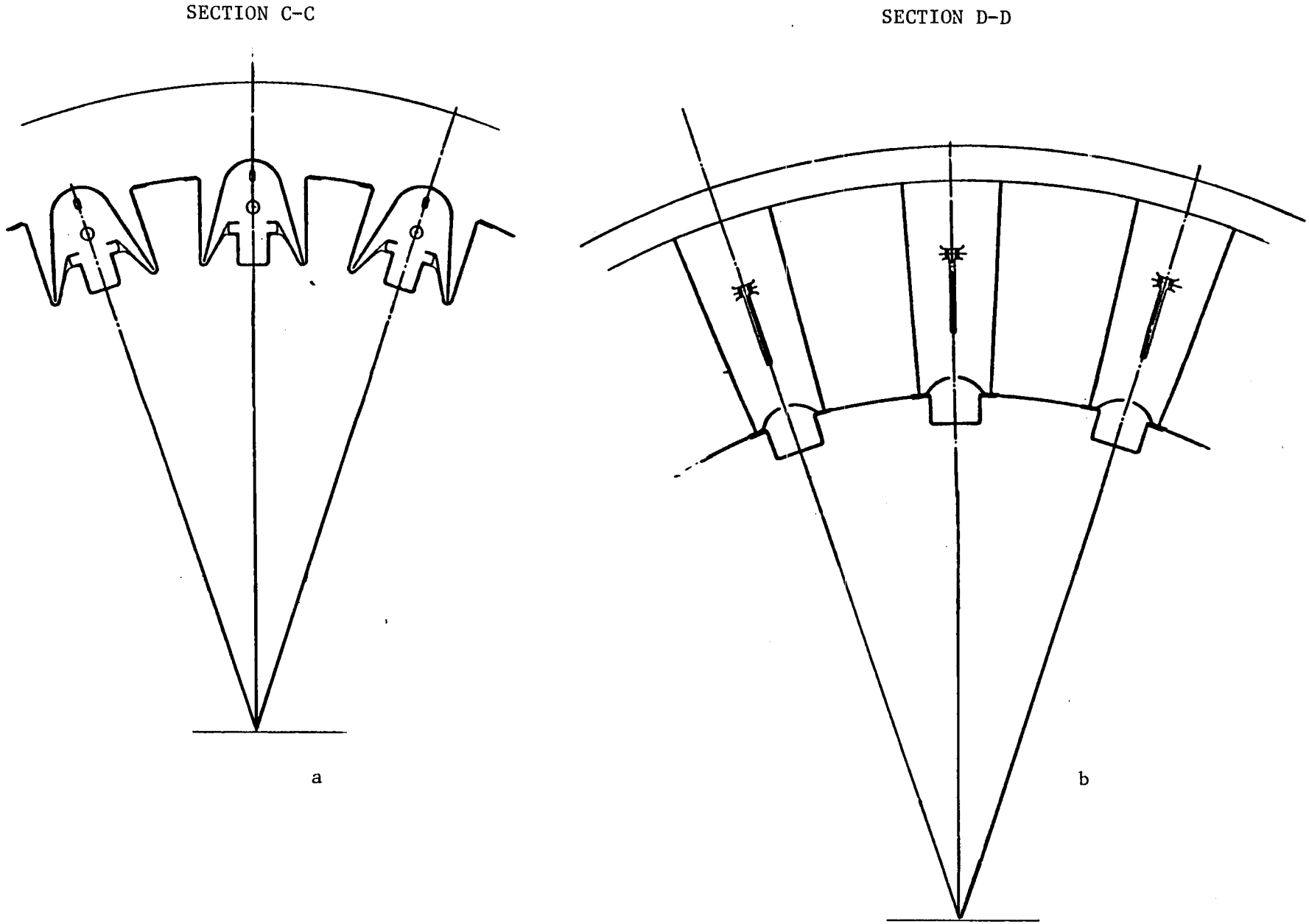

Figure 26. Section Drawings of Chutes Stowed and Deployed

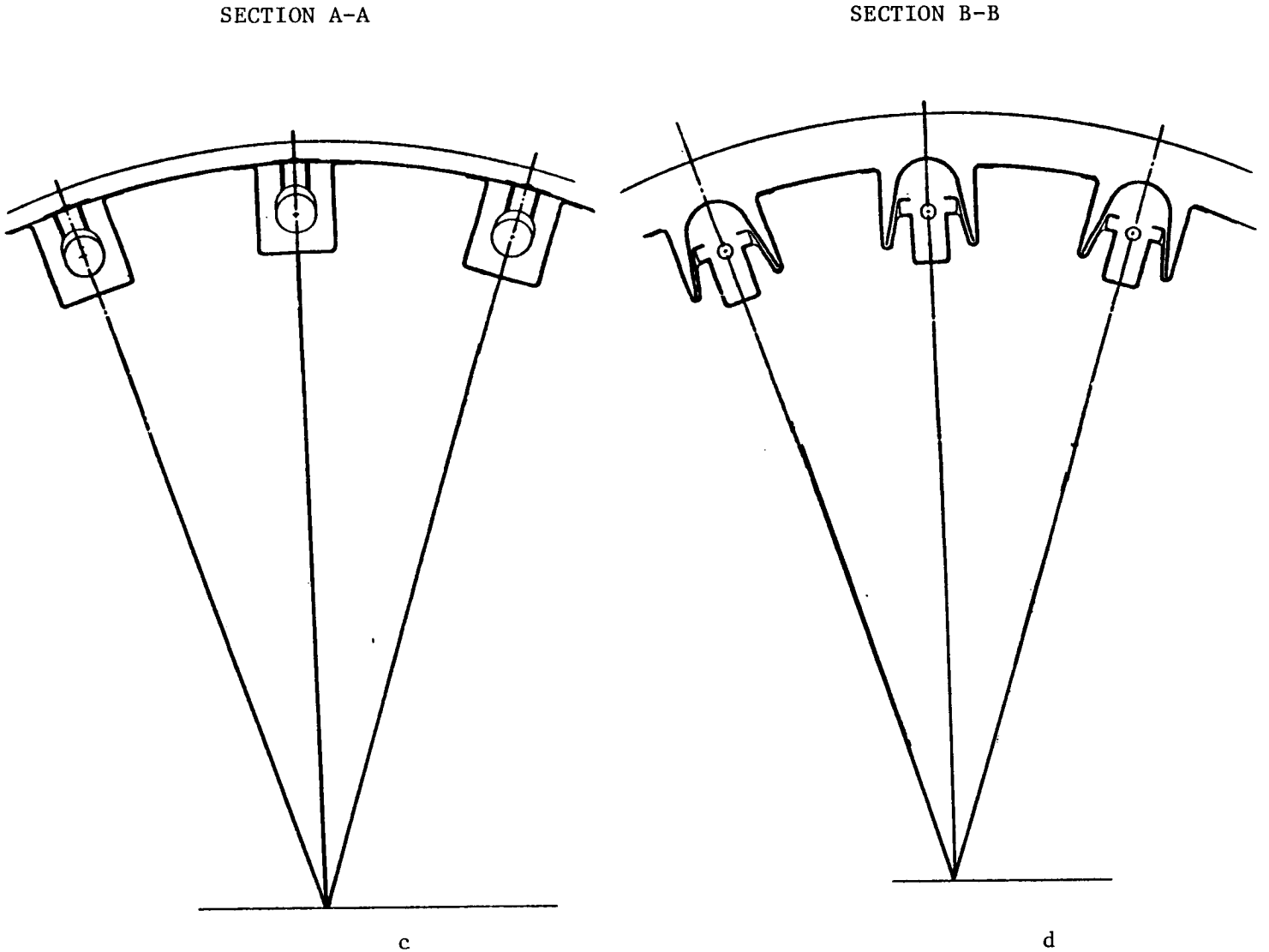

Figure 26. (Cont'd). Section Drawings of Chutes Stowed and Deployed.

SECTION E-E

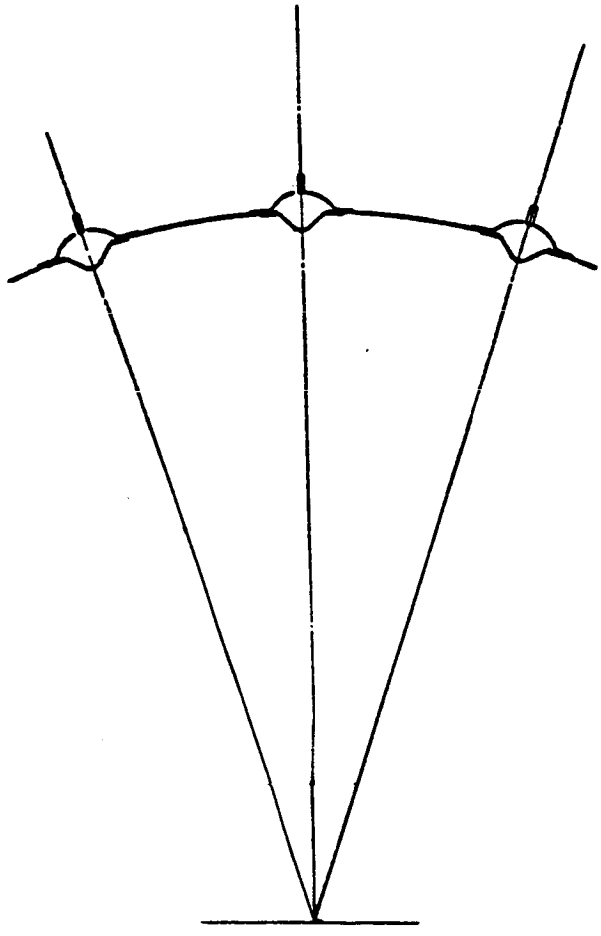

e

Figure 26. (Cont'd). Section Drawings of Chutes Stowed and Deployed.

Operating Modes

Figure 27 shows the relative positions of the components in the major operating modes as describe below.

Suppressed Takeoff, Figure 27a

The suppressor chutes are deployed and the translating outer shroud is positioned to mate with the chute outer edges. The translating shroud forms the outer flowpath of the high pressure outer stream, and the outer nozzle throat is formed between chutes at their aft edges. The ejector shroud is translated aft relative to the translating shroud to enable ejector ambient air induction and allow mixing of ambient air and the outer stream discharge from the suppressor chutes. The ejector flaps are positioned to match the full expansion area requirement of the mixed ambient air, outer stream and inner stream. Most of the bypass air flows from the bypass duct through the eight struts to the inner annulus and then exhausts through the open-positioned inner plug nozzle. Some of the bypass flow passes through the twenty-four Variable Area Bypass Injector (VABI) doors and is mixed with core flow. This feature allows the engine to be operated efficiently with the limited variation in the outer nozzle throat area.

Subsonic Cruise, Figure 27b

The suppressor chutes are in the stowed position. The outer shroud to be positioned to match the throat area, and the ejector inlet is closed. The ejector flaps are rotated to match the full expansion area of the outer and inner stream mixture.

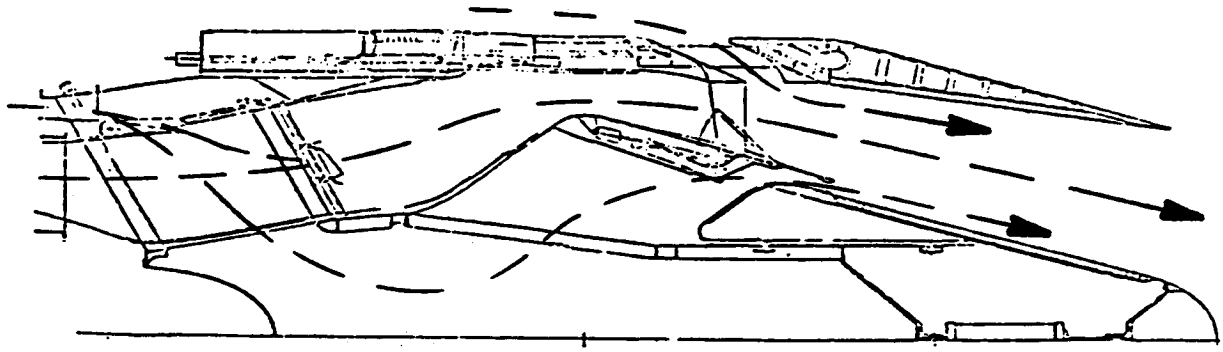

a - Takeoff

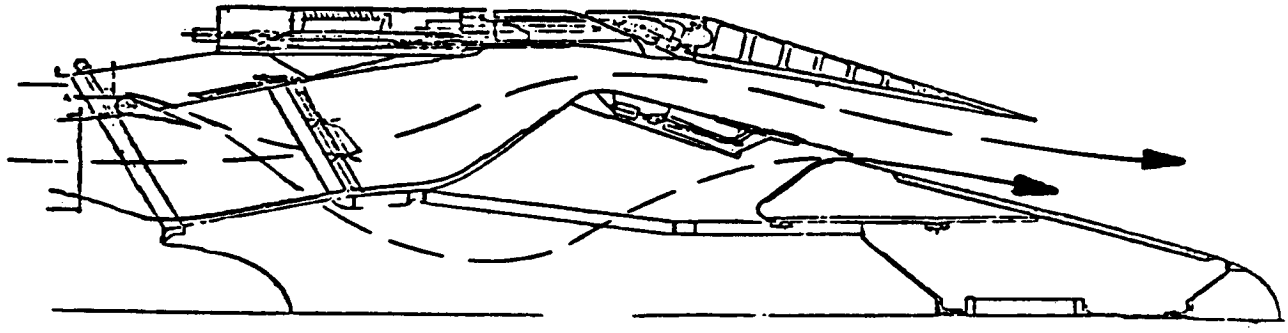

b - Subsonic Cruise

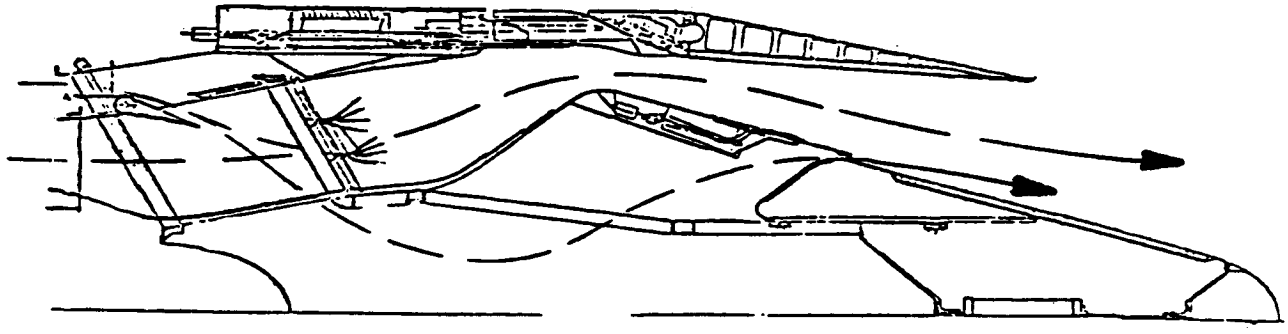

c - Transonic Acceleration

Figure 27. Ejector Shroud Flow Passages at Various Modes of Operation.

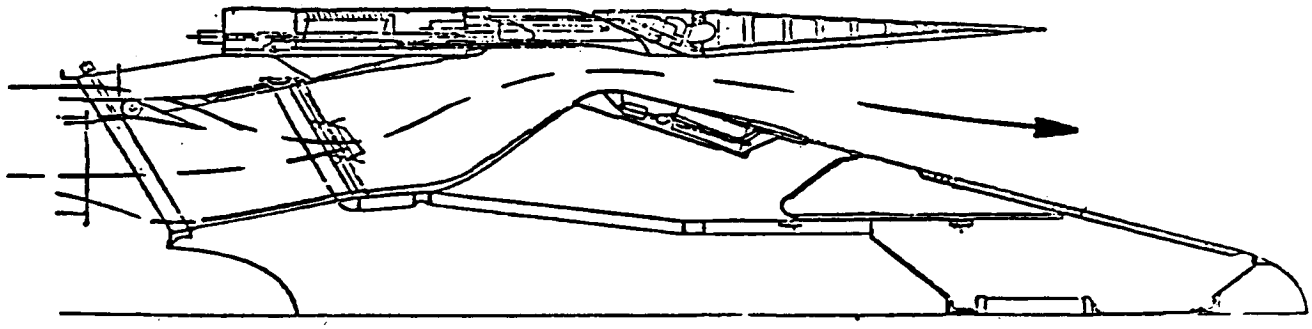

d - Supersonic Cruise

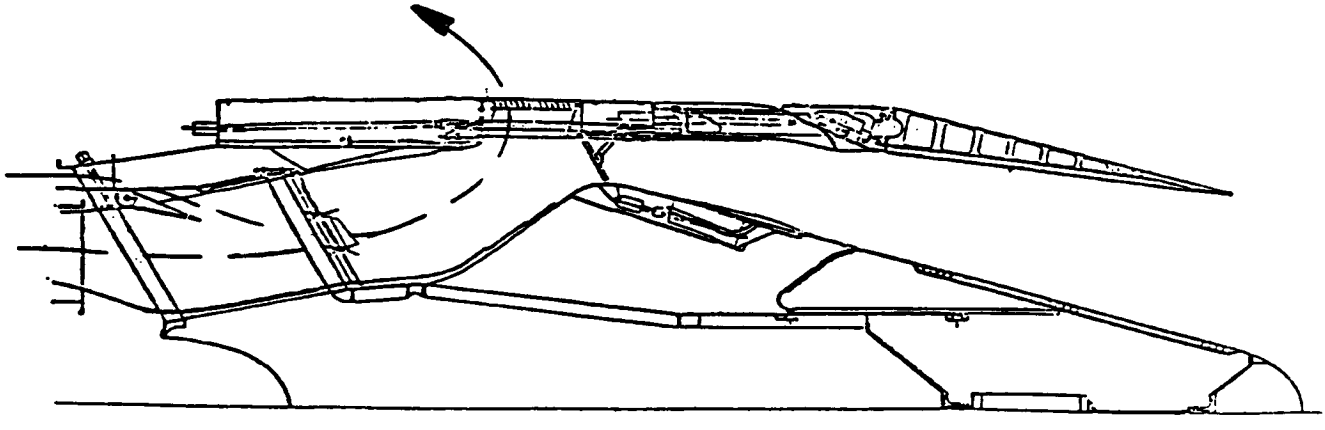

e - Reverse

Figure 27. (Cont'd). Ejector Shroud Flow Passages at Various Modes of Operation.

Acceleration, Figure 27c

The suppressor chutes are in the stowed position. The outer shroud is positioned to match the throat area, and the ejector shroud is positioned in the forward (closed ambient inlet) position relative to the translating shroud. The trailing edges of the ejector flaps are positioned to match the full expansion area of the outer and inner stream mixture. The flap positions vary from partially closed to fully open as the nozzle pressure ratio increases during the climb/acceleration portion of the flight profile. The low temperature rise (600-1000°) augmentor is operating to provide the required climb/acceleration thrust. The bypass airflow is regulated by the VABI and the inner plug nozzle to match the total airflow requirements consistent with the outer nozzle throat area. Most of the bypass air is mixed with the outer stream for high internal performance. Thus, the inner nozzle is nearly closed.

Supersonic Cruise, Figure 27d

The suppressor chutes are in the stowed position. The outer shroud is positioned to match the cruise throat area. The ejector inlet is closed, and the ejector flaps are positioned fully open to minimize base drag and optimize internal expansion area requirements for high supersonic performance. The bypass air is mixed with the core stream for highest internal performance, and the translating center plug nozzle is closed.

Reverser Thrust, Figure 27e

The suppressor chutes are in the stowed position. The outer shroud is fully extended to expose the reverser cascades to the outer stream flowpath and the ambient air. In this position blocker doors are deployed from the shroud at the plug crown to divert the outer stream to the cascades. The discharge from the

reverser cascades is controlled by cascade circumferential location and cascade vane orientation to prevent aircraft impingement and engine reingestion. The ejector is in the closed inlet position, and the ejector flaps are near closed, matching the approach area position. The center plug is closed, and VABI doors are open to mix the bypass air with the outer stream so that most of the engine airflow is utilized for reverse thrust. Tables 4 through 6 show the Cycle Sizing Data, Exhaust System Design Parameters and Actuation Systems respectively.

Exhaust System Materials Results

Advanced materials and processes that will permit use of better materials are continuously monitored for application to products such as the AST exhaust system. For high strength to density ratios at intermediate temperatures, the Titanium Aluminide materials (TiAl and Ti_3Al) appear to be very promising. These materials would be applied to the outer shroud and inner plug components. At higher temperatures, MA956 and the Rene' series of nickel base alloy would be used. MA956 is expected to be an improved liner material replacing Hastalloy X and HS188. The Rapid Solidification Plasma Deposition (RSPD) manufacturing approach is expected to broaden the application of the Rene' superalloys such as R120 and R125 from casting and forgings to sheet metal forms of construction, thus increasing the strength to weight ratio and temperature capabilities of sheet metal components now fabricated with I718 or R41. These superalloys will be applied to the structure outer plug, ejector structure and ejector flaps. For very high temperatures, ceramics and Carbon-Carbon are promising materials. Silicon ceramic is applied to the flameholder and oxidation inhibited Carbon-Carbon is applied to the sound absorption panels on the ejector flaps and inner plug surface. These materials along with the gas pressures and temperatures are shown in Figure 28.

TABLE 4

CYCLE SIZING DATA

	COANNULAR	20 CHUTE	EJECTOR
A8 Rotation, Square Inches	1135	1275	1275
A8 Supersonic Cruise, Square Inches	1291	1291	1291
A8 Max, Square Inches	1450	1450	1450
A8 Min, Square Inches	1110	1110	1110
A88 Rotation, Square Inches	247	248	248
A88 Supersonic Cruise, Square Inches	5	5	5
A88 Max, Square Inches	500	400	400
A9,Square Inches	4112	4592	----
A9, Flaps Open, Square Inches	----	----	5505
A9, Flaps Closed, Square Inches	----	----	3097
Ambient Inlet Aero, Square Inches	----	----	1220
T8, Max Augmented, Degrees Rankine	2360	2360	2360

TABLE 5

EXHAUST SYSTEM DESIGN PARAMETERS

	COANNULAR BASE	20 CHUTE BASE	20 CHUTE + EJECTOR
NOZZLE			
Max Diameter, Inches	77.44	80.98	90.86
Shroud Exit Diameter D9, Inches	72.36	76.46	76.46
Plug Angle, Degrees	15	15	15
No. of Struts	8	8	8
Nozzle Length from Engine Mount, Inches	179.5	181.6	181.6
Length, Engine Mount to A/C Interface	11.74	12.29	29.41
Inner Plug Exit Diameter D89, Inches	44.72	47.26	47.26
THRUST REVERSER			
Cascade Exit Length, Inches	12.60	12.05	10.73
Discharge Circumference, Degrees	270	270	270

	COANNULAR BASE	20 CHUTE BASE	20 CHUTE + EJECTOR
SUPPRESSOR			
Radius Ratio (R9/throat inside radius)	.856	.717	.717
Area Ratio (base area/throat aero)	1.0	1.75	1.75
Chute Depth/Width Ratio	----	1.0	1.0
Chute Inner Width/Outer Width Ratio	----	.717	.717
Chute Forward Edge Angle, Degrees	----	7.6	7.0
No. of Chutes	0	20	20
EJECTOR			
Flap Inside Diameter, Open, Inches	----	----	83.76
Flap Inside Diameter, Closed Inches	----	----	62.80
No. of Flaps	----	----	20

TABLE 6

ACTUATION SYSTEMS

	TYPE	QUANTITY		
		COANNULAR	20 CHUTE	EJECTOR
Translating Shroud	Hydraulic Screw jack	4	4	4
VABI Door	Rotary Hydraulic	8	8	8
Translating Inner Plug	Hydraulic Cylinder	1	1	1
Suppressor Chute	Hydraulic Screw jack	-	20	20
Ejector Translation	Hydraulic Screw jack	-	-	4
Ejector Flaps	Hydraulic Cylinder	-	-	20

- RSPD - Rapid Solidification Plasma Deposition
- TiAl - Titanium Aluminide
- Silicomp - Silicon Carbide

	M	Alt Ft.
TAKEOFF-ROTATION	.3	0.0
ACCELERATION - CLIMB	1.2	34,500
SUPERSONIC CRUISE	2.32	53,540

P_t - PSIA; T_t = °F; W = lbs/sec

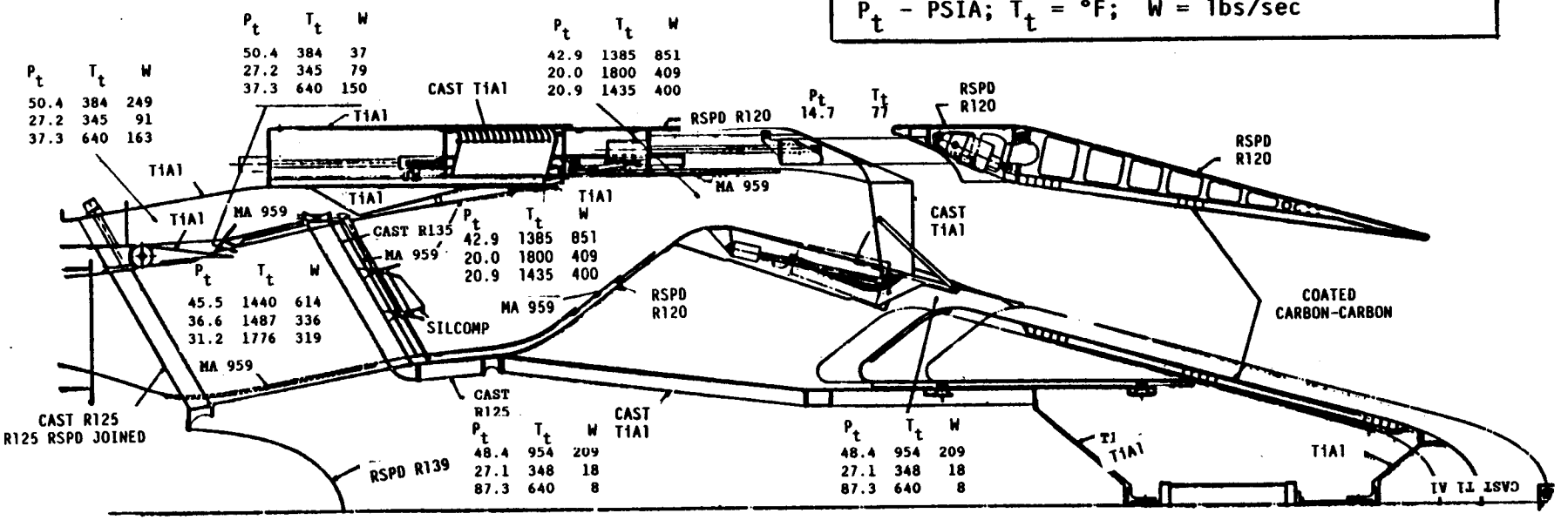

Figure 28. Ejector Shroud Nozzle Materials.

Exhaust System Weight Results

The preliminary weight estimate of the ejector exhaust system is 6,215 lbs. This is an increase of 1,910 lbs. relative to the 20-chute suppressor design and 2,456 lbs. relative to the coannular nozzle. The nozzles studied for this report were based on a 15° plug half-angle. The lower plug angle not only increases the plug length but also increases the outer shroud travel which in turn increases the length of the forward structure of the nozzle. All of these increase the weight of the nozzle. The increase in weight of the 20-chute with the 15° plug relative to one with an 18° plug is 345 lbs. Exhaust System Weight Summary is shown in Table 7.

TABLE 7

EXHAUST SYSTEM WEIGHT SUMMARY

COANNULAR BASELINE	3759 LBS
20-CHUTE SUPPRESSOR	4305 LBS
EJECTOR	6215 LBS

7.0 MISSION ANALYSIS

Methodology

Aircraft mission performance is a function of aircraft system weight, payload, trip fuel, acoustics and installed performance; hence, the effect of these subsystems on TOGW was determined through the mission analysis process to define performance versus TOGW tradeoffs.

Using the performance data generated in the conceptual design section the mission analysis was performed for the GE21-V50C engine cycle. The mission analysis computer program was set up to represent the aerodynamic and weight characteristics of the NASA AST-2 airplane shown in Figure 29 and the AST Mission B profile shown in Figure 30, which includes a 1,111 km (600 nmi) subsonic cruise segment and a supersonic cruise at Mach 2.32 on a hot (+8°C) day.

Engine performance data was generated for key mission flight conditions (supersonic cruise, subsonic cruise, climb, acceleration, takeoff and landing) for the engine cycle. The engine cycle was then run in the mission for a range of engine takeoff airflow sizes. The mission range was held constant at 7,408 km (4,000 nmi), and the TOGW varied with engine airflow size. Curves of TOGW versus engine takeoff airflow size ($W\sqrt{\theta}/\delta$) for a 7,408 km (4,000 nmi) mission "B" were generated as shown in Figure 31. These curves were generated for the three exhaust systems, namely, the ejector shroud, the 20-chute suppressor and the coannular baseline nozzles. The curves correlate airplane TOGW against engine size without regard for noise.

TOGW = 345,643 kg (762,000 lb)
Wing Area = 926 m^2 (9,969 ft^2)
292 Passengers
Payload = 27,670 kg (61,000 lbm)

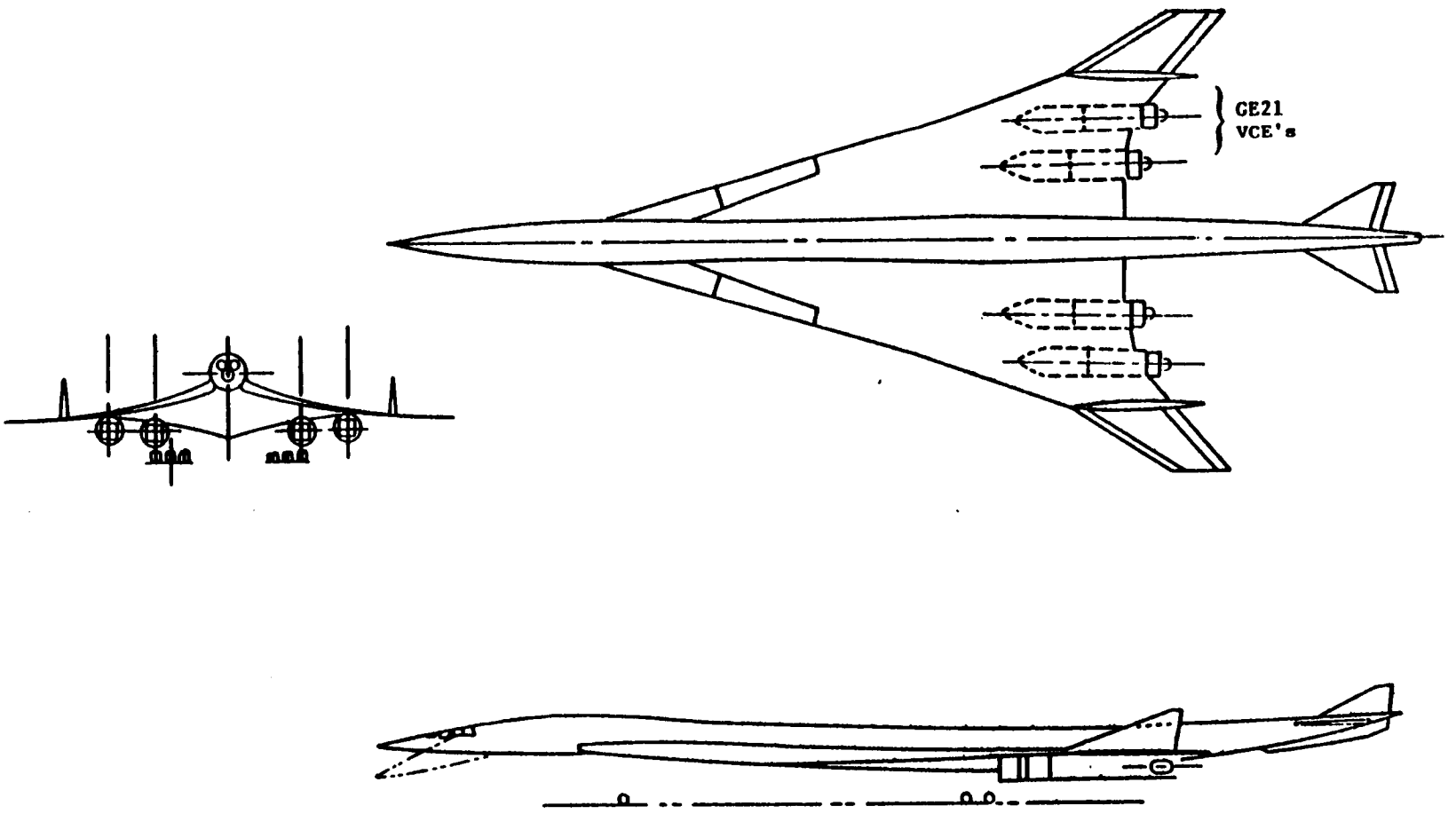

Figure 29. NASA Reference Aircraft Configuration

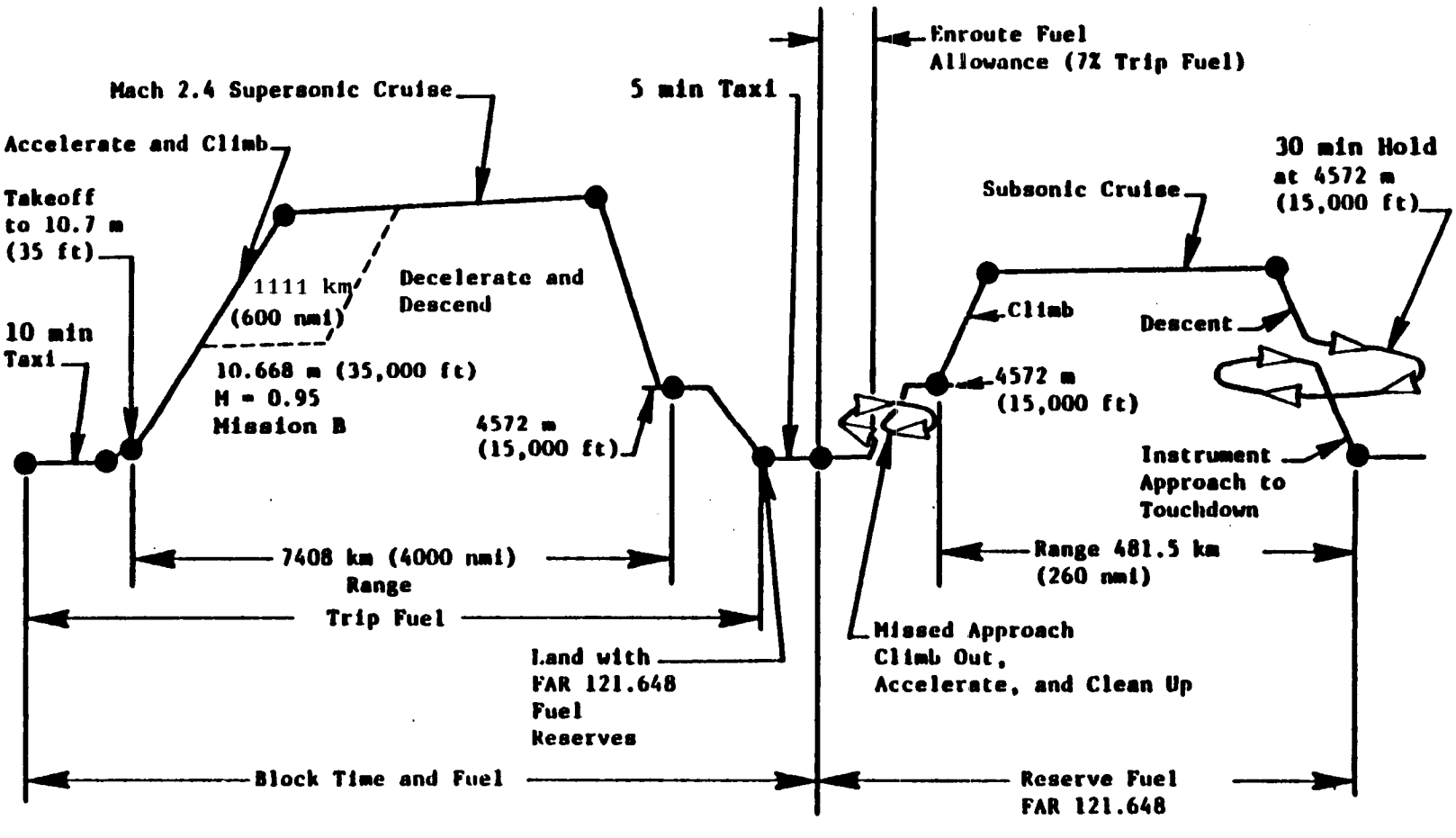

Figure 30. AST Mission

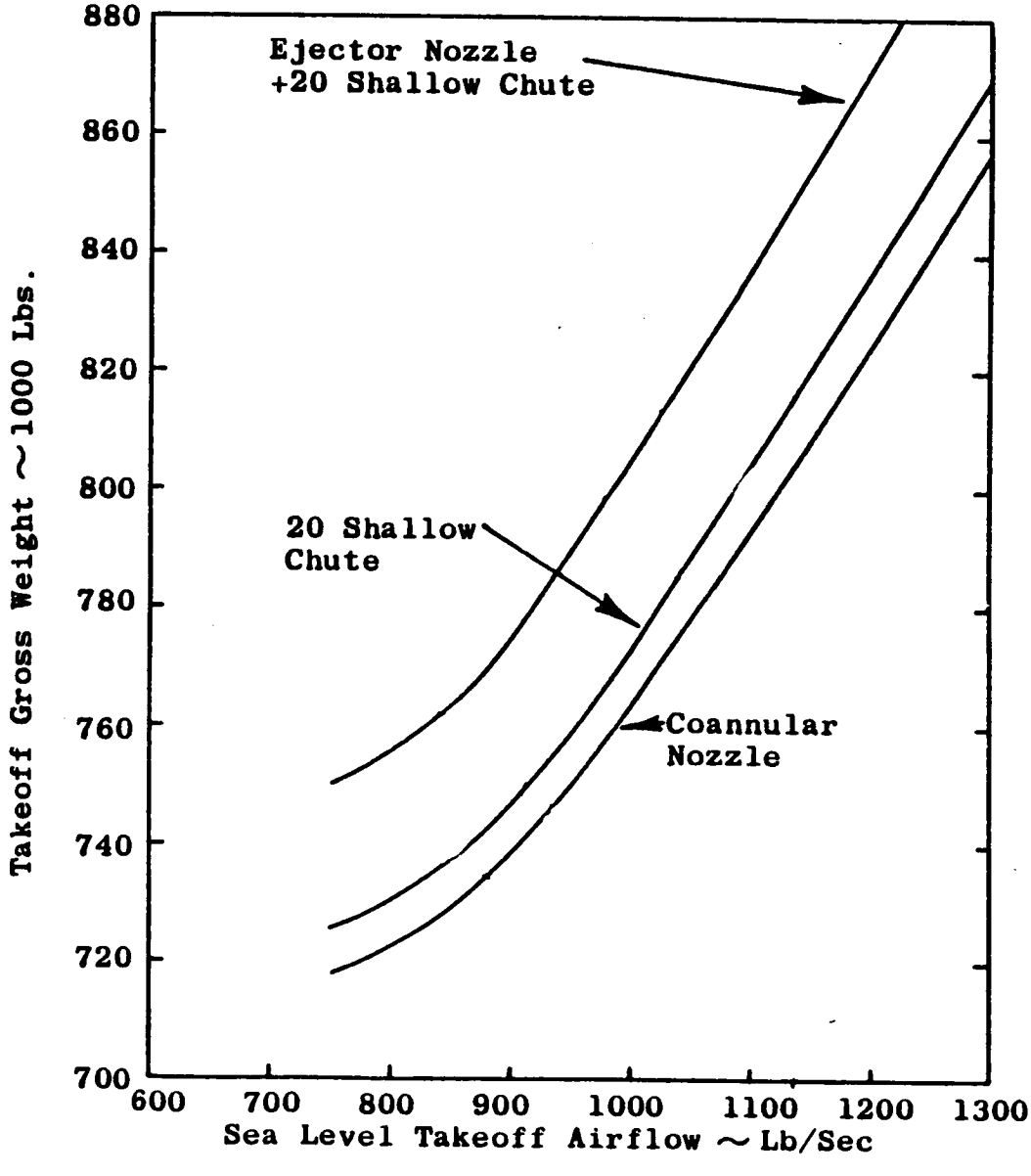

Figure 31. AST Mission "B" Performance, Airflow Versus TOGW.

Engine and Noise Sizing for Takeoff

The sizing analysis for engine and noise at takeoff conditions included the following subtasks:

- Generation of TOGW vs. airflow characteristics for the Ejector Shroud, 20-chute suppressor and the coannular unsuppressed nozzles to meet mission requirements.
- Engine sizing for takeoff distance of specified field length.
- Aircraft/engine noise estimation using noise levels (per FAR 36).

Figure 32 describes the flow of work and the interrelation of the subtasks.

Engine Cycle/Acoustic Data

As indicated earlier in the text, there are three types of noise suppression schemes as follows:

- Coannular noise suppression
- Multi-chute (20) mechanical noise supppressors
- Acoustically treated ejector shroud.

The noise suppression effectiveness was evaluated individually and the net suppression arrived at through an acoustic addition algorithm depending on the combinations to be evaluated.

Acoustic data generated by previous FAA study (Reference 5) were used to estimate coannular suppression noise level (EPNdB) versus mass averaged exhaust jet velocities (V_{mix}) and exhaust jet velocity ratio ($V_R=V_{jcold}/V_{jhot}$). These ideal critical noise parameters, V_{mix} and V_R), were "tailored" during cycle matching to achieve a maximum coannular noise suppression.

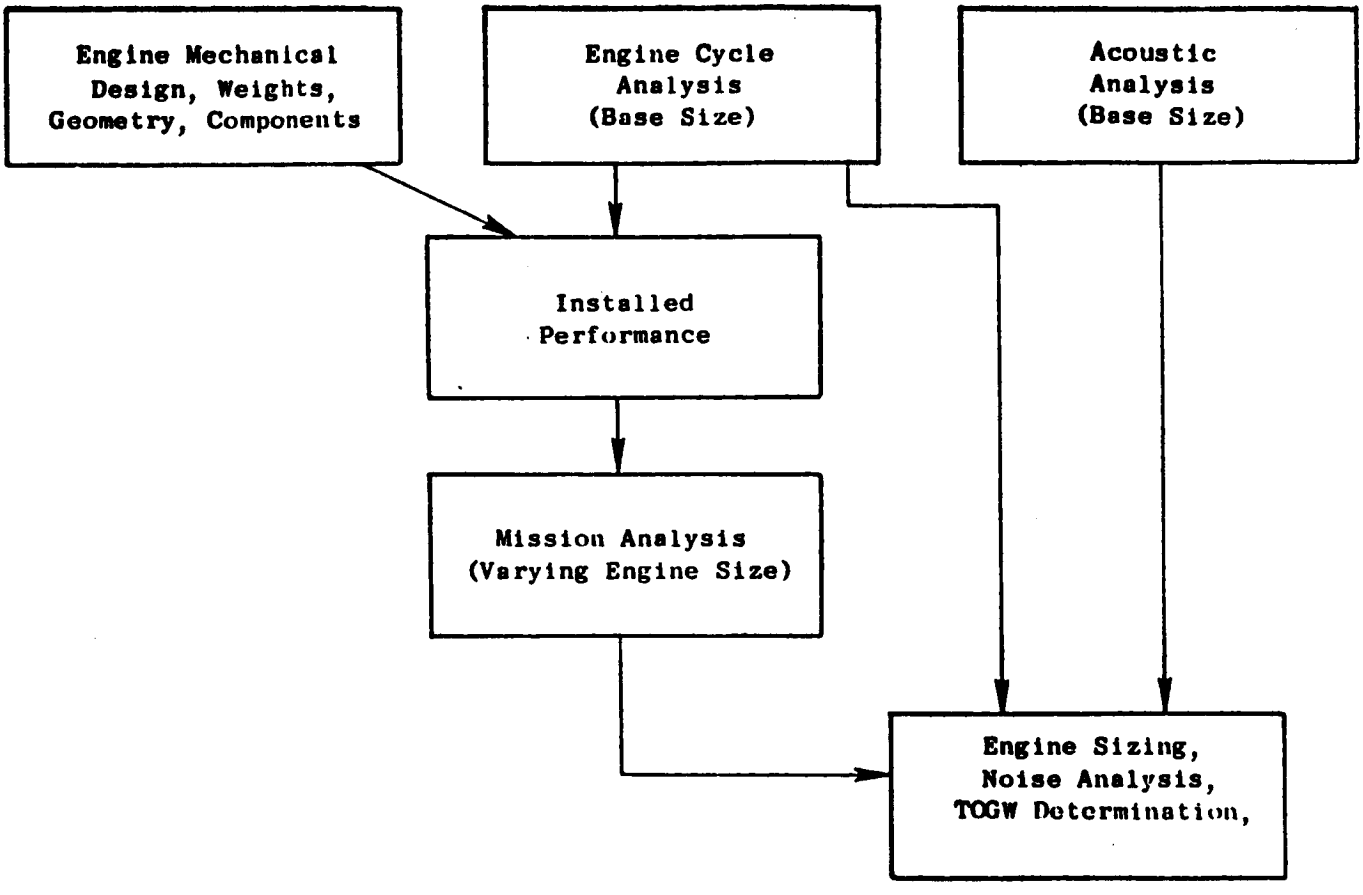

Figure 32. AST Mission Analysis Method.

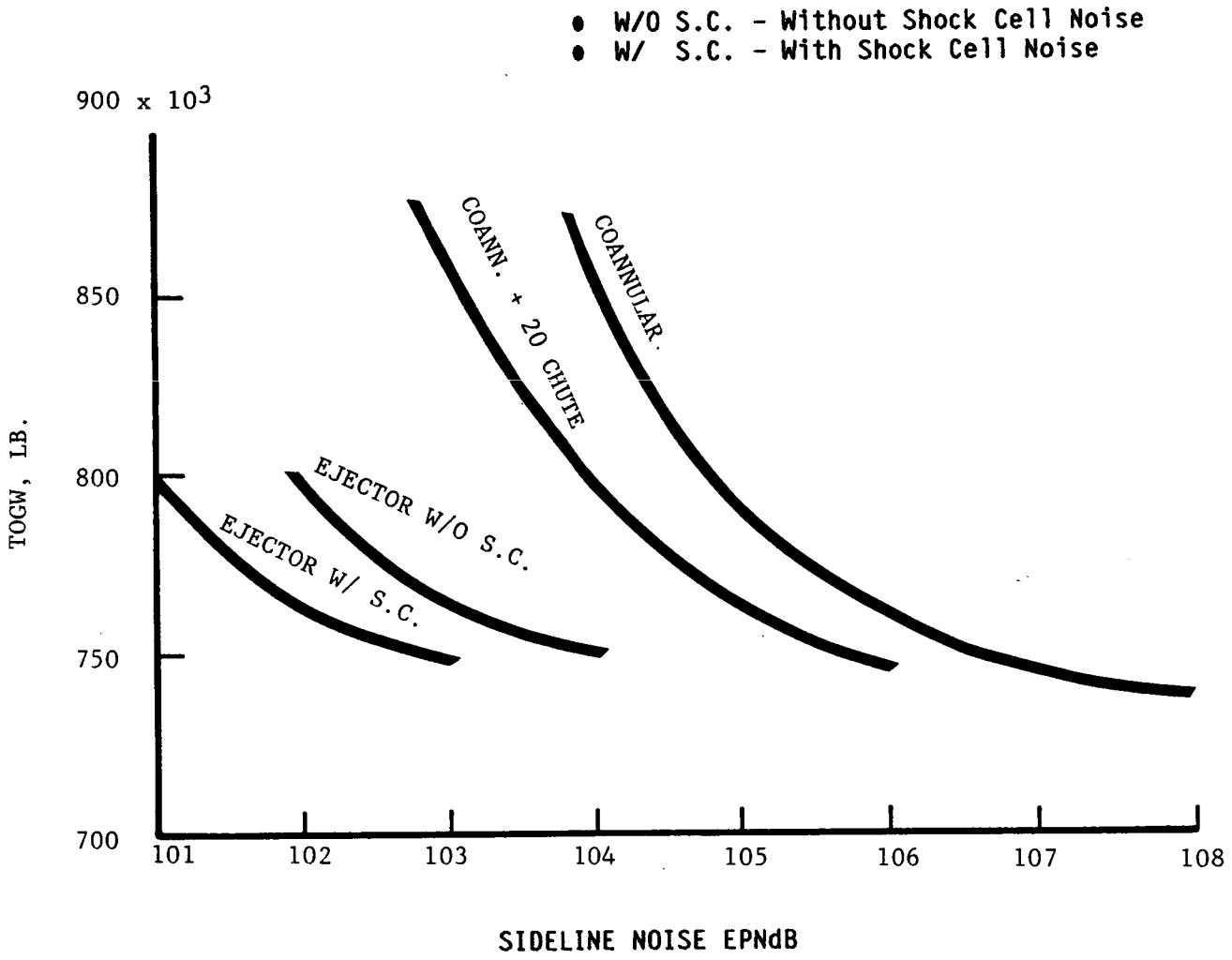

Figure 33. Predicted Noise Versus Aircraft TOGW.

The results produced two plots:

- Variation of TOGW with V_{mix}
- Variation of noise (FAR 36 Stage 3) with V_{mix}.

Eliminating the independent variable V_{mix} produced a crossplot of TOGW [for 7,408 km (4,000 nmi) range] versus traded noise. Superimposing the noise suppression due to the 20-chute mechanical suppressor, and further, that due to the acoustically treated ejector shroud on the coannular suppression produced TOGW versus noise for various degrees of noise suppression as shown in Figure 33. There are two curves for the Ejector Shroud nozzle, one with and one without shock cell control. The superiority of the ejector nozzle concept at low noise levels is clearly evident from this plot.

The combination of the TOGW versus takeoff airflow (lb/sec) and noise versus airflow plot produced a third plot, Figure 34, which enables any two of the variables, TOGW, takeoff airflow and noise to be determined, given the noise level and the type of nozzle. For example, to find the commensurate airflow and TOGW for an ejector shroud nozzle, no shock cell noise control at 104.7 EPNdB noise level, enter 104.7 on the noise level axis to determine approximately 860 lb/sec airflow and about 765,000 lbs TOGW. To achieve equivalent noise reduction using the 20-chute suppressor will require 862,000 lbs TOGW.

The above curves were generated by assuming the following:

1. Installed performance at levels estimated in conceptual design phase.
2. Fixed pay load
3. Aircraft range of 7,408 km (4,000 nmi).

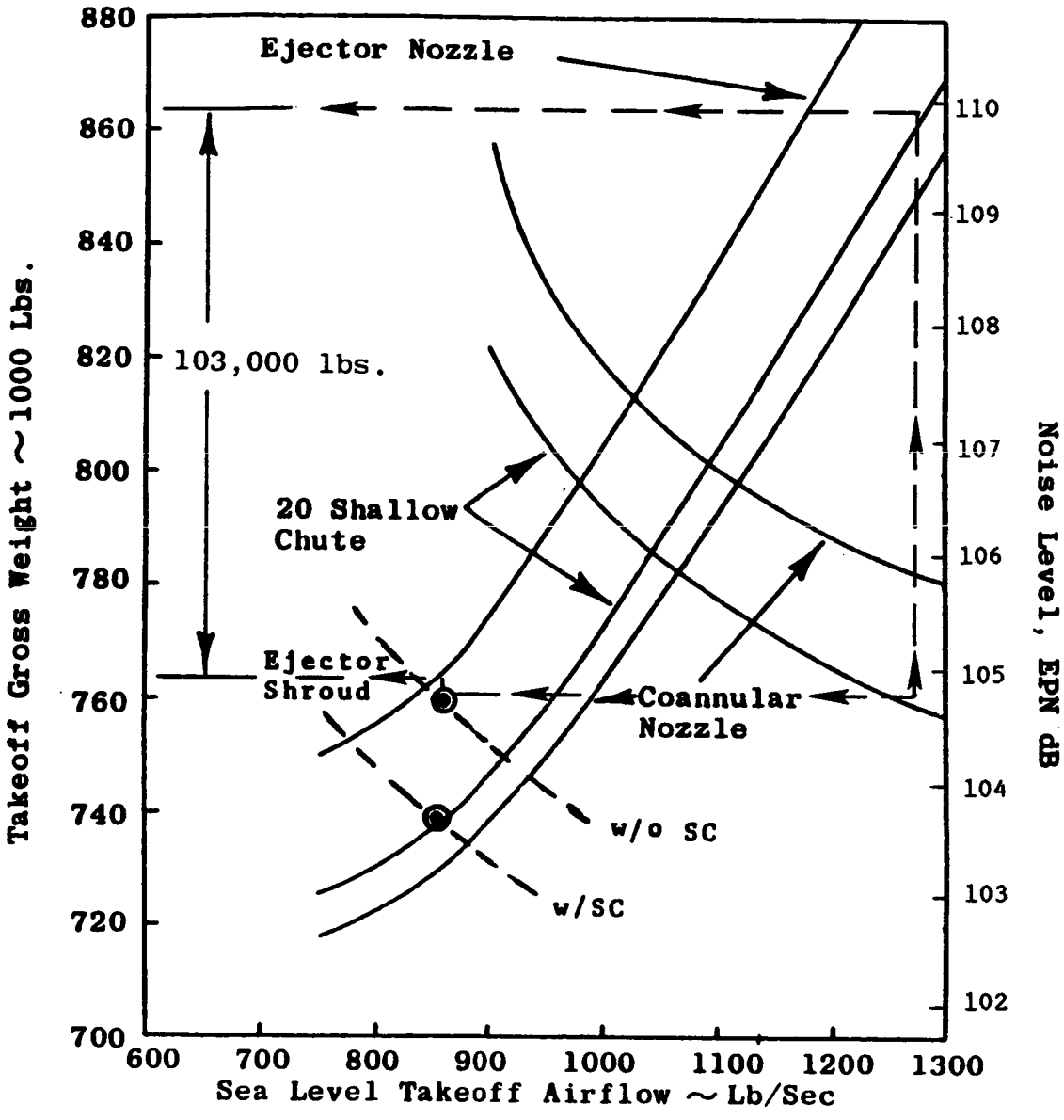

Figure 34. AST Mission Analysis Results for the Coannular, 20-Chute and Ejector Shroud Exhaust Systems.

Table 8 summarizes Mission Analysis results on the basis of installed performance estimated during the conceptual design phase. The above results were modified to reflect test performance after the test program which follows.

TABLE 8

PRELIMINARY MISSION ANALYSIS RESULTS SUMMARY SHOWING COMMENSURATE AIRFLOW AND TOGW NECESSARY TO SATISFY A NOISE GOAL OF 103 (TRADED) USING PREDICTED PERFORMANCE DATA

NOZZLE	SIDELINE EPNL dB	AIRFLOW lb/sec	TOGW lbs.
Ejector Shroud	104.74	858	765,000
20-Chute Suppressor	104.74	1,270	862,000
Coannular	104.74	Not Realistically Achievable	Not Realistically Achievable

8.0 TEST FACILITY DESCRIPTION

The tests described in this report were run in a static test stand and a transonic wind tunnel at the FluiDyne Medicine Lake Aerodynamic Laboratory.

8.1 STATIC THRUST STAND

The static thrust stand is the static (M = 0) wind tunnel setup and checkout facility. It consists of the piping which supplies dried, heated air from the 2,500 psia air storage systems to the sting-mounted flow-through force balance. This facility, shown schematically in Figure 35a, allows static checkout of the model balance, instrumentation and data acquistion systems before the sting is installed in the wind tunnel. Proper performance of this facility was verified by testing a standard ASME nozzle.

Nozzle pressure ratios up to 30 were achieved by enclosing the model in a 48-inch diameter test cabin equipped with a second-throat diffuser. This arrangement operated as a no-flow ejector whereby the model provided altitude simulation through the pumping effect of its own exhaust flow. Ambient pressure (nozzle exhaust pressure) was calculated as the average of 16 sidewall static taps. The 16 taps showed essentially constant pressure in the test cabin. Circulation velocities were measured using fore- and aft-facing total pressure probes and were found to be low (less than 50 ft/sec). Test cell interference effects were found to be negligible for most configurations. Test cabin bleed ports were provided as a means of stabilizing cabin pressure.

8.2 TRANSONIC WIND TUNNEL

The transonic wind tunnel has a 66 in. x 66 in. slotted-wall test section, and Figure 35b shows the tunnel

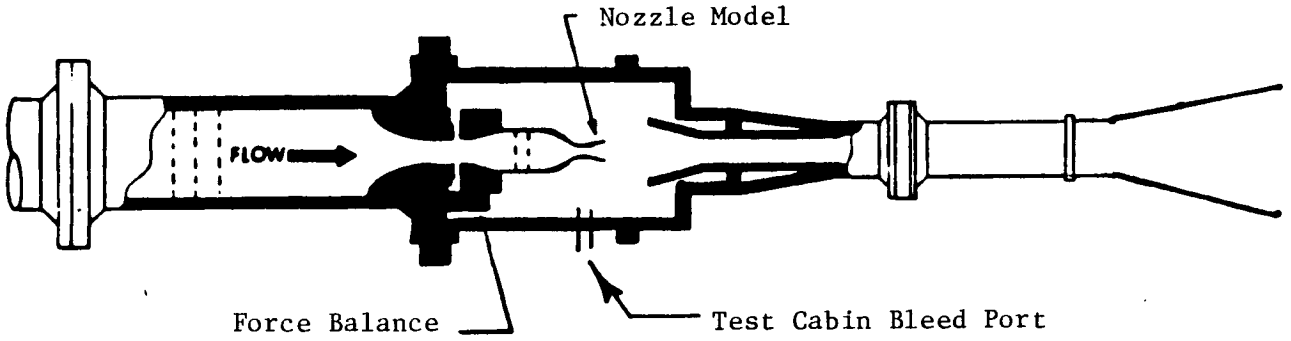

a. FluiDyne Static Thrust Stand

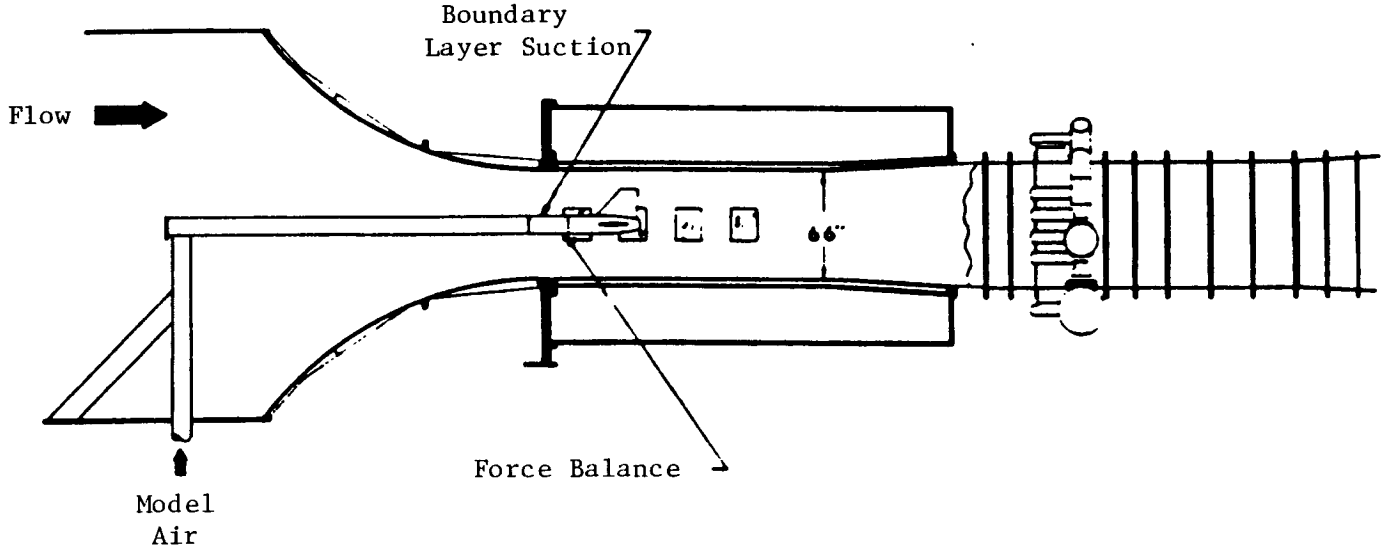

b. FluiDyne 5-1/2 x 5-1/2 foot Transonic Wind Tunnel

Figure 35. FluiDyne Test Facility Schematics.

installation schematic. Figure 36 shows an overall view of the tunnel. This is an induction-type tunnel in which atmospheric air is drawn through the test section using air ejectors to reduce the downstream pressure. The required test section Mach number is obtained by controlling the mass flow to the ejectors. Water condensation in the test section is avoided by burning propane upstream of the inlet.

Tunnel Mach numbers for the tests spanned Mach Numbers M = .35, .45 and .90.

The exhaust nozzle model and the force balance system were supported in the test cell by a cantilevered 10-inch diameter tube. The model support tube consists of two concentric pipes, with the dried and heated model air (obtained from a 2,500 psi storage system) being supplied to the model through the inner pipe. Thinning of the boundary layer on the support tube was achieved by using the facility vacuum system (33,500 ft^3) to remove the low energy air adjacent to the tube through a perforated section upstream of the test model.

8.3 FORCE BALANCE SYSTEM

Performance data taken in the static and wind tunnel test stands were obtained by force measurement using a dual-passage flow-through strain-gage force balance system. This system consists of two choked ASME metering nozzles, two flexible seals, and an axial force flexure. Figure 37 shows a schematic of the in-flight force balance system, test model assembly, and station nomenclature.

The force balance calibration determined the output characteristics of both the force balance flexure and the two elastic seals. The balance was first calibrated with the seals unpressurized to determine the "straight pull" calibration coefficient,

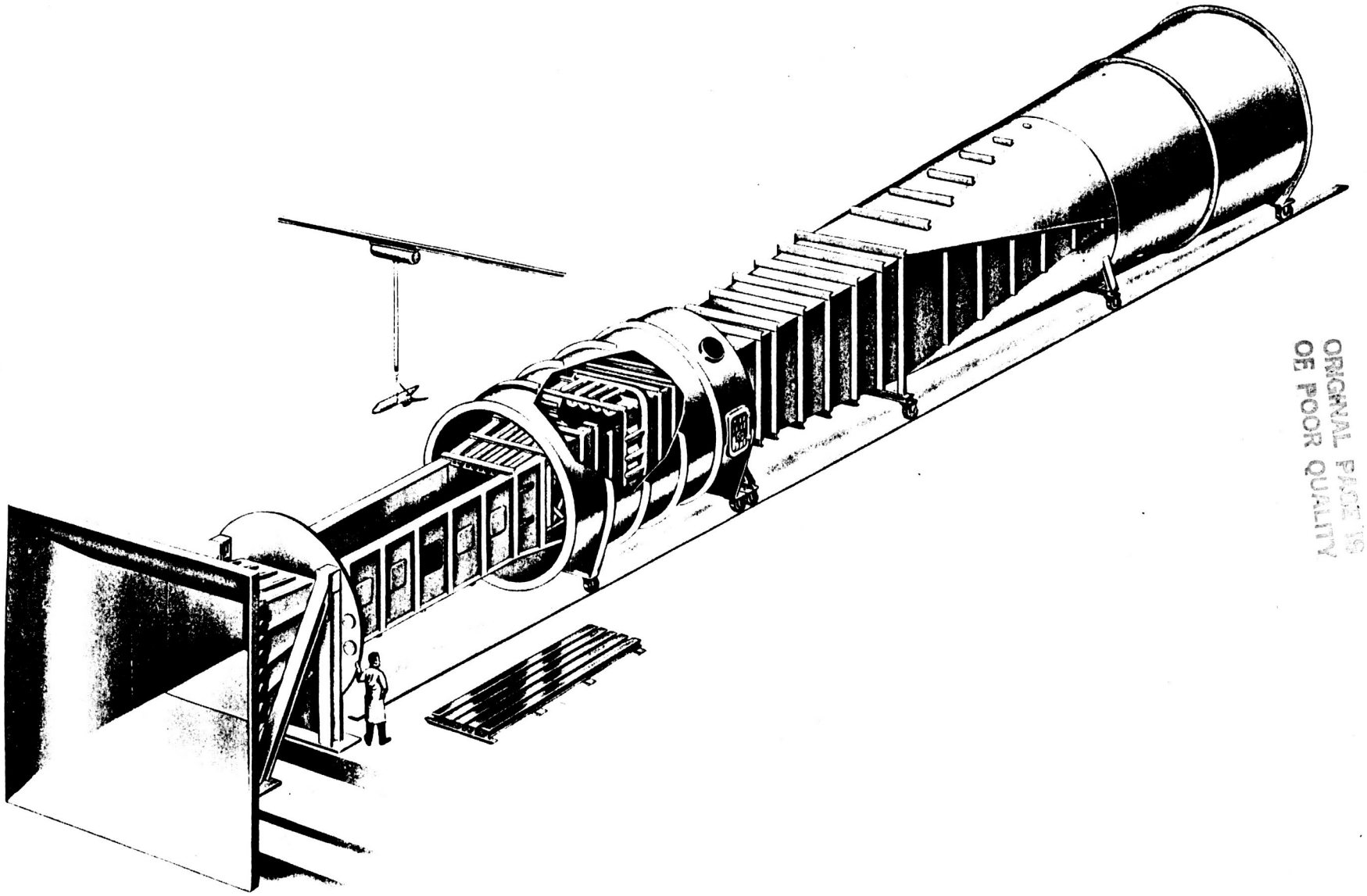

Figure 36. FluiDyne Transonic Wind Tunnel

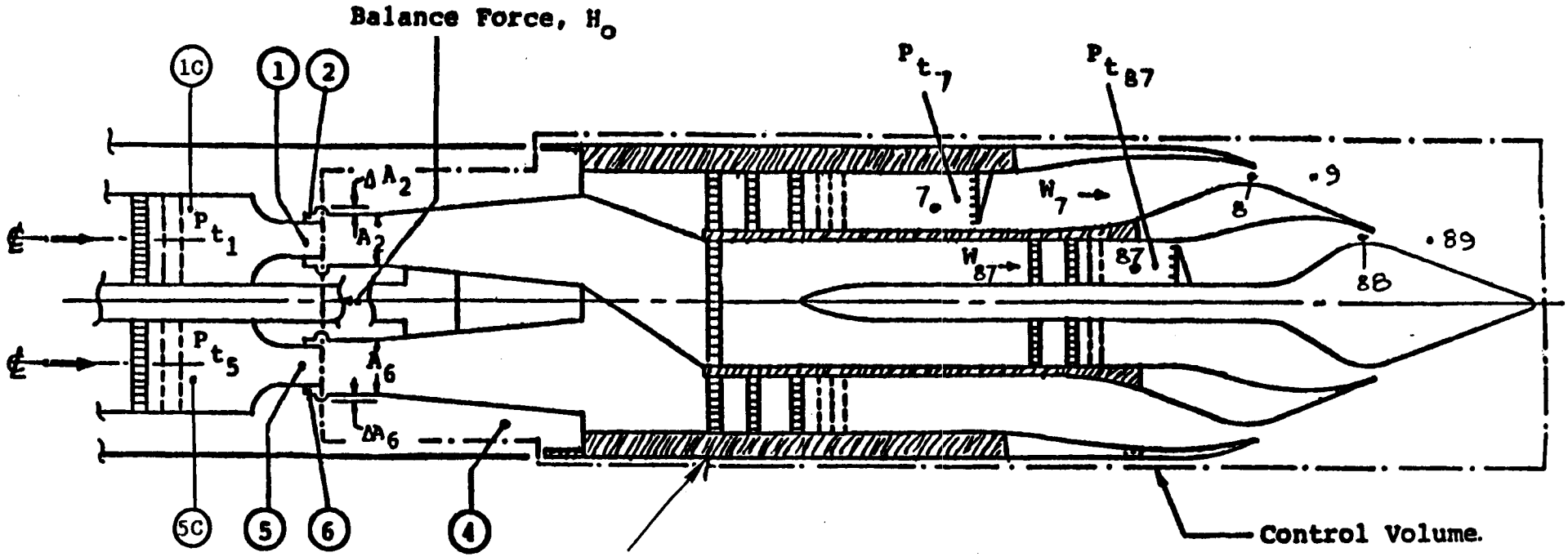

Station	Description
1	ASME meter throat (inner passage)
2	Flexible seal
4	Balance cavity
5	ASME meter throat (outer passage)
6	Flexible seal
7	Outer nozzle charging station
8	Outer nozzle throat station
9	Outer nozzle discharge
87	Inner nozzle charging station
88	Inner nozzle throat station
89	Inner nozzle discharge

(1C) **ASME meter changing station (inner passage)**

(5C) **ASME meter changing station (outer passage)**

Figure 37. Station Nomenclature, Suppressor and Ejector Nozzles

K_2. The balance interior was then pressurized to produce seal pressure differentials, ΔP. This pressure loading produces a downstream force on the balance. Additional loads (W_x) are applied to decrease or increase the net load to simulate actual test conditions of load and ΔP.

A summation of forces at the seal station indicates the axial balance force:

$$H_o = C_2K_2 = \Delta P_2 \, (A_2 + \Delta A_2) + \Delta P_6 \, (A_6 + \Delta A_6) + W_x.$$

Since ΔP acts upon each of two identical seals in this dual nozzle system, ΔA_2 is assumed equal to ΔA_6 when both seals are exposed to the same differential pressure and balance force (balance deflection) and an overall seal effective area increase (ΔA) is defined:

$$\Delta A = \Delta A_2 + \Delta A_6 = \frac{C_2K_2 - W_x - \Delta P \, (A_2 + A_6)}{\Delta P}$$

ΔA was then curve-fit as a function of H_o and ΔP so that a correction term could be included in the balance force calculation. When used to reduce test data, ΔA for each seal was defined by H_o and the ΔP at each seal.

Additional calibrations were performed for single passage tests. For these cases, the seal effective area increase was defined:

$$\Delta A_2 = \frac{C_2K_2 - W_x - \Delta P_2A_2}{\Delta P_2}$$

$$\Delta A_6 = \frac{C_2K_2 - W_x - \Delta P_6A_6}{\Delta P_6}$$

C-2

8.4 INSTRUMENTATION AND DATA ACQUISITION

The following instrumentation and data acquisition systems were used for these tests:

Measurement	Instrumentation	Acquisition
Balance force, H_o	Strain-gage force balance	Vidar IDVM
Facility temperatures	Shielded I-C thermocouple	
Facility meter, P_{t_5}	0-1,000 psi Statham transducer	
Facility meter, P_{t_1}	0-2,000 psi Statham transducer	
Facility seal, P_6	0-100 psi Statham transducer	
Facility seal, P_2	0-50 psi Statham transducer	
Balance cavity, P_4	0-30 psi multi-port transducer	PSI* Unit
Wind tunnel and test cabin ambient, P_a		
Model surface statics		
Model charging station	0-100 psi multi-port transducers	

*Pressure Systems, Inc.

8.5 OPERATIONAL PROCEDURES

The required nozzle flow was set by regulating the total air flow to obtain the desired P_{t_8}, while regulating a motorized flow-splitter to obtain the desired $P_{t_{87}}$. The external flow Mach number in the wind tunnel was set using the tunnel air ejectors, the boundary layer suction was adjusted with sting vacuum control, and the upstream tunnel propane burners were ignited to produce a desired freestream air temperature rise to prevent test section water vapor condensation. After the flow conditions and instrumentation systems stabilized, the outputs from the force balance, transducers and thermocouples were recorded. All systems were then shut down and recorder outputs were labelled and filed.

For tests performed in the static thrust test cabin, ambient pressure (and therefore model pressure ratio) was controlled by model mass flow rate. Test cabin in-bleed was used to provide fine tuning of cabin pressure for supersonic cruise configurations.

9.0 MODEL DESCRIPTION

Scale models representing the full scale baseline coannular, 20-chute suppressor, and the ejector shroud exhaust systems were tested. Each of these models consisted of several configurations which simulated nozzle operating modes of interest. The model support weldment, shown (hatched) in Figure 37, forms the outer passage charging station. The coaxial inner passage charging station for the inner plug is supplied by a separately metered flow. This charging station hardware is common to all the models tested. The outer and inner passage charging stations were instrumented with 4 ten-element and 2 five-element area-weighted total pressure rakes, respectively, with inner and outer wall static pressure taps located at each rake position.

The coannular plug system is common to all models and configurations. The inner nozzle throat area was adjusted by translating the center plug through the use of spacers. For configurations with the inner passage completely closed, the inner passage flow conditioning screens were replaced with a blank-off plate to avoid pressurizing the inner passage flexible seal. In this condition flow was delivered to the model through the outer passage meter only. Temperature data was acquired by calculating the Joule-Thomson temperature drop (adiabatic throttling) from the meter to the charging station. All interchangeable model components featured quick-disconnect O-ring type pressure instrumentation.

Static pressure taps were installed inlayed on outer surfaces of the nacelle and outer cowl except where static testing only was required. Static taps were also installed inlayed on the main plug, center plug, or surfaces of the inner and outer passages through the throat regions to the trailing edges of the cowls. Base taps were installed on all cowls and suppressor

chutes, and ejector shroud translating beams were instrumented with pressure taps as well. Table 9 summarizes test model instrumentation.

9.1 BASELINE COANNULAR MODEL

The baseline coannular scale model flowpaths were based on full scale coannular (unsuppressed) nozzle with a 15° coannular plug system. Spool pieces were used to vary shroud positions to set throat and exit areas to simulate takeoff, subsonic and supersonic cruise modes. Figure 38 shows the coannular (unsuppressed) nozzle test configurations, and Figure 39 shows the coannular baseline nozzle dimensional information. Full scale details were duplicated to the greatest extent possible with the exception of introduction of additional model parting lines to facilitate configuration change over and reduce the likelihood of damage during assembly and disassembly. Typical coannular model assembly methods are shown in Figure 40. Coannular baseline configurations tested are shown in Table 10. The four configurations were tested under varying conditions of tunnel Mach number, nozzle bypass ratio (A_{88}/A_8) and outer and inner pressure ratios (λ_8, λ_{88}), respectively. Photographs of two coannular baseline nozzle configurations, supersonic and subsonic cruise modes, are shown in Figure 41.

9.2 BASELINE 20-CHUTE SUPPRESSOR MODEL

The design of the scale model flowpaths was based on a full scale 20-chute suppressor nozzle with a 15° coannular plug system. Spool pieces were used to vary shroud positions to set nozzle throat and exit areas to simulate takeoff, subsonic cruise and supersonic cruise modes. To avoid the complexity of suppressor chute actuating mechanisms, two different shroud pieces emulating the chute "deployed" and "stowed" modes were used. The "chute-stowed" shroud included shroud tip scalloped features left

TABLE 9

INSTRUMENTATION SUMMARY

NOZZLE TYPE	OPERATING CONFIGURATION	QTY. OF PS TAPS
COANNULAR BASELINE	TAKEOFF	53
	SUBSONIC	53
	SUPERSONIC	43
20 - CHUTE SUPPRESSOR	TAKEOFF	61
	SUBSONIC CRUISE	53
	SUPERSONIC	43
EJECTOR SHROUD	TAKEOFF	65
	SUBSONIC	60
	TRANSONIC	47
	SUPERSONIC	47

COMMON INSTRUMENTATION:

OUTER PASSAGE - 4 TEN-ELEMENT PT RAKES
4 PS TAPS

INNER PASSAGE - 2 FIVE-ELEMENT PT RAKES
6 PS TAPS

TEMPERATURE MEASUREMENT - JOULE-THOMPSON METERS

TABLE 10

NOZZLE TEST CONFIGURATIONS AND VARIABLES

	OPERATING MODE	A_{INNER}/A_{OUTER}	SUPPRESSOR FEATURES	NPR
COANNULAR BASELINE	TAKEOFF M=0,.35,.45	0 .2	NONE NONE	2.2 - 3.5
	SUBSONIC CRUISE M=.9	0 .13	NONE NONE	2.5 - 4.5
	SUPERSONIC CRUISE M=2.32 (STATIC)	0		14 - 22
20-CHUTE SUPPRESSOR	TAKEOFF M=0,.35,.45	0 .13 .2	DEPLOYED DEPLOYED DEPLOYED	2.2 - 3.5
	SUBSONIC CRUISE M=.9	0 .13	STOWED STOWED	2.5 - 4.5
	SUPERSONIC CRUISE M=2.32 (STATIC)	0	STOWED	14 - 22

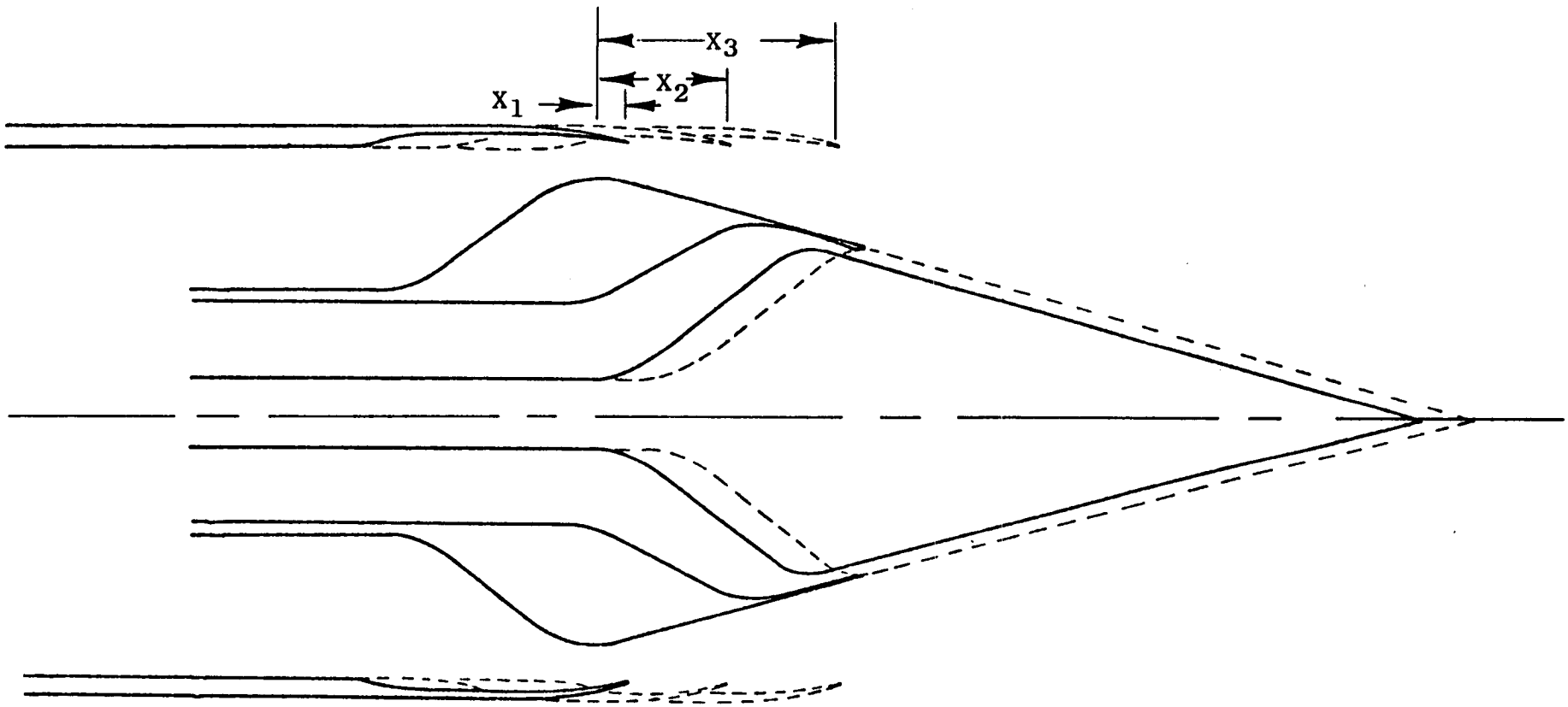

X_1 - TAKEOFF; X_2 - SUBSONIC CRUISE; X_3 - SUPERSONIC CRUISE

Figure 38. Coannular (Nozzle) Test Configurations

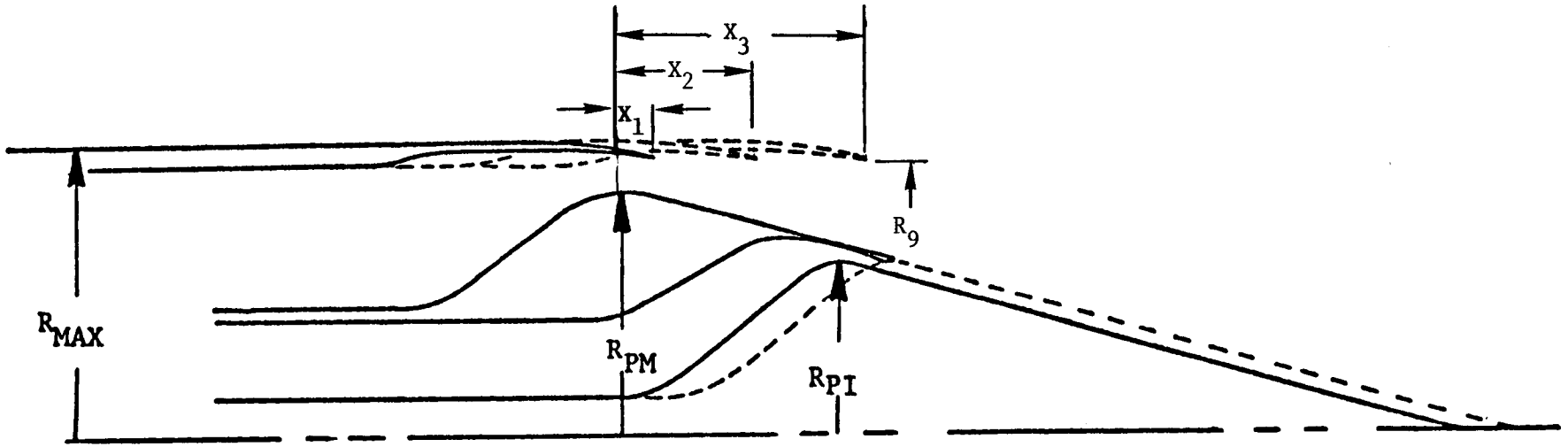

R_{max} = **38.72 in.**

$Rpm/Rmax$ = .807 $R9/Rmax$ = .934

$Rpi/Rmax$ = .572

$X1/Rmax$ = .092 - Takeoff

$X2/Rmax$ = .382 - Subsonic Cruise

$X3/Rmax$ = .835 - Supersonic Cruise

Model Scale Factor = .1318

Figure 39. Coannular Baseline Nozzle Dimensional Information

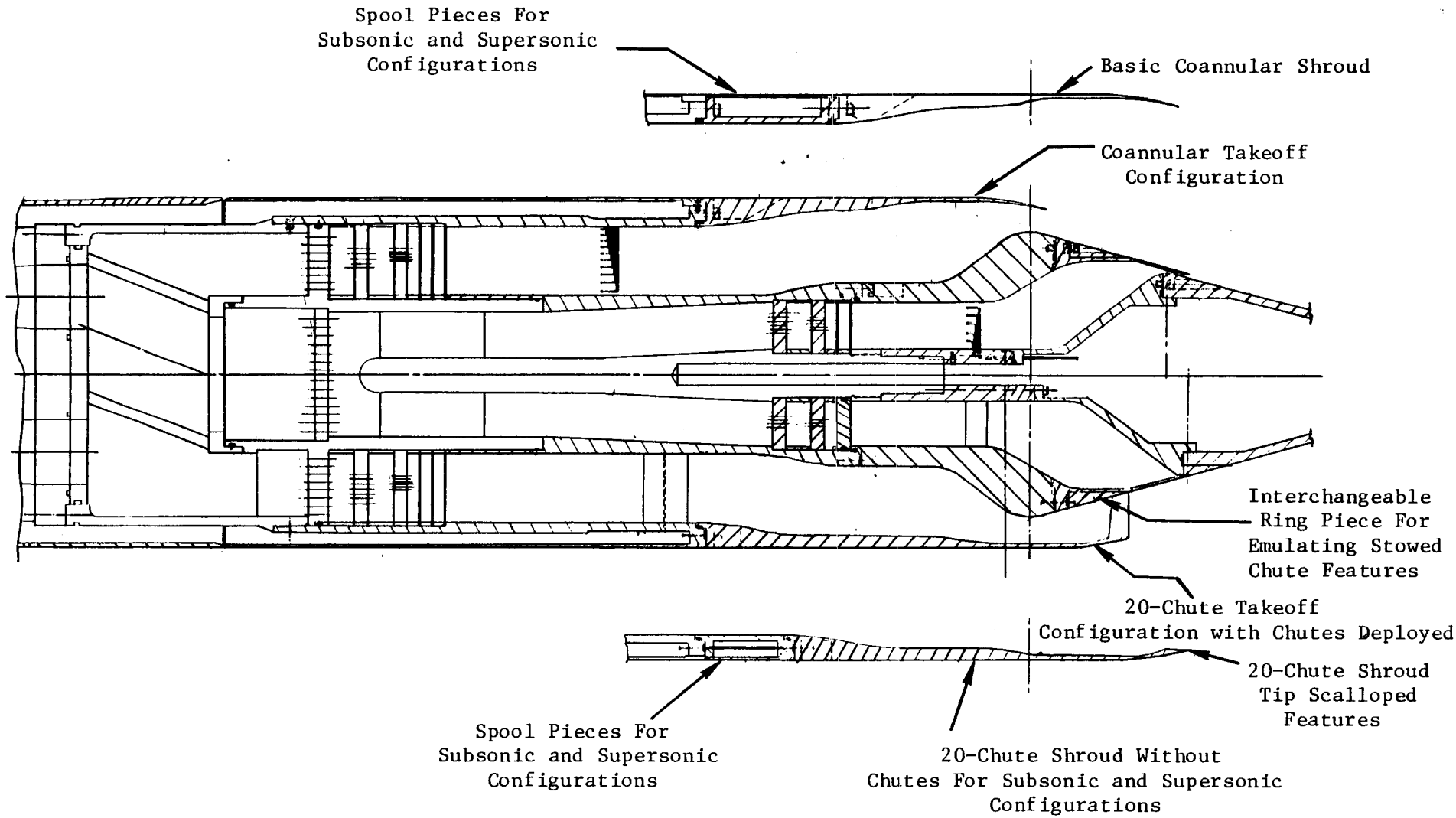

Figure 40. Coannular Baseline and 20-Chute Suppressor Model Assembly Methods

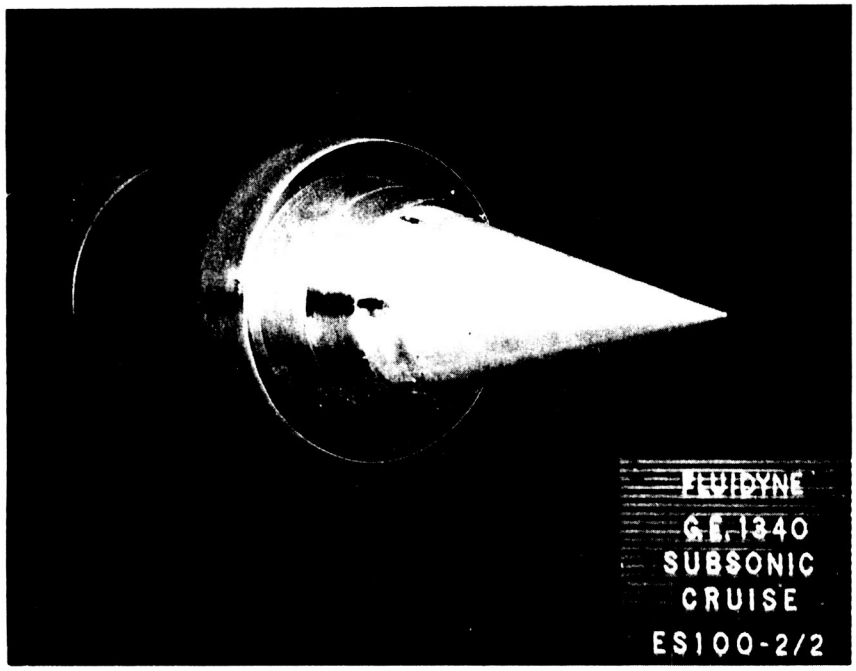

SUBSONIC CRUISE CONFIGURATION

INNER PASSAGE OPEN

SUPERSONIC CRUISE CONFIGURATION

INNER PASSAGE CLOSED

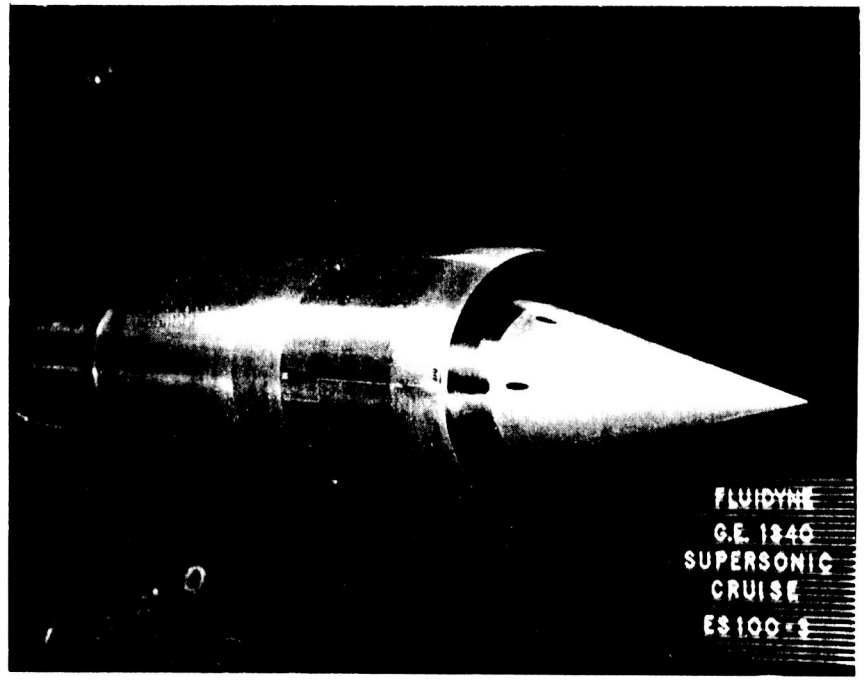

Figure 41. Coannular Baseline Model Photographs

by chute retraction, and commensurately, a ring component emulating "stowed chutes" was installed on the plug surface. This provided means for determining the effect of the stowed chutes on performance. Typical 20-chute model assembly methods are shown in Figure 40. Figure 42 shows the 20-chute suppressor test configurations, and Figures 43 and 44 show 20-chute nozzle dimensional information and chute profile respectively. The high radius-ratio requirement of the 20-chute nozzle for takeoff noise suppression required larger nacelle radius than the coannular; therefore, different scale factors had to be applied to enable the models to share a common plug system. The six configurations tested under varying conditions of tunnel Mach number, nozzle bypass ratio (A_{88}/A_8), and outer and inner nozzle pressure ratios (λ_8, λ_{88}) are shown in Table 1. Photographs of the 20-chute suppressor nozzle in various operating modes are shown in Figures 45 and 46.

9.3 EJECTOR SHROUD MODEL

The scale model flowpaths were based on full scale ejector shroud nozzle design with a 15° coannular plug system. Different ejector pieces were used to vary nozzle throat and exit areas to simulate takeoff, subsonic cruise, transonic acceleration, and supersonic cruise modes. Additional parting lines were introduced to facilitate model assembly and reduce the likelihood of damage.

The ejector shroud nozzle used the 20-chute suppressor nozzle as the basis for development. To accommodate the ejector shroud translation and flap rotation provisions, new forward shroud pieces had to be created. In so doing the ejector shroud nozzle nacelle diameter was increased relative to the 20-chute suppressor nozzle, but the chute deployment and stowage provisions remained intact along with the 15° coannular plug system.

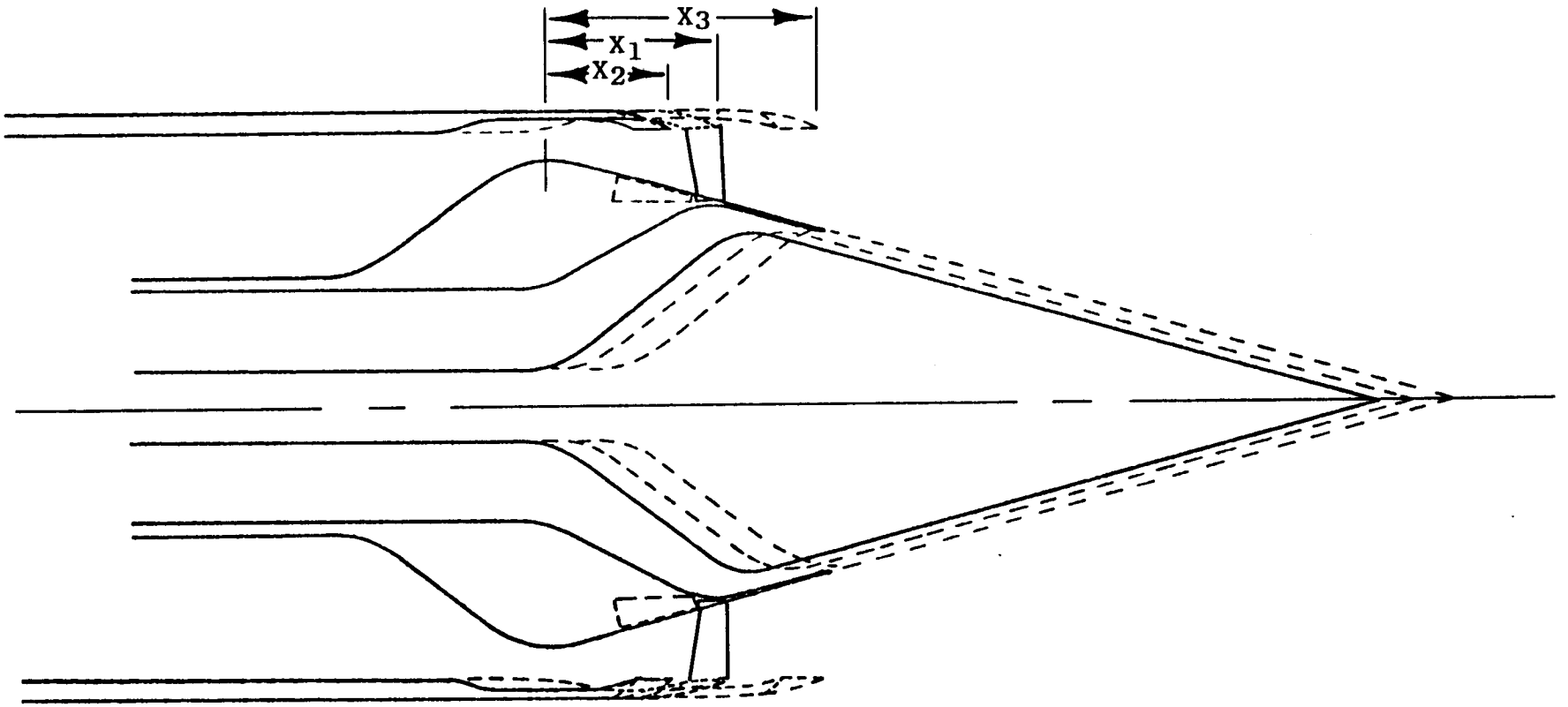

X_1 = TAKEOFF X_2=SUBSONIC CRUISE X_3=SUPERSONIC CRUISE

Figure 42. 20-Chute Suppressor Test Configurations

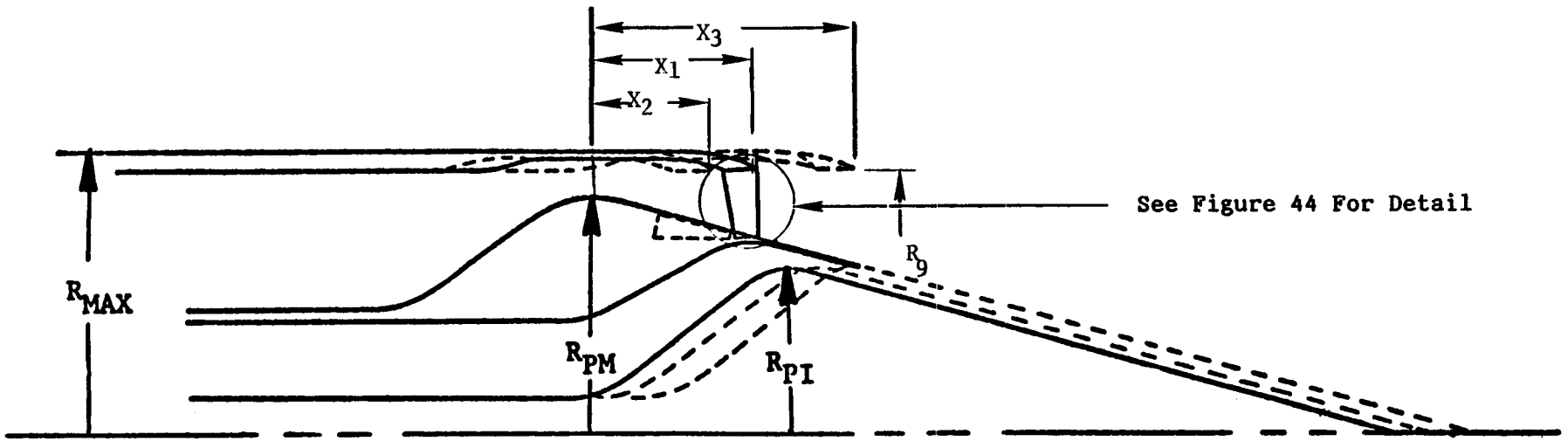

R_{max} = 40.49 in.

$Rpm/Rmax$ = .823 $R9/Rmax$ = .944

$Rpi/Rmax$ = .584

$X1/Rmax$ = .574

$X2/Rmax$ = .443

$X3/Rmax$ = .909

Model Scale Factor = .1235

Figure 43. 20-Chute Suppressor Nozzle Dimensional Information

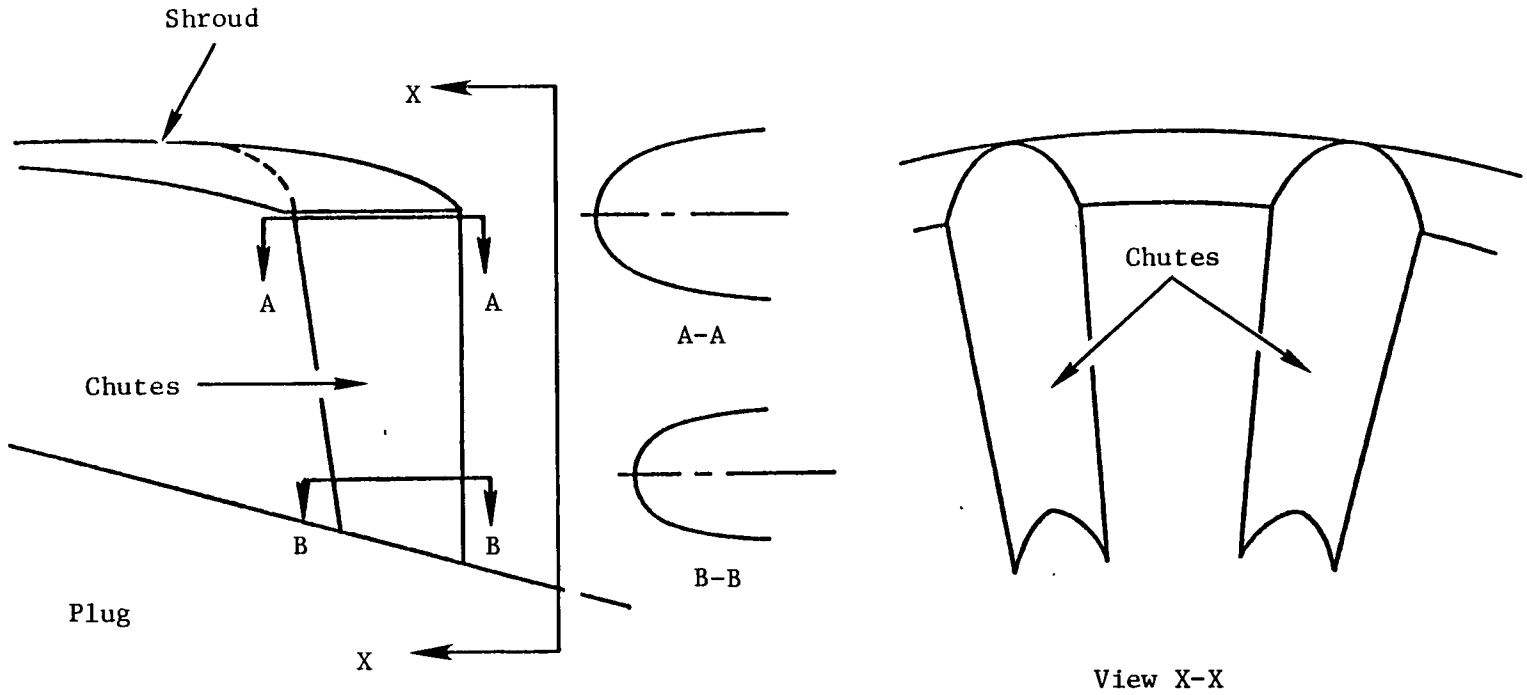

Figure 44. 20-Chute Suppressor Profile

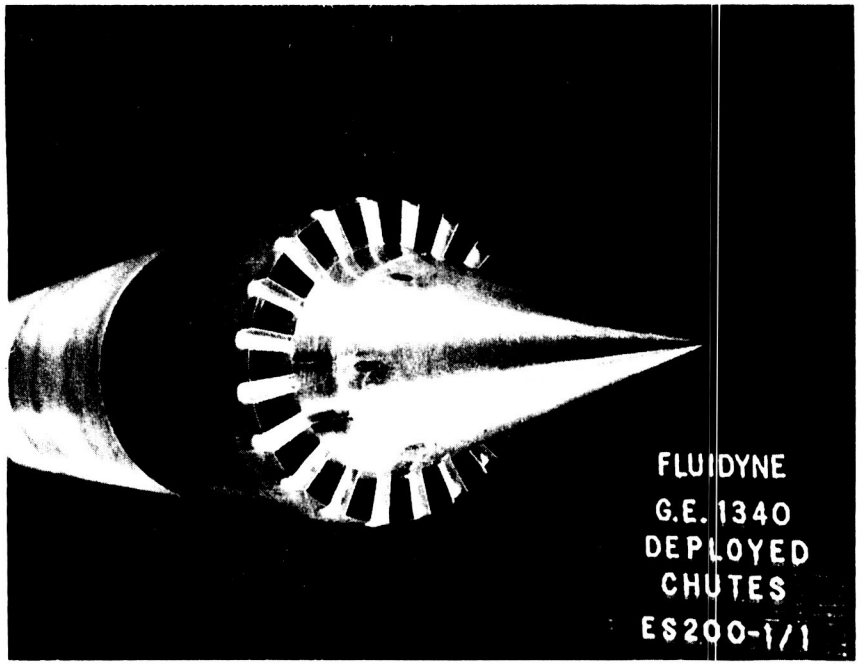

TAKEOFF CONFIGURATION

CHUTES DEPLOYED

SUBSONIC CRUISE CONFIGURATION

CHUTES STOWED

INNER PASSAGE OPEN

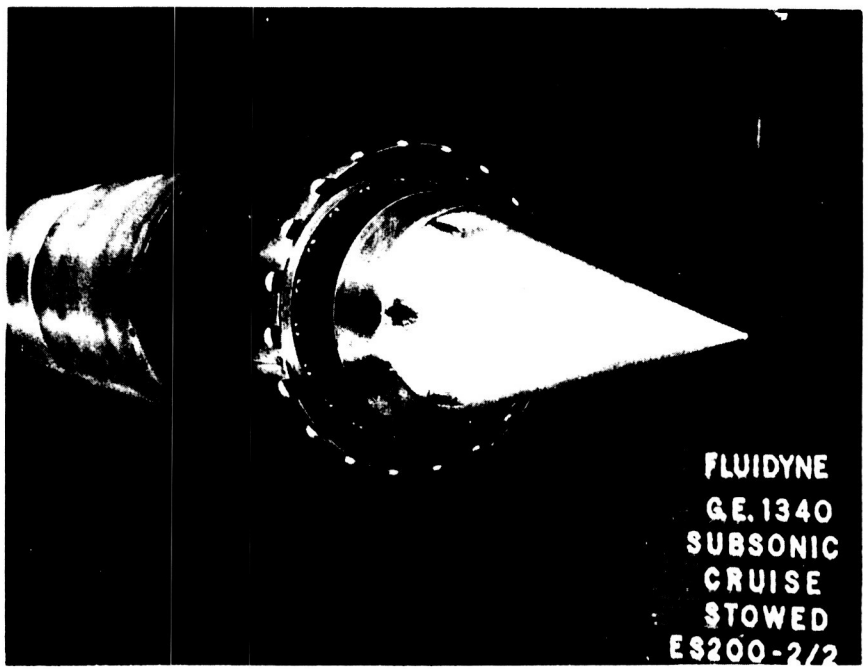

Figure 45. 20-Chute Suppressor Nozzle Model Photographs

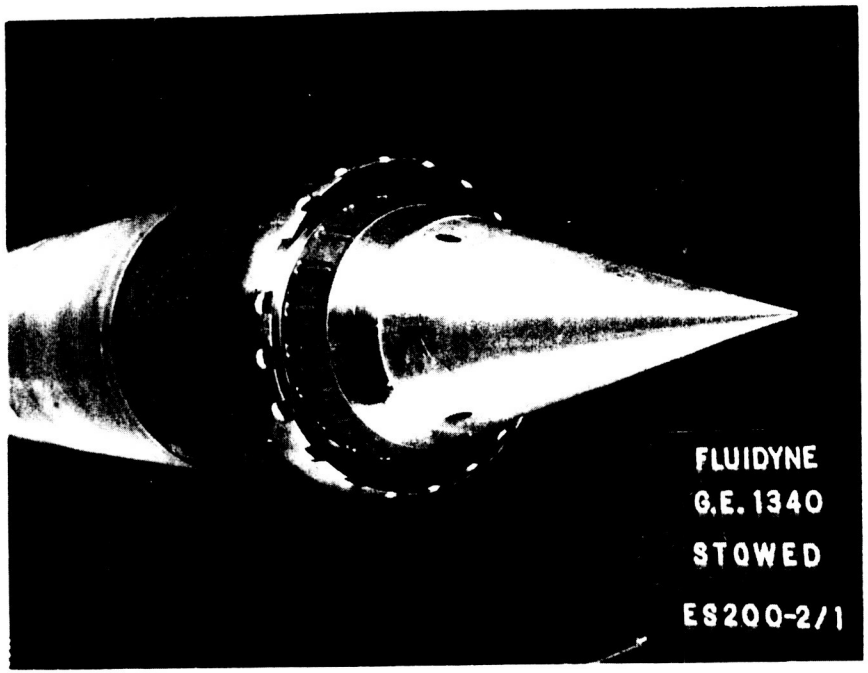

SUBSONIC CRUISE CONFIGURATION
CHUTES STOWED
INNER PASSAGE CLOSED

SUPERSONIC CRUISE CONFIGURATION
NO SUPPRESSOR FEATURES ON PLUG;
INNER PASSAGE CLOSED

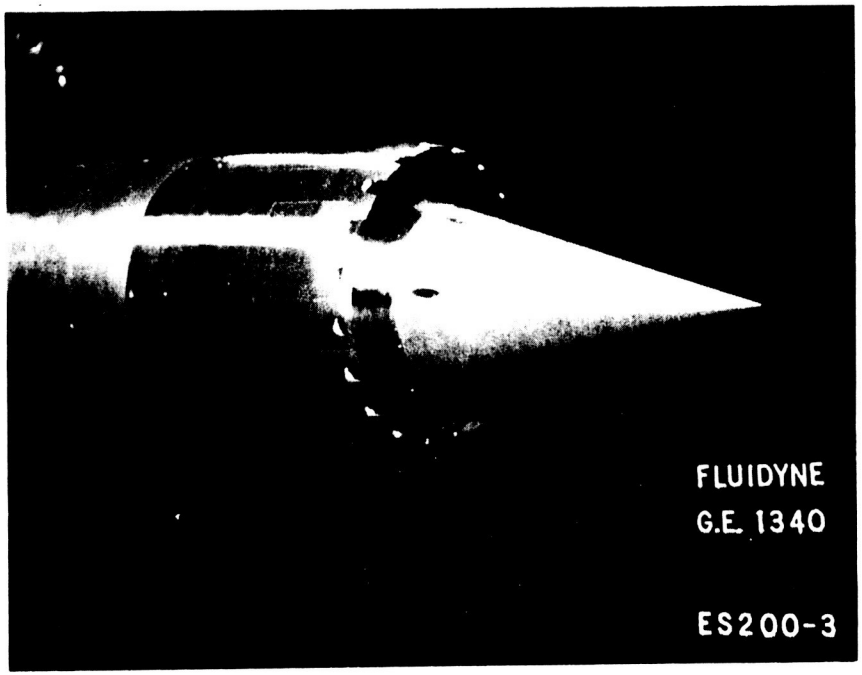

Figure 46. 20-Chute Suppressor Nozzle Model Photographs

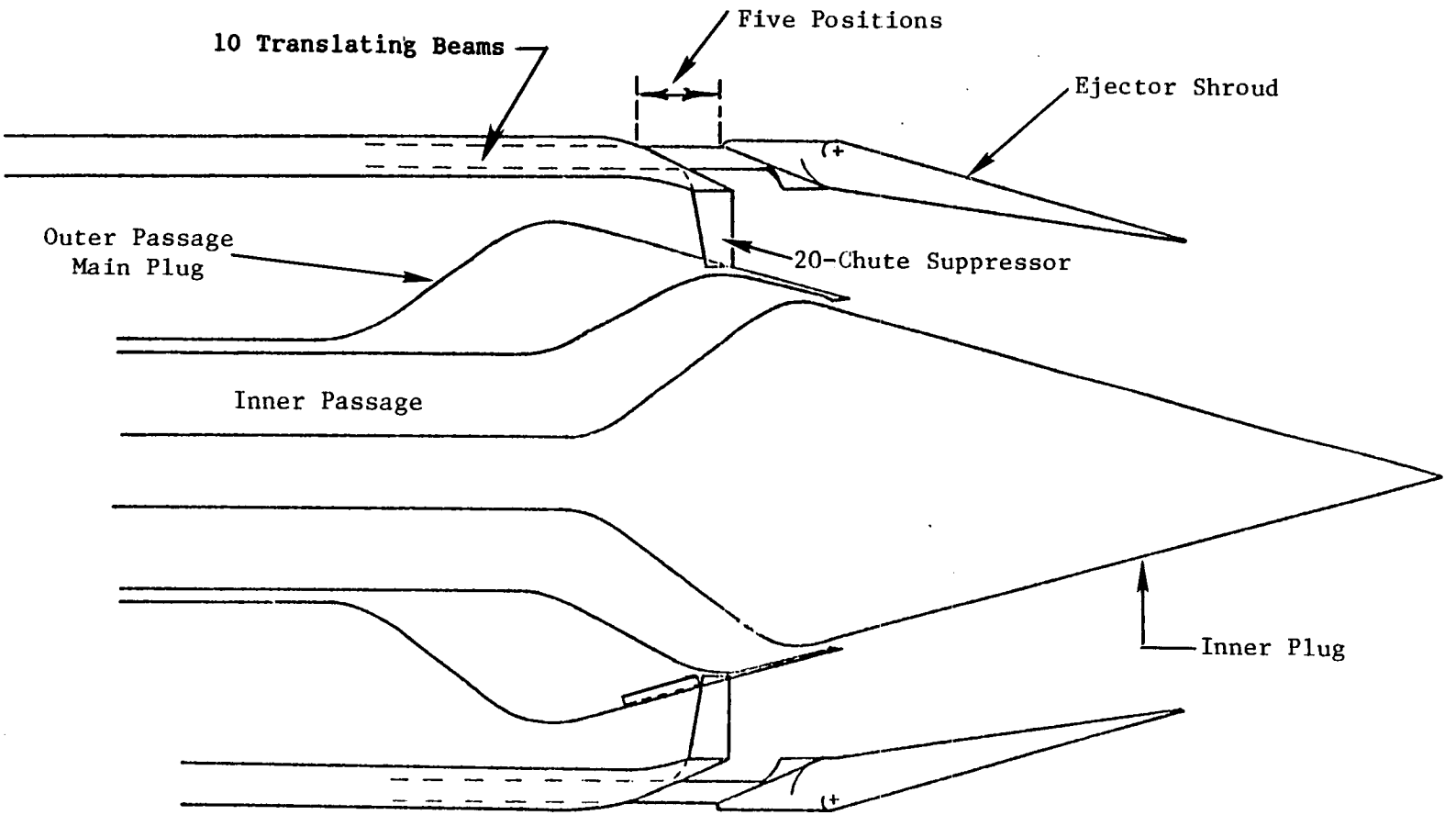

Figure 47. Ejector Shroud Test Configurations Take-Off Mode

The primary reason for the ejector shroud nozzle development is the noise abatement potential associated with it, but also inherent in the ejector design feature is the thrust augmentation benefits available during takeoff. Maximum thrust augmentation is realized at an optimum setback where setback is defined as the distance between ejector leading edge and nozzle shroud boattail faces as shown in Figure 47. To identify the optimum setback position experimentally, five setback provisions were made available, which invariably determined ejector inlet area and hence, the air induction characteristics. During subsonic cruise, transonic acceleration and supersonic cruise modes, the ejector setback is set to zero (equivalent to zero ejector inlet area); the suppressor is stowed and the shroud boattail scalloped cavities left by the stowed chute suppressors are filled by scalloped cavity fillers mounted on ejector leading edge face to provide a smooth path for gas expansion. Figures 47 and 48 show ejector nozzle test configurations, and Figures 49 through 52 show ejector nozzle model dimensional information. Since ejector shroud flap hinges for rotation purposes were not duplicated in the models, shroud model pieces representing the different flight regimes were made of interchangeable solid pieces. The thirteen configurations were tested under varying conditions of tunnel Mach number nozzle bypass ratio (A_{88}/A_8), and outer and inner nozzle pressure ratio (λ_8, λ_{88}) are shown in Table 11. Ejector nozzle model assembly methods are shown in Figure 53, and model photographs of the various Ejector Nozzle Configurations are shown in Figures 54 and 55.

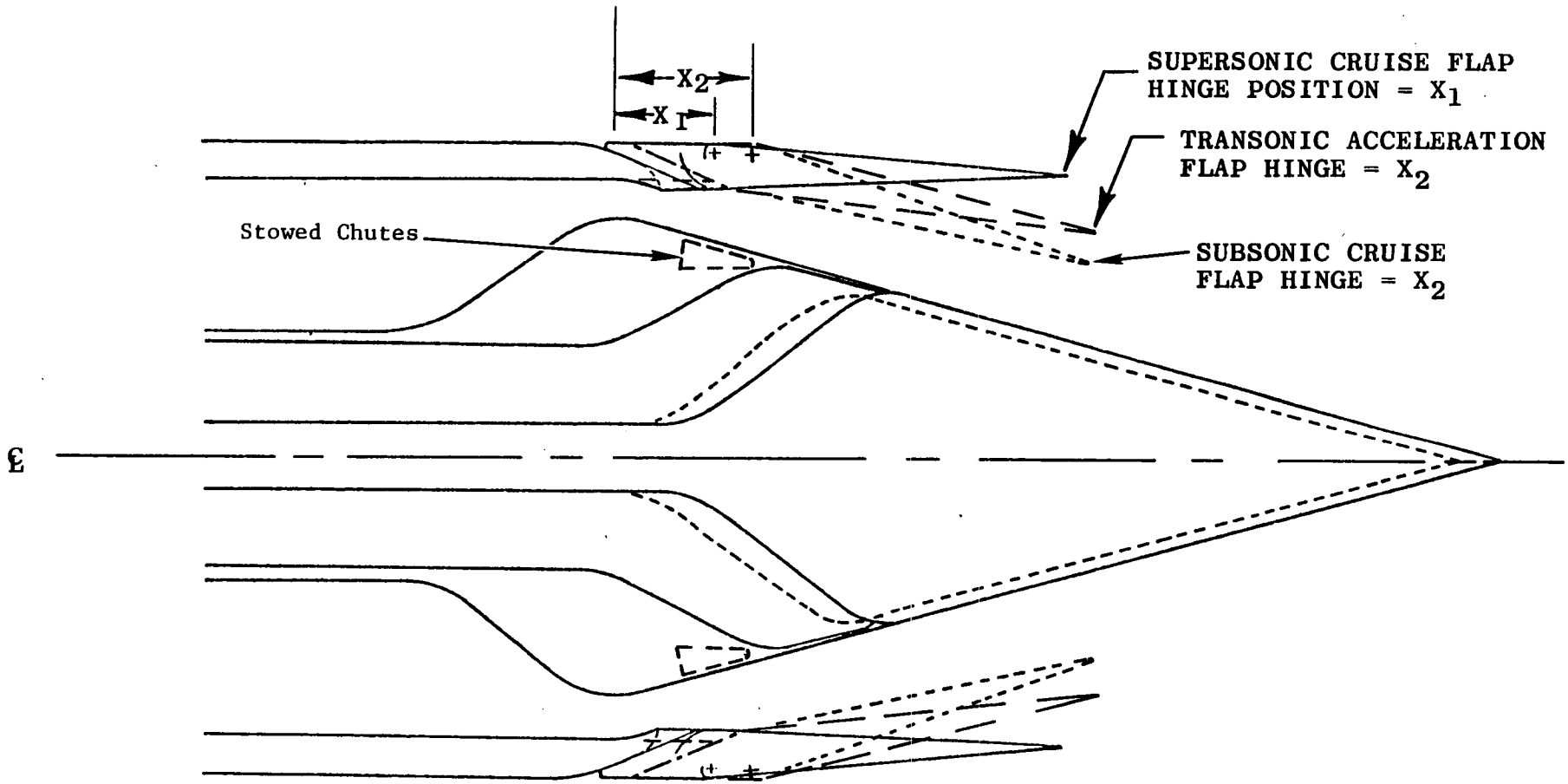

Figure 48. Ejector Shroud Test Configurations: Subsonic, Transonic and Supersonic Modes

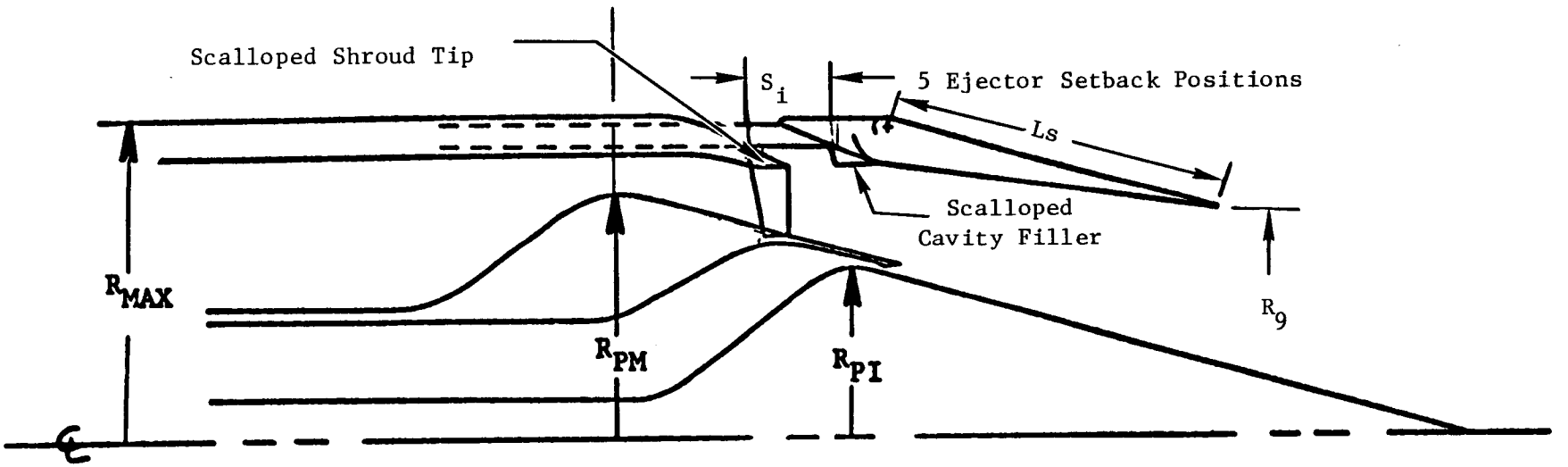

R_{max}	=	45.0 in.			
$Rpm/Rmax$	=	.741	$Ls/Rmax$	=	1.113
$Rpi/Rmax$	=	.525	$R9/Rmax$	=	.715
$S1/Rmax$	=	.089			
$S2/Rmax$	=	.178			
$S3/Rmax$	=	.267			
$S4/Rmax$	=	.356			
$S5/Rmax$	=	.400			

5 Ejector Setback (Inlet) Positions

Model Scale Factor = .1235

Figure 49. Ejector Shroud Nozzle Dimensional Information; Takeoff Configuration

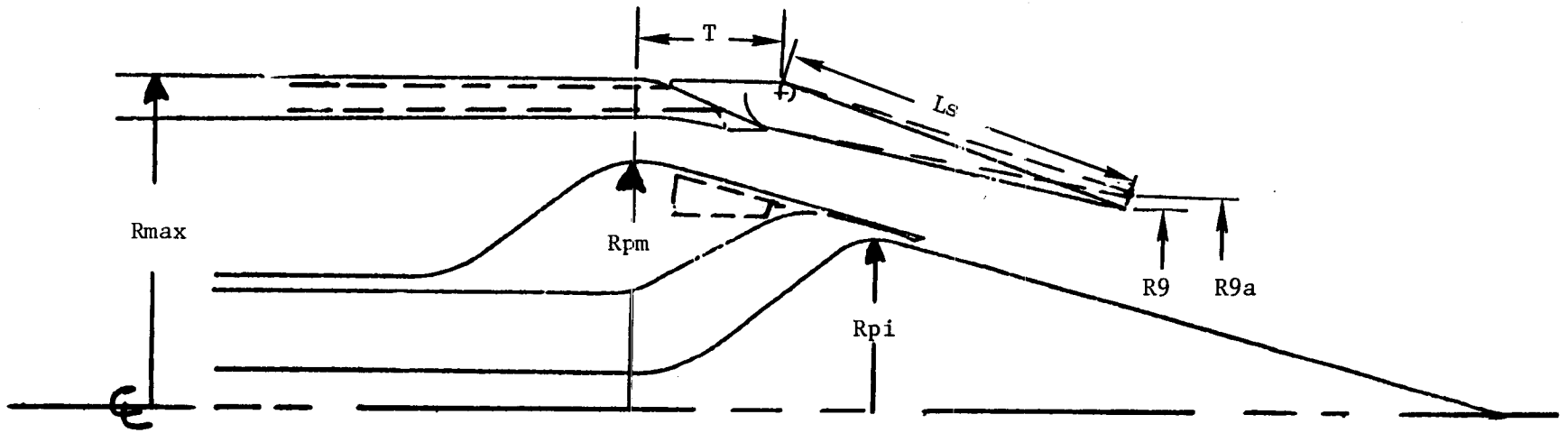

R_{max} = **45.0 in.**

$Rpm/Rmax$ = .741

$Rpi/Rmax$ = .525

$R9/Rmax$ = .629

$Ls/Rmax$ = 1.113

$T/Rmax$ = .401

Model Scale Factor = .1235

R9a =

Figure 50. Ejector Shroud Nozzle Dimensional Information; Subsonic Cruise Configuration

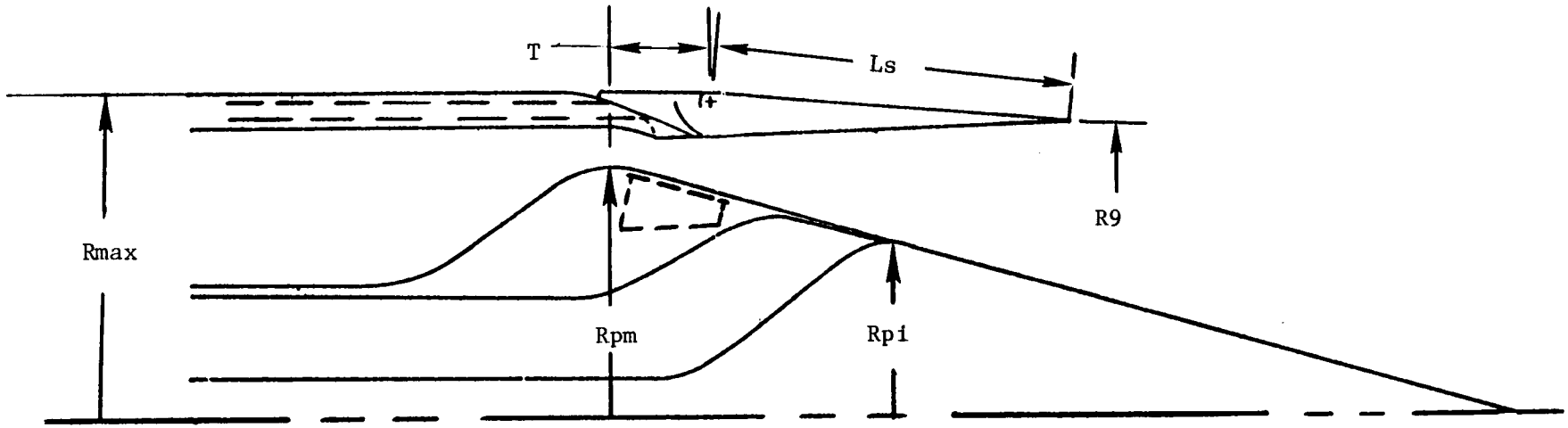

R_{max} = 45.0 in.

$Rpm/Rmax$ = .741

$Rpi/Rmax$ = .525

$R9/Rmax$ = .893

$Ls/Rmax$ = 1.113

$T/Rmax$ = .279

Model Scale Factor = .1235

Figure 51. Ejector Shroud Nozzle Dimensional Information; Supersonic Cruise Configuration

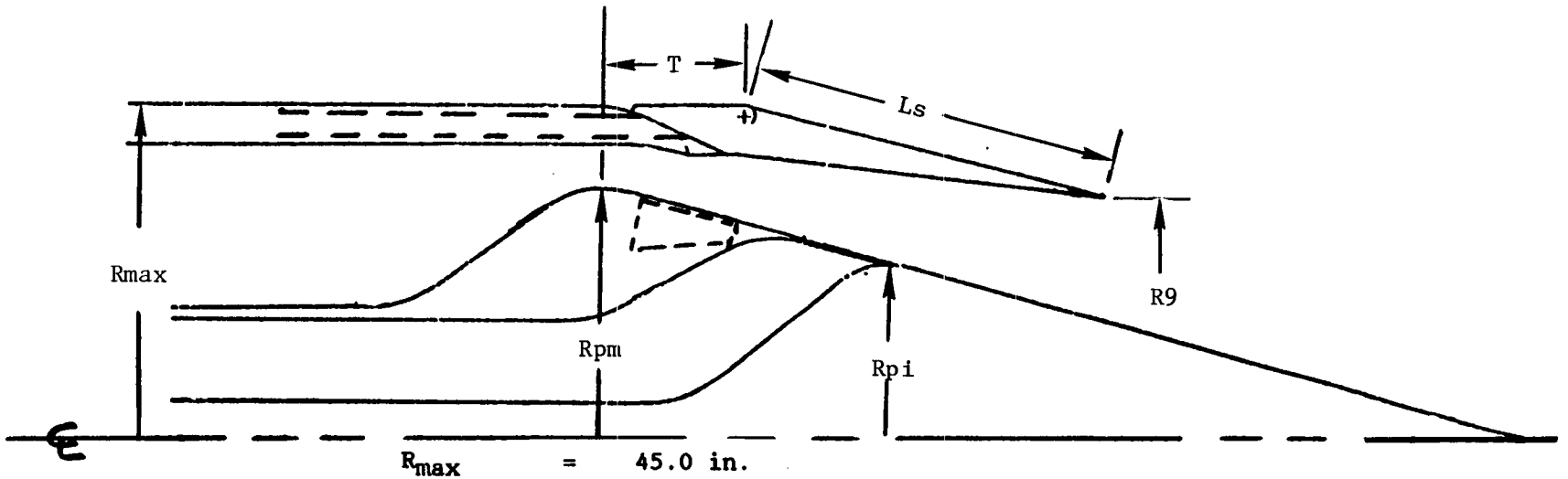

R_{max}	=	45.0 in.
$Rpm/Rmax$	=	.741
$Rpi/Rmax$	=	.525
$R9/Rmax$	=	.728
$Ls/Rmax$	=	1.113
$T/Rmax$	=	.401

Model Scale Factor = .1235

Figure 52. Ejector Shroud Nozzle Dimensional Information; Transonic Acceleration Configuration

TABLE 11

EJECTOR NOZZLE TEST CONFIGURATIONS & VARIABLES

OPERATING MODE	A_{INNER}/A_{OUTER}	SUPPRESSOR FEATURES	EJECTOR SETBACK FS (IN)	NPR
TAKEOFF M=0,.35,.45	.2 ↓ .2	DEPLOYED ↓ DEPLOYED	4 8 12 16 18	2.2 - 3.5
SUBSONIC CRUISE M=.9	0 .13	STOWED STOWED		2.5 - 4.5
TRANSONIC CRUISE M=1.2 (STATIC)	0 0	STOWED SMOOTH PLUG		5 - 9
SUPERSONIC CRUISE M=2.32 (STATIC)	0 0	STOWED SMOOTH PLUG		14 - 22

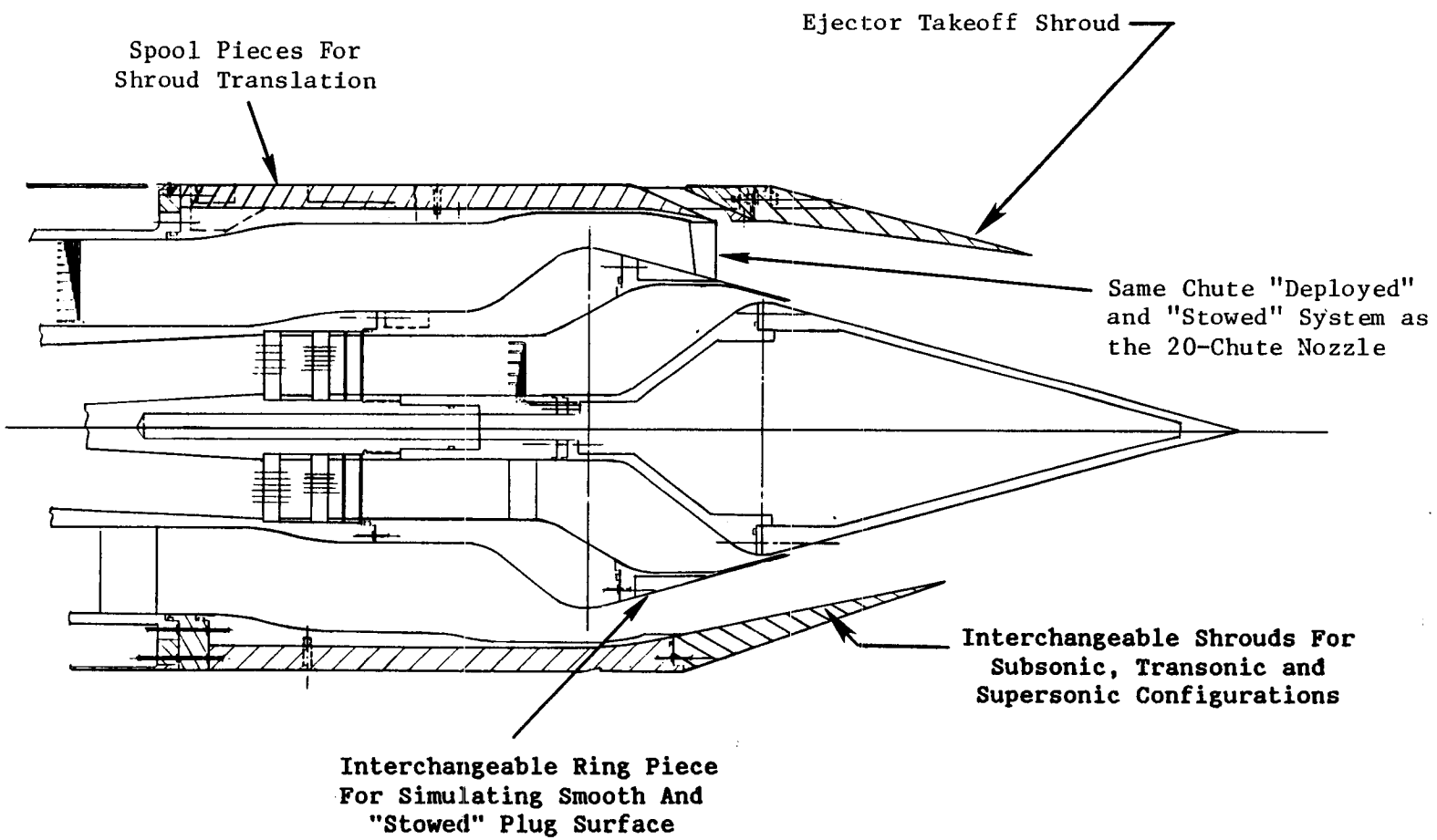

Figure 53. Ejector Shroud Nozzle Model Assembly Methods

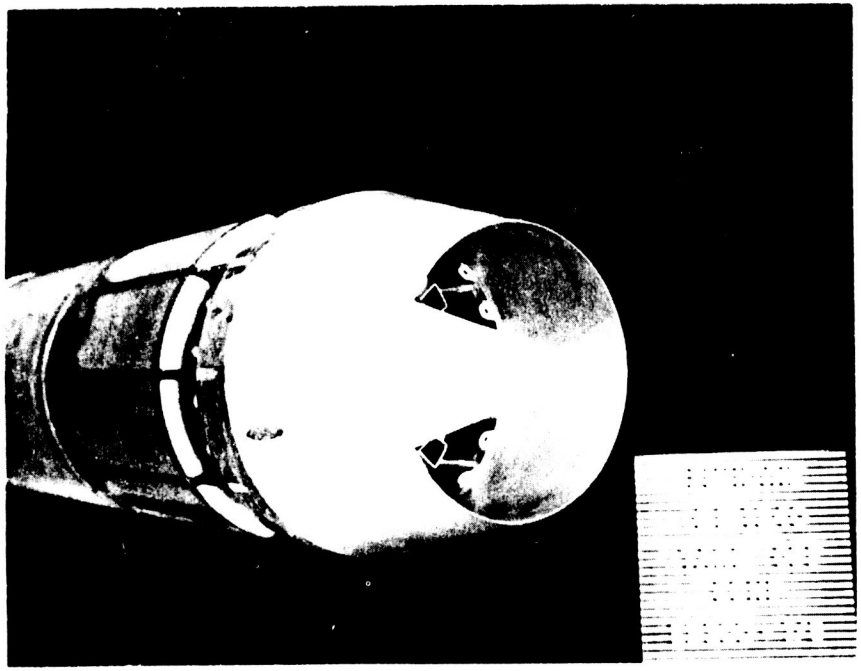

TAKEOFF CONFIGURATION
EJECTOR INLET OPEN
CHUTES DEPLOYED

TAKEOFF CONFIGURATION
VIEW LOOKING AFT

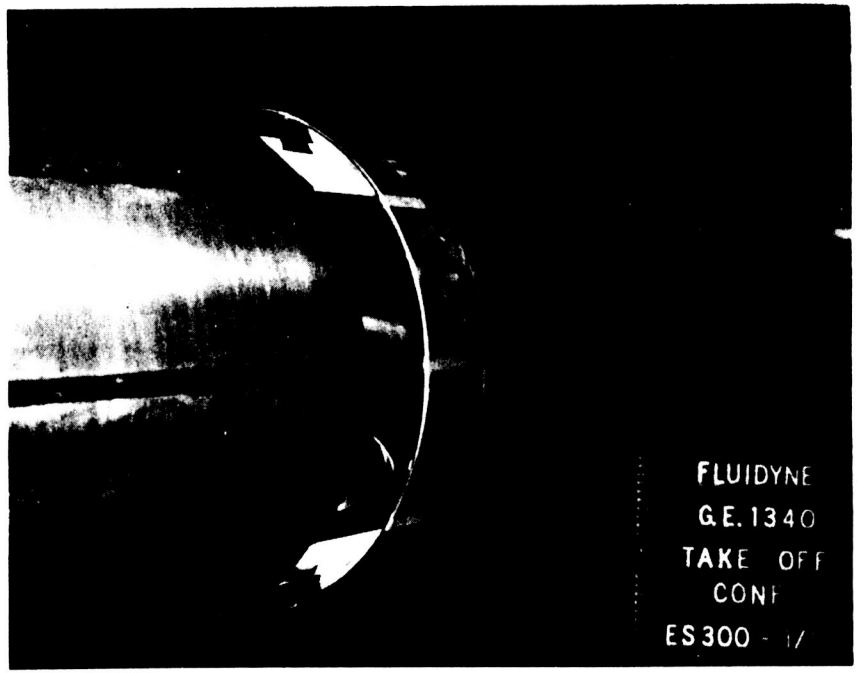

Figure 54. Ejector Shroud Nozzle Model Photographs

SUBSONIC CRUISE CONFIGURATION

EJECTOR INLET CLOSED

CHUTES STOWED

SUPERSONIC CRUISE CONFIGURATION

EJECTOR INLET CLOSED

CHUTES STOWED

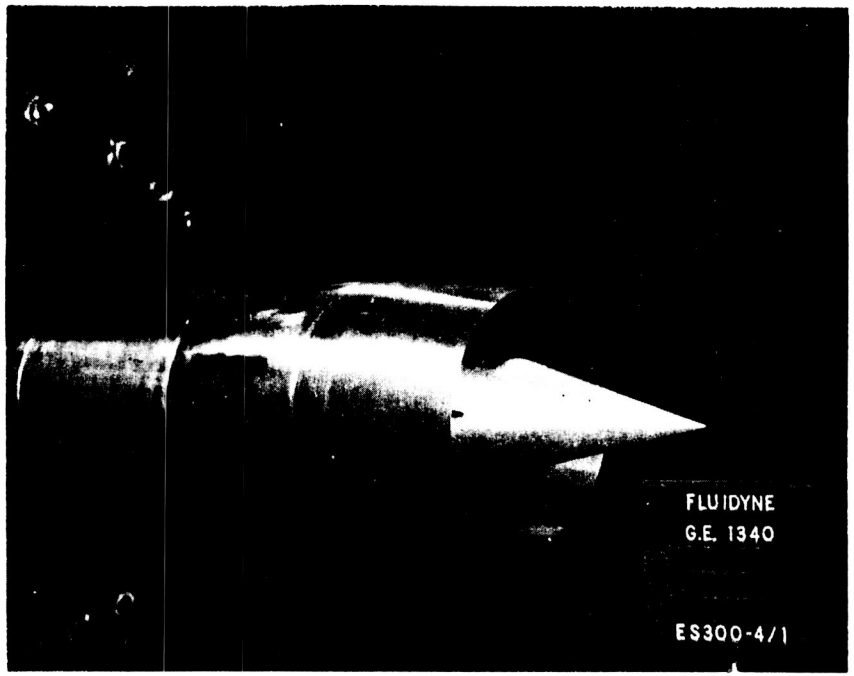

Figure 55. Ejector Shroud Nozzle Model Photographs

10.0 FACILITY DATA REDUCTION PROCEDURES

The following subsections describe facility data reduction procedures (flow rate and thrust measurements) as they apply to the coannular, suppressor and ejector shroud model tests performed in the static stand and in the wind tunnel. Model station notation is defined in Figure 37.

10.1 FLOW RATES

The mass flow rates through the test nozzles were determined using two choked ASME long-radius metering nozzles. The inner nozzle flow rate was determined at Station 1, and the outer nozzle flow rate was determined at Station 5, using the following equations.

$$W_1 = W_{88} = K_1 C_{D_1} A_1 P_{t_1} \Big/ \sqrt{T_{t_1}}$$

$$W_5 = W_8 = K_5 C_{D_5} A_5 P_{t_5} \Big/ \sqrt{T_{t_5}}$$

Total temperatures were measured at the meter charging stations and the critical flow factor, K, was calculated as a function of total pressure and total temperature using an equation of the form

$$K = A_1(T_t + T_t^2) + B_1(T_t + T_t^2)P_t + C_1(T_t + T_t^2)P_t^2$$

or

$$K = A + BP_t + CP_t^2$$

where $A = A_1(T_t + T_t^2)$, $B = B_1(T_t + T_t^2)$, and $C = C_1(T_t + T_t^2)$ and A_1, B_1, and C_1 are coefficients of the polynomial. This equation was obtained by curve-fitting data from Reference 4 and applies for $0 < P_t < 1000$ psia and $460 < T_t < 560$°R.

Meter discharge coefficients were calculated as a function of the throat Reynolds number, using a semi-empirical equation

$$C_D=1-0.184\ RN^{-0.2}$$

Meter geometric throat areas, A_1 and A_5, were 1.0790 and 1.0658 in^2, respectively, and the total pressure for each meter was calculated using the measured static pressure and the isentropic pressure ratio for the measured critical area ratio at the meter charging station. See Figure 37.

Therefore,

$$P_{t_1}=P_{1_c}/.9920 \text{ and } P_{t_5}=P_{5_c}/.9920$$

Calculated flow rates (lb_m/sec) for tests with the flow-through balance system were in the ranges shown:

$12 < W_5 < 23$;	$0 < W_1 < 5$	Wind tunnel tests
$10 < W_5 < 23$;	$0 < W_1 < 5$	Static stand tests

10.2 THRUST MEASUREMENT: DUAL FLOW

Static thrust of nozzle is defined as the axial momentum of the exhuast flow, plus the excess of exit pressure over ambient pressure times the exit area.

$$H=mV_e+(P_e-P_a)A_e$$

For wind tunnel tests, the measured thrust included form and friction drag on the external model surfaces. The actual thrust for the dual flow model tests was determined by applying the momentum equation to the control volume shown in Figure 37. The analysis of axial forces applied to the control volume included

entering stream thrusts (F_1 and F_5), the axial balance force (H_o), various pressure-area terms and the axial exit stream thrust ($H + P_a A_e$). Summing axial forces,

$$H=F_1+F_5+P_2(A_2+\Delta A_2-A_1)+P_6(A_6+\Delta A_6-A_5)+P_4(A_4-A_2-\Delta A_2-A_6-\Delta A_6)-P_a A_4-H_o$$

where p_4 is the pressure inside the cavity surrounding the seal and load cell, and A_4, the forward nacelle cross-sectional area at the support tube metric break station. A_4 ranged between 78.54 in^2 (20-chute) and 97.05 in^2 (ejector shroud). External nozzle boattail drag forces were accounted for in the above equation when models were run in the wind tunnel and are included in the H_o term.

P_a is the ambient pressure surrounding the model. For static stand tests P_4, the balance cavity pressure, is equal to the ambient pressure; and for static tests exhausting to atmosphere, P_a is barometric pressure. Ambient pressure for static tests in the test cabin is the average of test cell static pressure tap readings. Measured wind tunnel plenum pressures were corrected as a function of test section Mach number to determine P_a for wind-on tests.

The stream thrust (F_1 and F_5) is the exit stream thrust of the choked long-radius ASME nozzle and is calculated using a semi-empirical expression at the critical pressure ratio of 1.8929 as shown below:

$$F=GP_t(1+\gamma C_D C_T)(P^*/P_t)$$

The factor G corrects the stream thrust (calculated using ideal gas constants; γ=1.4 and P^*/P_t=.52828) for real gas effects.

Therefore,

$$G=1.00011+AP_t+BP_t^2-C(T_t-560)P_t^{1.9477}$$

where $A = .601347 \times 10^{-5}$
$B = 1.50556 \times 10^{-9}$
$C = 2.2751 \times 10^{-11}$

This equation was obtained by curve-fitting data from Reference 7 and applies for $460<T_t<560°R$ and $0<P_t<1000$ psia. Thrust coefficients C_{T_1} and C_{T_5} were thus calculated as follows:

$$C_T=1-0.109\ RN^{-0.2}$$

10.3 THRUST MEASUREMENTS: SINGLE PASSAGE

For single meter, single passage configurations, the redundant meter was blanked off at the meter charging station. Therefore, for outer passage only tests, Station 1 meter was blanked off and the inner passage flow conditioning screens replaced with a blank-off plate to avoid pressurizing (or evacuating the P_2 seal cavity. In this case the blank-off seal cavity was vented to Station 4, which is at ambient pressure for static stand tests and very nearly at ambient pressure for wind tunnel tests. This venting was necessary to prevent a large tare force which otherwise would result from the difference between barometric pressure (trapped in the blanked-off cavity) and P_4 during tests.

11.0 MODEL DATA REDUCTION PROCEDURES

The following subsections describe model data analysis procedures used for the coannular baseline, 20-chute suppressor, and the Ejector Shroud Nozzle tests. Station notation is defined in Figure 37.

11.1 MASS-MOMENTUM AVERAGE P_t

To obtain the best representative model charging station total pressures, the Mass Momentum Average Total Pressure technique was used. This method yields a better representative average total pressure in a nonuniform flow field by averaging flow properties that simultaneously satisfy both continuity and momentum equations.

For the tests, the total pressure profile at each of the charging station rakes was integrated using the mass-momentum technique, assuming a linear variation between the static pressures measured on the inner and outer walls at each rake. The average charging station total pressure was then defined as the average from the separate rake integrations.

11.2 PRESSURE DATA

Pressure instrumentation for facility and charging station were described previously. All other pressures in the model were measured using the PSI system. Model pressure data were reduced to absolute pressure (psia) and dimensionless ratios (P/P_a, $P/{}^{P}t_{88}$, $P/{}^{P}t_{8}$). See Table 12 for coannular, 20-chute and ejector shroud nozzle instrumentation summary.

TABLE 12

COANNULAR, 20-CHUTE AND EJECTOR SHROUD NOZZLE INSTRUMENTATION SUMMARY

NOZZLE TYPE	OPERATING CONFIGURATION	QTY. OF PS TAPS
COANNULAR BASELINE	TAKEOFF	53
	SUBSONIC	53
	SUPERSONIC	43
20 - CHUTE SUPPRESSOR	TAKEOFF	61
	SUBSONIC CRUISE	53
	SUPERSONIC	43
EJECTOR SHROUD	TAKEOFF	65
	SUBSONIC	60
	TRANSONIC	47
	SUPERSONIC	47

COMMON INSTRUMENTATION

OUTER PASSAGE - 4 TEN-ELEMENT PT RAKES
4 PS TAPS

INNER PASSAGE - 2 FIVE-ELEMENT PT RAKES
6 PS TAPS

TEMPERATURE MEASUREMENT - JOULE-THOMPSON METERS

11.3 DISCHARGE COEFFICIENTS

Nozzle discharge coefficients were defined as the ratio of actual flow rate through the nozzle, to the ideal isentropic flow rate at the overall nozzle pressure ratio. Defining nozzle pressure ratios as $\lambda_{88} = {}^{P}t_{88}/P_a$ and $\lambda_8 = {}^{P}t_8/P_a$ where P_a is the ambient pressure.

The discharge coefficients were calculated as

$$C_{D_{88}}=W_{88}/W_{88_i}=W_1/W_{88_i} \quad \text{and} \quad C_{D_8}=W_8/W_{8_i}=W_5/W_{8_i}$$

$$W_{88_i}={}^{P}t_{88}A_{88}K_{88}(A^*/A)_{88}\Big/\sqrt{T_{t_{88}}}$$

$$W_{8_i}={}^{P}t_8A_8K_8(A^*/A)_8\Big/\sqrt{T_{t_8}}$$

${}^{T}t_{88}$ and ${}^{T}t_8$ were calculated from the measured values of ${}^{T}t_1$ and ${}^{T}t_5$ by subtracting the temperature drop due to throttling of the flow between the meters and test nozzles. These temperature drops were calculated from Joule-Thomson throttling data.

K_{88} and K_8 are the critical flow factors defined earlier.

Model throat areas were determined from model throat measurements.

11.4 THRUST COEFFICIENTS

The thrust coefficient was defined as the ratio of actual thrust to the ideal thrust of the outer passage flow (expanded

from P_{t_8} to P_a) plus the ideal thrust of the inner passage flow (expanded from $P_{t_{88}}$ to P_a). Thus,

$$C_T = \frac{H}{m_{88}v_{i_{89}} + m_8 v_{i_9}} \quad \text{where H = Net thrust}$$

The ideal thrust (mv_i) was calculated from the actual mass flow and the dimensionless ideal thrust function based on nozzle pressure ratio. The ideal thrust was calculated as:

$$m_8 v_{i_8} = (A^*/A)_8 \; C_{D_8} A_8 P_{t_8} \; (m_i v_i / P_t A^*)_8$$

$$m_{88} v_{i_{88}} = (A^*/A)_{88} C_{D_{88}} A_{88} P_{t_{88}} (m_i v_i / P_t A^*)_{88}$$

where $$\frac{mvi}{P_t A^*} = \gamma \left(\frac{2}{\gamma+1}\right)^{\frac{\gamma}{\gamma-1}} \left(\frac{\gamma+1}{\gamma-1}\right)^{1/2} \left[1 - \left(\frac{1}{\lambda}\right)\frac{\gamma-1}{\gamma}\right]^{1/2}$$

In flight (wind-tunnel) thrust coefficients were referred to as "thrust-minus-drag-coefficients" because the measured thrust includes form and friction drag on the external model surfaces.

12.0 DATA ANALYSIS PROCEDURES

The exhaust system thrust coefficient defined as the actual thrust produced divided by the ideal thrust is a measure of exhaust system efficiency. However, the actual thrust measured is influenced by pressure losses due to flow duct aerodynamic design, instrumentation rakes, fan and turbine frames and struts, etc., as well as overall flow surface conditions. For instance, two identical nozzles, same areas, geometry, flow conditions, but different instrumentation, frames, struts and surface conditions will register different levels of actual thrust by virtue of different levels of pressure losses manifested by different flowpath obstacles. The differences in thrust coefficients for the above nozzles, therefore, are indicative of pressure losses associated with the flowpath obstacles and external influences and not the isolated nozzles in question. It becomes important, then, as a means of evaluating the efficiency of an isolated exhaust system to discount all hardware dependent losses in order to obtain a fair appraisal of the exhaust system geometry. The efficiency of such isolated nozzle is termed the exit thrust coefficient.

A similar situation exists between subscale and full scale exhaust systems where though similar, geometrically, are very different in many respects, such as absolute operating pressures and temperatures, Reynolds numbers, instrumentation, construction details, surface conditions, etc. For this reason it is imperative to establish a common reference of equivalence from where proper adjustments can be made to transform model coefficients to full scale coefficients and vice versa. This common reference is the exit thrust coefficient--a measure of nozzle geometry effectiveness for both the model and the full scale nozzle.

The exit thrust coefficient establishes a geometric similarity between test model and full scale nozzle and therefore represents the thrust coefficient of both nozzles with system

dependent calculable loss effects removed, i.e., skin friction, rake effects, base drag, protuberances, gaps, etc. To obtain full scale coefficients, full scale nozzle dependent losses of ducts, struts, links, rakes, bolts and other protuberances are calculated or tested and subtracted from the exit coefficients. In this case the loss items are flight path dependent due to Reynolds number effects and are treated accordingly.

The exit coefficient is appropriately a measure of nozzle angularity loss and expansion efficiency. Ideally, the exit coefficient for a perfect nozzle should be unity but a practical expectation is 0.995 $\pm$ .0025. Thus, a nozzle with an exit thrust coefficient near unity is an excellent performing design provided it is operating at peak design, and the nozzle cannot be made more favorable based on other trades. However, introduction of augmentation devices can cause the exit coefficient to go above unity as has been noted for ejector nozzles.

For this program, exit and full scale coefficient analyses were performed for all three nozzle systems. Model test coefficients were transformed to exit coefficients, to rid them of model dependent losses, and finally transformed to full scale coefficients to put back full scale dependent loss effects as evidenced by higher temperatures, Reynolds numbers, etc. The process was accomplished by adding the sum of model dependent losses to the model coefficients to obtain exit coefficients and similarly subtracting full scale dependent losses from the exit coefficients to obtain full scale coefficients. The full scale losses were calculated using full scale dimensions and actual flight path engine aero-thermodynamic variables.

13.0 PERFORMANCE RESULTS AND DISCUSSION

All nozzle concepts tested showed good exit coefficient characteristics within practical limits for conventional nozzles with the exception of the ejector subsonic cruise configuration and, to a lesser degree, the 20-Chute takeoff configuration as shown in Figure 56 in a bar chart form. These two configurations by virture of their unconventional features exhibited more exit losses.

The ejector subsonic cruise aerodynamic performance reduction resulted from the ejector takeoff acoustics and supersonic cruise aerodynamics optimization process which compromised subsonic cruise performance. In a similar manner the 20-chute takeoff aerodynamics was subordinated to the takeoff acoustics and hence the reduced performance, even though to a lesser degree. However, for the ejector takeoff configuration, which also embodies the 20-chute suppressor features, ejector thrust augmentation appears to make up for the suppressor exit losses. For this reason ejector takeoff exit coefficients show values sometimes higher than unity in static tests to demonstrate the effect of ejector thrust augmentation. The full scale wind-on installed thrust coefficients (Figures 57-60) appear fairly good for all configurations tested except, once again, the ejector subsonic cruise configuration. Stackup of performance and loss coefficients showed that for the ejector subsonic cruise configuration, the losses are mainly from internal expansion and boattail drag. The data will be particularly important for tuning the ejector takeoff and subsonic cruise configuration geometries to improve performance.

Despite the losses mentioned above, the ejector nozzle shows high potential for being an efficient expansion exhaust system. Development work should focus on improving the calculable loss items, enhancing the mechanical system, and tuning

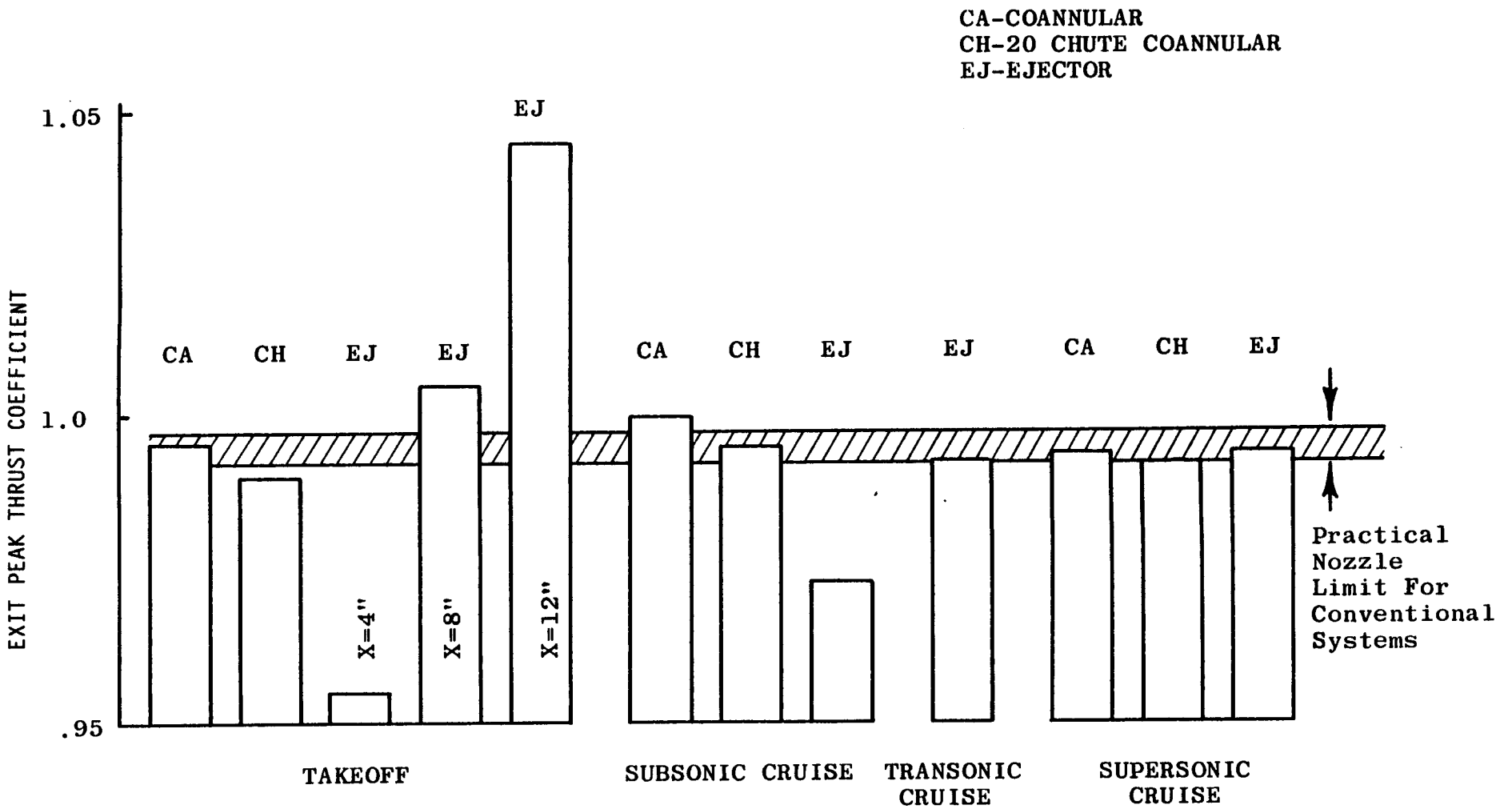

Figure 56. Nozzle Exit Peak Thrust Coefficient Results

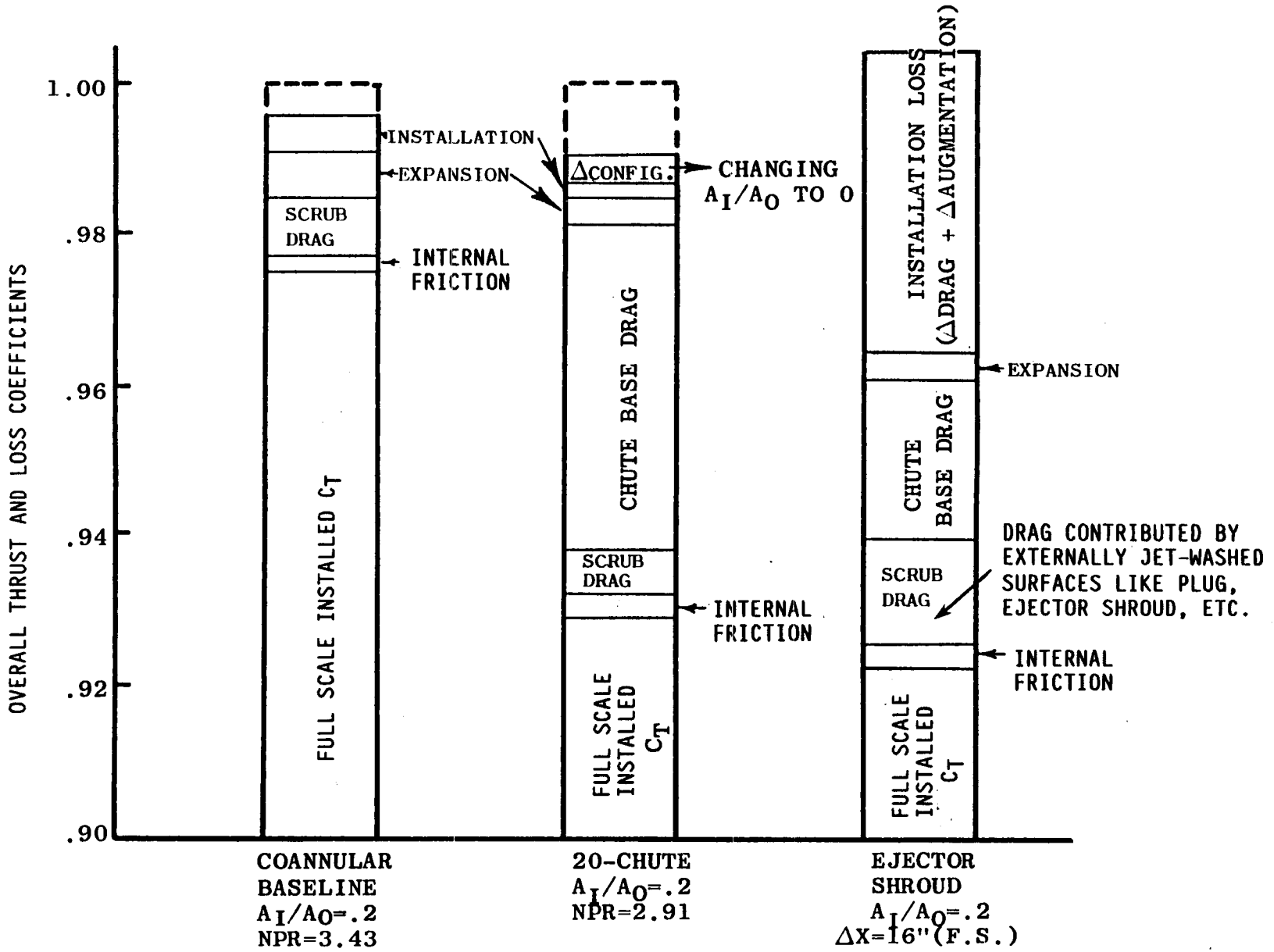

Figure 57. Nozzle Full Scale Thrust and Loss Coefficient Stackups Takeoff Mode; M = .35.

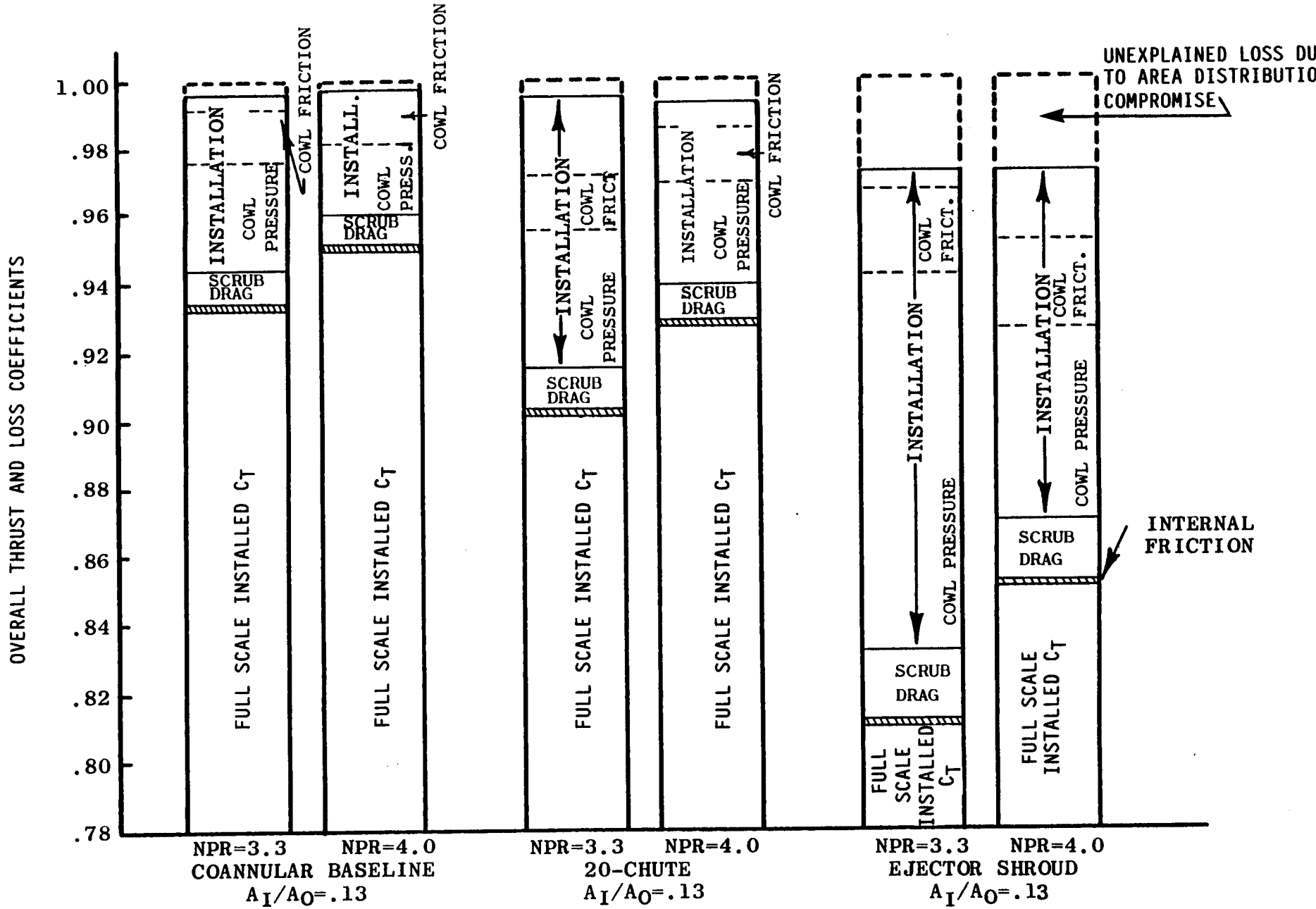

Figure 58. Nozzle Full Scale Thrust and Loss Coefficient Stackups Subsonic Cruise Mode; M = .9.

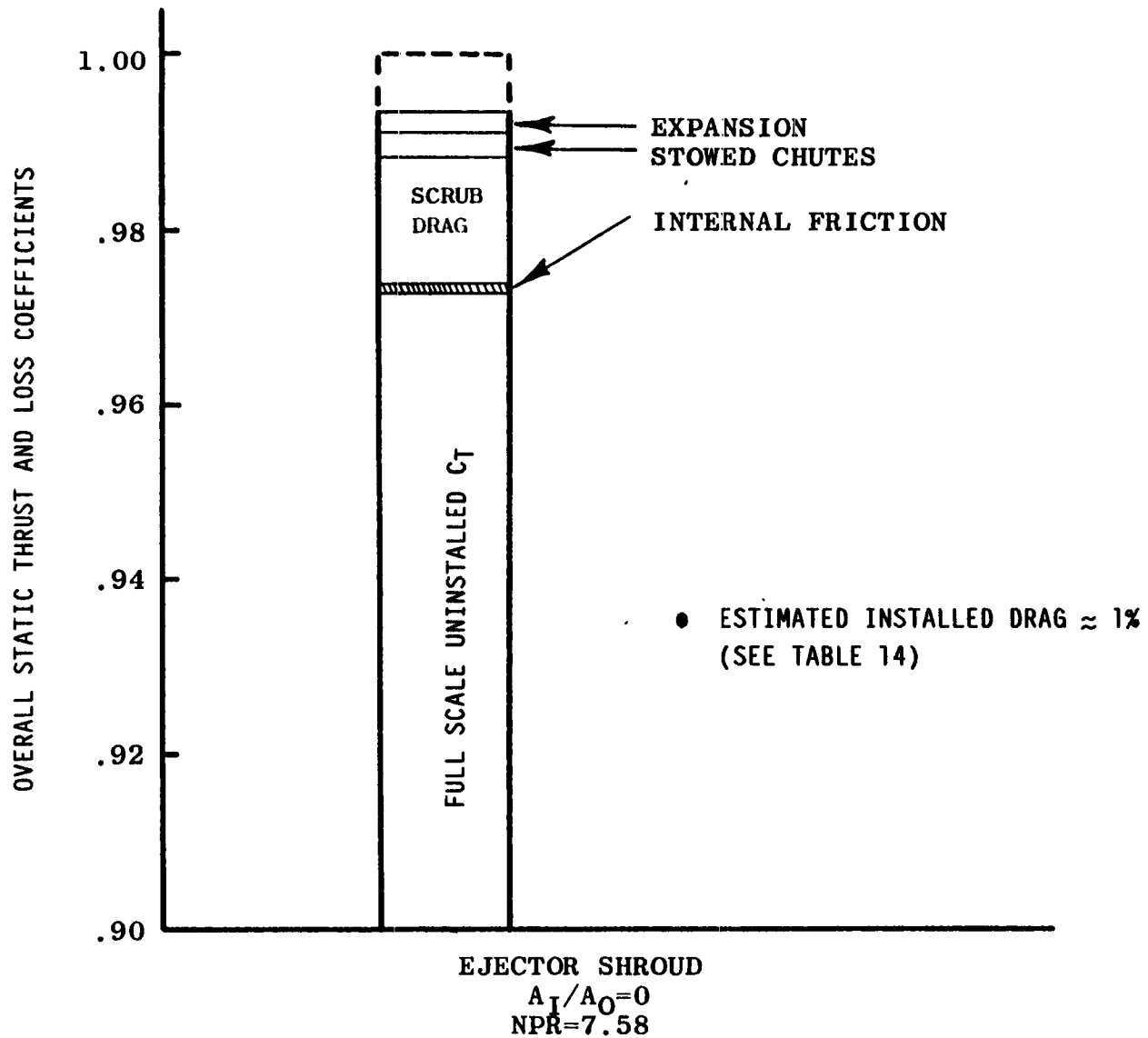

Figure 59. Nozzle Thrust and Loss Coefficient Stackups Transonic Acceleration Mode; M = 1.2 (Static).

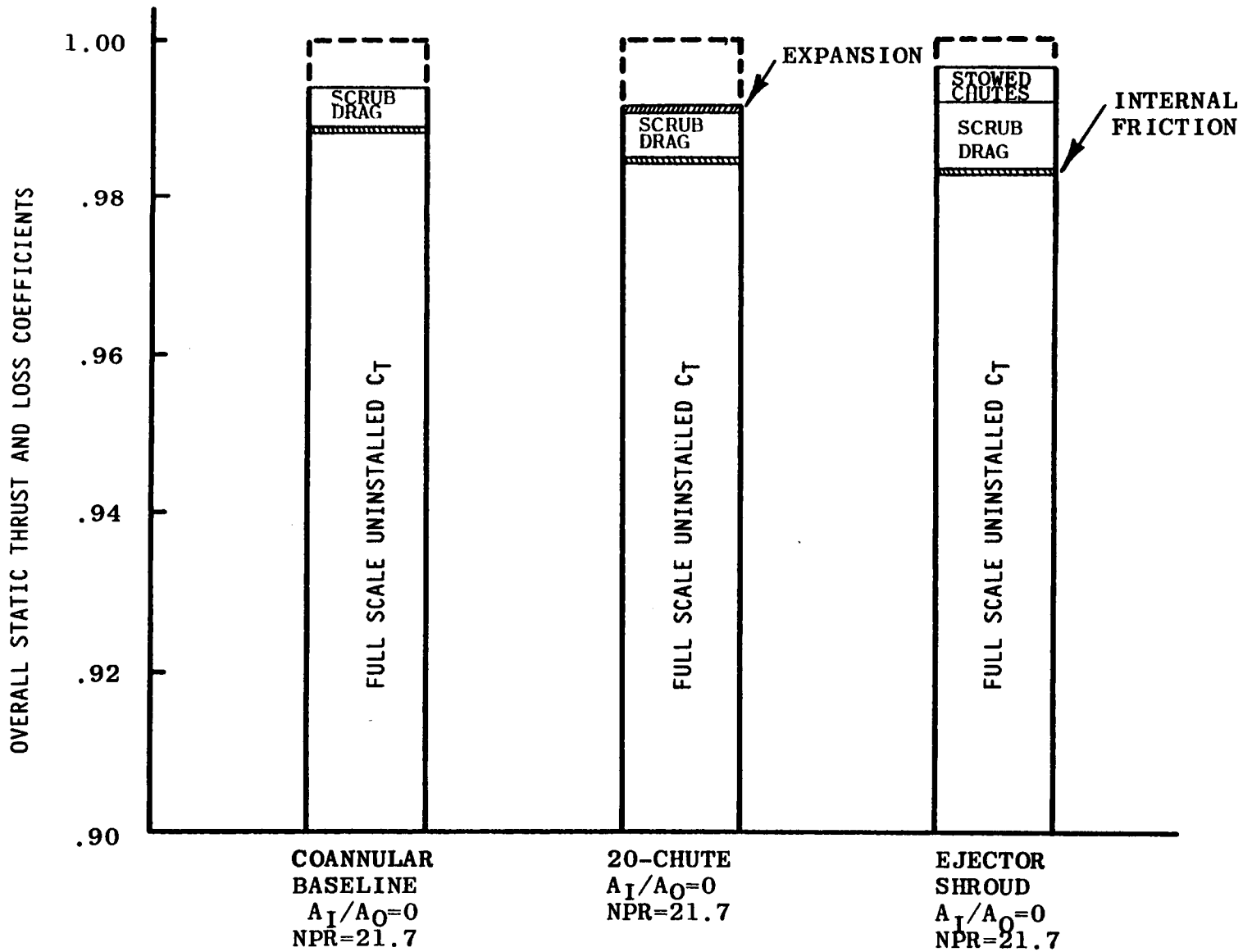

Figure 60. Nozzle Thrust and Loss Coefficient Stackups Supersonic Cruise Mode; M = 2.32 (Static).

individual configurations for the mission design points. The full scale thrust and loss coefficient stackup bar charts shown in Figures 57 through 60 are an important roadmap for identifying development needs.

Nozzle afterbody drag characteristics behave in relation to nozzle sizing parameter $A9_{external}/A_{max}$ as defined in Figures 61 and 62. Therein, the low afterbody drag nozzles like the coannular, the 20-chute, and the ejector supersonic cruise configurations show a relatively higher $A9_{external}/A_{max}$ ratios than the Ejector subsonic cruise configuration which shows high afterbody drag. One of the ways of improving the ejector subsonic cruise performance is to find a means of increasing the $A9_{external}/A_{max}$ ratio. Solutions along these lines are shown later.

As shown in Figure 62, the Ejector Area Ratio (EAR) varied with ejector setback due to model construction techniques. No specific test was conducted to ascertain what an optimum EAR should be. It is another potential area of investigation to bring substantial improvement to Ejector Shroud Nozzle System.

The following discussions provide a synopsis of the test data for each basic configuration.

13.1 COANNULAR NOZZLE

The coannular nozzle is an efficient thrust producing nozzle. It is generally smaller in diameter and has low boattail angle in relation to the other nozzles. Though endowed with high thrust coefficients, its poor overall acoustic suppression qualities limits its potential for the AST mission as shown in Task 2 mission analysis studies.

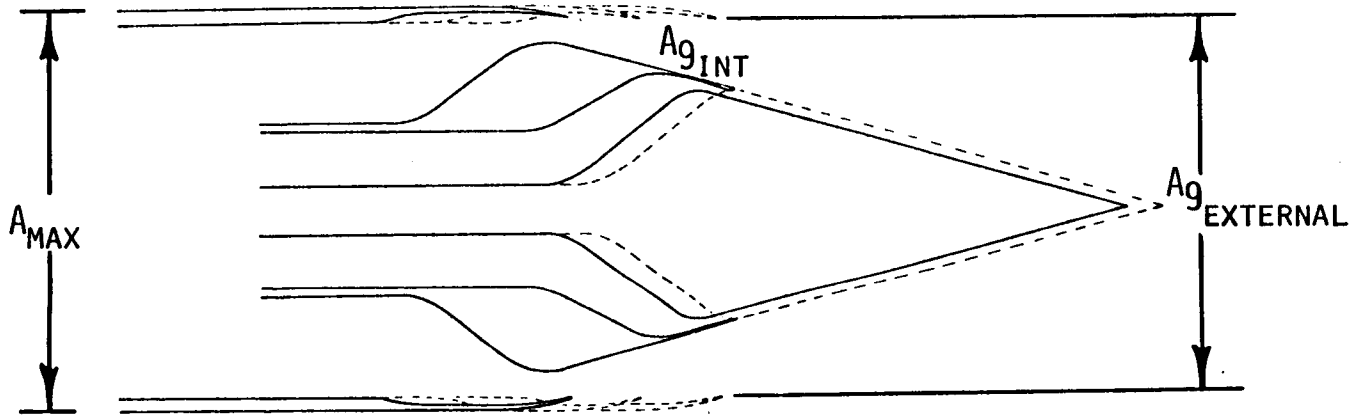

	CONFIGURATION	A_9 INTERNAL/A_8	A_9EXTERNAL/A_8	A_9EXTERNAL/A_{MAX}	NPR DESIGN
COANNULAR BASELINE:	TAKEOFF	1.0	3.62	.87	3.5
	SUBSONIC	1.15	2.84	.87	3.3
	SUPERSONIC	1.85	3.19	.87	21.7
20-CHUTE SUPPRESSOR:	TAKEOFF	1.0	3.60	.89	2.9
	SUBSONIC	1.15	3.17	.89	3.3
	SUPERSONIC	1.95	3.56	.89	21.7

Figure 61. Coannular and 20-Chute Nozzle Sizing Results

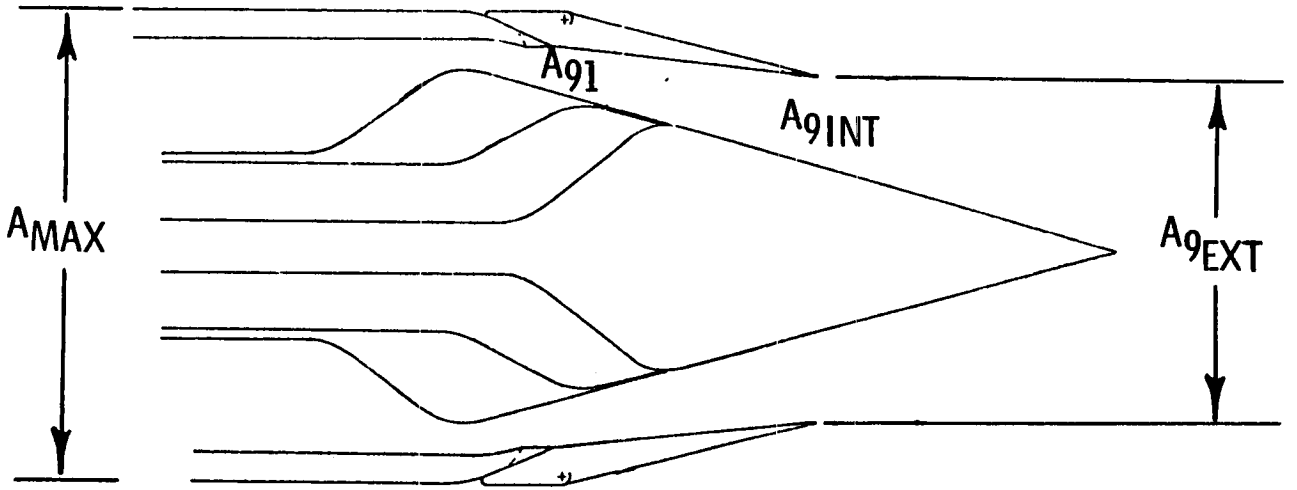

CONFIGURATION	EJECTOR SETBACK (FS)	A_{9INT}/A_8	A_{9EXT}/A_8	EJECTOR AREA RATIO A_{91}/A_{91NT}	NPR DESIGN	A_{EXT}/A_{MAX}
TAKEOFF	4	2.08	2.55	1.07	2.9	0.51
	8	2.14	2.55	1.03	2.9	0.51
	12	2.20	2.55	1.00	2.9	0.51
	16	2.25	2.55	0.97	2.9	0.51
	18	2.27	2.55	0.95	2.9	0.51
SUBSONIC	0	1.15	1.74	--	3.3	0.40
TRANSONIC	0	1.76	2.32	--	7.7	0.53
SUPERSONIC	0	3.22	3.93	--	21.7	0.80

Figure 62. Ejector Nozzle Sizing Results

Takeoff - Figures 56 and 57

The takeoff configuration is a conic nozzle for acoustic reasons and due to its smaller diameter the takeoff NPR is 3.5 as opposed to 2.9 for the others, to provide the necessary mass flow.

The measured peak exit coefficient is .996 at NPR=2.2, well within the expected values for conventional nozzles but it is operating off peak. The full scale expansion loss at 3.5 NPR is 1.5%; however, the plug recovers about 0.3%. The inner nozzle open condition provides a slight performance improvement due to lower friction. The installed performance loss is approximately 1% at takeoff.

Subsonic - Figures 56 and 58

The measured peak exit thrust coefficient is approximately unity, indicating that near ideal expansion has been achieved for the design. The inner nozzle in the open position suggests a slight improvement in installed performance. The subsonic cruise installed performance loss is approximately 3.5% at an NPR=3.3.

Supersonic - Figures 56 and 60

The measured peak exit thrust coefficient of 0.994 is a good design value, and the static installed performance is 0.989. Because of low afterbody drag characteristics for the coannular, the overall installed performance can be expected to be very good.

13.2 20-CHUTE NOZZLE

The 20-chute configuration design is similar to the coannular nozzle with the exception of the 20-chute mechanical suppressor for additional noise suppression at takeoff. For

non-takeoff operations it maintains some of the high thrust coannular-like features when the chutes are stowed. It has a larger diameter than the coannular as a condition for satisfying the high chute radius ratio requirements for acoustic effectiveness. The 20-chute sacrifices a little performance for acoustic suppression, and the slightly larger diameter exacts some drag losses.

Takeoff - Figures 56 and 57

The measured peak exit coefficient is 0.991 at NPR=2.2 and decreases when the inner nozzle is opened; a condition contrary to the coannular nozzle behavior. The difference here is that the deployed chutes at takeoff operate as twenty discrete conic nozzles whose jets mix only towards the end of the plug. This may be why it does not take advantage of the lower friction plug for inner-nozzle-open condition. The lower than expected exit coefficient is slightly below the practical conventional limits. The chutes account for over 1% internal friction loss at takeoff and an additional 1/2% installed. The net installed efficiency loss of the 20-chute relative to the coannular nozzle is approximately 4% at takeoff.

Subsonic Cruise - Figures 56 and 58

The measured peak exit coefficient is 0.995, an excellent value. The 20-Chute has approximately 3% additional installation loss relative to the coannular at subsonic cruise. This performance loss is attributable to the shape and higher projected area of the scalloped cowling.

Supersonic Cruise - Figures 56 and 60

The peak exit coefficient is 0.992 and is evaluated as fair. The reason may be the unconventional scalloped cowling. The static overall thrust coefficient is 0.985, a good value.

13.3 EJECTOR NOZZLE

The ejector nozzle is an integration of an acoustically treated ejector shroud and a 20-chute nozzle. The integration made it possible for the ejector nozzle to satisfy the AST mission goals. The overall performance was good except at the subsonic cruise point. The combination of good overall aerodynamic and acoustic performance provided the ejector nozzle with the best mission results of the three exhaust systems studied. The subsonic cruise configuration is vulnerable to high boattail drag and poor internal performance. This stems from AST engine/exhaust system sizing guidelines which size engine/exhaust systems for noise at takeoff and for aerodynamic efficiency at supersonic cruise. As a result, the intermediate subsonic and transonic cruise points are decided on "best available performance to satisfy thrust requirements" basis. In this particular case it appears the subsonic cruise cycle condition is not compatible with the configuration design. The result is higher than expected installation losses. Opportunity exits, however, to improve these intermediate cycle points, and that is addressed later.

Takeoff - Figures 56 and 57

The ejector nozzle takeoff performance has a strong dependence on ejector setback and the results indicated a maximum ejector augmentation corresponding with a setback between 16 and 18 inches, full scale . Variation of ejector takeoff performance with setback is shown in Figure 63. The measured exit static thrust coefficient is above unity for a setback of 12 inches (FS, Figure 56) indicating the extent of ejector augmentation at Mach zero. Incidentally, 12 inches is the largest setback tested statically. The gains in ejector augmentation were, however, slightly overcome by large installation and scrubbing drag losses as shown in Figure 57. It is particularly worthy of notice that

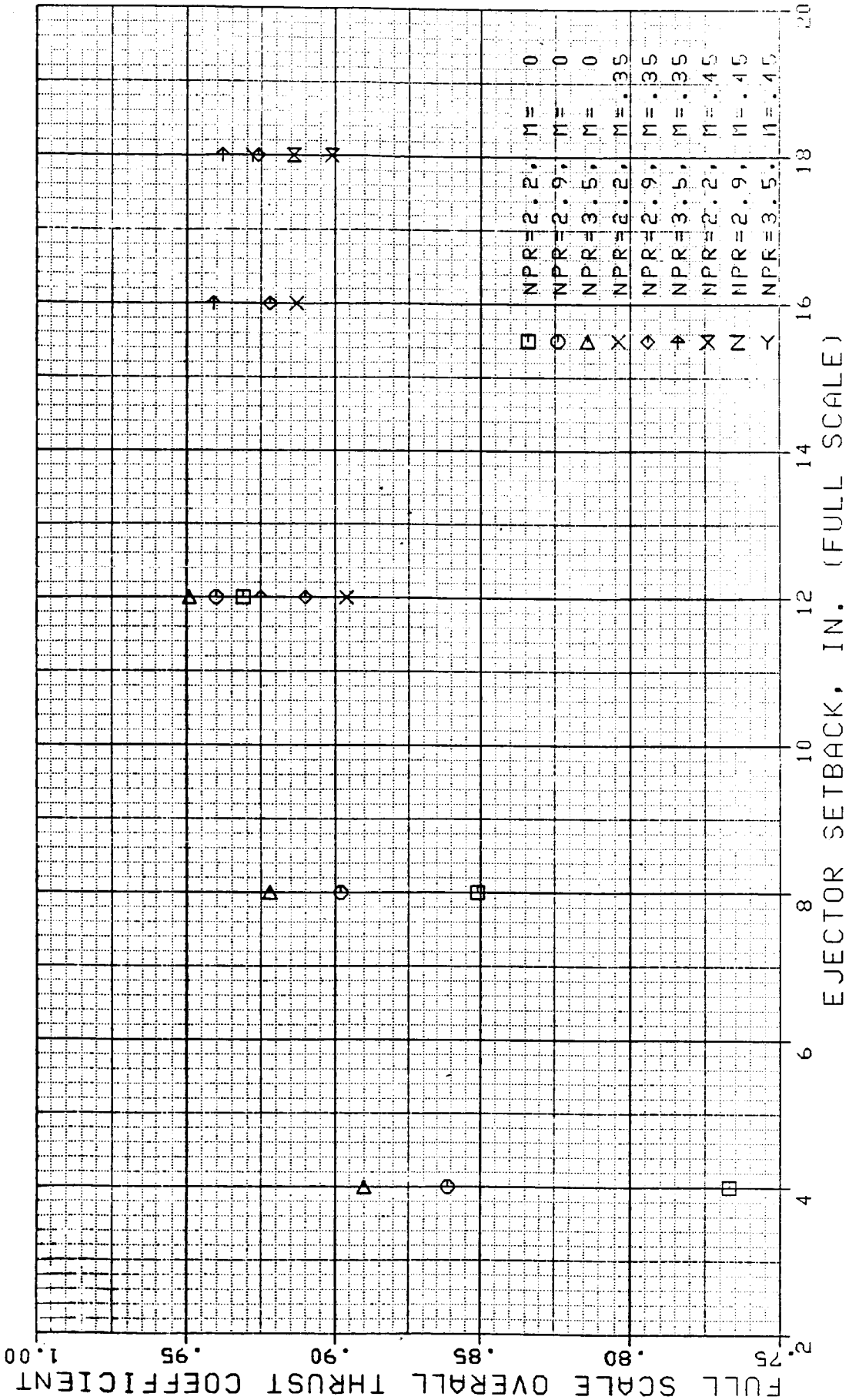

Figure 63. Variation of Ejector Takeoff Performance With Setback

the suppressor chute base drag was reduced by about half by the installation of ejector at the takeoff condition. The overall ejector takeoff installed performance is about .5% lower than the 20-chute nozzle.

Subsonic Cruise - Figures 56 and 58

The ejector subsonic cruise configuration is a compromise between takeoff acoustics and supersonic cruise aerodynamics. The measured peak exit thrust coefficient at Mach zero is 0.973, a low value. This compromise resulted in the internal nozzle expansion-contraction feature that may have caused over 2% loss in full scale thrust coefficient. This 2% loss estimate is conjectured on the basis of a large unexplained loss component on top of the ejector shroud subsonic cruise bar chart in Figure 58. Such large unexplained loss is usually indicative of some nozzle deficiency, and for the ejector shroud subsonic cruise nozzle configuration with less than ideal internal area distribution that anomaly becomes a prime suspect. The design compromise also resulted in a high boattail angle with about 13% installation loss. The installation loss has been verified by nozzle pressure integrations.

The ejector takeoff configuration was tested under subsonic cruise conditions to determine if the lower boattail angle could manifest itself in a lower boattail drag and an overall full scale thrust coefficient improvement. An overall performance loss of 6% relative to the bonafide subsonic cruise configuration was observed, and adjusting for chute base drag posted a gain of 4% for an overall loss of 2%. The test was conducted at 18 inches setback, full scale and chute may, also, have affected the ejector flow. Interestingly, the shallow boattail angle reduced the boattail drag by 91% relative to the bonafide subsonic cruise configuration. This brings to focus one

important aspect of setback ejector operation; though the ejector can produce a large static thrust augmentation, there is some forward velocity (tunnel Mach number) beyond which the ejector becomes a performance handicap, and it appears Mach .9 is within the velocity of diminishing returns. It is a fact that there is a performance lapse rate, as a function of tunnel Mach number, associated with any particular ejector inlet design, and it is equally conceivable that a shallower angle ejector inlet can decrease the performance lapse rate. Such optimism, however, should be tempered with the fact that shallower inlet angles necessitate longer shroud translations to achieve equivalent ejector inlet areas and the impact of weight is obvious. A performance versus ejector inlet design and weight impact study will be beneficial.

The problem with the ejector subsonic cruise configuration, though manifested as an aerodynamic problem, may be solved by subsonic cruise cycle redefinition and configuration area ratio rescheduling. The fundamental problem, it appears, is subsonic cruise cycle-hardware configuration incompatibility. However, the issue of compatibility can be resolved by performing a system trade study using the "Takeoff Acoustics-Supersonic Cruise Aerodynamics" compromise as boundary conditions.

In this way, the problem becomes an exercise in variational calculus whereby the goal will be to determine the cycle condition and area ratio schedule that will produce the required subsonic cruise thrust efficiently (i.e., at the least specific fuel consumption). The solution of this variational calculus problem will determine the appropriate cycle area ratio, boattail angle, etc., that will yield the least SFC and, consequently, the optimum subsonic cruise thrust coefficient. Figure 58 illustrates subsonic cruise performence improvement approach. To illustrate the potential improvement likely to be realized, the ejector subsonic cruise full scale thrust coefficient was evalu-

ated at an NPR of 4, a legitimate subsonic cruise cycle point. As can be seen from Figure 58, the full scale thrust coefficient at NPR of 4 is roughly 5% better than at the nominal NPR of 3.3. It is reasonable to expect that with the proper area ratio schedule and improved internal contours and some optimization techniques, an additional 7 to 10% improvement can be realized. Having achieved the means of efficient thrust production, tailoring the thrust available to the thrust required will be a simple matter, especially if there is more than required.

Transonic Cruise - Figures 56 and 59

The measured peak exit thrust coefficient at static conditions is 0.994, a good value. The stowed chutes show 0.3% decrement in full scale performance. The transonic cruise configuration can also benefit from a variational calculus exercise similar to the one prescribed for the subsonic cruise, but to a lesser extent. To properly assess installed performance at this condition, wind tunnel testing will have to be conducted.

Supersonic Cruise - Figures 56 and 60

The measured peak exit thrust coefficient is 0.994 based on constant stream thrust parameter. The stowed chutes show 0.2% in full scale performance loss. This is the performance anchor point and the performance was satisfactory with a static thrust coefficient of .9835. With a calculated external drag coefficient of about .0058, the full scale installed thrust coefficient registers at about .9777.

13.4 FLOW VISUALIZATION

The complexity of ejector aerodynamics is demonstrated by flow visualization pictures of the ejector takeoff configuration,

at optimum setback, as shown in Figures 64 through 66. The flowlines, as shown in Figures 64 and 65, seem to suggest that ejector air induction takes place primarily through inter-chute or inter-jet spaces. This is supported by the circumferential component of the flowlines direction at the nacelle base area and also at the surfaces of the ejector translation beams. If this is so, then it means the inducted air does not form an annular path, as previously envisioned, but rather a series of twenty isolated paths. This may explain why it took about twice as much ejector inlet opening than originally estimated to reach the optimum setback. From Figure 66, it appears the twenty discrete jets and the ejector inducted air finally coalesce about halfway through the ejector shroud as shown by the flowlines. More than one flow visualization test may be required in order to draw the precise relationship between all the important variables.

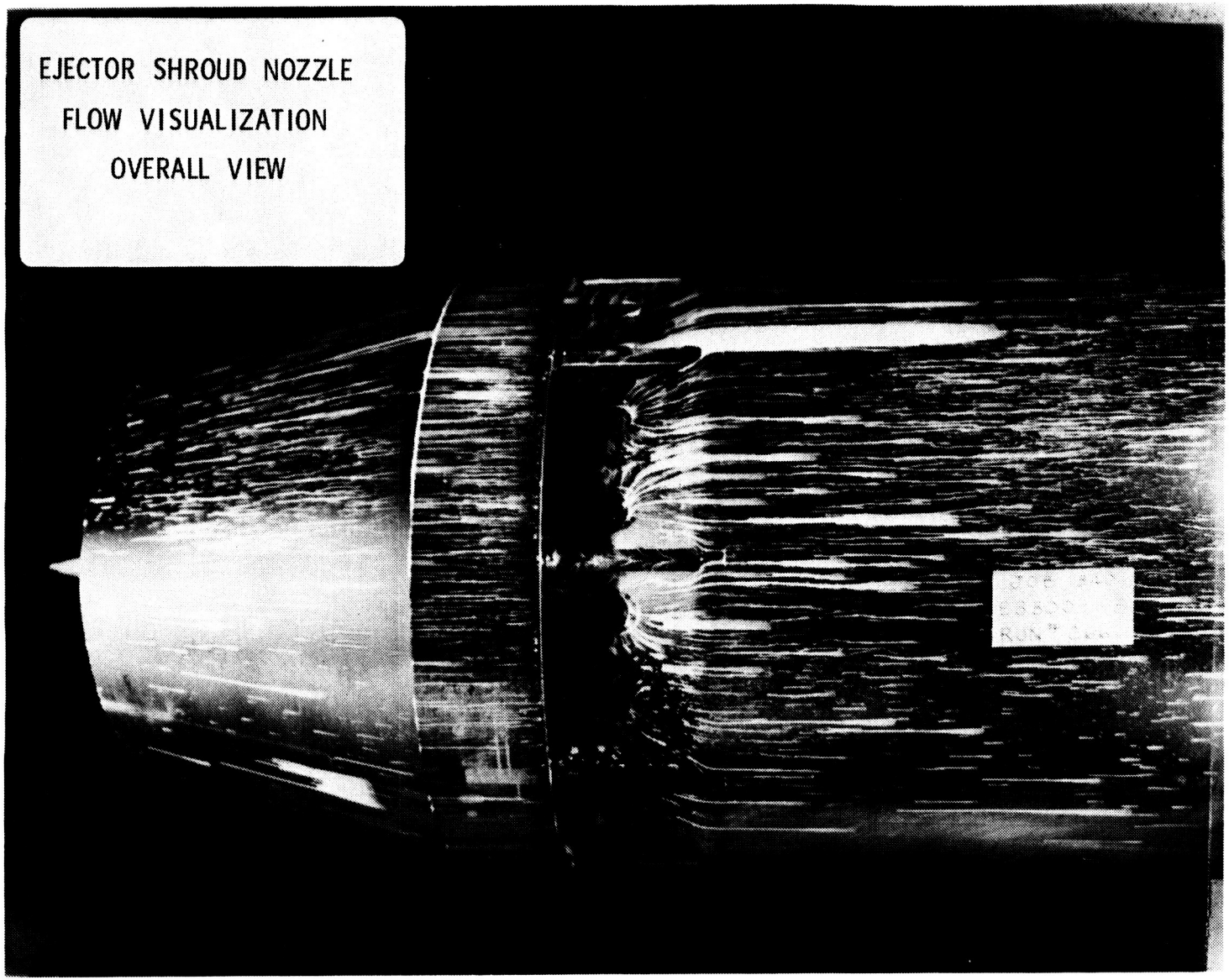

Figure 64. Ejector Shroud Nozzle Flow Visualization: Overall View

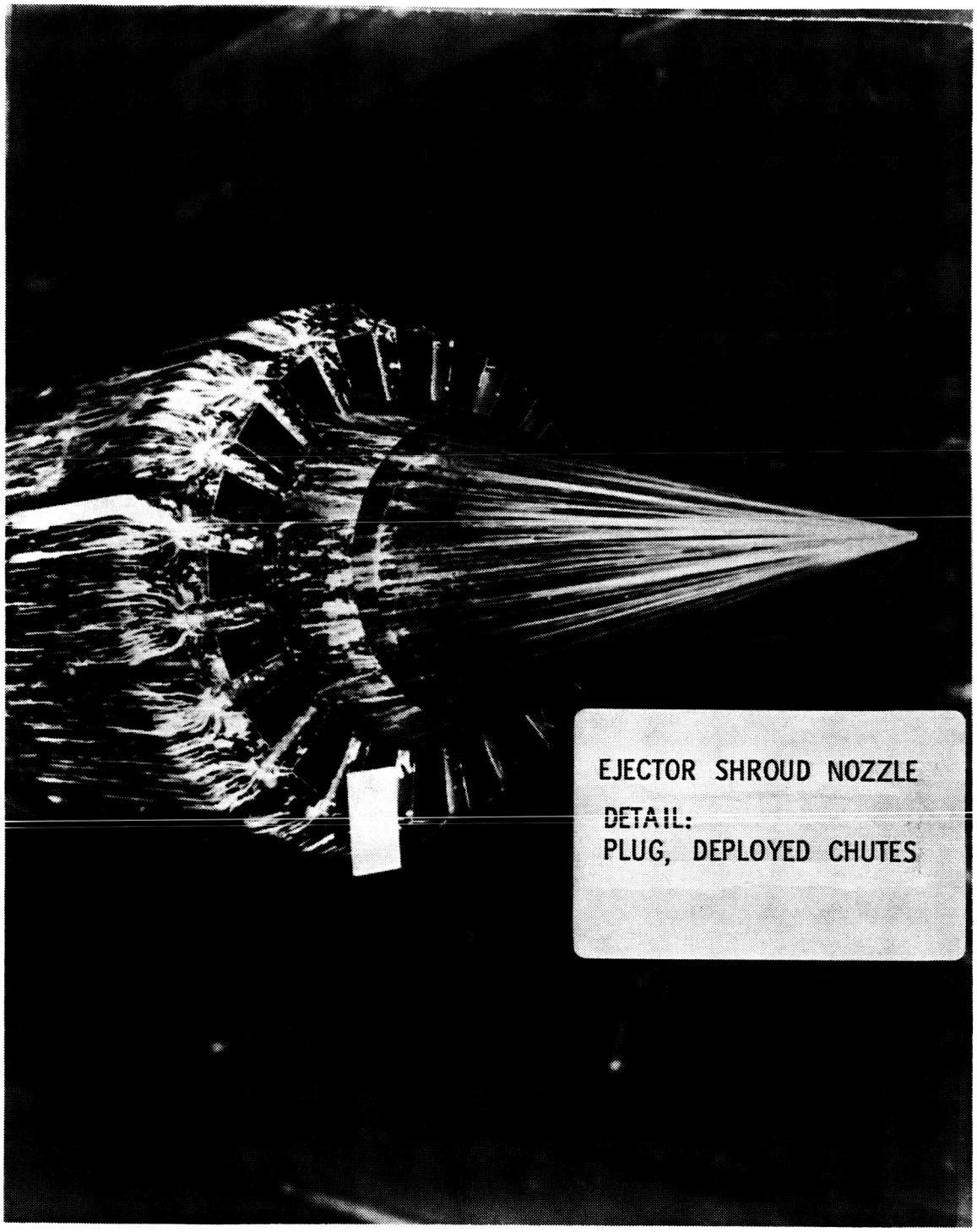

Figure 65. Ejector Shroud Nozzle Flow Visualization Showing Details of Plug and Deployed Chutes (Ejector Shroud Removed).

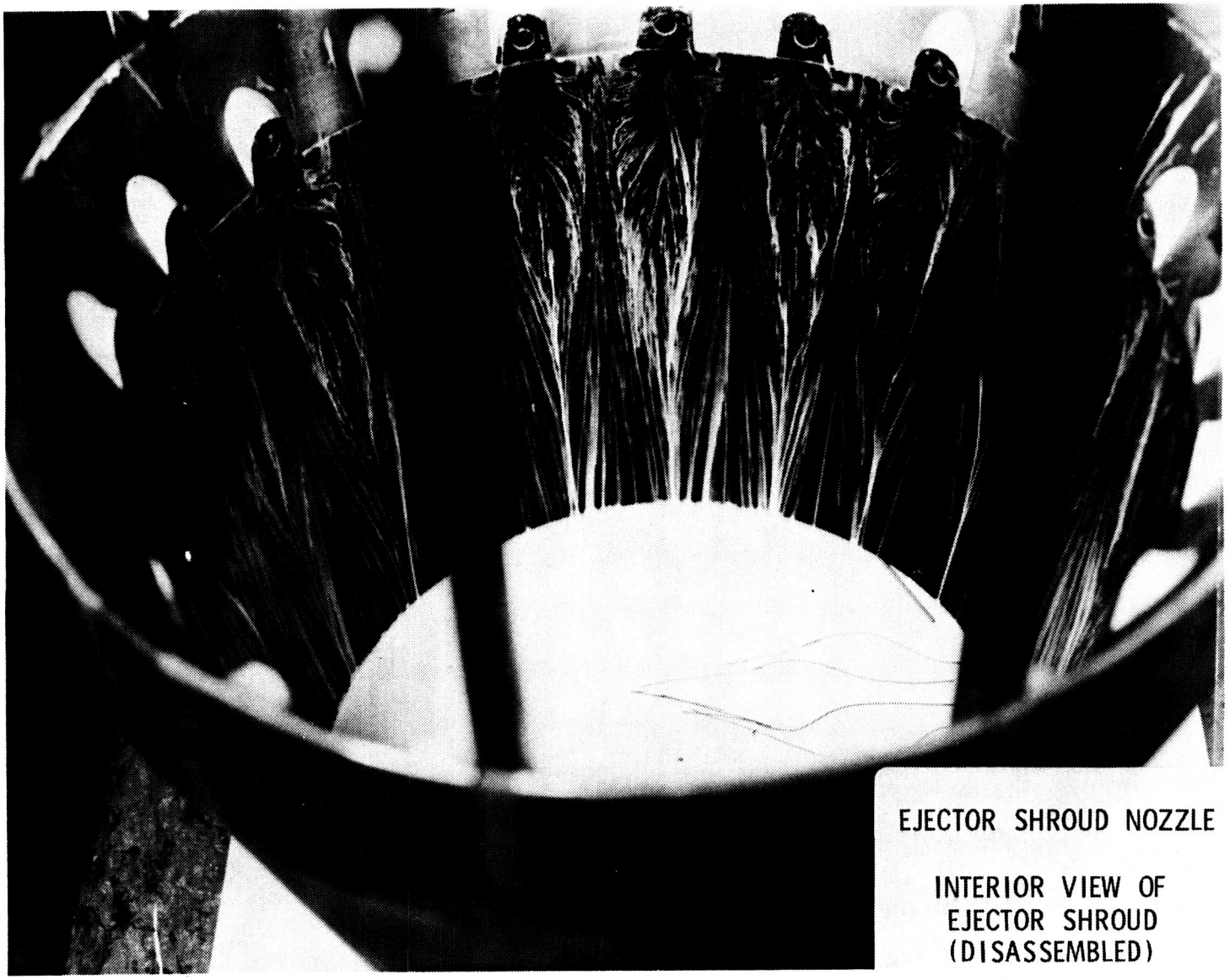

Figure 66. Ejector Shroud Nozzle Flow Visualization Showing Interior View of Ejector Shroud (Disassembled)

14.0 CONCEPTUAL DESIGN AND TEST PROGRAM RESULTS RECONCILIATION

The mission analysis study conducted in Section 7 utilized conceptual design performance data to establish aircraft TOGW necessary to fulfill the AST mission. This was done with the understanding that the TOGW could be adjusted later to reflect the installed performance when the test program was completed. During the course of the study, important performance sensitivities (derivatives) were generated to enable TOGW equivalents to be calculated for performance increments relative to the predicted installed performance established during the conceptual design phase. Table 13 shows performance sensitivities for the four flight regimes, i.e., takeoff, subsonic cruise, transonic acceleration and supersonic cruise. The small impact of takeoff performance on TOGW is very reasonable when the following is considered: the engine is sized primarily for acoustics so takeoff thrust is not critical, besides takeoff is a minute fraction of the mission. On the other hand, at supersonic cruise, which represents the largest block of mission time, a poor performance can be costly as shown by the 10,000 pounds penalty in TOGW for a 1% performance increment. Table 14 shows the individual and aggregate TOGW adjustments made as a result of reconciling the performance differences between the prediction and test installed performances. The final TOGW summaries referencing measured installed performance (except for those otherwise indicated) are shown in Tables 15 and 16 for the 20-chute and ejector shroud nozzles, respectively.

Final Mission Analysis Results

The mission analysis results indicate the ejector shroud as the best among the three nozzle systems studied for the AST mission, within the constraints of FAR 36 (1969) Stage 3 noise goal. Comparatively, the ejector nozzle system has 79,000 lbs advantage in TOGW over a commensurate aircraft fitted with the

TABLE 13

PERFORMANCE SENSITIVITIES

SUPERSONIC CRUISE AIRCRAFT

TAKEOFF:	- 1% CFG ≈ + 750 LBS IN TOGW
SUBSONIC CRUISE:	- 1% CFG ≈ + 3,000 LBS IN TOGW
TRANSONIC ACCELERATION:	- 1% CFG ≈ + 2,000 LBS IN TOGW
SUPERSONIC CRUISE:	- 1% CFG ≈ +10,000 LBS IN TOGW

TABLE 14

PREDICTED VS. MEASURED INSTALLED PERFORMANCE COMPARISON

NOZZLE	OPERATING MODE	PREDICTION	MEASURED	Δ
COANNULAR BASELINE	TAKEOFF	.9757	.9753	-.0004
	SUBSONIC	.9682	.9325	-.0357
	SUPERSONIC	.9827	.9853*	+.0026
20-CHUTE SUPPRESSOR	TAKEOFF	.9328	.9291	-.0037
	SUBSONIC	.9650	.9015	-.0635
	TRANSONIC	.9566	.9444*	-.0122
	SUPERSONIC	.9821	.9810*	-.0011
EJECTOR SHROUD	TAKEOFF	.9408	.9225	-.0183
	SUBSONIC	.9465	.8100	-.1365
	TRANSONIC	.9311	.9211*	-.0100
	SUPERSONIC	.9743	.9777*	+.0034

* WITH ESTIMATED EXTERNAL DRAG.

TABLE 15

TOGW ADJUSTMENTS: 20-CHUTE SUPPRESSOR NOZZLE
(BASED ON PREDICTED VS. MEASURED INSTALLED PERFORMANCE)

TAKEOFF:	Δ -.37% CT $\approx$ +	277 LBS. IN TOGW
SUBSONIC CRUISE:	Δ -6.35% CT $\approx$ +19,050	LBS. IN TOGW
TRANSONIC ACCEL:	Δ -1.22% CT $\approx$ + 2,440	LBS. IN TOGW
SUPERSONIC CRUISE:	Δ -.11% CT $\approx$ + 1,100	LBS. IN TOGW

NET CHANGE IN TOGW $\approx$ + 22,867

REFERENCE TOGW (MISSION ANALYSIS) $\approx$ 862,000 (TABLE 8. PAGE 85)

PROJECTED TOGW $\approx$ 885,000

TABLE 16

TOGW ADJUSTMENTS: EJECTOR SHROUD NOZZLE
(BASED ON PREDICTED VS. MEASURED INSTALLED PERFORMANCE)

TAKEOFF:	Δ- 1.83% CT	$\approx$ + 1,372 LBS. IN TOGW
SUBSONIC CRUISE:	Δ-13.65% CT	$\approx$ +40,950 LBS. IN TOGW
TRANSONIC ACCEL:	Δ- 1.0 % CT	$\approx$ + 2,000 LBS. IN TOGW
SUPERSONIC CRUISE:	Δ +.35% CT	$\approx$ -3,490 LBS. IN TOGW

NET CHANGE IN TOGW	$\approx$ + 40,832	
REFERENCE TOGW (MISSION ANALYSIS)	$\approx$ 765,000	(TABLE 8, PAGE 85)
PROJECTED TOGW	$\approx$ 806,000	

TABLE 17

TOGW SUMMARY
(MEASURED INSTALLED PERFORMANCE)

NOZZLE	SIDELINE NOISE EPNL dB	AIRFLOW LB/SEC	TOGW LBS.
EJECTOR SHROUD	104.74	858	806,000
20-CHUTE SUPPRESSOR	104.74	1,270	885,000
COANNULAR BASELINE	104.74	NOT REALISTICALLY ACHIEVABLE	NOT REALISTICALLY ACHIEVABLE

ΔTOGW EJECTOR SHROUD VS. 20-CHUTE SUPPRESSOR $\approx$ 79,000 LBS.

20-chute nozzle. The results further indicate that all three noise suppression systems will be required to meet the FAR 36 (1969) Stage 3 noise goals, not absolutely, but within the noise trading guidelines, with a reasonable engine size. In the same vein, the coannular is not an attractive concept for AST application where Stage 3 noise suppression is the measure of acceptability.

The increase in ejector/AST system TOGW from the preliminary estimate of 765,000 to 806,000 lbs, results from differences between predicted and measured performance. The aerodynamic explanation of the details of the performance decrement is covered under "Performance Discussions" in the test program results, but the bigger issue of not meeting performance prediction, as it relates specifically to the ejector subsonic cruise mode (shown in Table 17), has wider conceptual implications than aerodynamics of the subsonic cruise nozzle. As a rule, AST engines are sized for noise at takeoff and aerodynamically configured for peak performance at supersonic cruise, with intermediate points determined on the basis of best available performance. The former is imperative in order to maximize coannular noise suppression and the latter to minimize sfc and reduce mission block fuel consumption through high peak installed performance. The performance sensitivity shown in Table 13 supports this procedure by the fact that a 1% decrement in supersonic cruise performance is equivalent to 10,000 lbs gain in TOGW, whereas the same performance decrement at subsonic cruise increases TOGW by only 3,000 lbs. This is why ejector subsonic cruise nozzle remains second on the performance priority list.

Equally detrimental to the ejector subsonic cruise performance is the "High Radius Ratio" feature of the 20-chute suppressor system which makes it necessary to increase nozzle radius and, also, the low subsonic cruise thrust requirement which makes

it necessary to operate at a low area ratio schedule, thereby creating a high boattail angle. The low thrust requirement, and hence the low area ratio schedule, coupled with the high radial hinge points for the ejector shroud flaps combined unfavorably to create less than optimum internal nozzle expansion characteristics and a high boattail angle of 19°. Figure 67 illustrates the unfavorable features of the ejector subsonic cruise configuration characterized by a diverging-converging internal flowpath for what normally should be strictly divergent.

There are other subsonic cruise cycle points that, if adopted, may alleviate the current internal expansion-high boattail angle problem, though the accompanying high thrust output may not be desirable, particularly during the subsonic cruise leg following a missed approach (as shown in AST mission, Figure 30) when aircraft weight as well as thrust demand is low. However, the available thrust can be modulated to the required levels by rescheduling ejector shroud flap settings. Two options are available for resolving this problem, either by maintaining the as configured pressure ratio of 3.3 and manipulating flap position to improve and reduce internal performance and boattail drag respectively, or by operating at a higher pressure ratio cycle option (NPR=4) and modulating the thrust through control of area ratio settings. Figure 68 illustrates the two options discussed above. A slight modification of option 1 would be to operate with the ejector inlet open, suppressor chutes stowed, and ejector shroud flap more fully open to reduce boattail drag.

It is believed that the installed performance deficits incurred, particularly at the subsonic cruise point, can be restored by choosing the low or high pressure ratio subsonic cruise cycle point and performing the necessary area ratio rescheduling. It appears that choosing the high pressure ratio point (NPR=4) will be more prudent since that will assure thrust requirement availability at all times; besides the specific fuel

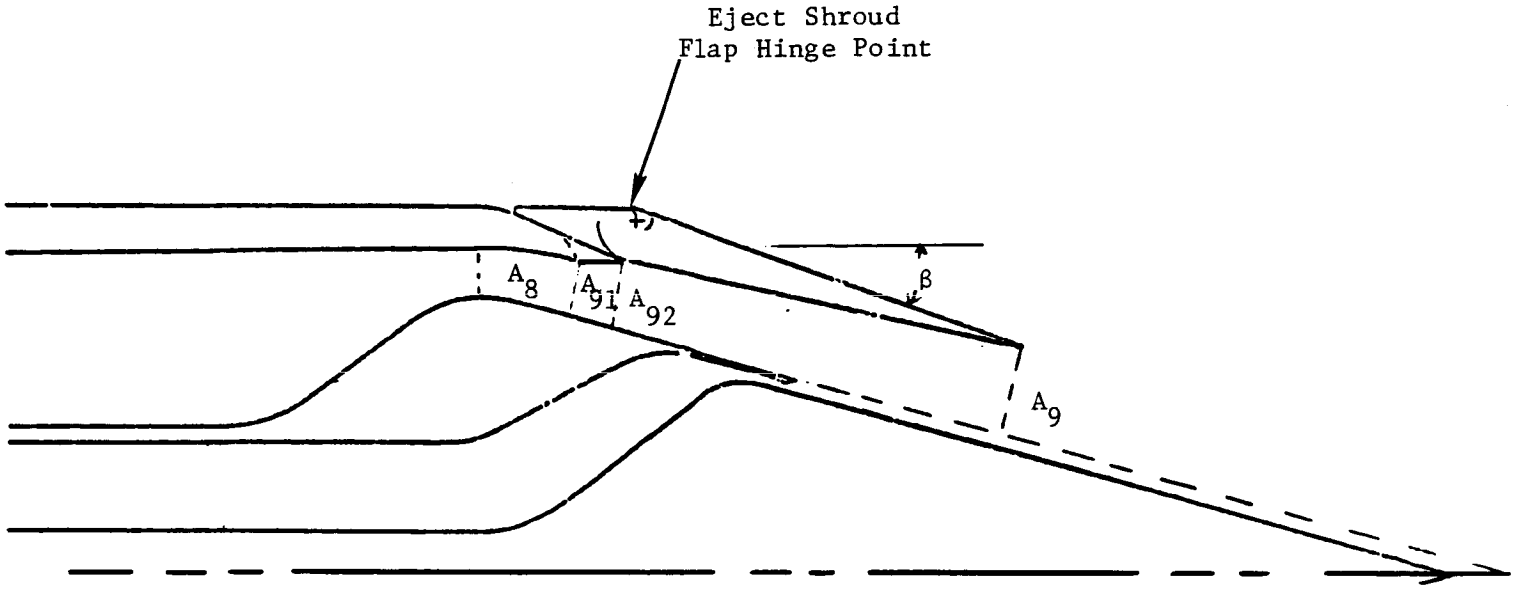

$A_8 = 1450$
$A_{91} = 1570$
$A_{92} = 1961$
$A_9 = 1667$
$\beta = 19^o$

} Full Scale, IN^2

Figure 67. Ejector Shroud Nozzle Subsonic Cruise Configuration Defined By Cycle Sizing Data Showing a Divergent-Convergent Divergent Section and High Boattail Angle

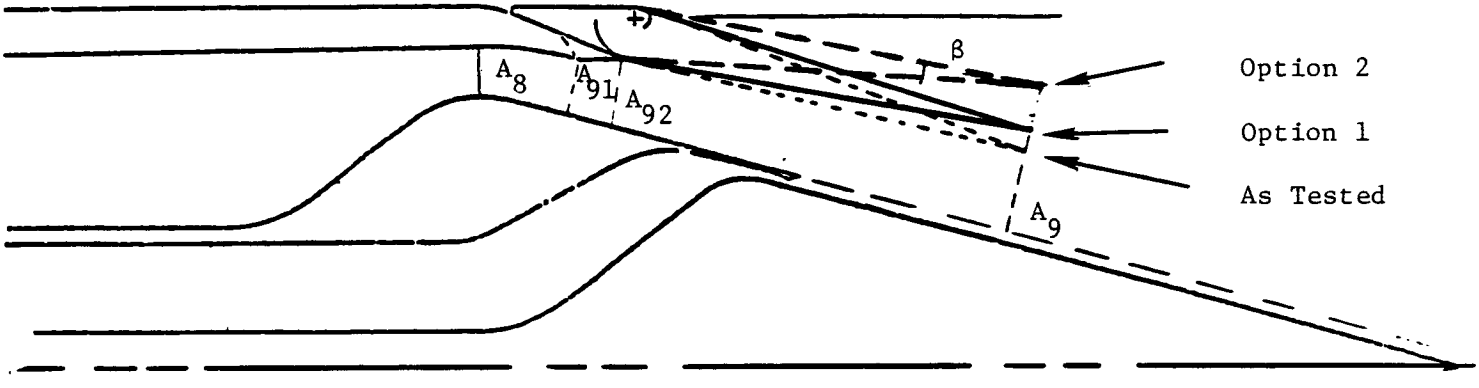

ITEM	CYCLE NPR	A9	β
Option 1	3.3	A_{92}	14.5
Option 2	4.0	$\geq A_{92}$	$\leq$ 14.5

Figure 68. Proposed Options For Subsonic Cruise Installed Performance Improvement Showing Possible Area Ratio Settings And Cycle Options To Match Thrust Requirements

consumption (sfc) is better at this point and the solution more consistent with AST mission objectives. The subsonic cruise point is determined by thrust and since there is a large thrust reserve (per cycle data) the solution becomes a matter of how efficiently the large thrust reserve can be tailored to meet requirements.

It is reasonable to expect the higher pressure ratio subsonic cruise cycle point in combination with the area ratio rescheduling to minimize installed performance losses and push the installed thrust coefficient towards the conceptual design goal.

15.0 CONCLUSIONS AND RECOMMENDATIONS

The program was successful in establishing the ejector shroud nozzle as an improved concept for Advanced Supersonic Transport application in relation to the baseline coannular and the 20-chute nozzles. The large data base accumulated stands ready for development initiation when required.

The integrated ejector shroud design is capable of providing adequate noise reduction to satisfy the FAR 36, Stage 3 guidelines under the "Noise Tradeoff" rules. At an estimated traded noise of 103 EPNdB, the ejector shroud nozzle leads to a calculated 79,000 pound saving in TOGW relative to the 20-chute suppressor nozzle, despite the existence of a highly non-optimized ejector flap geometry for subsonic cruise. The coannular nozzle, however, is not an attractive concept for FAR 36, Stage 3 noise requirement relative to the 20-chute or the ejector shroud nozzles.

Despite the success of this program, further investigation into certain aspects of ejector nozzle development will be beneficial in further enhancing aerodynamic performance and noise suppression. To this end, a clear understanding of ejector aerodynamics, particularly in the takeoff mode, must be pursued because of the wider implication it has, not only for aerodynamic performance but also for the acoustics as well. The noise absorption coefficient of the ejector shroud noise treatment is a function of the aerodynamic variables and therefore a better understanding of it will enable specific treatment techniques to be applied to improve the noise absorption coefficient.

The flow visualization test showed the complex interaction between the twenty discrete chute jets and the tertiary ejector air induction. It appears the tertiary flow is discretely inducted through inter-jet or inter-chute spaces and thus differs demonstrably from the conventional ejector characteristics

thought of as uniform and annular. For the ejector shroud, the ejector induction process appeared to be controlled by inter-jet areas rather than the physical ejector opening. This may explain why it took twice as much setback as originally calculated to reach optimum setback.

Further complicating the ejector aerodynamic analysis is the fact that the ejector shroud area ratio (1.07-0.95) varied with ejector setback. The importance of ejector area ratio in determining optimum ejector augmentation is undeniable but since identification of ejector optimum area ratio was not part of program objectives, the currently identified optimum ejector setback may only be provisional. Future development programs should focus on this as well as conduct more flow visualization studies to clarify the functional relationships between the important ejector takeoff configuration variables.

The present ejector nozzle subsonic cruise performance deficits may possibly be restored through subsonic cruise cycle redefinition and area ratio schedule changes. Future development programs should attempt to match engine cycle definition (NPR, etc.) to nozzle hardware configuration peculiarities in order to satisfy subsonic thrust requirements at a minimum loss.

The enhancement techniques suggested for the subsonic cruise configuration can be extended to the transonic acceleration configuration as well, even though the losses are less. The supersonic cruise configuration was the aerodynamic anchor point and therefore showed excellent performance. The potential exists for improving the ejector shroud exhaust system performance, aerodynamically and acoustically, if these recommendations are carried out to fruition.

16.0 REFERENCES

Task 2 Acoustically Treated Ejector Shroud

1. J. F. Brausch, W. S. Clapper, P. F. Scott, M. A. Smith, E. J. Stringas, R. W. Whittaker, "High Velocity Jet Noise Source Location And Reduction, FAA-RD-76-79, Tasks 1-6, R79AEG302, April 1979.

2. J. P. Wolf, "Preliminary Design of an AST Jet Engine Exhaust System Incorporating a 20-Chute Suppressor in the Outer Stream of an Annular Two Stream Plug Nozzle," GE TM No. 79-535, September 1979.

3. R. D. Allan, J. E. Johnson, W. Joy, R. H. Brown, H. J. Barrial, "Engine Cycle Studies", General Eletric Company, NASA, CR-159500, NAS3-21388, R80AEG428, August 1980.

4. R. D. Allan, B. G. Hines, W. L. Wines, "Effect of Design Temperature on Double Bypass Engines For SCR," General Eletric Company, NASA, CR167854, NAS3-22749, R82AEB225, September 1982.

5. J. Brausch, W. S. Clapper, P. R. Gliebe, et. al., "High Velocity Jet Noise Source Location and Reduction, Task 6 - Noise Abatement Nozzle Design Guide, FAA-RD-76-79, VI, April 1979.

6. A. Sieckman,, R. E. Motsinger, P. R. Gliebe, , "High Velocity Jet Noise Source Location and Reduction: General Supplement - Computer Programs; The Engineering Correlation (M*5) Jet Noise Prediction Method and Unified Aeroacoustic Prediction Model (M*G*B) for Nozzles of Arbitrary Shape," General Electric Company, FAA-RD-76-79, VIa, April 1979.

7. Ames Research Staff, "Equations, Tables, and Charts for Compressible Flow." NACA 1133, 1953.

8. SST Technology, Follow-on Program--Phase II, Vol. I-X. Noise Suppressor/Nozzle Development: Boeing Commercial Airplane Company. 1975.

9. Wyatt, DeMarquis D., "Analysis of Errors Introduced by Several Methods of Weighting Non-Uniform Duct Flows." NACA TN 3400. March 1955.

10. Reimer, R.M., "Computation of the Critical Flow Function, Pressure Ratio, and Temperature Ratio for Real Air." ASME Paper #62-WA-177. 1962.

11. Jordan, D.P. and Mintz, M.D., "Air Tables." McGraw-Hill Book Company, New York. 1965.

12. Johnson, R. C., "Real Gas Effects in Critical-Flow-Through Nozzles and Tabulated Thermodynamic Properties." NASA TN D-2565. 1965.

APPENDIX A

EJECTOR SHROUD PLOTTED DATA

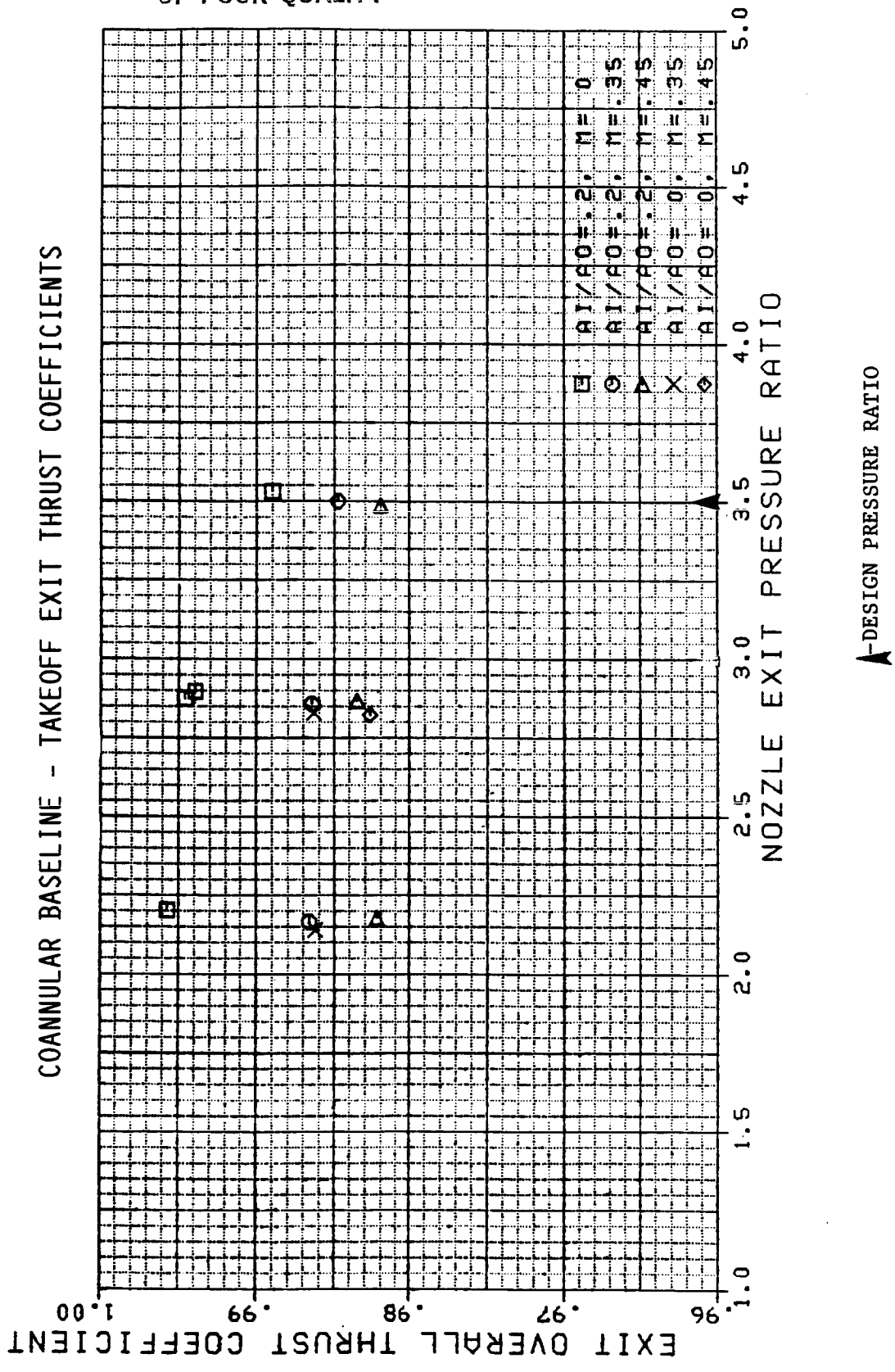

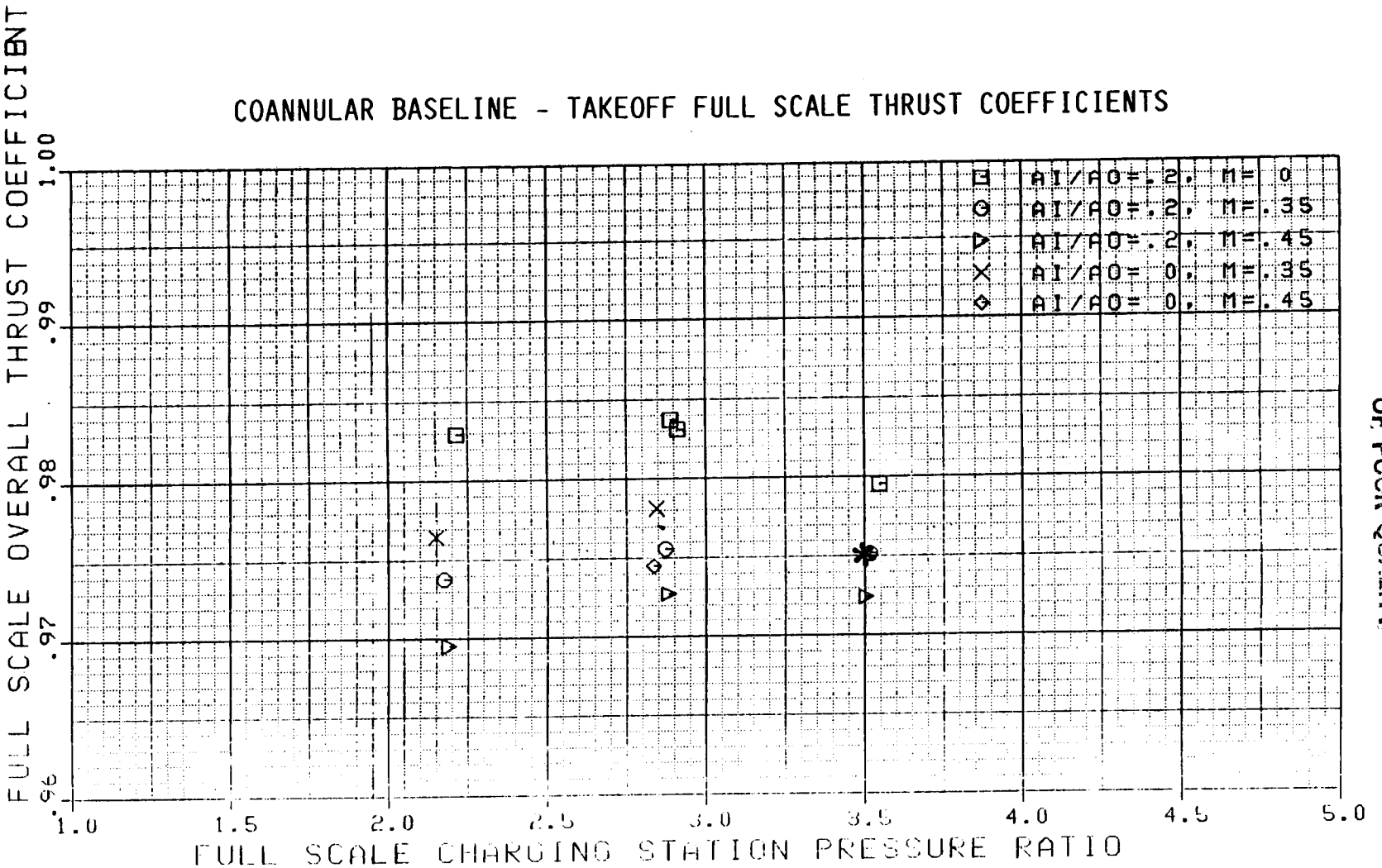

* - DESIGN PRESSURE RATIO

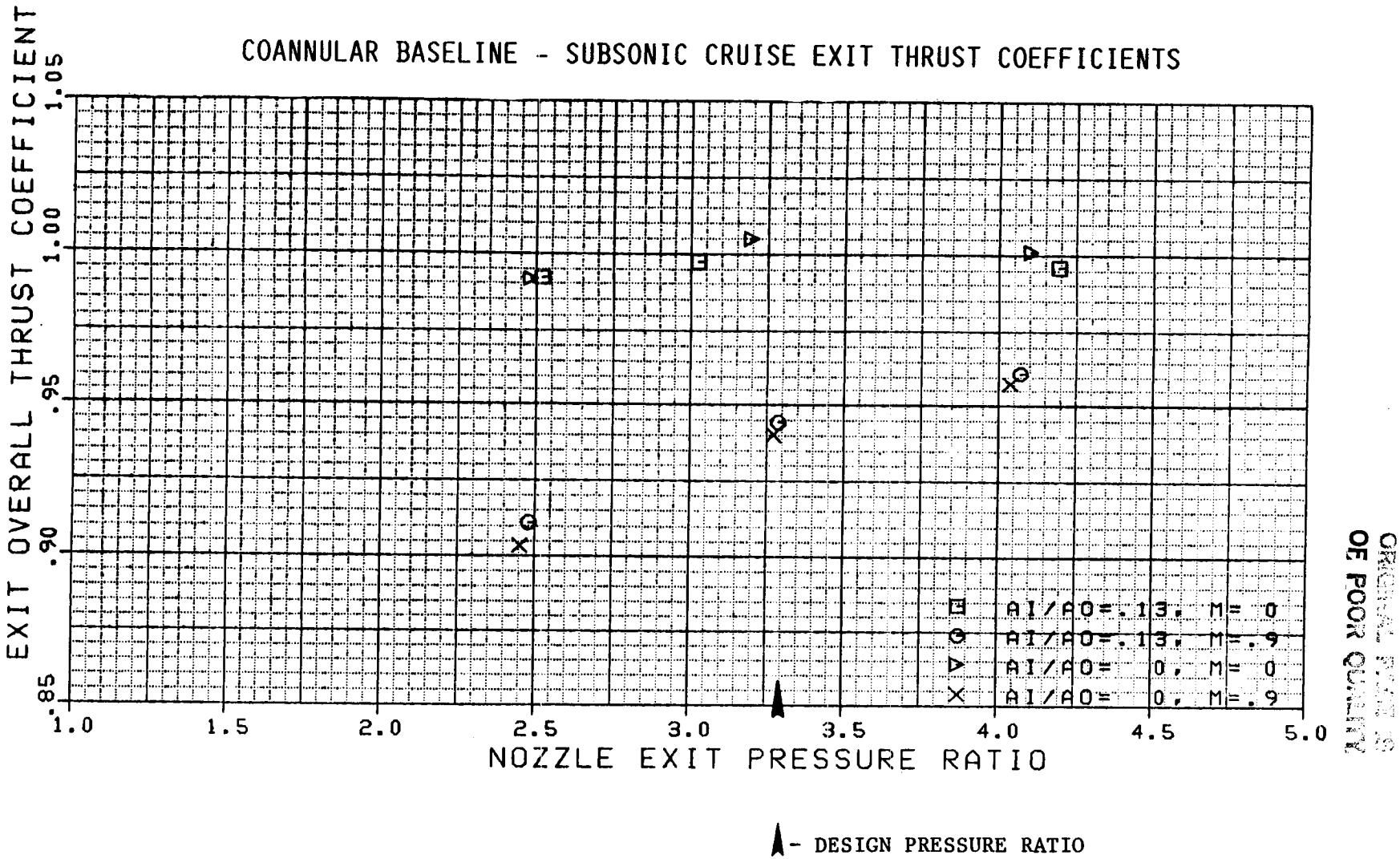

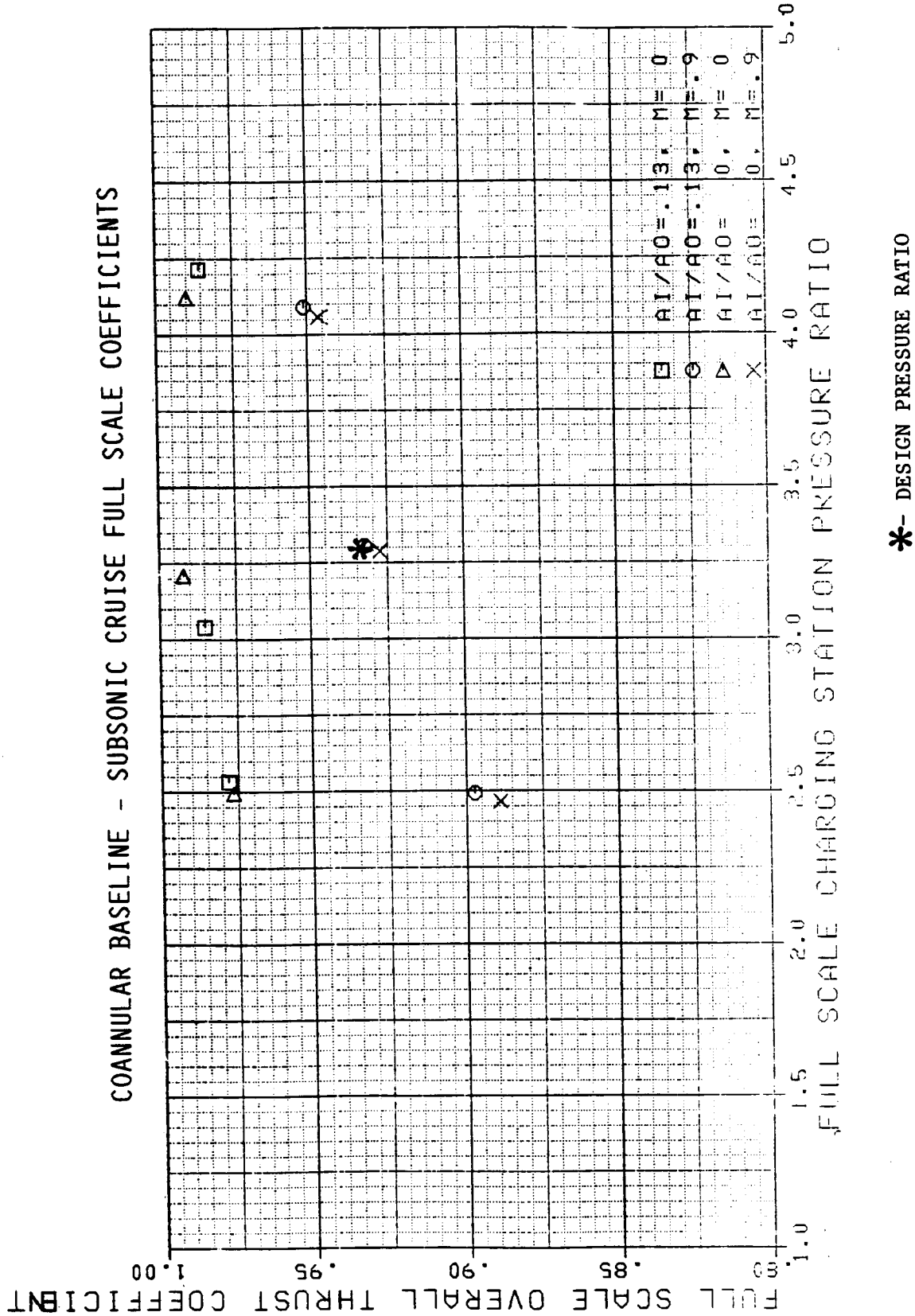

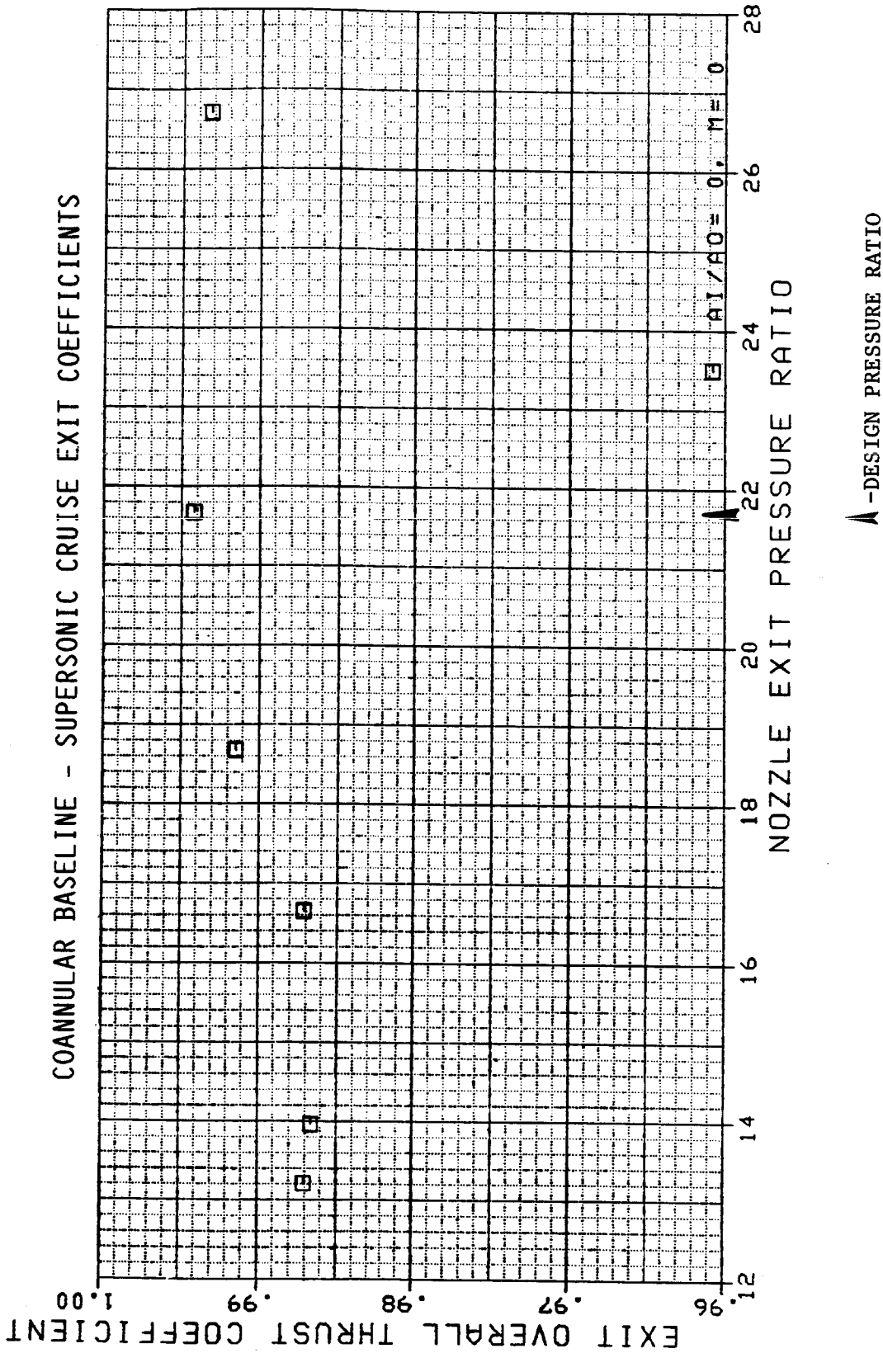

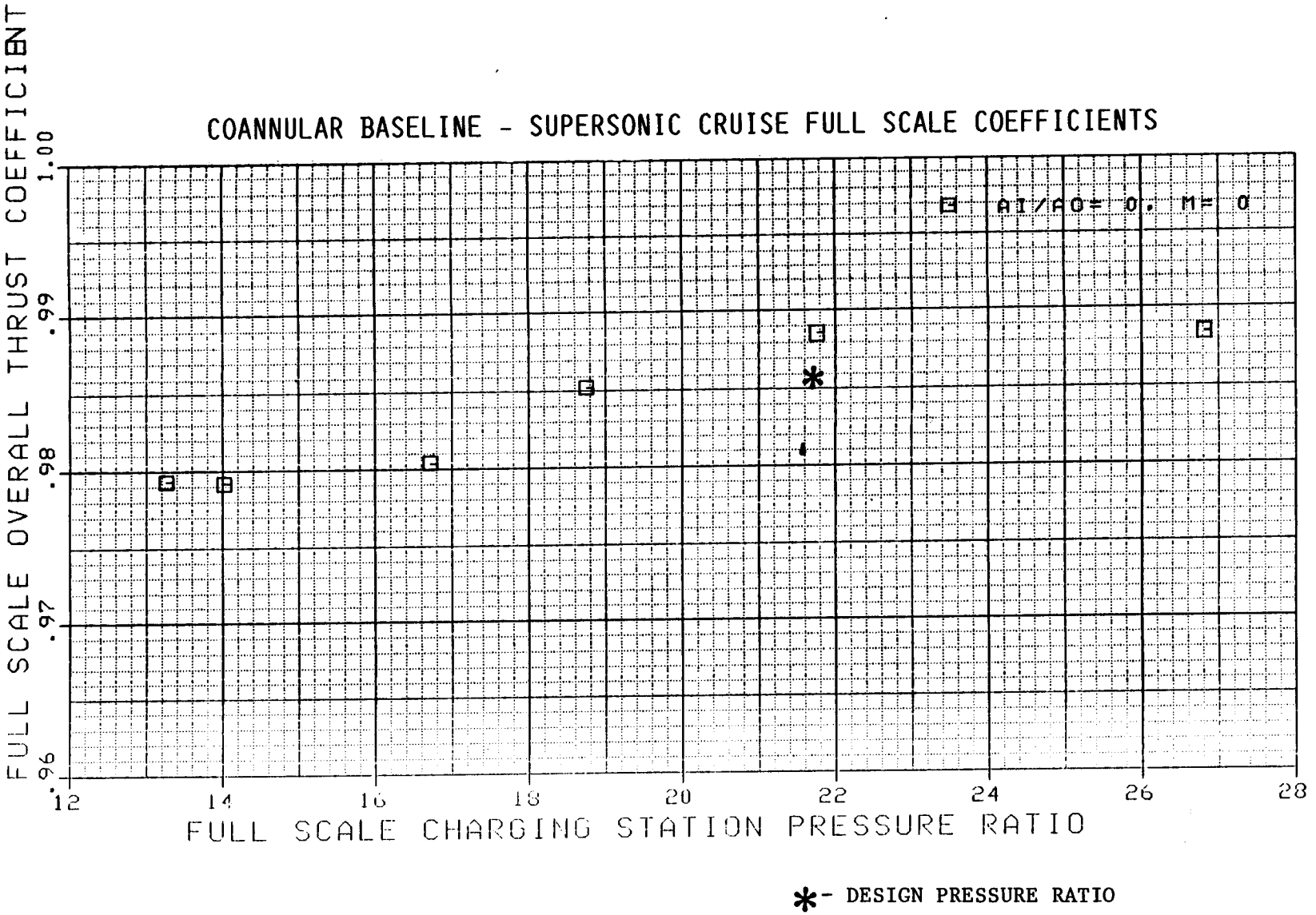
COANNULAR BASELINE - SUPERSONIC CRUISE FULL SCALE COEFFICIENTS
FULL SCALE OVERALL THRUST COEFFICIENT
1.00
.99
.98
.97
.96
12
14
16
18
20
22
24
26
28
FULL SCALE CHARGING STATION PRESSURE RATIO
A1/A0= 0. M= 0
*- DESIGN PRESSURE RATIO

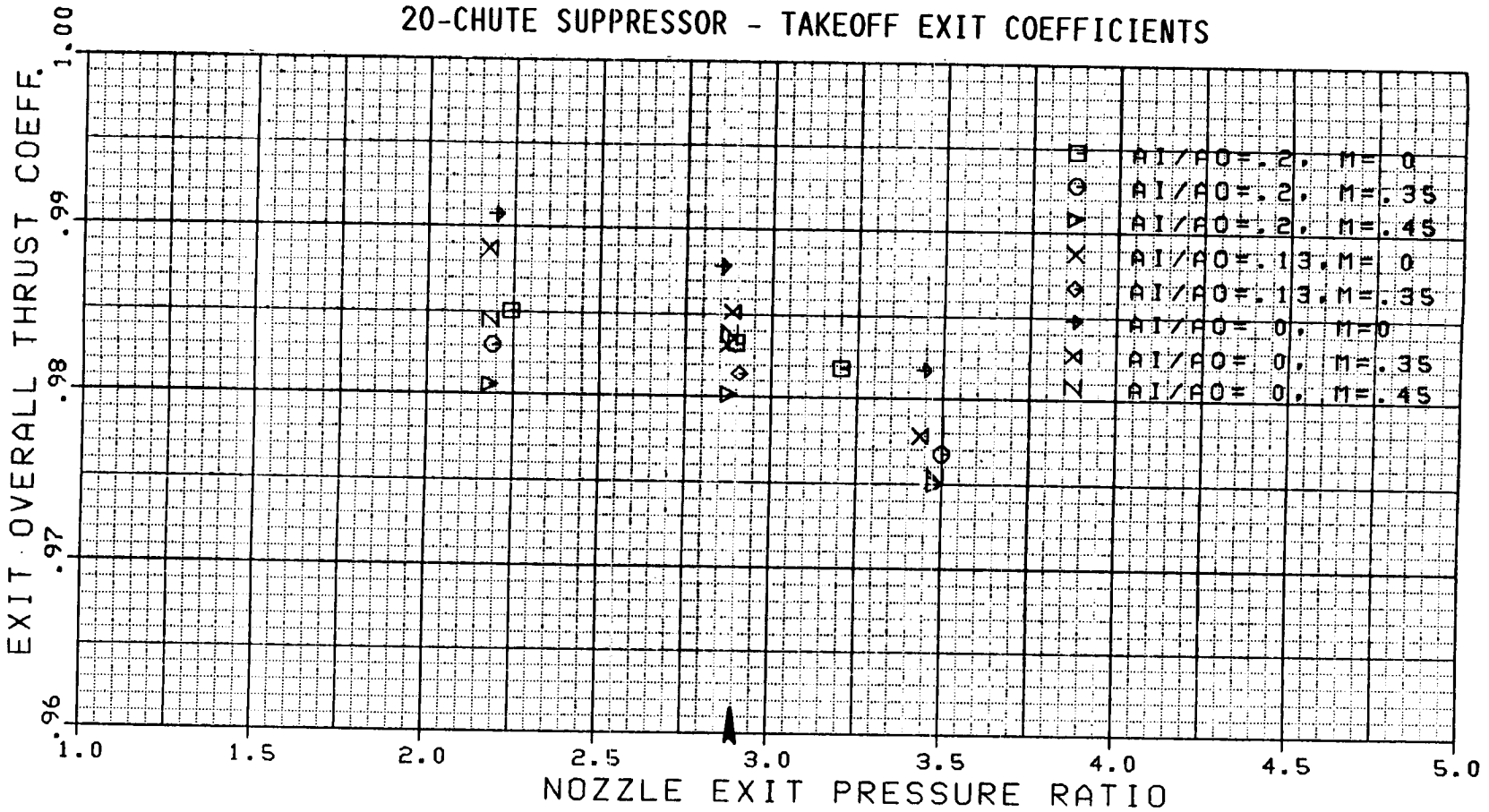

▲ -DESIGN PRESSURE RATIO

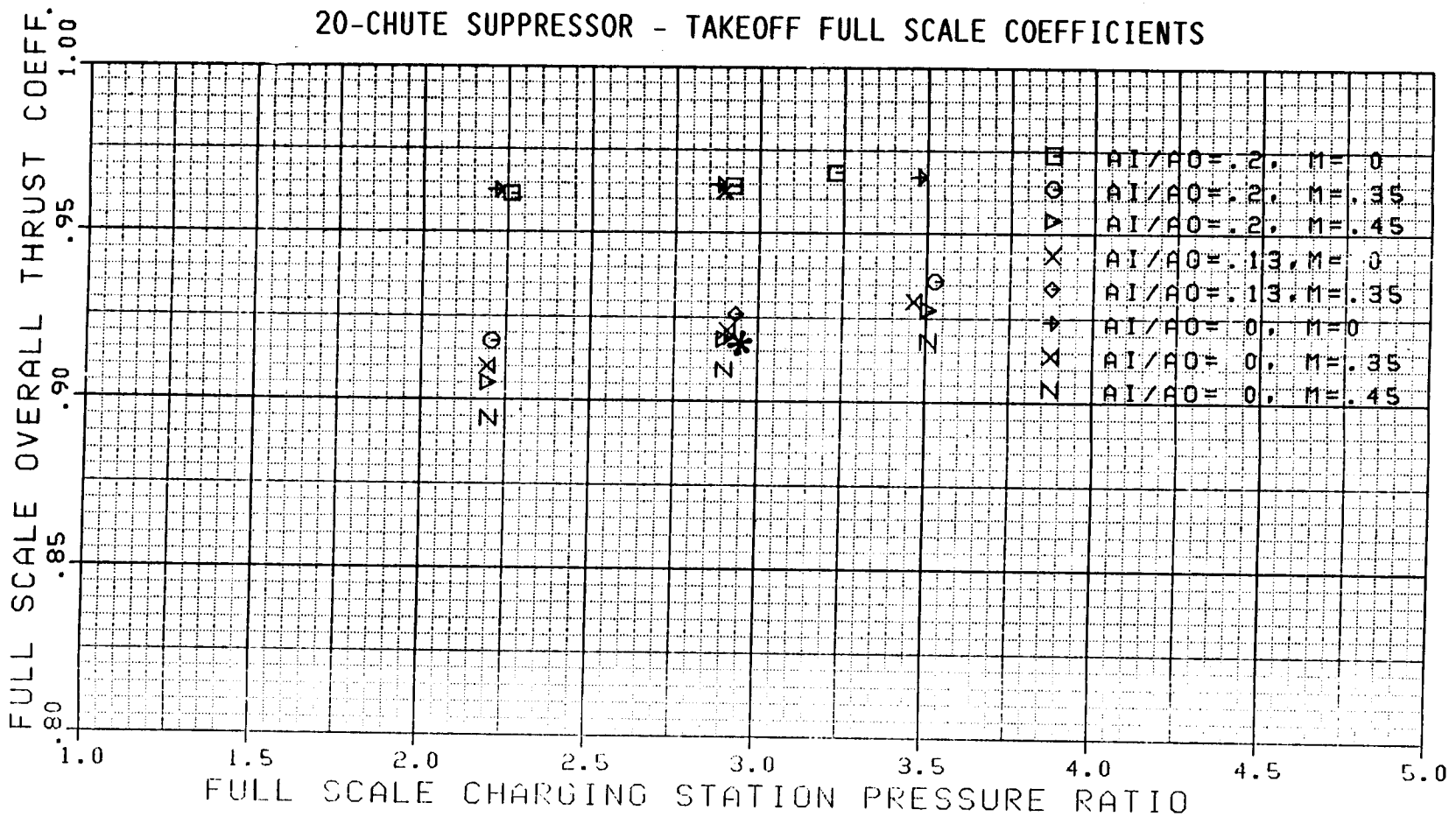

*- DESIGN PRESSURE RATIO

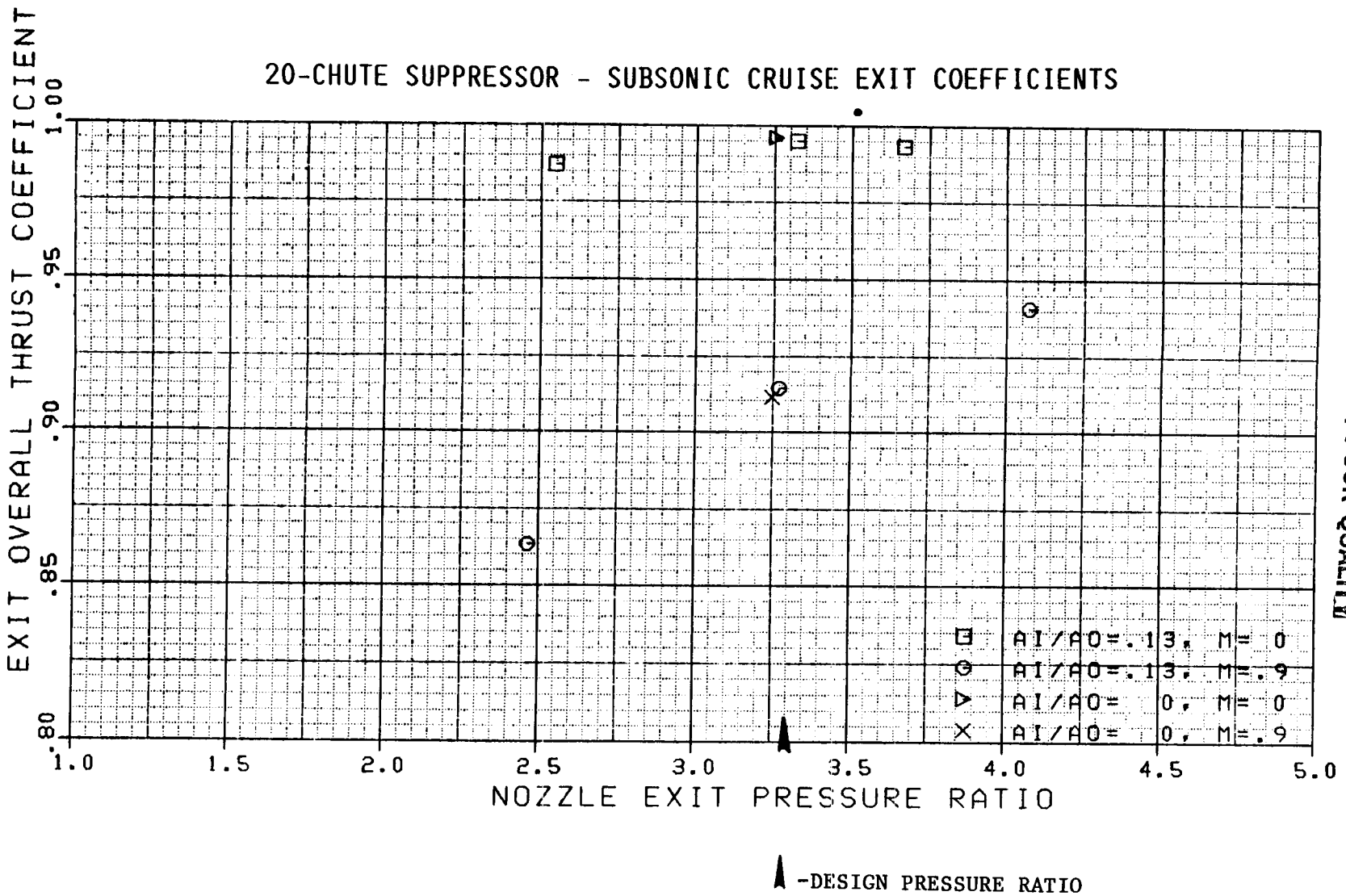

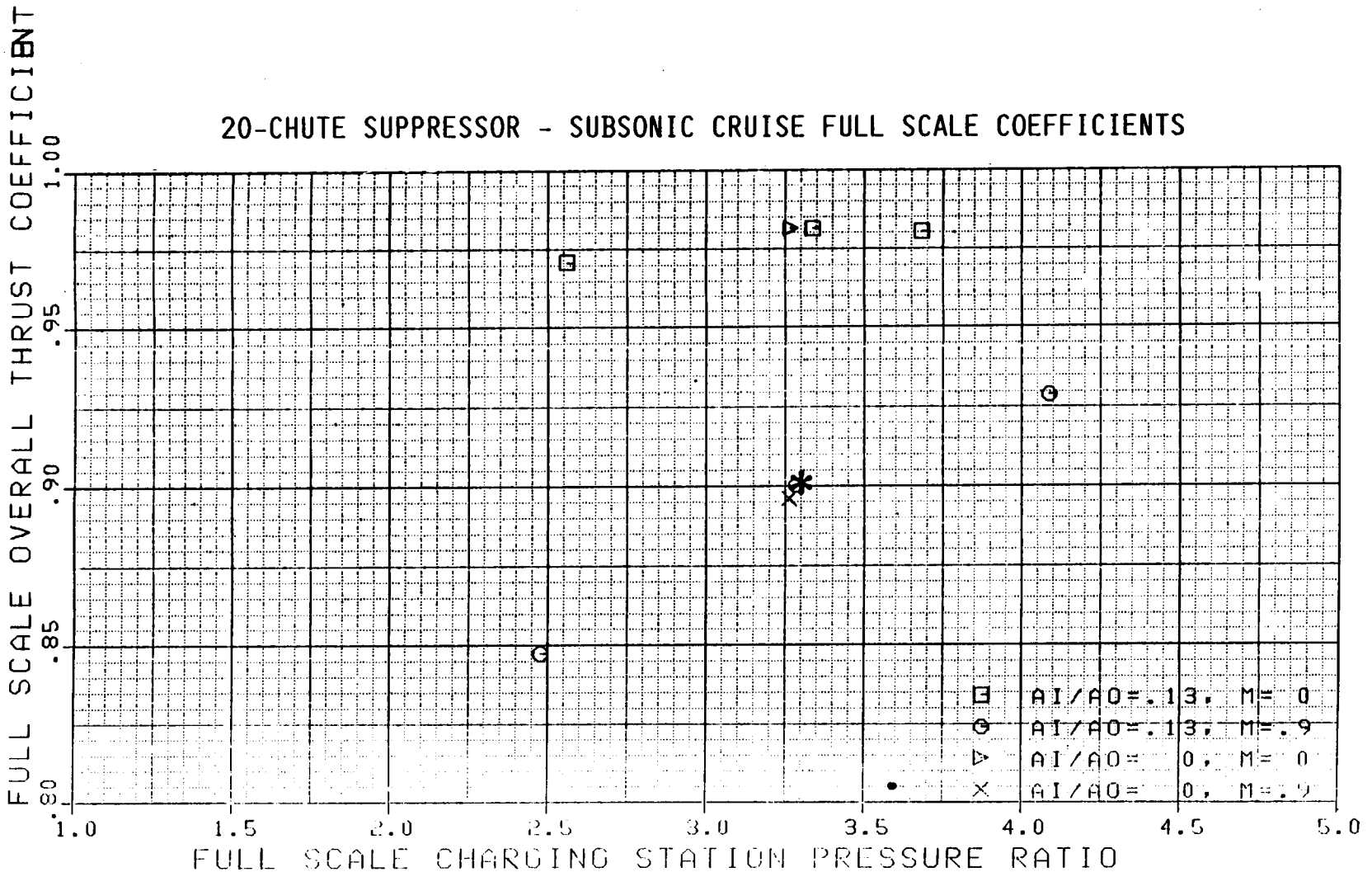

*- DESIGN PRESSURE RATIO

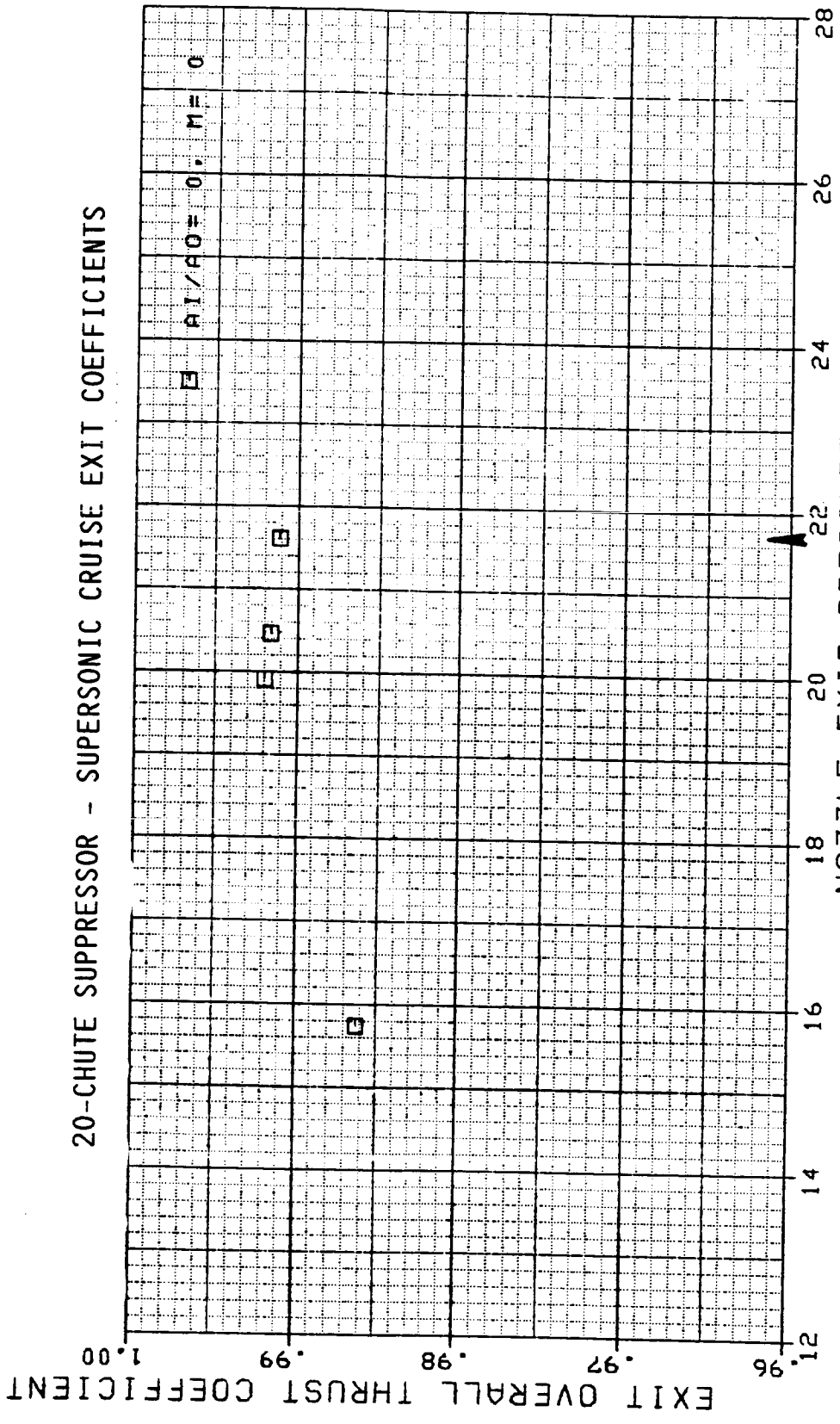

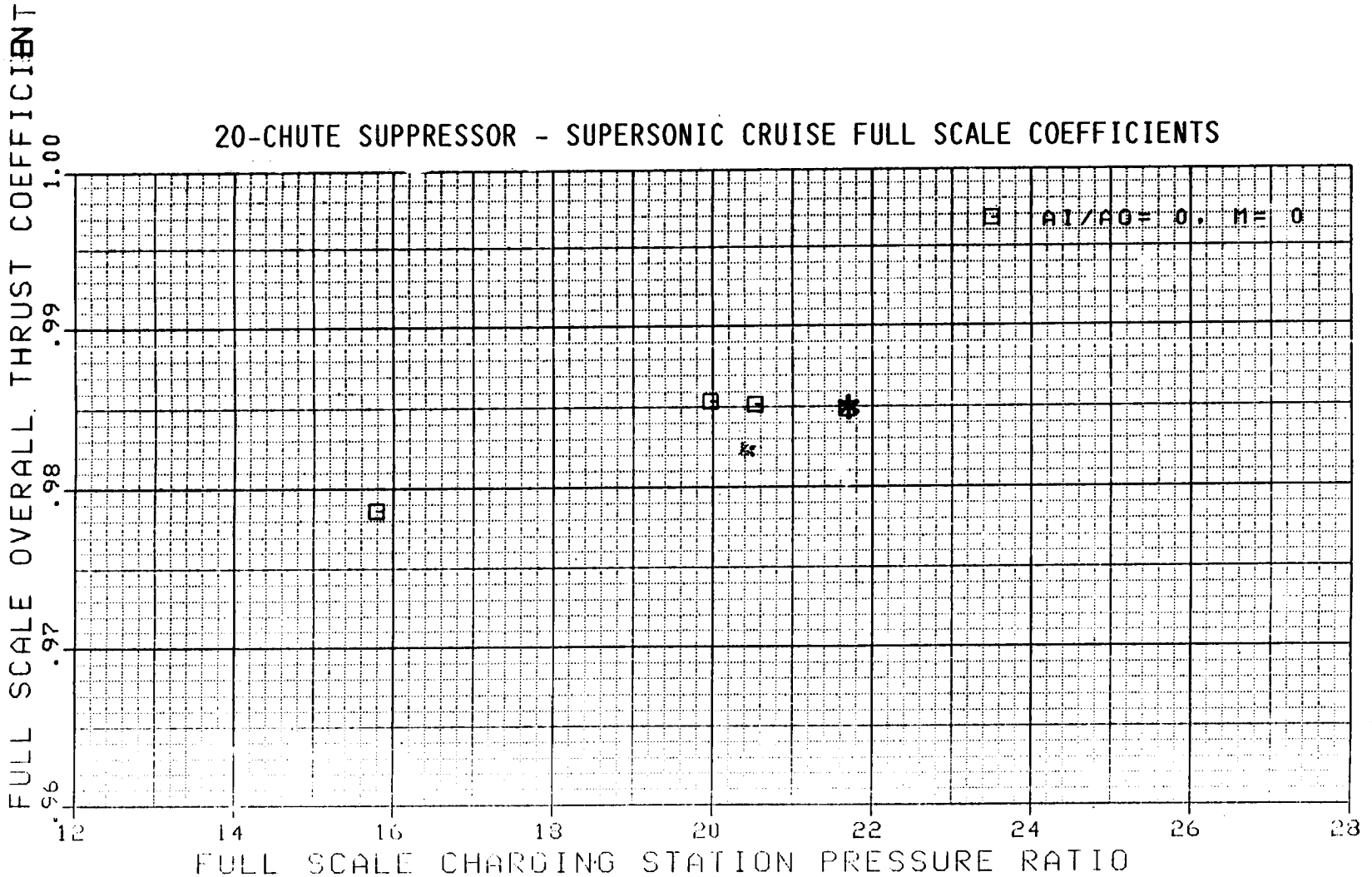

* - DESIGN PRESSURE RATIO

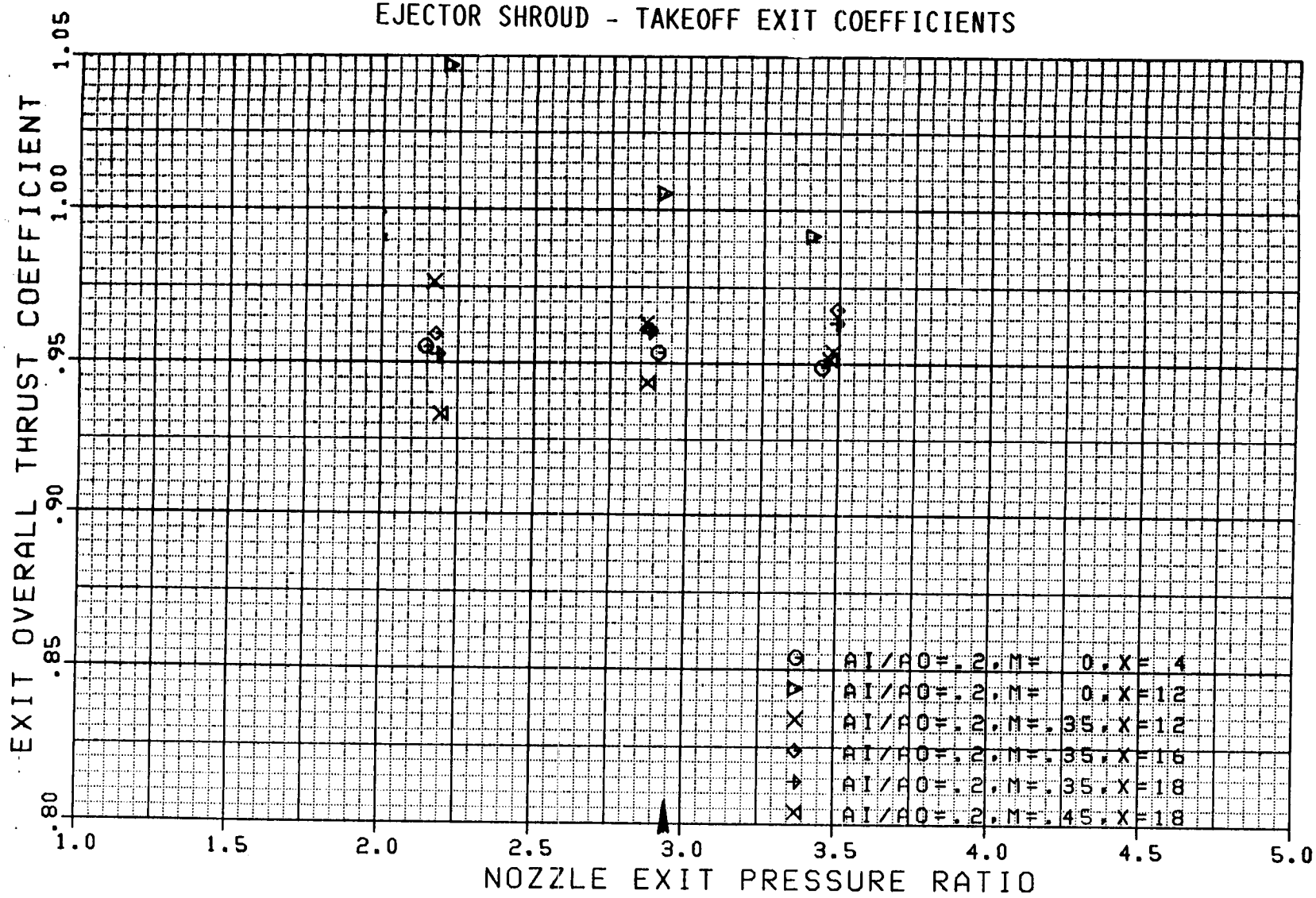

▲- DESIGN PRESSURE RATIO

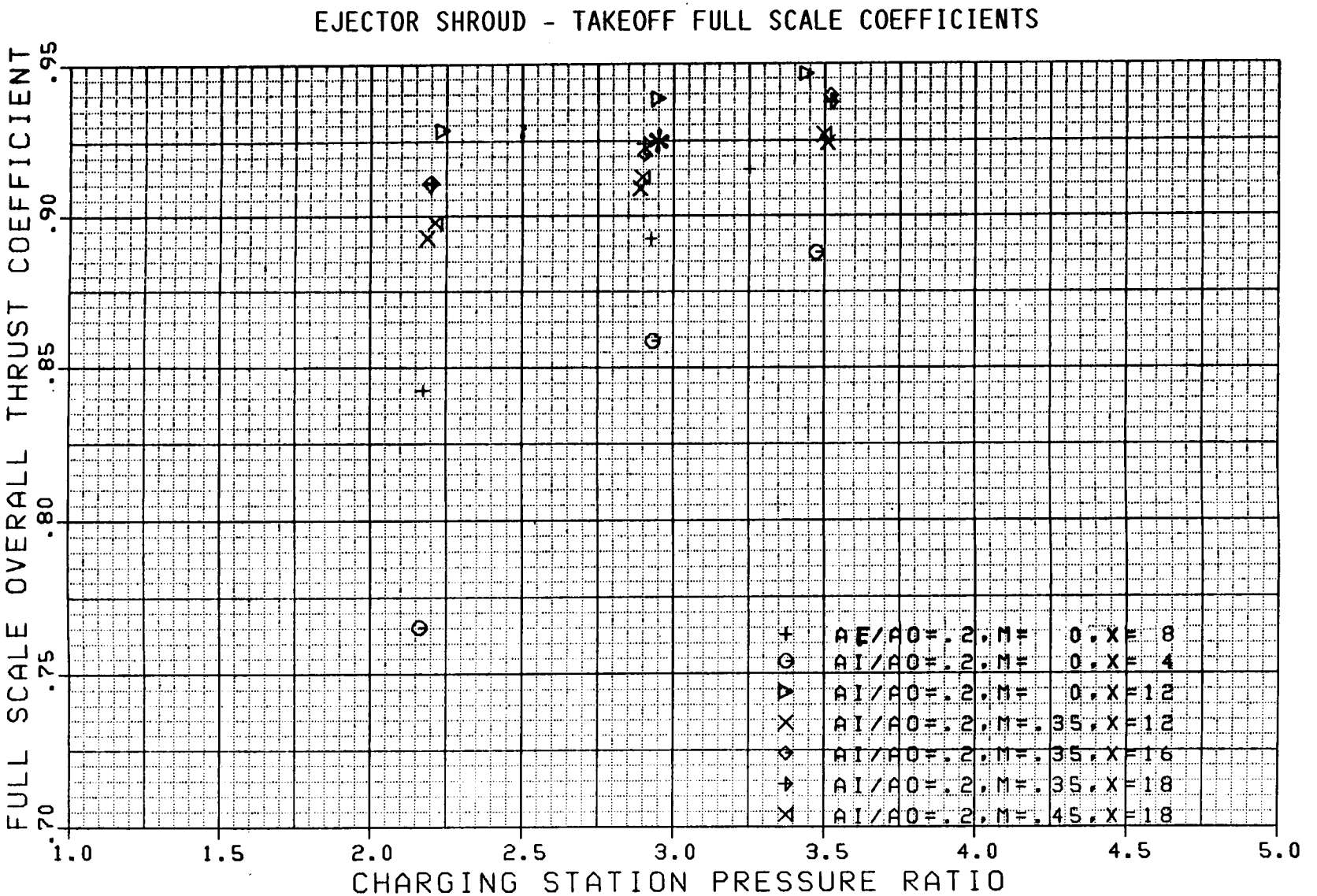

* - DESIGN PRESSURE RATIO

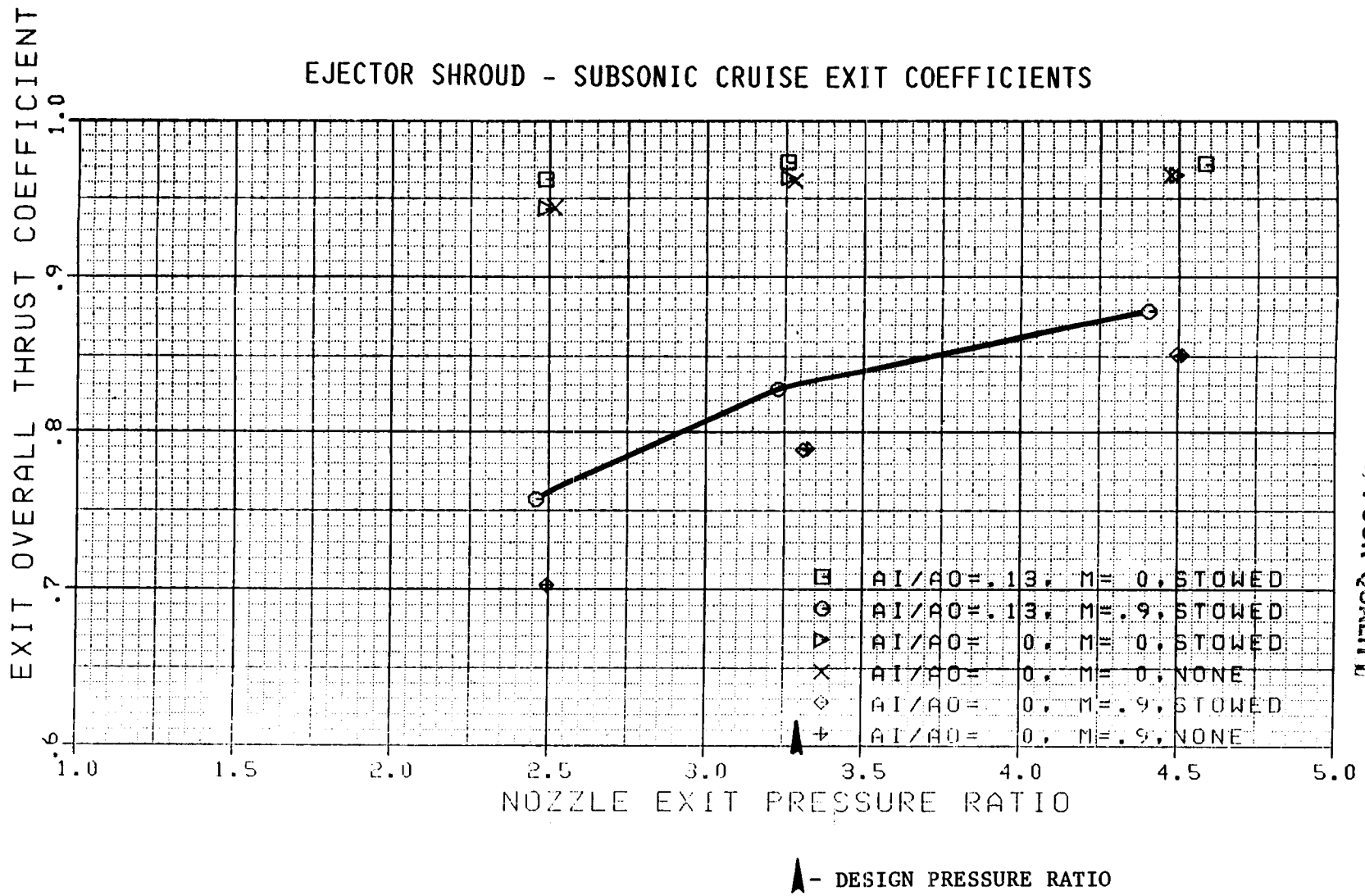

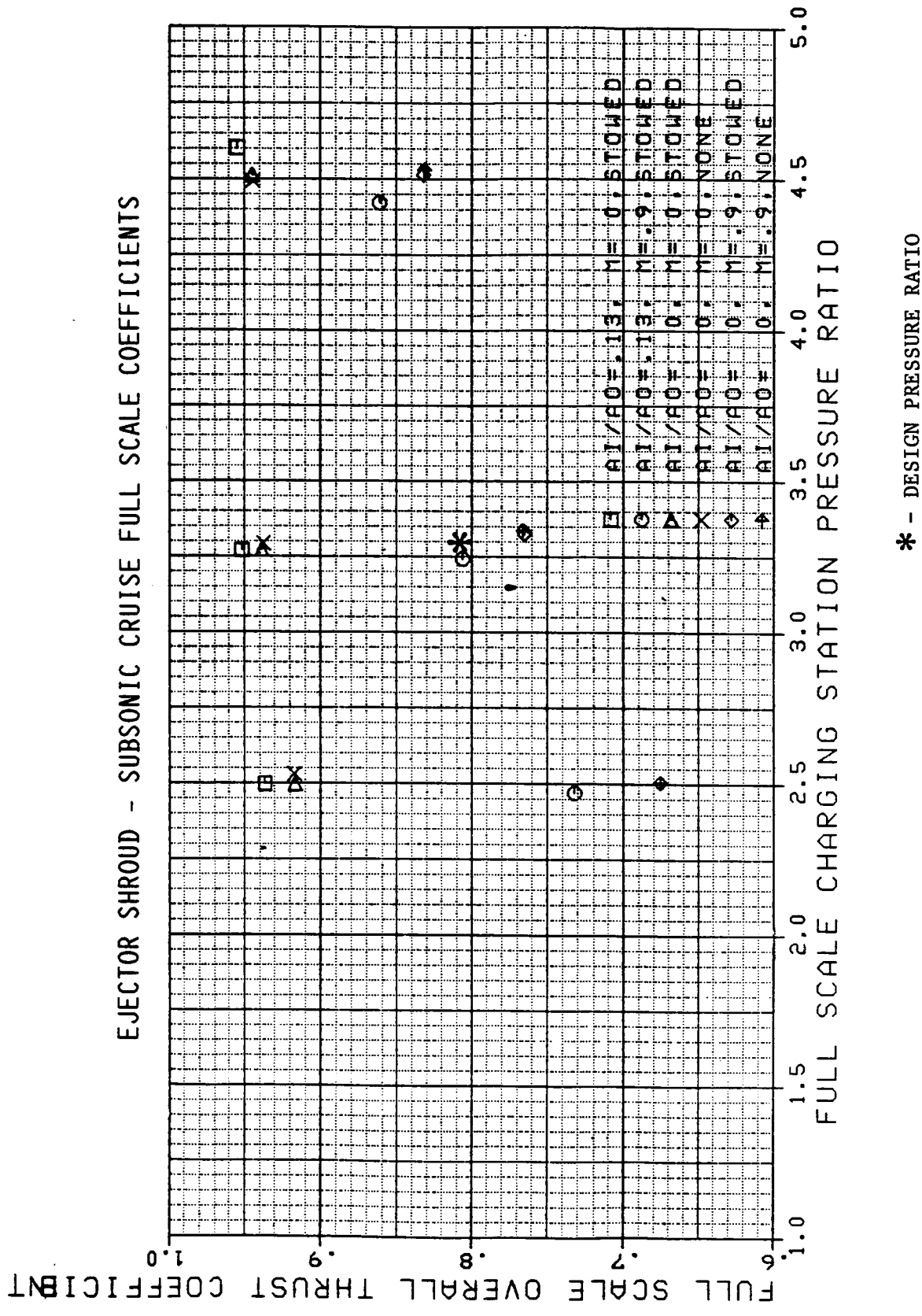

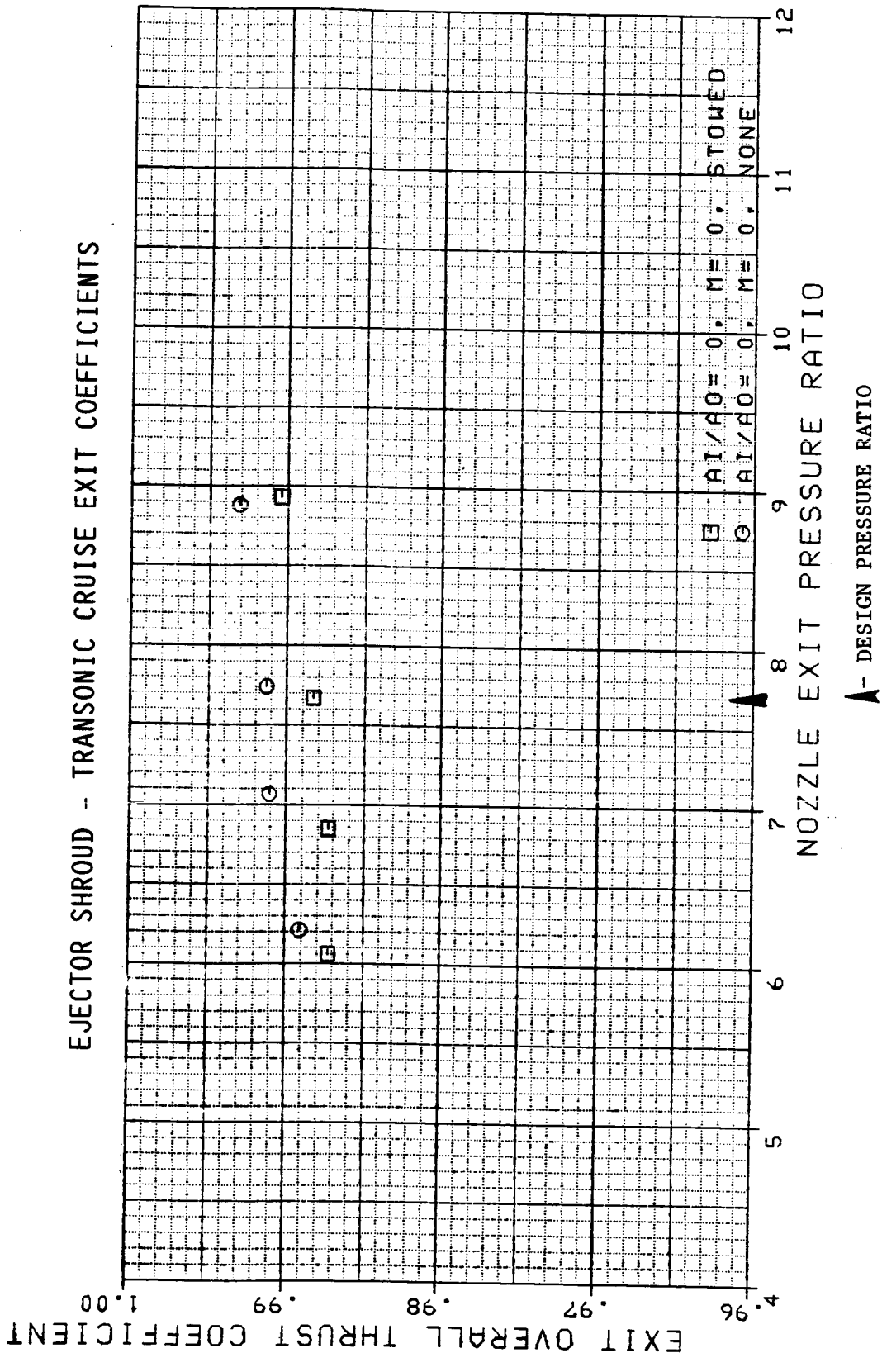

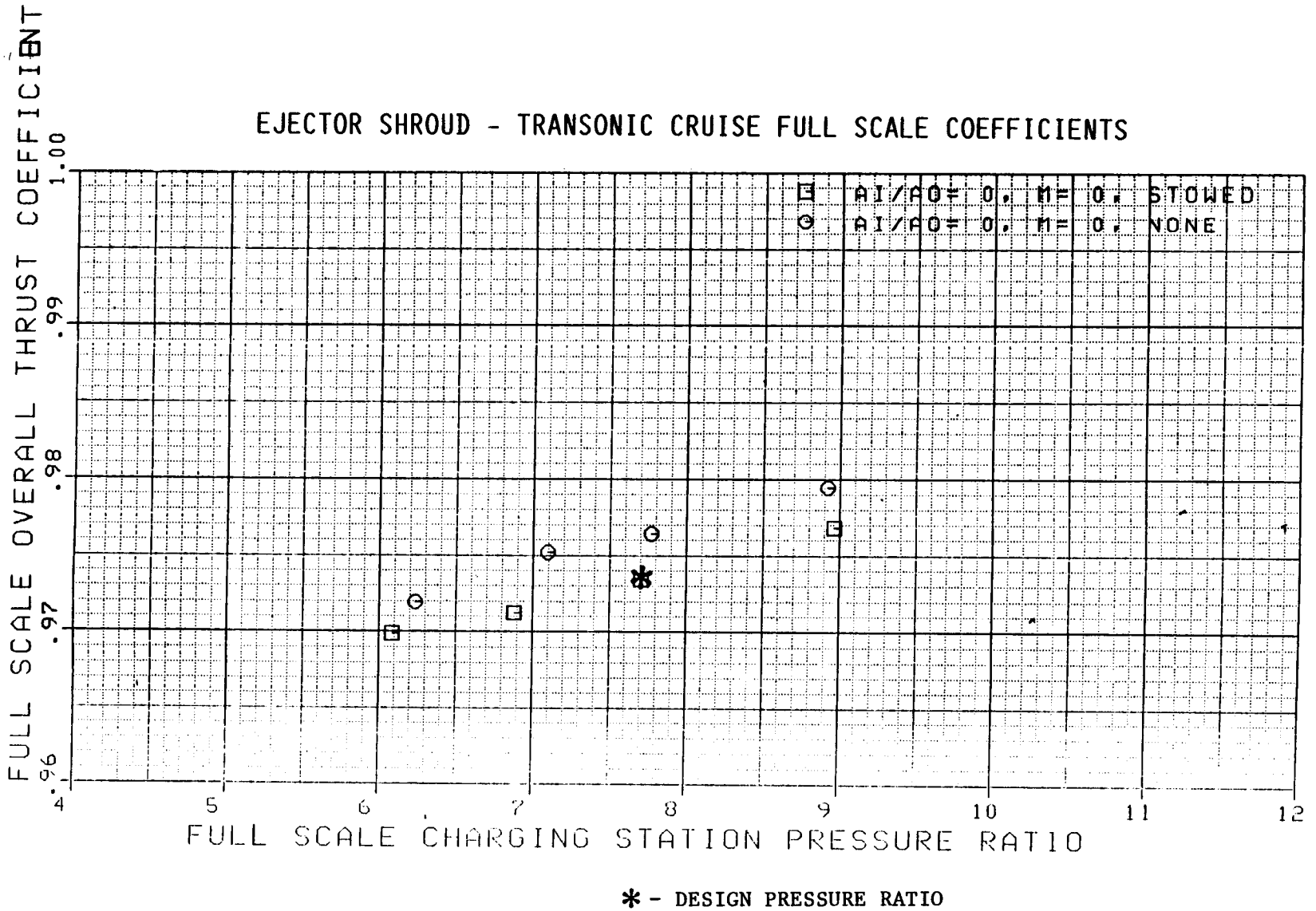
EJECTOR SHROUD - TRANSONIC CRUISE FULL SCALE COEFFICIENTS
AI/AO= 0, M= 0, STOWED
AI/AO= 0, M= 0, NONE
FULL SCALE OVERALL THRUST COEFFICIENT
1.00
.99
.98
.97
.96
4
5
6
7
8
9
10
11
12
FULL SCALE CHARGING STATION PRESSURE RATIO
* - DESIGN PRESSURE RATIO

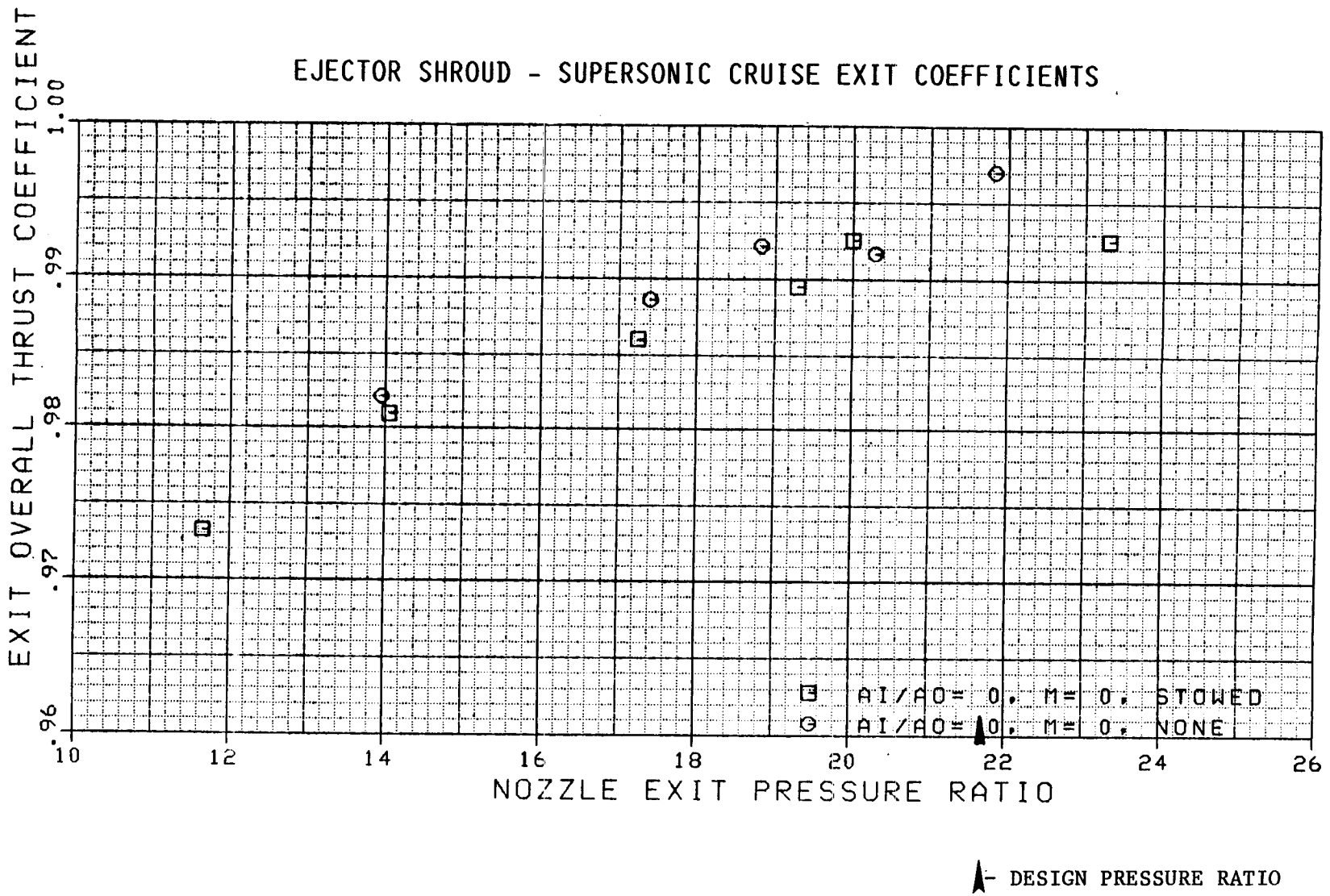
EJECTOR SHROUD - SUPERSONIC CRUISE EXIT COEFFICIENTS
EXIT OVERALL THRUST COEFFICIENT
1.00
.99
.98
.97
.96
10
12
14
16
18
20
22
24
26
NOZZLE EXIT PRESSURE RATIO
AI/AO= 0, M= 0, STOWED
AI/AO= 0, M= 0, NONE
DESIGN PRESSURE RATIO

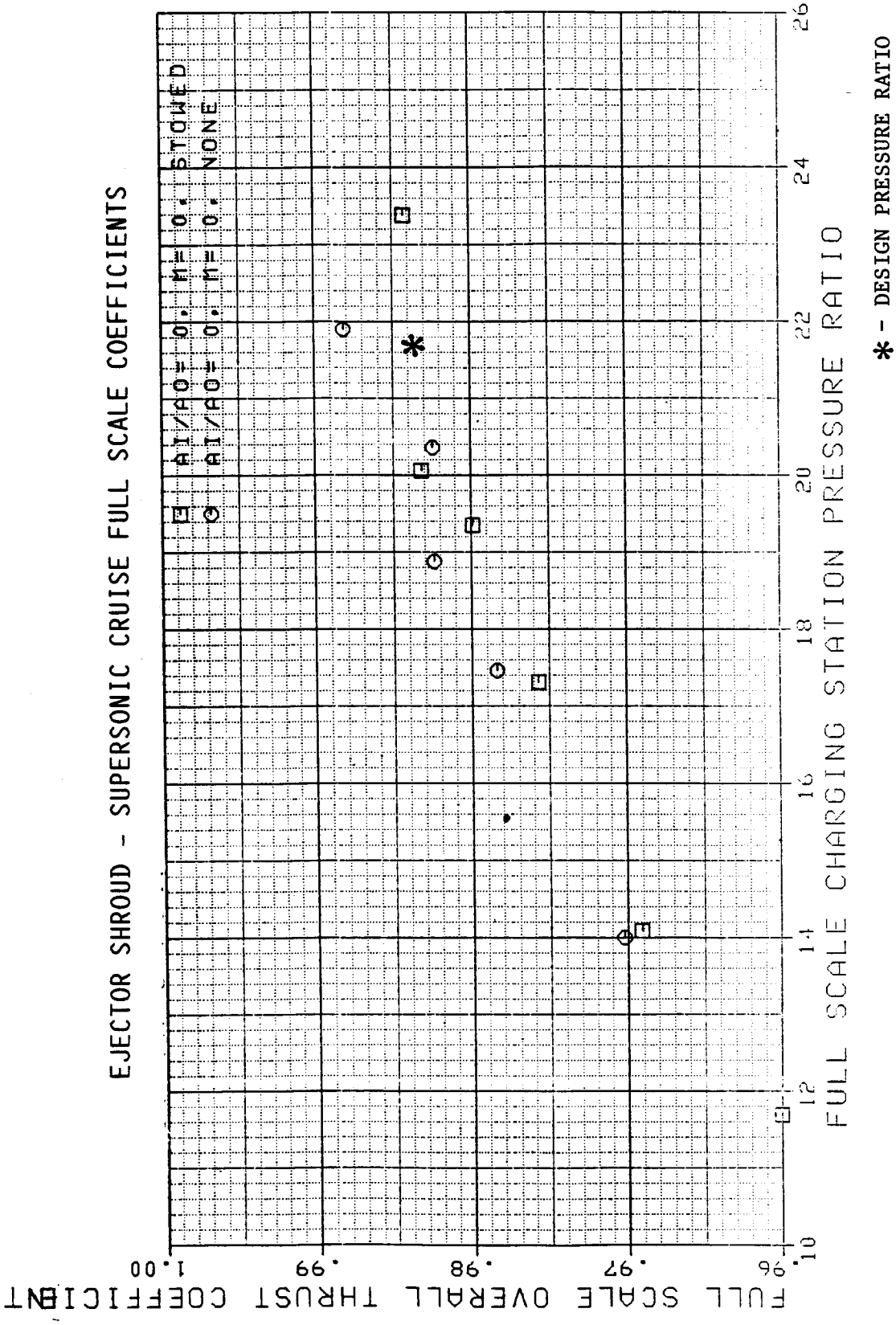

APPENDIX B

EJECTOR SHROUD TABULATED DATA

APPENDIX B

ANALYSIS RESULTS

Nomenclature:

RDG	Reading number
MACH	Mach number
PAMB	Ambient pressure
PR7M	Model outer nozzle charging station pressure ratio
CV7M	Model outer nozzle charging station velocity coefficient
CD7M	Model outer nozzle charging station flow coefficient
PR87M	Model inner nozzle charging station pressure ratio
CD87M	Model inner nozzle charging station flow coefficient
CTM	Overall model thrust coefficient
PR8	Main nozzle pressure ratio
CV9M	Model outer nozzle flow coefficient with scrubbing drag
CV8	Outer nozzle velocity coefficient
CD8	Outer nozzle flow coefficient
PR88	Inner nozzle pressure ratio
CV89	Inner nozzle velocity coefficient with scrubbing drag
CD88	Inner nozzle flow coefficient
CTOA9	Overall exit thrust coefficient with scrubbing drag
CTOA	Overall exit thrust coefficient without scrubbing drag
PR7FS	Full scale outer nozzle charging station pressure ratio

CV7FS	Full scale outer nozzle charging station flow coefficient
CV9FS	Full scale outer nozzle velocity coefficient with scrubbing drag
CD7FS	Full scale outer nozzle charging station flow coefficient
PR87FS	Full scale inner nozzle charging station pressure ratio
CV87FS	Full scale inner nozzle charging station velocity coefficient
CV89FS	Full scale inner nozzle velocity coefficient with scrubbing drag
CD87FS	Full scale inner nozzle charging station flow coefficient
CTFS	Overall full scale thrust coefficient

AST FLUIDYNE SCALE MODEL TEST RESULTS
COANNULAR BASELINE

F	400	530	520	600	15000	15100	15300	14800
MACH	0.	0.	0.	0.	.3523	.3535	.3608	.4449
PAMB	14.038	8.645	14.085	7.794	13.122	13.113	13.064	12.472
PR7M	2.2215	2.8991	2.9208	3.5591	2.1829	2.8801	3.5289	2.1962
CV7M	.98782	.98895	.98888	.9832	.97609	.97967	.97872	.97104
CD7M	.98378	.98513	.98365	.98554	.98507	.98516	.98363	.98471
PR87M	2.3016	2.9663	2.9292	3.5413	2.1529	2.8938	3.5056	2.1903
CD87M	.98121	.9841	.9835	.98517	.98625	.98615	.98463	.98431
CTM	.98067	.98145	.98194	.97766	.97125	.97411	.97423	.9669
PR8	2.2033	2.8748	2.8977	3.5297	2.1648	2.857	3.5012	2.1779
CV9M	.99238	.99232	.99203	.98588	.98077	.98288	.98128	.97568
CV8	.99904	.99857	.99769	.99144	.98759	.98871	.98638	.98254
CD8	.99189	.99345	.99149	.99378	.99329	.99314	.99141	.99297
PR88	2.2793	2.9367	2.9019	3.5063	2.1316	2.8663	3.4732	2.1685
CV89	.95106	.94816	.95028	.9524	.95161	.94971	.9541	.95113
CD88	.99081	.99403	.99275	.995	.99609	.99558	.9938	.99417
CTOA9	.9853	.98488	.98516	.98042	.97607	.97741	.97685	.97167
CTOA	.99571	.99459	.99394	.98902	.98658	.98645	.98477	.98227
PR7FS	2.2146	2.8894	2.9124	3.5473	2.176	2.8715	3.5187	2.1891
CV7FS	.9894	.99043	.98958	.98432	.97789	.98056	.97922	.97289
CV9FS	.99229	.9925	.99163	.98599	.98082	.98263	.98089	.97578
CD7FS	.98682	.98844	.98649	.98882	.9882	.98812	.98647	.98789
PR87FS	2.2983	2.9609	2.9259	3.535	2.1495	2.89	3.5017	2.1867
CV87FS	.95182	.95073	.95057	.95474	.95255	.9505	.95445	.95239
CV89FS	.95606	.95383	.9537	.95733	.95725	.95368	.95706	.95696
CD87FS	.98262	.9859	.98463	.98692	.98779	.98742	.98573	.98592
CD88	.9829	.9837	.98312	.97948	.97378	.97557	.97517	.96951

AST FLUIDYNE SCALE MODEL TEST RESULTS
COANNULAR BASELINE

RDG.	15200	14900	7.00	900	800	18200	18100	18000
MACH	.4499	.4582	0.	0.	0.	.8968	.8997	.8955
PAMB	12.434	12.374	14.074	7.993	6.522	8.3898	8.3743	8.3976
PR7M	2.8917	3.5141	2.5475	3.0609	4.2424	2.5099	3.326	4.1168
CV7M	.97603	.97533	.98137	.98869	.98925	.8888	.92931	.95034
CD7M	.98473	.98478	.98016	.98099	.9805	.98217	.9819	.98148
PR87M	2.8446	3.5115	2.6056	3.0995	4.314	2.5277	3.3322	4.0783
CD87M	.9864	.98484	.98341	.98392	.98313	.98677	.98801	.98693
CTM	.97112	.97133	.97643	.98284	.98415	.89435	.93075	.94985
PR8	2.8683	3.4864	2.5195	3.0259	4.1944	2.4807	3.2883	4.0711
CV9M	.97924	.9779	.98647	.99305	.99242	.8938	.93303	.95341
CV8	.98511	.98307	.994	1.0006	.99865	.90228	.94014	.95952
CD8	.99274	.99263	.99105	.99236	.99172	.99375	.99317	.9925
PR88	2.8174	3.4788	2.5826	3.0703	4.2742	2.5033	3.3013	4.0416
CV89	.94936	.95391	.9438	.94227	.94849	.94056	.94476	.94853
CD88	.99593	.99409	.99217	.99326	.99228	.99638	.99726	.99589
CTOA9	.97442	.97397	.98137	.98707	.98723	.89928	.9344	.95285
CTOA	.98351	.982	.99191	.99758	.99592	.91106	.94429	.96135
PR7FS	2.8829	3.5038	2.5315	3.0402	4.2139	2.4926	3.3038	4.09
CV7FS	.97698	.97591	.983	.99075	.99057	.89139	.93087	.95134
CV9FS	.97904	.97758	.98522	.99255	.99188	.89345	.93243	.95264
CD7FS	.98773	.98769	.98635	.98769	.98713	.98902	.98851	.98791
PR7FS	2.8407	3.5073	2.6052	3.099	4.3124	2.5274	3.3318	4.0778
CV87FS	.95039	.95452	.94138	.94306	.94936	.94153	.94511	.94841
CV89FS	.95364	.95712	.9453	.94628	.9517	.94563	.94811	.95087
CD87FS	.98775	.98602	.98317	.98431	.98351	.98729	.98827	.98702
CTFS	.97268	.97239	.97802	.98512	.98569	.89728	.93253	.95101

AST FLUIDYNE SCALE MODEL TEST RESULTS
COANNULAR BASELINE

RDG.	18600	18700	18800	100	300	200	18300	18400
MACH	.3535	.3571	.4506	0.	0.	0.	.8939	.8996
PAMB	13.101	13.075	12.414	14.292	8.591	7.337	8.4536	8.4205
PR7M	2.1571	2.853	2.8445	2.5112	3.2314	4.1492	2.4818	3.3088
CD7M	.98575	.98527	.98585	.98057	.98129	.98102	.98175	.98214
CV7M	.97462	.97717	.97349	.97504	.99044	.98876	.88609	.92605
CTM	.97462	.97717	.97349	.97504	.99044	.98876	.88609	.92605
PR8	2.1392	2.8301	2.8215	2.4835	3.1948	4.1027	2.4528	3.2713
CV9M	.97937	.98041	.97676	.98022	.99451	.99196	.89115	.92978
CTOA9	.97937	.98041	.97676	.98022	.99451	.99196	.89115	.92978
CV8	.98622	.98628	.98269	.99144	1.005	1.0011	.9036	.94021
CTOA	.98622	.98628	.98269	.99144	1.005	1.0011	.9036	.94021
CD8	.99398	.99326	.99389	.99151	.99252	.99216	.99334	.9934
PR7FS	2.1503	2.8445	2.8359	2.4955	3.2101	4.122	2.4647	3.2869
CV7FS	.97644	.97808	.97448	.97645	.99204	.98989	.88871	.92752
CTFS	.97644	.97808	.97448	.97645	.99204	.98989	.88871	.92752
CV9FS	.97944	.98017	.97657	.97872	.99377	.99125	.89082	.92909
CD7FS	.98887	.98822	.98884	.98674	.9878	.9875	.98855	.98869

AST FLUIDYNE SCALE MODEL TEST RESULTS
20-CHUTE SUPPRESSOR

RDG.	1600	17300	1300	1400	1510	15400	15500	15800
M	0.	.3508	0.	0.	0.	.349	.3555	.4516
PmB	14.516	12.934	14.21	14.219	8.646	12.993	12.96	12.3
PR7M	2.9034	2.9411	2.2673	2.93	3.24	2.2147	3.5355	2.2085
CV7M	.96536	.92397	.96216	.9664	.97097	.90924	.93206	.89447
CD7M	.95789	.95947	.95874	.95717	.95949	.95878	.95937	.95905
PR87M	2.9353	2.9547	2.256	2.9247	3.2637	2.228	3.514	2.192
CD87M	.9856	.99	.98151	.97789	.98113	.98205	.98128	.98366
CTM	.96135	.92473	.95953	.96307	.9669	.91542	.93523	.90297
PR8	2.8715	2.9083	2.2416	2.8978	3.2025	2.1892	3.4969	2.1829
CV9M	.96969	.9281	.96819	.97068	.97505	.91522	.93545	.90043
CV8	.98433	.98234	.98606	.98497	.98315	.98359	.97678	.98046
CD8	.96855	.9703	.96976	.96783	.97072	.96998	.96995	.97033
PR88	2.9156	2.9344	2.2342	2.8974	3.2315	2.2061	3.4815	2.1702
CV89	.93364	.93306	.95143	.95004	.95018	.95106	.95403	.95102
CD88	.99228	.99683	.9911	.98711	.9909	.99181	.99043	.99353
CTOA9	.96545	.92868	.9654	.96724	.97085	.92128	.93854	.90884
CTOA	.98322	.98147	.98507	.98329	.98184	.98306	.97674	.98053
PR7FS	2.8951	2.9322	2.2604	2.9216	3.2287	2.2075	3.5253	2.2012
CV7FS	.96598	.92463	.9634	.96701	.97187	.9106	.93245	.89588
CV9FS	.96926	.92773	.96787	.97026	.9748	.91497	.93502	.9002
CD7FS	.96064	.96237	.9617	.95993	.96285	.96191	.96214	.96225
PR87FS	2.9352	2.9543	2.2527	2.9211	3.2578	2.2244	3.5097	2.1882
CV87FS	.93628	.93645	.95178	.95028	.95228	.95192	.9543	.95209
CV89FS	.93879	.93895	.95612	.95339	.95506	.95634	.95688	.95663
CD87FS	.98563	.99014	.98295	.97911	.98289	.98364	.98246	.98533
CT[illegible]S	.96254	.92599	.96148	.96424	.9686	.91751	.93604	.90512

AST FLUIDYNE SCALE MODEL TEST RESULTS
20-CHUTE SUPPRESSOR

RDG.	15700	15600	1000	1200	1110	17900	17800	17700
MACH	.4496	.4489	0.	0.	0.	.8923	.8938	.8934
PAMB	12.317	12.321	14.013	7.949	7.539	8.4453	8.4335	8.4113
PR7M	2.9097	3.518	2.5695	3.3525	3.6982	2.488	3.2986	4.1059
CV7M	.91148	.92202	.97503	.98549	.9843	.83343	.89415	.92615
CD7M	.95949	.95991	.98009	.98136	.98127	.98235	.98193	.98133
PR87M	2.9178	3.45	2.5972	3.3924	3.7691	2.5369	3.3144	4.1524
CD87M	.98312	.98322	.98495	.98609	.98645	.98772	.98995	.98833
CTM	.91725	.92666	.9703	.97986	.97915	.84501	.89915	.92806
PR8	2.877	3.4793	2.5481	3.3237	3.6666	2.4661	3.2703	4.0714
CV9M	.91564	.92541	.97882	.98846	.98698	.83701	.89688	.9284
CV8	.98115	.97478	.98842	.99749	.99551	.84781	.90594	.93617
CD8	.97039	.97057	.98833	.98987	.98974	.9911	.99042	.98963
PR88	2.89	3.4178	2.5762	3.3638	3.7375	2.5147	3.2865	4.1186
CV89	.94945	.95333	.93828	.94022	.9433	.93472	.93979	.94464
CD88	.9926	.99248	.99295	.99448	.99479	.99644	.99835	.99644
CTOA9	.92133	.92999	.97406	.98279	.98181	.84862	.90188	.93031
CTOA	.9801	.97502	.98702	.99496	.99331	.86318	.91409	.9408
PR7FS	2.9007	3.5076	2.5588	3.3376	3.6819	2.4765	3.284	4.0883
CV7FS	.91219	.92245	.97563	.98651	.98515	.83509	.895	.92653
CV9FS	.91529	.925	.97756	.98795	.98646	.83681	.89634	.92765
C FS	.96245	.96276	.98416	.98575	.98564	.9869	.98629	.98555
P..87FS	2.9137	3.4456	2.5974	3.3928	3.7695	2.5372	3.3148	4.1529
CV87FS	.9503	.95381	.93693	.94176	.94475	.93704	.94098	.9452
CV89FS	.95343	.95644	.94058	.94448	.9472	.94081	.94377	.94745
CD87FS	.98453	.98447	.98457	.98616	.98651	.98799	.98997	.98819
CTFS	.91853	.92753	.97109	.98125	.98037	.8472	.90035	.92872

AST FLUIDYNE SCALE MODEL TEST RESULTS
20-CHUTE SUPPRESSOR

RDG.	5100	5200	5300	19300	19400	19200	19700	19600
MACH	0.	0.	0.	.3533	.3597	.3462	.4524	.4488
PAMB	14.021	14.034	8.733	13.003	12.967	13.168	12.314	12.342
PR7M	2.223	2.8859	3.4856	2.202	2.9173	3.4735	2.2081	2.9092
CD7M	.95808	.95829	.95886	.95962	.96004	.96041	.95887	.96008
CV7M	.96108	.96407	.96618	.90814	.92018	.92948	.89263	.90849
CTM	.96108	.96407	.96618	.90814	.92018	.92948	.89263	.90849
PR8	2.1976	2.854	3.4457	2.1766	2.8847	3.4356	2.1825	2.8765
CV9M	.96729	.96844	.96991	.91416	.92434	.93292	.89857	.91264
CTDA9	.96729	.96844	.96991	.91416	.92434	.93292	.89857	.91264
CV8	.99068	.98783	.9818	.98874	.98516	.9778	.9845	.98383
CTDA	.99068	.98783	.9818	.98874	.98516	.9778	.9845	.98383
CD8	.96915	.969	.96996	.97082	.97089	.97101	.97015	.971
PR7FS	2.216	2.8776	3.4739	2.195	2.9085	3.4636	2.2008	2.9003
CV7FS	.96273	.96485	.96733	.9099	.92105	.92999	.89451	.90945
CTFS	.96273	.96485	.96733	.9099	.92105	.92999	.89451	.90945
CV9FS	.96734	.96817	.97005	.91432	.92418	.93261	.89884	.91255
CD7FS	.96106	.96104	.96211	.96271	.96291	.96314	.96206	.96302

AST FLUIDYNE SCALE MODEL TEST RESULTS
20-CHUTE SUPPRESSOR

RDG.	19500	5400	19800	6500	6300	6400	6600	
MACH	.4549	0.	.8883	0.	0.	0.	0.	
PAMB	12.297	8.345	8.4597	3.123	2.496	2.443	2.379	
PR7M	3.5184	3.283	3.2759	15.849	20.045	20.605	21.758	
CD7M	.95986	.98041	.98195	.98743	.98641	.98718	.98707	
CV7M	.91763	.98026	.89531	.97917	.98593	.98566	.98541	
CTM	.91763	.98026	.89531	.97917	.98593	.98566	.98541	
PR8	3.4797	3.2549	3.2478	15.739	19.907	20.462	21.608	
CV9M	.92101	.98325	.89805	.97998	.98665	.98637	.9861	
CTOA9	.92101	.98325	.89805	.97998	.98665	.98637	.9861	
CV8	.9754	.9961	.91091	.98622	.99196	.9916	.99111	
CTOA	.9754	.9961	.91091	.98622	.99196	.9916	.99111	
CD8	.97053	.98889	.99045	.99429	.99326	.99406	.99393	
PR7FS	3.5081	3.2687	3.2615	15.79	19.971	20.528	21.677	
CV7FS	.91822	.98116	.8961	.97858	.98536	.98513	.98487	
CTFS	.91822	.98116	.8961	.97858	.98536	.98513	.98487	
CV9FS	.92077	.98265	.89746	.97898	.98571	.98548	.98521	
CD7FS	.96268	.98472	.98626	.99109	.99007	.99086	.99073	

AST FLUIDYNE SCALE MODEL TEST RESULTS
EJECTOR SHROUD

RDG.	2120	2200	2600	2700	2800	2300	2400
MACH	0.	0.	0.	0.	0.	0.	0.
PAMB	9.252	8.166	14.249	9.399	8.444	14.26	14.26
PR7M	2.8574	3.5852	2.1686	2.9423	3.4845	2.2433	2.9573
CV7M	.88498	.91362	.72896	.84168	.87566	.92474	.93678
CD7M	.95631	.95612	.95658	.95768	.95624	.9558	.95609
PR87M	2.9328	3.5625	2.1566	2.9151	3.4627	2.2152	2.9674
CD87M	.98162	.98155	.98166	.98231	.98099	.98081	.97991
CTM	.89529	.91962	.76523	.85875	.88785	.92832	.93846
PR8	2.8242	3.544	2.1439	2.9083	3.4445	2.2178	2.9248
CV9M	.88924	.91707	.73385	.84559	.87906	.93062	.94088
CV8	.98686	.96683	.94995	.94908	.94353	1.06	1.0113
CD8	.96756	.96723	.96763	.9689	.96735	.96679	.96671
PR88	2.9037	3.5275	2.1356	2.8862	3.4287	2.1937	2.9398
CV89	.9483	.95267	.95196	.94826	.95192	.95164	.95029
CD88	.99144	.99128	.99132	.99213	.99071	.99042	.98912
CTOA9	.89947	.92301	.77023	.86265	.89121	.93409	.94247
CTOA	.98479	.96848	.95517	.95338	.949	1.0469	1.0052
PR7FS	2.8475	3.5727	2.1619	2.9322	3.4724	2.2364	2.9488
CV7FS	.88709	.91536	.73079	.84361	.87737	.92671	.93761
CV9FS	.89016	.91785	.7344	.84644	.87982	.93107	.94073
CD7FS	.95965	.95947	.95958	.96099	.95957	.95877	.95884
PR87FS	2.9275	3.5561	2.1533	2.9099	3.4566	2.2119	2.9638
CV87FS	.95029	.9546	.95219	.95026	.95383	.95191	.9504
CV89FS	.9534	.95715	.95683	.95339	.95645	.95636	.95347
CD87FS	.98338	.9833	.98314	.98407	.98272	.98227	.9811
CTFS	.89789	.92181	.76724	.8611	.88994	.93083	.93974

AST FLUIDYNE SCALE MODEL TEST RESULTS
EJECTOR SHROUD

RDG.	2500	16100	16200	16000	16500	16400	16300	
MACH	0.	.3514	.3542	.3583	.3451	.3501	.3522	
PAMB	8.212	13.038	13.013	13.001	12.996	12.964	12.951	
PR7M	3.4512	2.1948	2.8992	3.5193	2.203	2.9138	3.53	
CV7M	.94601	.8819	.90138	.91884	.90318	.91566	.93719	
CD7M	.95647	.95951	.95969	.95883	.95882	.95973	.95892	
PR87M	3.4826	2.2298	2.8915	3.5136	2.1845	2.9415	3.5331	
CD87M	.98226	.98409	.98289	.98112	.98397	.98396	.98141	
CTM	.9465	.89287	.90882	.92424	.91028	.92084	.93956	
PR8	3.4114	2.1695	2.8668	3.4809	2.1775	2.8813	3.4915	
CV9M	.94973	.88778	.90549	.92219	.90917	.9198	.9406	
CV8	.99483	.97564	.96103	.94947	.95519	.95812	.96592	
CD8	.96762	.97072	.97054	.9694	.97003	.97057	.96948	
PR88	3.4484	2.2079	2.864	3.4811	2.163	2.9137	3.5005	
CV89	.95206	.95113	.94956	.95406	.95134	.94979	.95424	
CD88	.99201	.99386	.99232	.99026	.99377	.99336	.99054	
CTOA9	.95012	.89865	.91286	.92752	.91618	.92489	.94289	
CTOA	.9917	.97646	.96337	.95399	.95947	.96097	.96771	
PR7FS	3.4391	2.1877	2.8904	3.5091	2.1958	2.9051	3.5199	
CV7FS	.94787	.88428	.90258	.91951	.90559	.91683	.93786	
CV9FS	.95055	.88858	.90565	.92205	.90998	.91994	.94045	
CD7FS	.95983	.96264	.9626	.9616	.96196	.96263	.96168	
PR87FS	3.4764	2.2262	2.8875	3.5094	2.181	2.9376	3.5289	
CV87FS	.95399	.95193	.95024	.95429	.95212	.95038	.95443	
CV89FS	.9566	.95635	.9534	.95687	.95668	.95349	.957	
CD87FS	.984	.98566	.98424	.98229	.98557	.98528	.98257	
CTFS	.94889	.89573	.91045	.92525	.91323	.92245	.9406	

AST FLUIDYNE SCALE MODEL TEST RESULTS
EJECTOR SHROUD

RDG.	16800	16700	16600	16900	17200	17000	17100	
MACH	.3515	.3467	.3511	.4528	.4525	.4547	.8926	
PAMB	12.958	12.974	12.943	12.263	12.416	12.38	8.4836	
PR7M	2.2098	2.9111	3.5306	2.2198	2.9055	3.5078	3.4754	
CV7M	.90334	.91952	.93434	.88814	.90568	.9218	.71289	
CD7M	.95919	.95938	.95968	.95832	.95934	.95943	.9592	
PR87M	2.244	2.9268	3.5286	2.2024	2.8796	3.5018	3.3955	
CD87M	.98285	.98301	.9822	.98274	.98334	.98209	.98386	
CTM	.9106	.924	.93717	.89767	.91232	.92665	.75136	
PR8	2.1843	2.8786	3.492	2.1939	2.8729	3.4692	3.4354	
CV9M	.9093	.92368	.93774	.89401	.90982	.9252	.71567	
CV8	.94715	.95718	.96096	.9238	.93747	.94638	.77235	
CD8	.9704	.97022	.97027	.9696	.97025	.97009	.97038	
PR88	2.2219	2.899	3.496	2.1805	2.852	3.4692	3.362	
CV89	.95099	.9497	.95415	.95089	.94933	.95374	.95132	
CD88	.99262	.99242	.99137	.99261	.99283	.99132	.99365	
CTOA9	.91644	.92808	.94049	.90347	.91639	.92998	.75423	
CTOA	.95283	.96018	.96357	.93327	.94371	.95141	.80567	
PR7FS	2.2026	2.9023	3.5203	2.2123	2.8966	3.4974	3.4633	
CV7FS	.90573	.92071	.93505	.8907	.90701	.92264	.71447	
CV9FS	.9101	.92383	.93763	.89497	.91009	.9252	.71647	
CD7FS	.96232	.96228	.96246	.96153	.96231	.96228	.96255	
PR87FS	2.2404	2.9228	3.5244	2.1986	2.8755	3.4973	3.3894	
CV87FS	.95185	.95033	.95441	.95203	.9502	.95421	.95334	
39FS	.95623	.95345	.95699	.95653	.95338	.9568	.95602	
87FS	.98444	.98434	.98338	.98443	.98475	.98334	.98561	
CTFS	.91354	.92565	.93825	.90077	.91409	.92785	.75299	

AST FLUIDYNE SCALE MODEL TEST RESULTS
EJECTOR SHROUD

RDG.	1700	1800	1900	1760Ø	1750Ø	1740Ø		
MACH	Ø.	Ø.	Ø.	.8954	.8929	.891		
PAMB	14.296	8.045	6.552	8.481	8.5138	8.5415		
PR7M	2.508	3.2839	4.6241	2.4813	3.257	4.4408		
CV7M	.93671	.95179	.95451	.70271	.78729	.84964		
CD7M.	.98545	.98551	.98457	.98666	.98642	.98578		
PR87M	2.5316	3.3386	4.6322	2.5314	3.2828	4.4296		
CD87M	.97662	.98317	.98183	.98553	.98586	.98453		
CTM	.93644	.95004	.95325	.72984	.80474	.86053		
PR8	2.4871	3.2557	4.5849	2.4594	3.229	4.4038		
CV9M	.94047	.95471	.95664	.70574	.78972	.85156		
CV8	.9598	.9728	.97142	.72719	.80785	.86613		
CD8	.99375	.99405	.99299	.99544	.99495	.99405		
PR88	2.5112	3.3106	4.5939	2.5094	3.2553	4.3941		
CV89	.93797	.93969	.94565	.93467	.93927	.94597		
CD88	.98457	.99149	.99001	.99417	.99419	.99251		
CTOA9	.94018	.95293	.95536	.73296	.80722	.86247		
CTOA	.96182	.97315	.97189	.75691	.82747	.87876		
PR7FS	2.4977	3.2693	4.6037	2.4699	3.2425	4.422		
CV7FS	.9366	.95289	.95523	.70432	.78809	.8496		
CV9FS	.93852	.95432	.95627	.70578	.78928	.85056		
CD7FS	.98953	.9899	.98892	.99121	.9908	.98996		
PR87FS	2.53	3.3352	4.6274	2.5283	3.2795	4.4262		
CV87FS	.93764	.9417	.94761	.9377	.94118	.94683		
CV89FS	.94096	.94414	.94941	.94103	.94366	.9487		
CD87FS	.97724	.98417	.98284	.98675	.98684	.98529		
CTFS	.93672	.95156	.95434	.7322	.80607	.86087		

AST FLUIDYNE SCALE MODEL TEST RESULTS
COANNULAR BASELINE

RDG.	18500	5500	5510	5620	5900	5710	6700	
MACH	.8956	0.	0.	0.	0.	0.	0.	
PAMB	8.4539	3.183	3.078	2.636	2.332	2.039	1.702	
PR7M	4.0829	13.314	14.078	16.786	18.829	21.845	26.929	
CD7M	.98174	.98548	.98478	.98495	.98388	.98367	.98505	
CV7M	.9453	.97966	.97954	.98082	.98565	.98896	.98866	
CTM	.9453	.97966	.97954	.98082	.98565	.98896	.98866	
PR8	4.0376	13.207	13.965	16.651	18.679	21.671	26.715	
CV9M	.94837	.98069	.98054	.98173	.98651	.98976	.98938	
CTOA9	.94837	.98069	.98054	.98173	.98651	.98976	.98938	
CV8	.95739	.98703	.98661	.9871	.99144	.99419	.9932	
CTOA	.95739	.98703	.98661	.9871	.99144	.99419	.9932	
CD8	.99277	.99345	.99272	.99288	.99179	.99156	.99295	
PR7FS	4.0567	13.259	14.02	16.717	18.753	21.756	26.818	
CV7FS	.94617	.97932	.97915	.98042	.9852	.98854	.98843	
CTFS	.94617	.97932	.97915	.98042	.9852	.98854	.98843	
CV9FS	.94748	.97984	.97966	.98089	.98565	.98895	.9888	
CD7FS	.9881	.98955	.98883	.98899	.9879	.98769	.98913	

AST FLUIDYNE SCALE MODEL TEST RESULTS
EJECTOR SHROUD

RDG.	2910	3010	3100	20100	20000	19900	3200	3300
MACH	0.	0.	.0.	.8995	.9033	.8974	0.	0.
PAMB	14.182	8.517	7.081	8.3391	8.3066	8.3558	14.154	8.482
PR7M	2.5088	3.2864	4.5309	2.5177	3.3397	4.5332	2.5394	3.3062
CD7M	.98302	.98379	.98262	.98641	.98667	.98626	.98351	.98235
CV7M	.91689	.93791	.94471	.67385	.76471	.83248	.9177	.93662
CTM	.91689	.93791	.94471	.67385	.76471	.83248	.9177	.93662
PR8	2.4879	3.2583	4.4927	2.4954	3.311	4.4954	2.5182	3.2779
CV9M	.92058	.94077	.94683	.6767	.76701	.83433	.92133	.93946
CTOA9	.92058	.94077	.94683	.6767	.76701	.83433	.92133	.93946
CV8	.94404	.9625	.9647	.70247	.78863	.85174	.94465	.96117
CTOA	.94404	.9625	.9647	.70247	.78863	.85174	.94465	.96117
CD8	.9913	.99227	.99097	.99519	.99521	.99453	.99179	.99082
PR7FS	2.4985	3.2721	4.5115	2.5062	3.3251	4.5143	2.529	3.2918
CV7FS	.91642	.93856	.94488	.67549	.76523	.83213	.91721	.93729
CTFS	.91642	.93856	.94488	.67549	.76523	.83213	.91721	.93729
CV9FS	.91831	.93999	.94595	.67688	.76637	.83307	.91908	.9387
CD[illegible]S	.98706	.98808	.98684	.99092	.99099	.99038	.98755	.98664

AST FLUIDYNE SCALE MODEL TEST RESULTS
EJECTOR SHROUD

RDG.	3400	20400	20300	20200	3900	4000	4100	4200
MACH	0.	.9005	.9038	.9002	0.	0.	0.	0.
PAMB	7.075	8.3262	8.2966	8.3352	5.702	5.231	4.792	4.243
PR7M	4.5122	2.5171	3.3511	4.548	6.1101	6.9077	7.7364	9.0042
CD7M	.98318	.98632	.98588	.98614	.98572	.98584	.98546	.98531
CV7M	.94432	.67399	.7654	.8316	.97079	.9721	.97425	.97763
CTM	.94432	.67399	.7654	.8316	.97079	.9721	.97425	.97763
PR8	4.4742	2.4949	3.3224	4.5101	6.0591	6.8501	7.6721	8.9295
CV9M	.94646	.67684	.7677	.83344	.97251	.97368	.97572	.97896
CTOA9	.94646	.67684	.7677	.83344	.97251	.97368	.97572	.97896
CV8	.96442	.70258	.78929	.85083	.98727	.98731	.98836	.99038
CTOA	.96442	.70258	.78929	.85083	.98727	.98731	.98836	.99038
CD8	.99154	.9951	.99441	.99442	.99403	.99413	.99373	.99356
PR7FS	4.4929	2.5057	3.3365	4.529	6.0845	6.8787	7.7041	8.9667
CV7FS	.94457	.67559	.76591	.83126	.96986	.97121	.97338	.97678
CTFS	.94457	.67559	.76591	.83126	.96986	.97121	.97338	.97678
CV9FS	.94564	.67698	.76705	.8322	.97076	.97204	.97415	.97748
CD7FS	.98741	.99083	.9902	.99027	.98988	.98999	.9896	.98944

AST FLUIDYNE SCALE MODEL TEST RESULTS
EJECTOR SHROUD

RDG.	3500	3600	3700	3800	.01	4600	4300	4400
MACH	0.	0.	0.	0.	0.	0.	0.	0.
PAMB	5.536	5.048	4.711	4.253	3.735	3.183	2.713	2.481
PR7M	6.2634	7.1252	7.8045	8.9563	11.728	14.146	17.372	19.425
CD7M	.98202	.98423	.98339	.98548	.98968	.99005	.98958	.98935
CV7M	.97281	.97611	.97727	.98035	.96052	.96976	.97642	.98066
CTM	.97281	.97611	.97727	.98035	.96052	.96976	.97642	.98066
PR8	6.211	7.0658	7.7396	8.8821	11.646	14.047	17.251	19.29
CV9M	.97451	.97767	.97873	.9817	.96147	.97062	.9772	.9814
CTOA9	.97451	.97767	.97873	.9817	.96147	.97062	.9772	.9814
CV8	.98909	.99104	.99131	.99312	.9732	.98088	.98604	.98949
CTOA	.98909	.99104	.99131	.99312	.9732	.98088	.98604	.98949
CD8	.99029	.9925	.99164	.99371	.99668	.99702	.99651	.99624
PR7FS	6.237	7.0953	7.7718	8.919	11.683	14.093	17.307	19.353
CV7FS	.9719	.97522	.97639	.97947	.95998	.96912	.97572	.9799
CTFS	.9719	.97522	.97639	.97947	.95998	.96912	.97572	.9799
CV9FS	.97278	.97604	.97715	.98018	.96043	.96953	.9761	.98026
CD7FS	.98617	.98838	.98752	.98959	.99346	.9938	.9933	.99303

AST FLUIDYNE SCALE MODEL TEST RESULTS
EJECTOR SHROUD

RDG.	4410	4510	4700	4800	5010	5000	4900
MACH	0.	0.	0.	0.	0.	0.	0.
PAMB	2.401	2.069	3.176	2.654	2.599	2.332	2.176
PR7M	20.137	23.469	14.049	17.524	18.947	20.433	21.981
CD7M	.98912	.98992	.9899	.98963	.98948	.98943	.9895
CV7M	.98398	.98479	.97079	.97906	.98321	.9831	.98883
CTM	.98398	.98479	.97079	.97906	.98321	.9831	.98883
PR8	19.997	23.307	13.951	17.402	18.816	20.291	21.828
CV9M	.9847	.98546	.97165	.97983	.98395	.98381	.98953
CTOA9	.9847	.98546	.97165	.97983	.98395	.98381	.98953
CV8	.99257	.99256	.982	.98864	.99214	.99171	.99701
CTOA	.99257	.99256	.982	.98864	.99214	.99171	.99701
CD8	.996	.99683	.99689	.99657	.99636	.99636	.99642
PR7FS	20.062	23.382	13.996	17.458	18.877	20.356	21.898
CV7FS	.98321	.98423	.97018	.97837	.98238	.98245	.98821
CTFS	.98321	.98423	.97018	.97837	.98238	.98245	.98821
CV9FS	.98356	.98456	.9706	.97875	.98274	.98279	.98855
CD7FS	.99279	.99363	.99367	.99336	.99315	.99315	.99321

DISTRIBUTION LIST

			No. of Copies
NASA Lewis Research Center 21000 Brookpark Road Cleveland, OH 44135			
Attn:	Report Control Office	MS 60-1	1
	Library	MS 60-3	2
	R. E. Coltrin	MS 86-7	2
	L. H. Fishbach	MS 6-12	1
	W. C. Strack	MS 6-12	1
	L. C. Franciscus	MS 6-12	1
	A. G. Powers	MS 86-7	1
	J. B. Whitlow	MS 86-7	5
NASA Scientific and Technical Information Facility P. O. Box 8757 Baltimore/Washington International Airport, MD 21240			
Attn:	Accessioning Department		20
NASA Headquarters Washington, DC 20546			
Attn:	W. S. Aiken, Jr.	Code RJ	1
	J. Levine	Code RX	1
	J. A. Suddreth	Code RJ	1
	G. Banerian	Code RP	1
NASA Langley Research Center Hampton, VA 23665			
Attn:	D. Maglieri	MS 249B	1
	C. Driver	MS 249A	1
	S. J. Morris	MS 249B	1
	C. E. Mercer	MS 280	1
	Research Information Center	MS 151A	1
NASA Dryden Flight Research Center P. O. Box 273 Edwards, CA 93523			
Attn:	F. W. Burcham	MS D-OFAP	1
	R. S. Baron	MS D-FP	1
NASA Ames Research Center Moffett Field, CA 94035			
Attn:	C. Thomas Snyder	MS 200-3	1
Air Force Aero Propulsion Lab Wright Patterson AFB, OH 45433			
Attn:	E. E. Bailey	AFWAL/NASA-PO	1

DISTRIBUTION LIST (Continued)

		No. of Copies
Pratt & Whitney Aircraft **Commercial Products Division** **East Hartford, CT 06108**		
Attn: R. B. Hunt	Eng. 3NJ	1
R. W. Hines	Eng. 3NJ	1
The Boeing Commercial Airplane Company **P. O. Box 3707** **Seattle, WA 98124**		
Attn: F. Neumann	MS 9H-46	1
P. Johnson	MS 9H-46	1
G. Evelyn	MS 9H-46	1
G. W. Klees	MS 9H-46	1
Lockheed-California Company **P. O. Box 551** **Burbank, CA 91503**		
Attn: J. Clauss	Dept. 75-21 Bldg. 63-3 Plant A-1	1
L. Bangert	Dept. 75-21 Bldg. 63-3 Plant A-1	1
Douglas Aircraft Company **3855 Lakewood Boulevard** **Long Beach, CA 90801**		
Attn: R. D. FitzSimmons	Code 35-74	1
W. Rowe	Code 35-74	1
General Electric Company **1 Neumann Way** **Cincinnati, OH 45215**		
Attn: D. J. Dusa	M/D H-43	1
C. D. Wagenknecht	M/D H-43	2
R. W. Whittaker	M/D H-43	1
E. D. Bediako	M/D H-43	5
R. Lee	M/D G-42	1
J. F. Brausch	M/D G-42	1
R. K. Majjigi	M/D G-42	1
B. A. Janardan	M/D G-42	1
J. P. Wolf	M/D H-6	1
R. D. Allan	M/D H-6	1
Evendale Technical Information Center	M/D N-32	6
Lynn Technical Information Center	24001	3
Technical Information Exchange, Schenectady	Bldg. 5 Rm. 221	3

1. Report No.	2. Government Accession No.	3. Recipient's Catalog No.
NASA CR-174860		

4. Title and Subtitle	5. Report Date
Aerodynamic Performance Investigation of Advanced Mechanical Suppressor and Ejector Nozzle Concepts for Jet Noise Reduction	February 1985
	6. Performing Organization Code
7. Author(s)	8. Performing Organization Report No.
C. D. Wagenknecht and E. D. Bekiako	R83AEB122-3
	10. Work Unit No.
9. Performing Organization Name and Address	11. Contract or Grant No.
General Electric Company Aircraft Engine Business Group Cincinnati, OH 45215-6301	NAS3-23038
	13. Type of Report and Period Covered
12. Sponsoring Agency Name and Address	Final Report 1981 - 1984
National Aeronautics and Space Administration Washington, DC 20546	14. Sponsoring Agency Code

15. Supplementary Notes

Project Manager, John B. Whitlow, Jr.
Propulsion Systems Division
NASA Lewis Research Center
Cleveland, OH 44135

16. Abstract

Advanced Supersonic Transport jet noise may be reduced to Federal Air Regulation limits if recommended refinements to a recently developed ejector shroud exhaust system are successfully carried out.

This report describes a two-part program consisting of a design study and a subscale model wind tunnel test effort conducted to define an acoustically treated ejector shroud exhaust system for supersonic transport application. Coannular, 20-chute, and ejector shroud exhaust systems were evaluated. Program results were used in a mission analysis study to determine aircraft takeoff gross weight to perform a nominal design mission, under Federal Aviation Regulation (1969), Part 36, Stage 3 noise constraints.

Mission trade study results confirmed that the ejector shroud was the best of the three exhaust systems studied with a significant takeoff gross weight advantage over the 20-chute suppressor nozzle which was the second best.

17. Key Words (Suggested by Author(s))	18. Distribution Statement
Ejector, Exhaust Nozzle, Acoustic, Suppressor, Aircraft, Propulsion	[redacted] (Until February 15, 1986)

19. Security Classif. (of this report)	20. Security Classif. (of this page)	21. No. of Pages	22. Price*
UNCLASSIFIED	UNCLASSIFIED	208	

* For sale by the National Technical Information Service, Springfield, Virginia 22161